# Bio-Inspired Anti-Wetting Materials Derived from Natural Components

A Thesis Submitted by

**Arpita Shome**

**Roll No: 176122042**

to

**Indian Institute of Technology Guwahati**

for the award of the degree of

**Doctor of Philosophy**

**Department of Chemistry,**

**Indian Institute of Technology Guwahati**

**North Guwahati-781039**

**Assam, India**

**28th Feb 2022**

Dedicated to My Maa and Papa

**Indian Institute of Technology Guwahati**

**Department of Chemistry**

# STATEMENT

I hereby declare that the work incorporated in the thesis entitled "**Bio-Inspired Anti-Wetting Materials Derived from Natural Components**" is the result of investigations of research work carried out by me in the Department of Chemistry, under the supervision of Dr. Uttam Manna, Associate Professor, Department of Chemistry, Indian Institute of Technology Guwahati, Assam, India.

Research material used in this thesis from any other source has been fully cited and acknowledged. This work is original and has not been submitted elsewhere for the award of any degree.

**28th February 2022**

**IIT Guwahati** **Arpita Shome**

**Indian Institute of Technology Guwahati**
**Department of Chemistry**

# CERTIFICATE

This is to certify that the work presented in this thesis entitled **“Bio-Inspired Anti-Wetting Materials Derived from Natural Components”** by **Arpita Shome**, a Ph.D. student of Department of Chemistry, Indian Institute of Technology Guwahati, for the award of degree of Doctor of Philosophy has been carried out under my supervision and this work has not been submitted elsewhere for the award of any degree.

**28th February 2022**

**Dr. Uttam Manna**
Thesis Supervisor
Department of Chemistry
Indian Institute of Technology Guwahati
North Guwahati–781039, Assam, India.

*'Truth, Determination and Perseverance'*

These words were hardly comprehensible for the 6-year old child in me, who devotedly chanted it at every morning prayer for the next 10 years at school. The words lingered on, and the underlying meaning became the motto that instigated and inspired me to keep my sail steady in the sea of life.

Foremost, my whole-hearted acknowledgement is reserved for my supervisor, Dr. Uttam Manna. With a lot of uncertainty yet tenacity, I started the voyage of PhD constantly guided, supported, motivated and protected by my supervisor. I am forever indebted to my supervisor for transforming my academic perspective and re-inciting an ambition in me. I have earned numerous recognitions and appreciation for my research works, an unbelievable dream that was made achievable due to the constant efforts of my supervisor to nourish and present the best in me. I will cherish every academically enlightening as well as the strict, difficult times spent with you that has helped me to become a more careful and sincere human being. Words are insufficient to express my gratitude towards you. Thank you, Sir!

I would like to extend my sincere acknowledgement to my doctoral committee members Prof. Parameswar K. Iyer, Prof. Debapratim Das and Dr. Dipankar Srimani for their valuable suggestions and guidance in improving my research works. I thank the technical staff at Central Instrumentation facility and Department of Chemistry, IIT Guwahati for extending their timely help in instrumentation facilities. I also thank Prof. Thalappil Pradeep and Prof. Biman B. Mandal for their advice and expertise in the collaborative works.

The five wonderful years spent at CHEL-302, Bio-inspired Polymeric Lab has been an academically enriching and personally renewing journey. I thank my former and current lab mates for creating a conducive working environment. The fun-filled memories would be well-guarded treasures for a lifetime. Dr. Adil Majeed Rather, a strict mentor, an inspiring senior and a loyal friend has been a blessing in disguise since 2017. Truly, my PhD journey would have been different without the constant, self-less learnings and help from you. I will fondly reminisce the delightful times spent with Mrs. Tumpa Manna Jana and the adorable bundle of joy, Irsia Manna. I feel blessed and indebted to have found the best set of friends at IIT Guwahati who have extended their selfless support, love and care in every phase of my journey. My heart-felt gratitude to Shilpa Bhuyan, Monikha Chetia, Angana Borbora, Sourav Bhowmick, Rakesh Majumdar, Krishan Mudgal and Joseph Christakiran for loving and accepting me considerably. I am especially thankful to Shilpa Bhuyan and Angana Borbora for helping me to stay optimistic and relish the other aspects in life during the difficult and stressful times.

In Guwahati, I thank my childhood friends from school Manjusha Deka, Tandrali Baruah and Atiqur Rahman for their compassionate friendship through all these years. My gratitude to all my teachers from Maria's Public School and Delhi Public School, Guwahati for imparting a very high standard of education and ethical values. Over the years, I have realised the importance of a good schooling environment and felt grateful for the schools I have attended.

Life in Delhi was a transition for me from the adolescent phase to an adult and finding faithful friends like Mimisha Khamrai, Monalisa Chowdhary, Treesha Pranjali, Dhruv Khandpal, Prakriti Rathi, Fouzia Khan and Vivek Soni has helped me stay grounded to my moral values while fulfilling my academics goals. I am glad to have met each and every one of you and extremely thankful for all the happy days we have spent together. I thank the immensely supportive professors during my graduation days at Sri. Venketeswara College, Delhi University and post-graduation at Jamia Millia Islamia for inculcating the basics of chemistry and introducing me to a new world of imagination and possibilities. Delhi has definitely taught me to dream big, fly limitlessly high and live carefree, since we only live once.

The journey endured so far in life wouldn't have been possible without the unwavering love, care and support of my parents, Mrs. Manjula Devi and Mr. Biswajit Shome. Their self-less sacrifices all through the years for providing the best possible education has contributed in shaping my individuality both professionally and personally. For me, my mother is an epitome of a courageous, fiercely independent woman with immense elegance and smartness. My strive towards excellence through hard-work and patience has and will always be driven by my ambitious father. I thank the unknown power, the lord and eternity for being born as their daughter. I thank my aunt, Dr. Arundhuti Devi for her valuable academic counselling and direction throughout my career. I whole-heartedly express my sincere regards and respect for my aunt, Mrs. Gita Devi and uncle, Mr. Ashish Shome for extending their unwavering strength and support towards our family during the toughest unimaginable times. My younger brother, Mr. Pinak Shome, has been a constant source of both joy and pain in my life. You are and will always be my little, irritating brother who has grown upto to be this smart, extremely intelligent and far-sighted young man who I am proud of.

## 1. Abstract:

The existence of liquid repellent interfaces in nature has stimulated widespread research towards fabrication of bio-inspired anti-wetting materials utilizing numerous synthetic and naturally derived components. However, the earlier reported approaches of naturally derived bio-inpsired materials suffer from durability concerns on prolonged exposure to challenging physical and aqueous chemical settings. Most importantly, the existing approaches mostly fail to provide a facile basis to further induce the desired chemical functionalities in the interfaces ‘three-dimensionally’ to tailor the liquid wettability and also modulate other physical parameters. The substitution of synthetic components with naturally derived eco-friendly alternatives with residual reactivity to tailor both the liquid wettability and mechanical property for developing robust bio-inspired anti-wetting materials can prove vital for biomedical applications and tackling environmental issues. In this synopsis report, I have strategically exploited low-cost, naturally abundant polymers and hydrogel to develop robust, three-dimensional, abrasion-tolerant anti-wetting materials exploiting the catalyst-free Michael addition reaction and facile Schiff base reaction. The use of Michael addition reaction allowed the ‘three-dimensional’ induction of residual chemical reactivity into the substrates that gave the opportunity to tailor the liquid wettability through appropriate post covalent modification with the desired chemical functionalities and also modulate the mechanical property. The synopsis report entitled **‘Bio-Inspired Anti-Wetting Materials Derived from Natural Components’** is divided into seven chapters. **Chapter 1** introduces the basics of liquid wettability, the challenges associated with the existing bio-mimicked anti-wetting materials and the probable solutions. In **Chapter 2**, I have developed ‘reactive’ protein nanoparticles for obtaining robust superhydrophobicity wherein the presence of ‘reactivity’ allowed to tailor the water wettability for controlled release of bioactive molecules. In **Chapter 3**, I have utilized the silk-biopolymer to construct mechanically tailorable sponges through ethanol assisted embedment of beta sheet structures. The same mechanically tailorable sponges were rendered with chemical reactivity through Michael addition reaction to allow the modulation of water wettability. In **Chapter 4**, I judiciously aimed for waste management by exploiting a single chemical approach to convert waste paper into mechanically tailorable, superhydrophobic sponges for resolving another major environmental concern of oil spillages. In **Chapter 5**, BSA protein and Schiff base reaction were strategically extended for developing sustainable underwater superoleophobicity. In **Chapter 6**, the underwater superoleophobic property of Aloe Vera mucilage was discovered and directly utilized for fabricating stretchable and abrasion tolerant underwater oil repellent coatings for filtration-based oil/water separation. **Chapter 7**

summarizes the synopsis report and provides a futuristic direction to the existing works discussed in the report.

## 2. Chapter 1: Introduction

In 1944, Cassie and Baxter first introduced the water-repellent characteristics of the duck's feathers widely recognized as superhydrophobicity (Figure 1B). The structural morphology of the duck's feathers was found to satisfy the theoretical requirements of achieving water repellence in accordance to the Cassie-Baxter heterogenous model of liquid wetting on a rough solid surface (Figure 1A). To survive and adapt to the harsh environment, plants and animals in the water kingdom have been gifted with underwater superoleophobic property referring to extreme oil repellence underwater (Figure 1D-F). In 2009, Liu *et al*, first discovered the underwater oil repellence of fish-scales with hierarchal featured scales made up of calcium phosphate, proteins and a thin mucus layer (Figure 1E). Bio-mimicking i.e. fabricating artificial interfaces inspired by the design of naturally occurring plants/insects requires the presence of a) hierarchal or micro/nano topography to entrap the metastable air (for superhydrophobicity) or water layer (in case of underwater superoleophobicity) and b) low/high surface energy coating for superhydrophobicity and underwater superoleophobicity respectively. Over the years, various synthetic components including fluorinated molecules, hydrocarbons, polymers and naturally derived counterparts including cellulose, chitosan, clay, phytic acid, etc have been used for constructing bio-inpsired anti-wetting materials for applications in oil/water separation, self-cleaning etc.

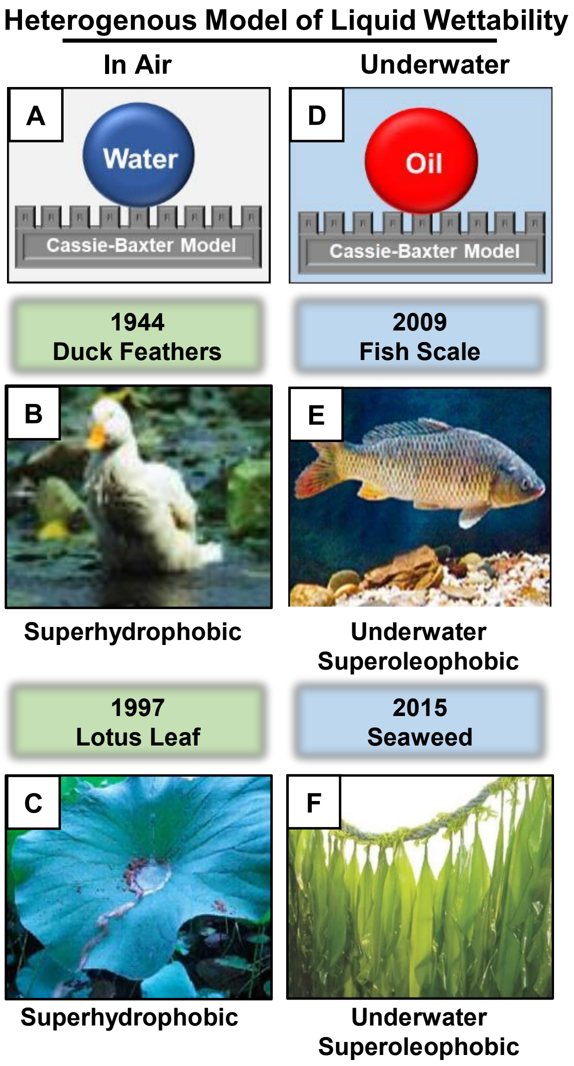

**Figure 1.** A) Cassie-Baxter model of heterogenous water wettability on a solid surface in air. B-C) Image of non-adhesive superhydrophobic duck feather's (B) and lotus leaf (C). D) Cassie-Baxter model of heterogenous oil wettability on a solid surface underwater. E) Image of underwater superoleophobic fish scales. F) Image of underwater superoleophobic clam's shell. H) Image of underwater superoleophobic seaweed. Adapted with permission from *J. Mater Chem. A*, 2021, **9**, 824. Copyright 2021, The Royal Society of Chemistry.

Generally, metal-ion interactions, metal-thiol bonding, polyelectrolytes assembly, inert fluorine chemistry involving synthetic/natural components have been adopted for fabrication purposes, wherein the essential chemical optimization is restricted to only the top surface of the substrate imparting a ‘thin’ layer (order of few nanometers) of the relevant surface functionalization. Thus, subjecting the thin layer of surface coating to severe physical abrasion leads to its removal and eventually compromises the embedded liquid wettability. Moreover, durability of the polyelectrolytes and metal-ions under prolonged aqueous exposure leads to its disintegration whereas hydrogels that are widely used for developing underwater superoleophobicity, are also known to be extremely delicate and deformable. Further, in some cases, the surfaces are rendered with hierarchal features through complex chemical treatments or corrosion and thereby, the waste by-products formed will pose additional environmental threats. Subsequently, a few robust covalent chemistries were explored for association with the hierarchal topography or imparting the essential surface energy to tackle the durability issues, but these lacked the ability to further functionalize the interfaces ‘three-dimensionally’ with the desired chemical functionalities to tailor the embedded liquid wettability and also modulate other physical parameters. Moreover, the derivation of durable bio-inspired wettability from naturally existing components are extremely rare in the literature. Thus, the strategic association

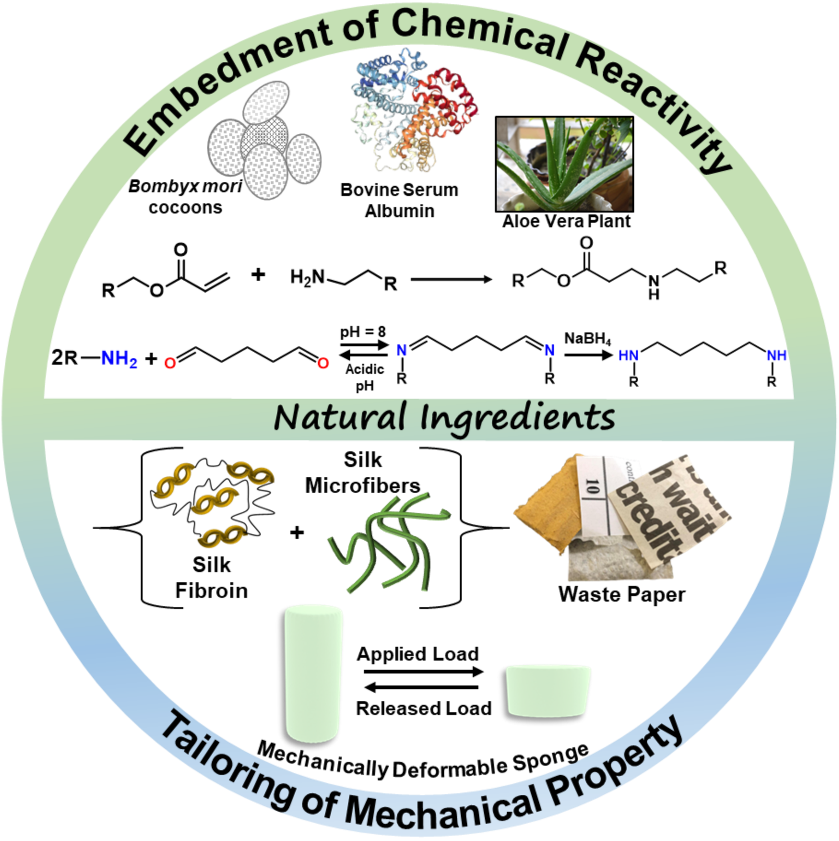

**Figure 2.** Schematic representing the integration of various naturally derived components with a facile chemical approach for embedment of chemical reactivity that would further allow to tailor the liquid wettability. Furthermore, such natural ingredients can be strategically integrated to tailor the mechanical property.

of naturally abundant ingredients with a facile chemical approach imparting residual reactivity is an unprecedented pathway for developing eco-friendly, bio-inpsired anti-wetting materials for extensive real-world applications. Michael addition reaction between a synthetic amine-containing polymer and acrylate functional small molecule was explored recently for developing abrasion-tolerant, three-dimensional anti-wetting materials but the use of synthetic ingredients is likely to pose hindrance for bio-medical applications and combating environmental issues.

In this thesis work, the major aim was to strategically exploit this facile, catalyst-free Michael addition reaction and Schiff base reaction to integrate various well-known naturally abundant, eco-friendly, low-cost ingredients including natural polymers and hydrogels to develop robust anti-wetting materials. The use of Michael addition reaction provided an unprecedented chemical avenue to tailor the water wettability ‘three-dimensionally’ as well control the mechanical property of the as-fabricated materials (Figure 2). Such facile association of a strategic chemical approach with naturally abundant materials has immense potential for drug delivery, wound healing and remediation of major environmental concerns.

## 3. Chapter 2: Protein Derived Chemically ‘Reactive’ Interface for Obtaining Durable Superhydrophobicity

Bovine serum albumin (BSA) is an abundant plasma protein derived from cows that is known for its biocompatibility, non-toxicity and biodegradability and has been widely used for therapeutic applications. The chemical modification of the amino acid residues of BSA has been explored in the past utilizing specialized chemistries. However, there is a dearth of chemical approaches that exploits the amine residues to cross-link the protein network and render residual chemical ‘reactivity’ to the proteins that would allow to install various desirable chemical functionalities. In this chapter, BSA nanoparticles were synthesized following de-solvation technique with ethanol as the anti-solvent and subsequently exposed to dipentaerythritol pentaacrylate (5Acl) (Figure 3A-B), to develop chemically ‘reactive’ and covalently cross-linked protein nanoparticles with an average diameter: 487 nm ±16.85. The amine groups of BSA readily reacted with the acrylate groups of 5Acl following the catalyst-free Michael addition reaction (Figure 3C). The appearance of the IR peaks due to (a) the asymmetric C–H stretching (at 1410 $cm^{-1}$) of β carbon of the vinyl group and (b) stretching of the carbonyl group (at 1736 $cm^{-1}$) together revealed the presence of unreacted acrylate groups in the BSA nanoparticles as shown in Figure 3D. Hence, these residual acrylate groups provided further scope for post-covalent modification with primary amine containing small molecule i.e. octadecylamine (ODA) as indicated by the decrease in peak intensity at 1410 $cm^{-1}$ (Figure 3D, red). Thus, these post modifiable nanoparticles were believed to be capable of producing durable superhydrophobicity.

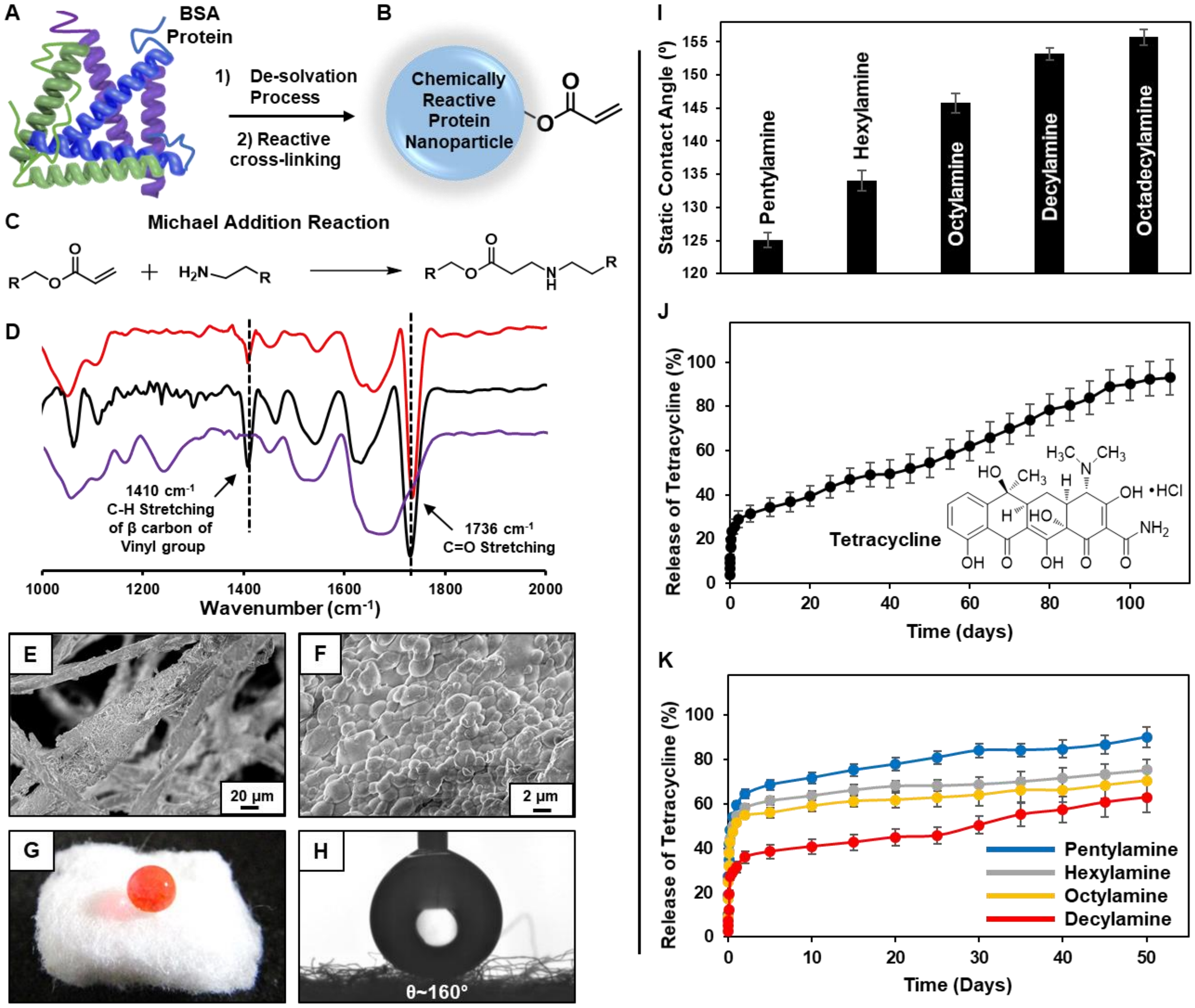

**Figure 3.** A-C) Schematic illustrating the formation of the chemically 'reactive' bovine serum albumin nanoparticles through Michael addition reaction between amine residues of BSA and multi-functional acrylate (5Acl). D) FTIR spectra of BSA nanoparticle (violet) after covalent cross-linking (black) with 5Acl, and after post-modification with octadecylamine, ODA (red). E-F) FESEM images of the BSA nanocomplexes coated cotton fibres. G-H) Digital image (G) and static water contact angle (H) of a beaded water droplet on the BSA derived superhydrophobic cotton. I) Plot depicting the static water contact angles on cotton after post modification with different alkylamines. J) Plot depicting the sustained release of tetracycline from the ODA treated cotton. K) Plot illustrating the controlled release of tetracycline loaded into the BSA nanoparticles coated 'reactive' cotton that was selectively post modified with different alkylamines. (*Nanoscale Adv.* 2019, **1**, 1746-1753, *ACS Sustainable Chem. Eng*., 2019, **7**, 7502-7509)

In the presence of naturally abundant fibrous medical cotton, the same de-solvation process was repeated for directly depositing the BSA nanoparticles on cotton. Upon addition of ethanol, (a) BSA nanoparticles were immediately deposited on cotton, and (b) upon treatment with 5Acl molecules, a covalently cross-linked uniform coating of BSA nanocomplexes on cotton was obtained as characterized by FESEM (Figure 3E-F). The granular domains randomly aggregated and provided the essential hierarchical topography for achieving extreme water repellence. The 5Acl treated BSA coating with residual acrylate groups provided a facile basis for covalent association of ODA to achieve a superhydrophobic cotton (Figure 3G-H). The presence of a shiny interface on submerging the superhydrophobic cotton underwater, validated the existence of metastable trapped air that conferred the heterogenous water wettability.

Different physical manipulations, i.e. bending, twisting, winding, and severe physical abrasion tests, i.e. adhesive tape test, sand paper abrasion were performed on the BSA derived superhydrophobic cotton that revealed the interiors of the fibrous substrate. However, the anti-wetting property remained intact both on the surface as well as on the newly exposed interiors of cotton with static water contact angles >155°, thus, revealing the presence of bulk superhydrophobicity. The superhydrophobic cotton was also exposed to extremes of pH, artificial sea water, river water and surfactant contaminated aqueous phases, UV radiation for 30 days without any perturbation in the water repellence property.

Such a durable, 'reactive' fibrous substrate was further subjected to post covalent modification with amine containing different small molecules including pentylamine, hexylamine, octylamine, and decylamine to tailor the water wettability from hydrophobic, adhesive superhydrophobic and non-adhesive superhydrophobic as shown in Figure 3I. The presence of metastable trapped air allowed the sustained release of the loaded drug molecules owing to the slow impregnation of aqueous phase into the bulk of the substrate. Subsequently, the ODA modified superhydrophobic cotton loaded with tetracycline displayed an initial burst release which was attributed to the loosely bound drug molecules on the outer exposed surface followed by a sustained release over a period of 100 days from the bulk of the fibrous substrate (Figure 3J). Post covalent modification with different alkylamines altered the water wettability of the fibrous substrate and consequently, allowed to control the rate of drug release (Figure 3K). Increasing the hydrophobicity led to an extended time period of release, wherein it was observed that pentylamine modified cotton (with water contact angle ~128°) released ~64% tetracycline over 2 days whereas decylamine (with water contact angle ~157°) modification led to ~36% release in 2 days. Moreover, anti-bacterial studies revealed that the released drug remained bio-active against *E.coli* and *S. aureus*.

## 4. Chapter 3: Silk Cocoon derived Superhydrophobicity with Tailorable Mechanical Property

In the previous chapter, the 'reactive' protein nanoparticles allowed the facile tailoring of the water wettability for extended drug delivery applications but the simultaneous modulation of the mechanical property in the substrate was not viable. In this chapter, the naturally derived silk cocoon of *Bombyx mori* silkworm was exploited to fabricate mechanically deformable and chemically 'reactive' silk sponges denoted as silk microfiber reinforced silk fibroin sponge (SMFRSFS). Silk fibroin (protein) is a widely known biodegradable protein biopolymer that is present in α-helical and random coil conformations in its liquid state. Liquid silk fibroin experiences immense shear when spun by silkworms that causes β-sheet crystallization and generates stable microfibers with high tensile strength. Inspired from this concept of β-sheet microfibers spun by silkworms, the current work on silk cocoon derived sponges involves the use of silk microfibers as reinforcements in a silk fibroin matrix to modulate the mechanical property as shown in Figure 4A-B.

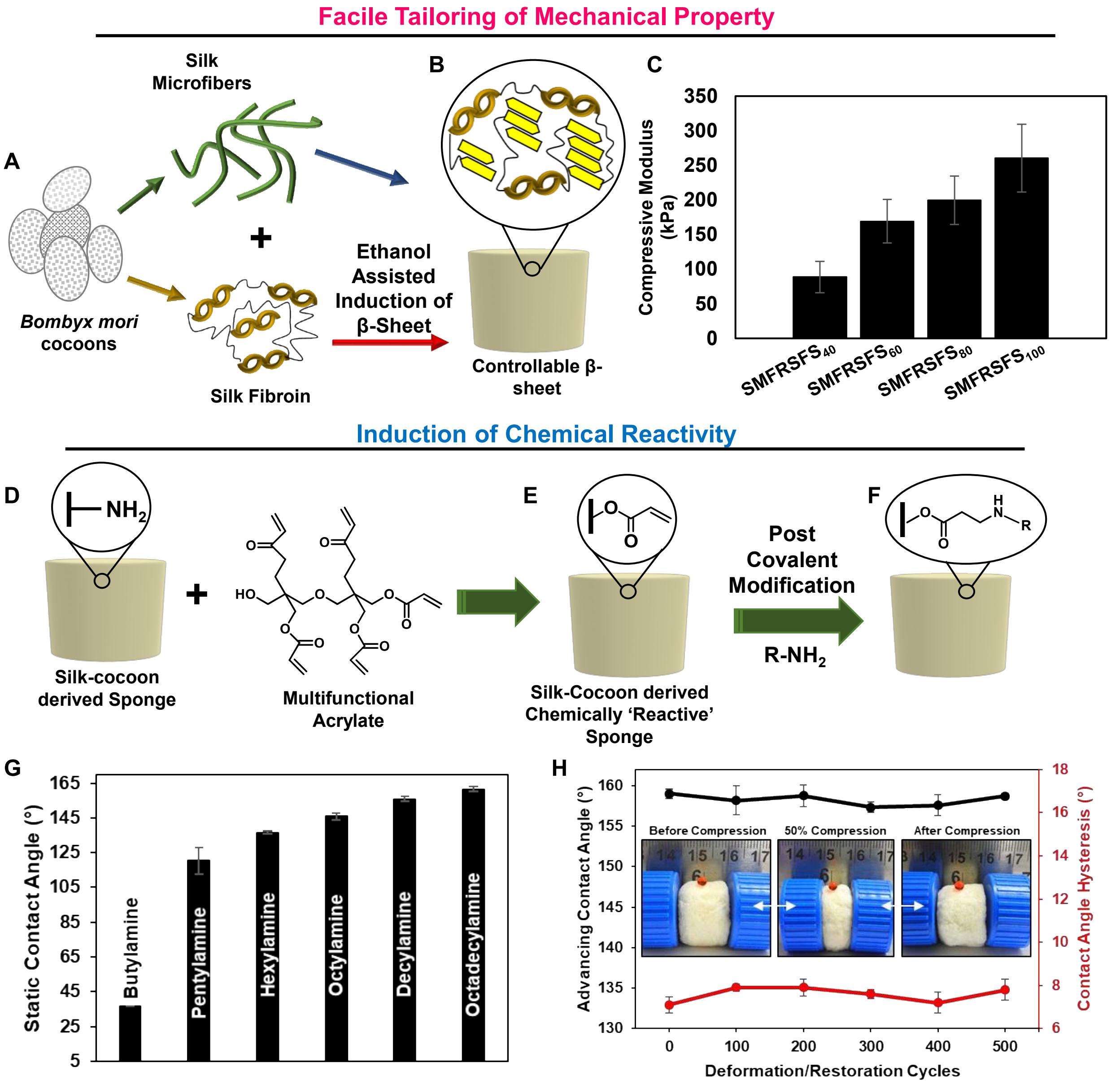

**Figure 4.** A-B) Silk fibroin, which is predominantly present in α-helical and random coil structures, can undergo transformation to β-sheet structures on exposure to ethanol, thus providing a facile basis to tailor the mechanical property by varying the ethanol concentration. C) Plot accounting for the compressive modulus of the different variants of sponges. D-E) The presence of amine residues in the silk cocoon derived sponge paves way for associating chemical reactivity following the facile, catalyst-free Michael addition reaction between amine and a multifunctional acrylate crosslinker at ambient conditions to obtain a chemically 'reactive' sponge (E). F-G) The appropriate post-covalent modification of the residual acrylate groups with selected alkylamines allowed to tailor with the desired water wettability. H) Plot representing the advancing contact angle (black) and contact angle hysteresis (red) of the beaded water droplet on the silk cocoon-derived superhydrophobic sponge that was subjected to 50% manual compression. (*ACS Appl. Mater. Interfaces*, 2021, **13**, 24258-24271).

The ethanol-assisted controlled induction of β-sheets in the silk fibroin skeletal framework allowed to tune both the compressive (90-290 kPa) and tensile (180-980 kPa) moduli while the ethanol treatment did not perturb the conformation of the silk microfiber reinforcement that is already present in stable beta sheet form (Figure 4C). Keeping the content of silk fibroin and microfiber similar, the increase in concentration of ethanol (40-100 v/v%) led to an increase in the beta sheet content and subsequently, an increase in the compressive/tensile modulus. The silk microfiber reinforcement imparted mechanical stability to the sponges that aided in self-recovery after physical deformation of the as fabricated sponges. Further, the catalyst-free Michael addition reaction between the amine residues of silk protein and 5Acl provided a facile basis to fabricate a chemically 'reactive' silk cocoon derived material (Figure 4D-E). The residual reactive acrylate functionalities of the cross-linker rendered the synthesized material chemically 'reactive' for facile and rapid covalent post functionalization with different primary amine-containing desired molecules (Figure 4F-G) to embed a wide range of water wettability (36°-161°) including hydrophobicity, rose petal-inspired adhesive superhydrophobicity and lotus leaf-inspired non-adhesive 'bulk' superhydrophobicity. The embedded water wettability in the silk cocoon derived sponges remained unperturbed even after 500 cycles of repetitive compression (50%) as shown in Figure 4H, 28 days of UV exposure and severe physical abrasions that revealed the interiors of the sponge. The silk cocoon sponges with three-dimensional water repellence were capable of repelling chemically contaminated aqueous droplets (acidic, basic, salt and surfactant contaminated) with water contact angles above 150° and contact angle hysteresis below 10°.

## 5. Chapter 4: Conversion of Waste Products into Robust Functional Materials

In this chapter, the aim revolves around the sustainable waste management by catalyst-free chemical conversion of discarded waste paper into lightweight, porous, highly compressible sponges for remediation of another major environmental concern. The strategic condensation of the cellulosic hydroxyl groups (of waste paper) with the hydroxyl groups of an amine functionalized binder i. e. 3-(2-aminoethylamino)-propyltrimethoxysilane (AEPTMS)[11] during the sponge fabrication process (Figure 5), provided a facile basis to modulate both the a) porosity and b) compressive modulus of the paper-derived sponges. The polymerization of the selected binder (also comprising of primary amines) provided a covalently cross-linked network that imparted mechanical stability to the paper sponge thus, exhibiting high compressibility. Increasing the concentration of the binder led to an increase in the compressive modulus hence, providing an unprecedented basis to modulate the mechanical property through this facile chemical approach. Further, the catalyst-free Michael addition reaction cross-linking of the amine functionalized waste paper with 5Acl induced the desired chemical 'reactivity' in the waste paper derived sponge. The presence of residual acrylate groups in the covalently cross-linked, chemically 'reactive' waste paper derived compressible sponge provided a simple basis to tailor the water wettability from hydrophobic, adhesive superhydrophobic to non-adhesive superhydrophobic with water contact angles ~25° to 161°, following the post covalent modification with the appropriate alkylamines adopting the Michael addition reaction.

The as developed waste paper based 'bulk' superhydrophobic sponges could sustain repetitive compression (60% compressive strain) for 1000 cycles, severe physical abrasions including sand paper abrasion, sand drop test, prolonged (30 days) exposure to harsh chemical aqueous conditions and UV irradiation without compromising the embedded anti-wetting property. Furthermore, the robust waste paper sponge with the highest compressibility (lowest young's modulus), was successfully extended for repetitive (25 times) absorption-based separation of various oils from chemically contaminated aqueous phases without compromising the embedded water repellence and physical integrity of the sponge. Furthermore, the analogous waste paper derived membranes with the highest porosity and subsequently, highest oil flux rate, was utilized for repetitive (50 times) gravity-driven filtration-based

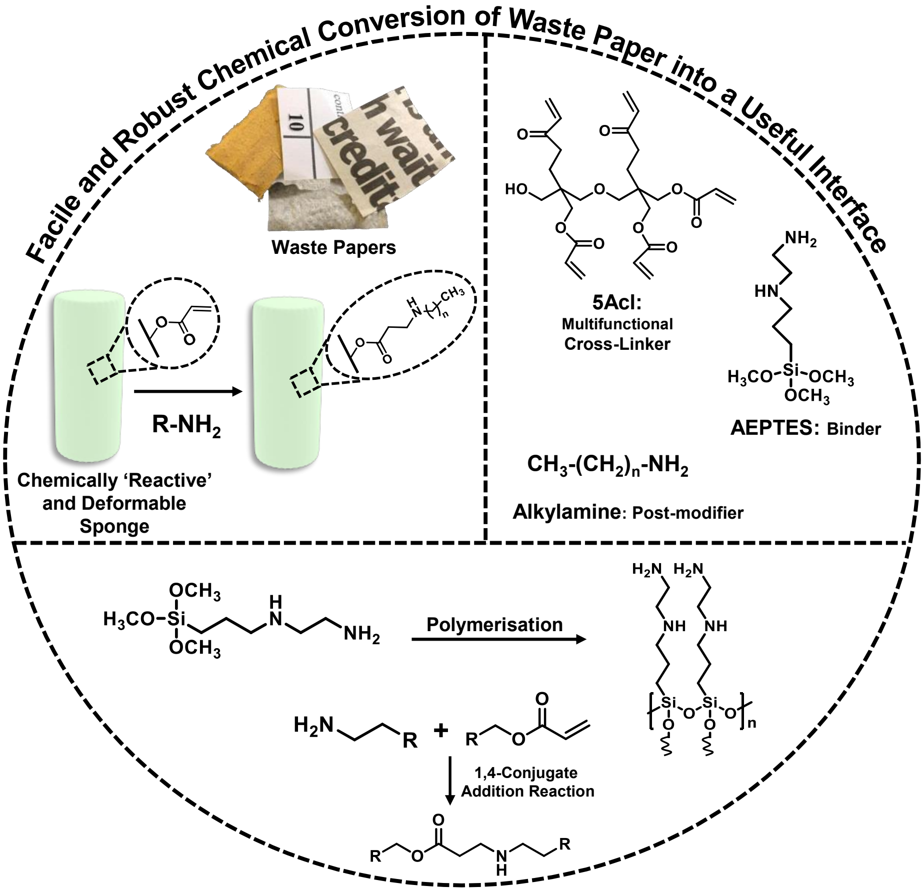

**Figure 5.** A-C) Schematic illustrating the facile chemical conversion of waste papers into a deformable and chemically 'reactive' sponge following the hydrolytic condensation of the amine functionalized silane binder with the hydroxyl groups of waste paper. The polymerization of the binder provided mechanical stability to the sponge to withstand repetitive compression. The Michael addition reaction between the amine functionalized deformable sponge and acrylate cross-linker provided chemical reactivity to the sponge that allowed the fine tailoring of the water wettability on post covalent modification with the selected alkylamines. (*Chem Asian J.* 2021, **16**, 1988-2001).

oil/water remediation with oil separation efficiency above 95%. Thus, a single chemical approach allowed the facile tailoring of both the mechanical property and the water wettability of the robust functional material.

## 6. Chapter 5: Protein derived Sustainable Underwater Superoleophobicity

Nature is a vast reserve that has provided both inspiration as well as the ingredients for the fabrication of artificial anti-wetting materials. Fish-scales were revealed to exhibit underwater oil repellence owing to the hydrophilic protein building blocks that provided both the essential micro/nano topography and high surface energy. Inspired by the hydrophilic, protein constituent of fish-scales, in this chapter I have judiciously exploited bovine serum albumin to construct robust underwater oil-repellent interfaces.

In this chapter, reversible imine bond formation between amine and aldehyde followed by reduction of imine to obtain stable cross-linkages (Figure 6A) was associated with BSA to achieve durable underwater oil repellence. The cross-linking of the aldehydic groups of glutaraldehyde with the amine residues of the protein chain led to the formation of Schiff's base (imine) as one of the expected products (Figure 6B). The deposition of the dynamically cross-linked BSA derived imine on a fibrous substrate provided a) the essential topography to trap the aqueous layer for exhibiting the anti-oil repellent property and b) the presence of hydrophilic amino acid residues enhanced the stability of the trapped aqueous phase. However, since the imine bond is well-known to be labile under acidic media, thus, the embedded underwater superoleophobicity was expected to be compromised. Therefore, reduction of the imine linkage is essential to obtain a stable underwater oil-repellent coating (Figure 6G). A commercially available fibrous substrate was coated with the dynamically cross-linked BSA to obtain a fluorescent underwater oil repellent interface with oil contact angle ~161° in alkaline media (Figure 6C-D). However, exposure of the BSA derived imine coated fibrous substrate to acidic media (pH 1) led to compromise of the embedded oil repellence with oil contact angle reducing to ~107° (Figure 6E-F). To obtain a stable protein derived underwater superoleophobic coating on the substrate, reduction of the imine with sodium borohydride was carried out and it was observed that the selected oil repellence was preserved in acidic media as shown in Figure 6H-I with oil contact angle ~162°, upto 30 days. The presence of granular aggregates on the otherwise featureless fibrous substrate after deposition of the BSA-derived reduced imine, plays a key role in exhibiting heterogenous oil wettability (Figure 6J-K). Exposure of the BSA-derived reduced imine coated fabric to various harsh aqueous conditions and UV radiation for 30 days, severe physical abrasions failed to deter the embedded oil repellence. Furthermore, even stretching the fibrous substrate from 0 to 150% tensile strain for 1000 times failed to perturb the underwater oil wettability.

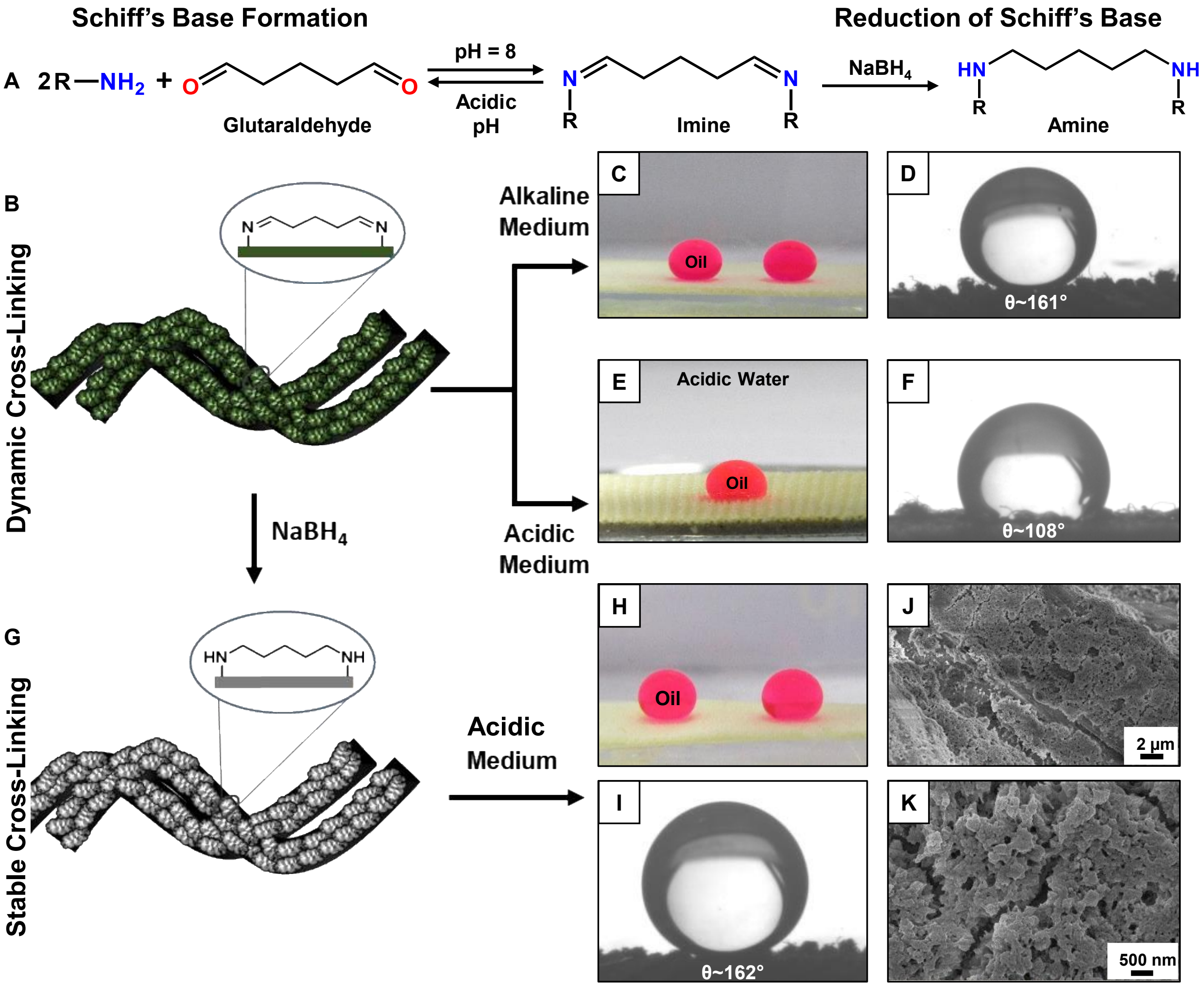

**Figure 6.** A) Illustrating the Schiff base reaction between amine and glutaraldehyde resulting in an acid reversible imine bond. This imine bond can be reduced to a secondary amine using sodium borohydride. B–F) The facile and dynamic cross-linking process between the amine residues of bovine serum albumin protein and glutaraldehyde yielded a fluorescent coating on a fibrous substrate that displayed underwater superoleophobicity in alkaline media (C, D). The coating failed to perform in acidic media owing to the hydrolysis of the imine (E, F). The reduction of the imine bond resulted in a stable crosslinked BSA coating (G) that continued to display unperturbed underwater superoleophobicity in acidic media (H, I). J-K) FESEM images at of the BSA-derived reduced imine coating on the fibrous substrate. (*J. Mater. Chem. A*, 2020, **8**, 15148-15156)

## 7. Chapter 6: Aloe Vera Mucilage derived Abrasion Tolerant Underwater Superoleophobicity

In the previous chapters, nature inspired liquid repellence was integrated with naturally abundant components to construct anti-wetting materials. In this chapter, Aloe Vera mucilage (AVM) a naturally existing hydrogel, was discovered to be inherently underwater superoleophobic (Figure 7B, D) and hence, was directly utilized for developing a stretchable, abrasion-tolerant underwater oil repellent coating. Aloe Vera mucilage consists of an immobilized aqueous phase (~99 wt%) (Figure 7A-B) whereas the outer green peel with water content ~7%, displayed underwater oil contact angle ~67° (Figure 7B-C). The presence of an immobilized aqueous layer in the mucilage aided in displaying excellent non-adhesive oil repellence underwater that remained unperturbed even after exposure to boiling water (100°C) for 1 h, liquid nitrogen (-196°C) for 24 h and extremes of aqueous conditions for 30 days. This prompted to exploit the naturally abundant hydrogel to coat on a commercially available, inherently oleophilic (oil contact angle 0°) fibrous substrate to obtain an underwater superoleophobic coating. However, exposure of the AVM coated fabric to severe physical abrasions i.e. adhesive tape test sand paper abrasion, knife scratch test and sand drop test led to compromise of the embedded bio-mimicked wettability with oil contact angles <100°.

To ensure a stable attachment of the coated AVM on the selected fibrous substrate, a covalent cross-linking chemistry was introduced. The inherently underwater superoleophobic AVM consisting of amine functionalities was covalently modified with a multi-functional cross-linker (5Acl) following the facile and catalyst-free Michael addition reaction between amine and acrylate. This simple chemical approach provided a basis for both covalent cross-linking and essential post modification of the entire deposited AVM to obtain a robust AVM coating. The 5-Acl modified AVM exhibited highly adhesive underwater superoleophobicity with advancing oil contact angle ~152° and contact angle hysteresis ~ 14°, but it comprised of residual acrylate groups. Hence, the residual acrylate functionalities on the covalently cross-linked AVM aided in associating a high surface energy

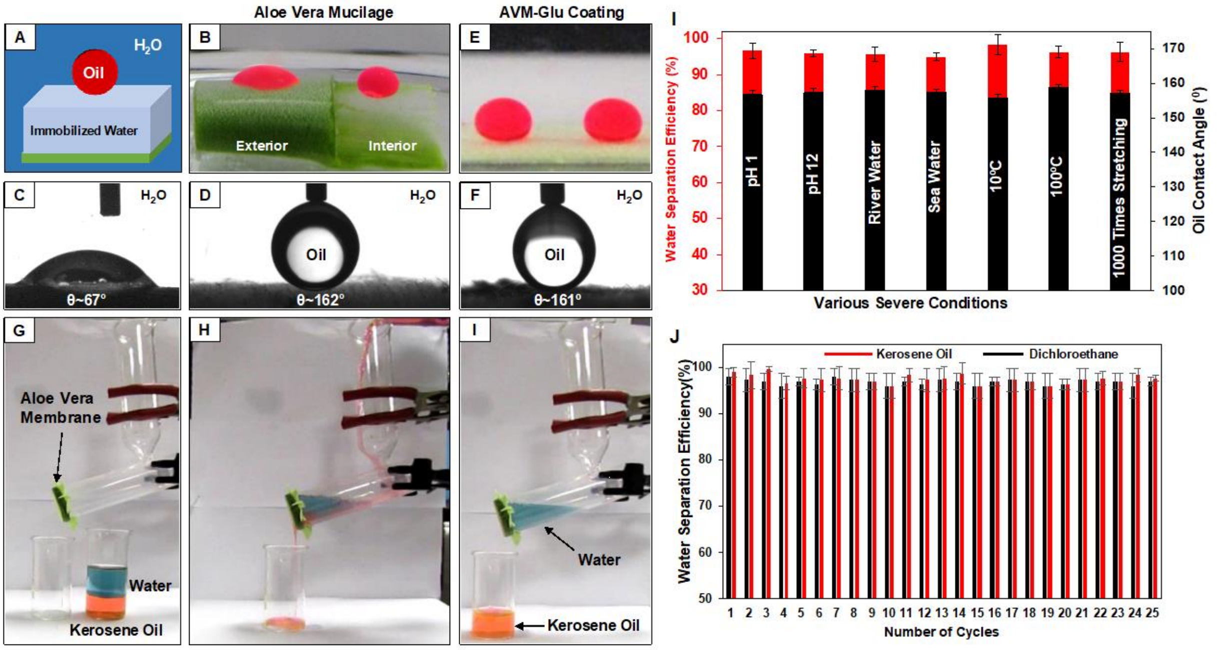

**Figure 7.** A) Schematic representing oil wettability on an immobilized-aqueous phase under water. B–D) Digital image (B) and contact angle images (C, D) of beaded oil droplets on the exterior (C) and interior (D) of the Aloe Vera leaf under water. E-F) Digital image (E) and contact angle image (F) of the beaded oil droplet on the AVM-Glu coated fibrous substrate under water. G–I) Digital images showing the gravity-driven separation of kerosene oil/water mixture by selective filtration of aqueous phase through the AVM-Glu coated stretchable bio-mimicked membrane. I) Plot showing the water separation efficiency (red) through the AVM-Glu coated membrane for motor oil/water mixture under various harsh aqueous chemical conditions. J) Plot illustrating the water separation efficiency after repetitive (25 times) use of the same Glu-AVM coated fibrous substrate for kerosene oil/water mixture (red) and dichloroethane/water mixture (black). (*J. Mater. Chem. A*, 2018, **6**, 22465-22471)

molecule i.e. glucamine to achieve non-adhesive underwater superoleophobicity with advancing contact angle ~161° and contact angle hysteresis ~6° (Figure 7E-F). The glucamine modified coating (denoted as AVM-Glu) withstood 150% tensile strain for 1000 times sustained severe physical abrasions and exposure to several chemically contaminated aqueous phases.

This robust nature-inspired interface was further exploited for gravity-driven oil/water separation of both light (kerosene, Figure 7G-I) and model heavy (dichloroethane, DCE) oils, wherein the aqueous phase selectively passed through the AVM-Glu coated fibrous substrate and the oil phase remained suspended at the top. Furthermore, even after contamination of the water phase with acid, base, salt, surfactant, extremes of temperatures (10°C and 100°C) and physical deformation (150% tensile deformation) of the membrane ensured efficient, selective filtration of the aqueous phases with unperturbed underwater non-adhesive superoleophobicity as shown in Figure 6I. The same AVM-Glu coated membrane was repetitively used for the separation of both light and heavy oils for a minimum of 25 times with water separation efficiency above 97% (Figure 7J).

## 8. Chapter 7 : Conclusion and Future Directions

In conclusion, the work reported in this synopsis strategically utilizes the naturally abundant, low-cost components including natural polymers and hydrogel to develop abrasion-tolerant, three-dimensional bio-inspired liquid repellent materials. The strategic use of Michael addition reaction allowed the embedment of chemical 'reactivity' into protein nanoparticles for developing durable superhydrophobicity and also tailor the water wettability for controlling the release profile of the loaded drugs. The controlled induction of beta sheet in a silk fibroin matrix reinforced with silk microfibers generated mechanically modulable sponges that were further imparted chemical reactivity exploiting the Michael addition reaction between amine residues of silk protein and an acrylate cross-linker. The deformable sponges exhibited extremely durable superhydrophobic property. Further, a single chemical approach allowed precise control over the mechanical property as well as the water wettability in waste paper derived sponges. The superhydrophobic paper sponges that displayed impeccable physical and aqueous chemical durability, were further extended for selective, repetitive absorption of the oil phase from various oil/water mixtures even under harsh aqueous settings. The association of amine residues of proteins with an aldehydic cross-linker followed by reduction of the as obtained imine bond generated sustainable underwater superoleophobic coatings. Aloe Vera mucilage, a naturally existing, undiscovered underwater superoleophobic hydrogel was explored in an unprecedented approach for developing stretchable and robust underwater superoleophobicity on a fibrous substrate for selective filtration of the water phase from various oil/water mixtures at challenging aqueous settings.

Superhydrophobic, blood-repellent coatings have recently accumulated attention for minimizing blood loss, easier wound dressing removal and triggering faster clotting. In that context, the protein derived superhydrophobic coatings on fibrous substrates that was demonstrated for proof-of-concept drug delivery can be extended to develop mechanically deformable, blood-repellent bandage materials for use as external wound healing patches. The ability to tailor the water wettability in such bio-viable materials would prove useful to control the rate of release of the drugs loaded in the blood-repellent patches, thus, preventing excessive blood loss and enabling faster clotting, as desirable. The silk-cocoon derived sponges with tailorable mechanical property and water wettability possess immense potential for tissue engineering applications, where bio-compatibility and bio-degradability plays an important role. The controlled embedment of ethanol-assisted beta sheet content tunes the mechanical property which in turn can aid in controlling the degradability of the sponge when used as implants *in vivo*. The opportunity for simultaneous tailoring of the water wettability in such deformable implants would provide a platform for stem cell differentiation. Moreover, the integration of superhydrophobic, mechanically deformable substrates (silk or waste paper derived) with electrical conductivity can also be useful in developing bio-compatible, wearable electronics, where embedment of water repellence would enhance the longevity of the devices. The eco-friendly, stretchable and abrasion-tolerant underwater superoleophobic coatings can be used for anti-platelet adhesion purposes, underwater wearable electronics etc. Such naturally derived coatings with tuneable liquid wettability can be used as coatings for medical devices without imparting any side effects. Thus, naturally derived components integrated with a smart chemical approach possess potential for a variety of bio-medical applications and remediating environmental concerns.

# Table of Contents

# Chapter 1. Introduction

## 1.1. 'Nature': A Reservoir of Inspiration and Innovation for Science and Technology

Over the years, investigations on the pointed beak of the kingfisher,[1] echo-sounding of bats and dolphins,[2] the hump-back of whales,[3] etc, has formed the basis of bionics.[4] These observations have led to the invention of airplanes, bullet trains, Velcro, turbines etc, that has instigated technological transformation.[5-6] The study of the interaction of a liquid droplet on a solid surface constitutes a major branch of surface science that has opened up multiple interdisciplinary research areas. Interestingly, the in-depth research and analysis in this area has also drawn its inspiration from the infinite reserve of nature.[7] Thus, nature is invariably the one stop solution for all the problems plaguing science and technology. The extreme water-repellent behaviour exhibited by the lotus-leaf, rose-petal, legs of the water strider or the extreme oil repellent behaviour displayed by the fish-scales, clam's shell, sea-weed, bestows its survival under harsh aqueous conditions.[8-9] Mimicking the extreme liquid (water/oil) repellent behaviour exhibited by the naturally existing species is widely termed as bio-mimicked anti-wetting behaviour.[10] Adaptation of the liquid repellence behaviour of such naturally existing species has revolutionized the development of bio-mimicked anti-wetting functional materials for widespread applications in engineering, healthcare and environmental remediation.[11-12] For the replication of the characteristic anti-wetting properties of naturally existing species, considerable attention was focussed on examining the structural and chemical composition of these species.[10] Over the years, synthetic polymers[13] or small molecules[14-15] and even naturally abundant, bio-compatible components[16-17] have been strategically integrated together to develop numerous bio-mimicked anti-wetting materials for various potential applications.[18-19]

In the following sections, an extensive discussion on the origin of liquid wettability in nature and its theoretical aspects studied over the years have been provided. Moreover, a brief evaluation of the essential parameters for mimicking the characteristic anti-wetting properties of the naturally existing species has also been discussed in detail. Further, the advancement in the development of natural components derived bio-mimicked anti-wetting interfaces, the problems associated and the probable solutions for extending it for practical applications is the main motive of this thesis that has been outlined in detail in this chapter.

## 1.2. Exploring the Naturally Existing Anti-Wetting Interfaces

The hidden treasures of nature have always astonished mankind and paved away for revolutionizing industrialization. In 1923, Thomson in a pioneering approach, elaborated the structural features of the duck's feathers that displays extreme water repellence behaviour (Figure 1.1A).[20] Later in 1997, Barthlott and Neinhuis discovered the water repellence property of the lotus leaf, wherein the water droplet remained perfectly spherical on the surface of the leaf and easily rolled off on tilting the surface carrying the deposited dirt along with it, thus, exhibiting self-cleaning property (Figure 1.1B).[21]

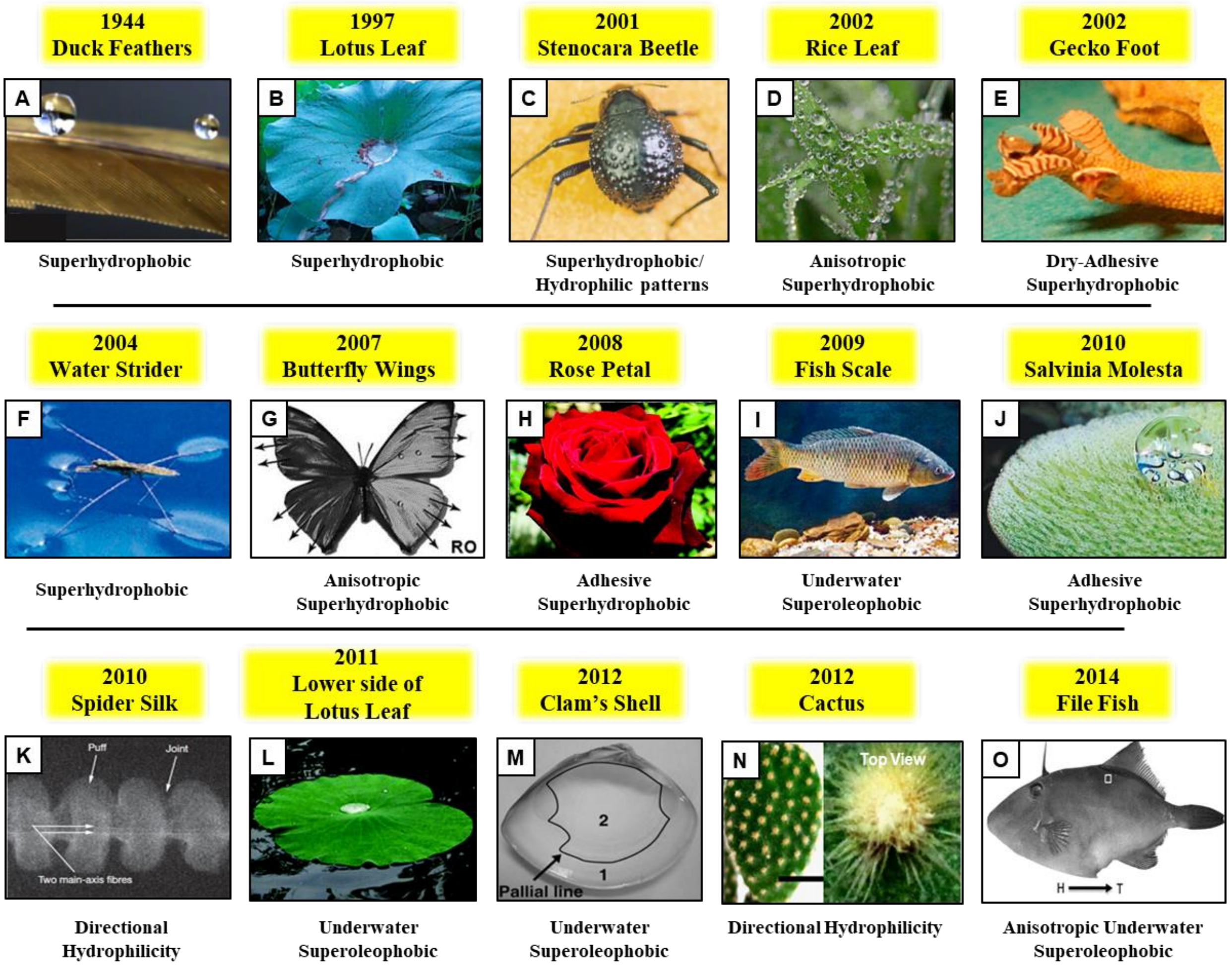

**Figure 1.1.** A) Water-repellent duck feather. Reprinted with permission from (*Proc. Natl. Acad. Sci. U. S. A.*, 2017, **114**, 6930-6935). Copyright 2017, National Academy of Sciences. B) Rolling of the water droplet carrying dust along with it from the surface of the lotus leaf. C) Extremes of wettability patterned back of the Stenocara beetle. D) Directional water wettability of the rice leaf. E) Highly adhesive water-repellent foot of Gecko. F) Water-repellent legs of the water strider that helps it to stay afloat on water. G) Directional water wettability of the butterfly wings. H) Adhesive water-repellent surface of the rose petal. I) Underwater oil-repellent fish-scales. J) Adhesive water-repellent surface of Salvinia Molesta. K) Directional water wettability of spider silk. L) Underwater oil-repellent lower side of the lotus leaf. M) Underwater oil-repellent Clam's shell. N) Directional water wettability of cactus. O) Underwater, directional oil-repellent property of file fish. Reprinted with permission from (*J. Mater. Chem. A*, 2021, **9**, 824-856). Copyright 2021, The Royal Society of Chemistry.

Detailed investigation on the surface of the lotus leaf revealed micro-meter sized papillae (~5-9 µm) which were further decorated with nanometre sized epicuticular wax crystalloids (~200 nm) secreted by the leaf itself, thus, resulting in a dual degree of surface roughness as shown in Figure 1.2A-C. The dual degree or two-tier roughness along with the hydrophobic wax coating was responsible for the extreme water repellence behaviour exhibited by the lotus leaf.[21-22] In 2002, the anisotropic water wettability of the rice leaf was revealed, where the beaded water droplet rolled off along the direction parallel to the leaf edge but remained pinned in the perpendicular direction (Figure 1.1D).[23] This anisotropic behaviour was attributed to the parallel arrangement of micro-papillae along the leaf edge and randomly in the other directions, as shown in Figure 1.2D-F. The highly water adhesive behaviour of the surface of rose petal was discovered in 2008 (Figure 1.1H), where the presence of a close array of micro-papillae decorated with nano-folds led to the extreme adhesion of the beaded water droplet even on inverting the surface upside down as shown in Figure 1.2G-J.[24]

The extreme water repellence behaviour is not just restricted to the plant kingdom. Several insects present in nature have also been gifted with this marvellous water repellence property that aids in their survival under harsh conditions. The stenocara beetle has an astounding water collection mechanism

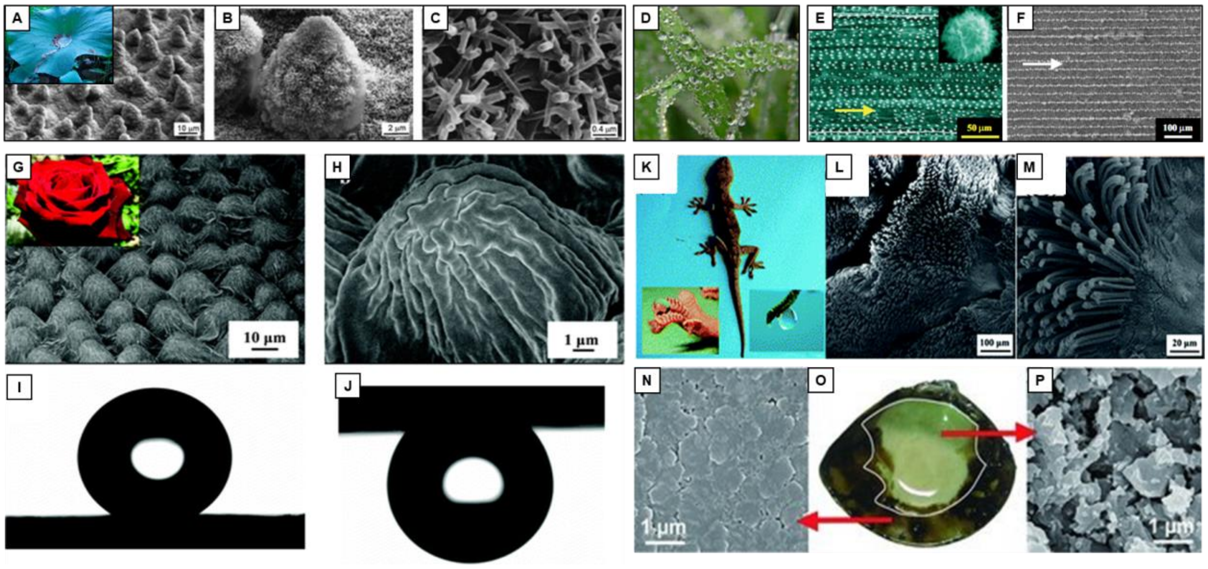

**Figure 1.2.** A-C) Scanning electron microscopic images of the lotus-leaf. Reprinted with permission from (*Soft Matter*, 2009, **5**, 1386-1393). Copyright 2009, The Royal Society of Chemistry. D-F) Scanning electron microscopic images of rice leaf that displays anisotropic water wettability. Reprinted with permission from (*Adv. Mater.*, 2002, **14**, 1857-1860). Copyright 2002, Wiley-VCH Verlag GmbH & Co. KGaA, Weinheim. G-H) Scanning electron microscopy images of the surface of rose petal. I-J) Water contact angle images on the surface of rose petal in the upward direction (I) and on inversion (J). Reprinted with permission from (*Langmuir*, 2008, **24**, 4114-4119). Copyright 2008, The Royal Society of Chemistry. K-M) Scanning electron microscopy images of the highly adhesive gecko foot. Reprinted with permission from (*Nanoscale Horiz.*, 2019, **4**, 52-76). Copyright 2019, The Royal Society of Chemistry. N-P) Scanning electron microscopy images of the outer (N) and inner (P) portions of the clam's shell. Reprinted with permission from (*Adv. Mater.*, 2012, **24**, 3401-3405). Copyright 2012, Wiley-VCH Verlag GmbH & Co. KGaA, Weinheim.

embedded on its back (Figure 1.1C). In 2001, Parker *et al.* revealed that the beetle back comprises of randomly distributed hydrophilic smooth bumps (0.5 mm diameter) and wax coated extreme water-repellent (superhydrophobic) valleys forming micro-structures.[25] The water droplet bounces off on hitting the superhydrophobic valleys and accumulates at the hydrophilic regions until a size is reached wherein it can easily slide off from the beetle back. Over the years, the directional water repellence property of spider silk (Figure 1.1K)[26] and cactus (Figure 1.1N)[27] was also discovered that provided inspiration for designing its artificial counterparts. In 2002, Autumn *et al*. were the first to report the highly adhesive water-repellent feature of the Gecko foot (Figure 1.1E) that comprises of thousands of hydrophobic, micro-meter sized keratinous setae that are further split into hundreds of nanoscale ends as shown in Figure 1.2K-M.[28] The legs of the water strider comprise of numerous oriented needle-shaped setae with diameters ranging from 3 µm to several hundreds of nano-meters. Nanoscale grooves atop the micro-setae along with a hydrophobic wax coating helps the water strider to float on the surface of water (Figure 1.1F).[29]

To survive and adapt to the harsh aqueous environments, the various species in the water kingdom have been bestowed with special anti-wetting properties for their survival. In 2009, Liu *et al.* first reported the extreme oil repellence exhibited by fish-scales that helps it to stay clean and survive even in oil contaminated aqueous phases (Figure 1.1I).[30] Hierarchically featured fish-scales were revealed to be made up of hydrophilic components comprising of calcium phosphate, protein and a thin layer of mucus. The scales consist of radially arranged micro-papillae (length ~100-300 µm and width 30-40 µm) topped with nanoscale structures. The presence of this dual degree of roughness and hydrophilic coating aided in exhibiting extreme underwater oil repellence. Apart from the fish scales, the lower side of the lotus leaf (Figure 1.1L),[31] clam's shell (Figure 1.1M, 1.2N-P),[32] snail shell,[33] file fish[34] (Figure 1.1O) and seaweed[35] were also discovered to exhibit extreme underwater oil repellence. Investigations of structural and chemical properties of these naturally existing species have led to the widespread development of bio-mimicked anti-wetting functional materials over the years for numerous 'real' world applications.

## 1.3. Theoretical Origins of Liquid Wettability on a Solid Surface

To adapt the characteristic anti-wetting features of the naturally existing species, detailed understanding on the theoretical models of liquid wettability is significant. Wettability of a solid surface is an important property since controlled wettability has prospective applications.[18-19] The wetting of a liquid on a solid surface can be determined experimentally by measuring the angle between the surface and the liquid meniscus at the line of contact known widely as the contact angle.[10] Contact angles can be classified as static contact angle and dynamic contact angles. Static contact angle is an equilibrium angle which is obtained when the beaded liquid drop has acquired a steady state on the solid interface as shown in Figure 1.3A. Dynamic contact angles are non-equilibrium contact angles which are further recorded during the advancing and receding of a liquid droplet on a solid surface. Advancing contact angle is measured during the growth of a liquid droplet i.e., when the liquid droplet wets the solid interface (Figure 1.3B), whereas receding contact angle is measured during the shrinkage of the droplet i.e., when the droplet de-wets the surface (Figure 1.3C). The timeline of the theoretical evolution of liquid wettability on a solid surface is discussed below in detail.

### 1.3.1. Young's Model of Liquid Wettability:

The wetting of a liquid droplet on a smooth, homogeneous solid surface was first explained by Thomas Young in 1805, wherein it was observed that the liquid droplet continued to expand on the solid surface until the equilibrium state is achieved as shown in Figure 1.3D.[36] The contact angle of the liquid droplet on the flat, homogeneous solid surface was mainly dependent on the interfacial energy between the solid-vapor, solid-liquid and liquid-vapor interfaces expressed as follows:

$$cos\theta = \frac{\Upsilon_{SV} - \Upsilon_{SL}}{\gamma_{LV}}$$

where, $\theta$ is Young's contact angle, $\Upsilon_{SV}$ is the solid-vapor interfacial energy, $\Upsilon_{SL}$ is the solid-liquid interfacial energy and $\Upsilon_{LV}$ is the liquid-vapor interfacial energy.

The Young's model of liquid wettability in 'air' can also be extended for explaining the wetting of an oil droplet on a flat solid surface placed underwater, resulting in a solid/water/oil three phase interface.[9] The contact angle of an oil droplet in the underwater Young's state can be expressed as follows,

$$cos\theta_{OW} = \frac{\Upsilon_{SO} - \Upsilon_{SW}}{\gamma_{OW}}$$

where, $\theta_{OW}$ is the Young's underwater contact angle, $\Upsilon_{SO}$ is the solid-oil interfacial energy, $\Upsilon_{SW}$ is the solid-water interfacial energy and $\Upsilon_{OW}$ is the oil-water interfacial energy. But, in real-world scenarios, the solid surfaces are not smooth or homogeneous and consist of a certain degree of roughness. This condition led to the failure of the Young's model at practical settings.

### 1.3.2. Wenzel Model of Liquid Wettability:

In 1936, Wenzel explained the liquid wettability on a non-homogenous, non-uniform solid surface by considering a dimensionless roughness factor (Figure 1.3E).[37] It was stated that water conformally filled the rough surface asperities on the solid surface forming a continuous line of wetting and the equilibrium state equation for such surfaces is expressed as follows,

$$cos\theta_W = rcos\theta_Y$$

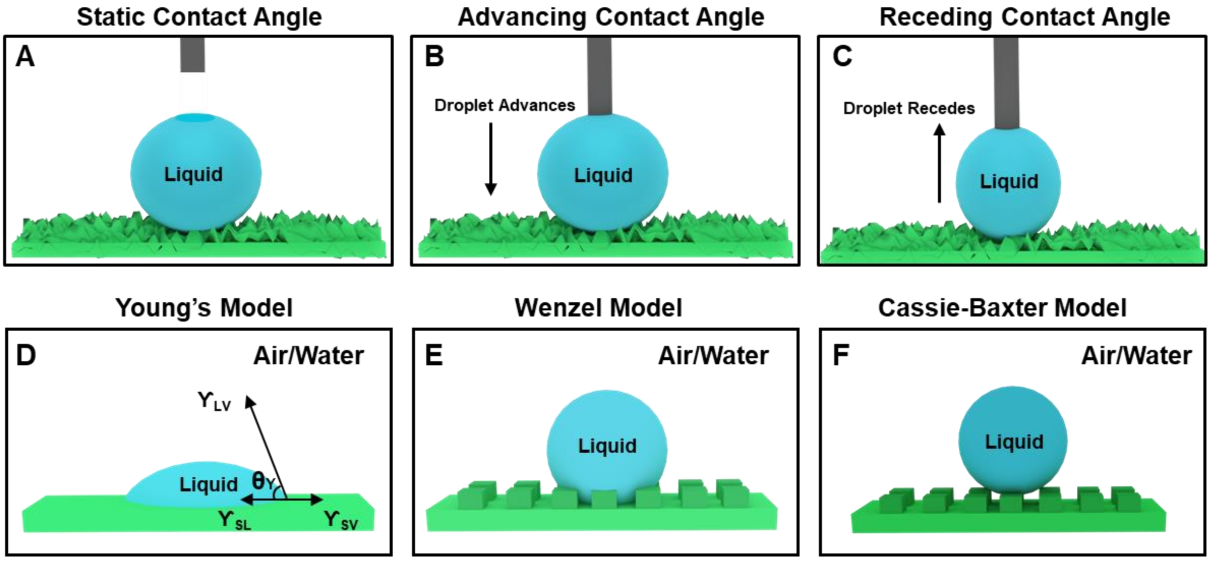

**Figure 1.3.** A-C) Schematic illustrating the static contact angle (A), advancing contact angle (B) and receding contact angle (C). D-F) Schematics depicting the different models of liquid wettability on a solid surface including Young's model (D), Wenzel model (E) and Cassie-Baxter model (F).

where, $\theta_w$ is the apparent contact angle in the Wenzel state, $\theta_Y$ is the Young's contact angle on a flat surface and r is the roughness factor = $\frac{Actual\ surface\ area}{Projected\ surface\ area}$

Thus, surfaces with static water contact angles less than 90º are known as hydrophilic surfaces while surfaces with static water contact angles greater than 90º are known as hydrophobic surfaces as shown in Figure 1.4B-C. According to the Wenzel model, the hydrophobicity of a surface can be further increased by enhancing the surface roughness, however in reality, for roughness values greater than 1.7, the cosine limits are not defined and thus, the Wenzel model fails.

In the underwater Wenzel state, the oil droplet fills the rough asperities of the solid substrate and the relationship between the oil contact angle and surface roughness can be expressed as follows,[9]

$$\cos\theta^*_{OW} = r\cos\theta_{OW}$$

where, $\theta^*_{ow}$ and $\theta_{ow}$ are the oil contact angles underwater on a rough and smooth surface respectively.

### 1.3.3. Cassie-Baxter Model of Liquid Wettability:

In 1944, Cassie-Baxter explained that on increasing the roughness factor beyond 1.7, the liquid droplet remained suspended atop the rough surface asperities, thus, forming a discontinuous line of contact with the solid surface as shown in Figure 1.3F.[7] The rough surface features were revealed to trap an external third phase i.e. a metastable layer of air that aided in minimizing the contact of the beaded liquid droplet with the solid surface. The sum of contributions from all the different phases account for the apparent contact angle as expressed below,

$$\cos\theta^{CB} = f_1\cos\theta_1 + f_2\cos\theta_2 \ldots\ldots\ldots\ldots\ldots\ldots\ldots\ldots(1)$$

where, $\theta^{CB}$ is the apparent contact angle, $f_1$, $f_2$ are the fraction of the solid-liquid, liquid-vapour surfaces in contact, respectively and $\theta_1$, $\theta_2$ are the contact angles of the solid-liquid, liquid-vapour phases. The contact angle of the liquid droplet with air, $\theta_2$ can be considered to be 180°. Moreover, if the solid fraction of a rough surface is $f$, the air fraction can be considered to be 1-$f$, thus equation 1 sums up as follows,

$$cos\theta^{CB} = f(1 + cos\theta) - 1$$

Where, $\theta^{CB}$ is the apparent contact angle and $f$ is the fraction of solid in contact with the beaded liquid phase.

In the underwater Cassie state, the trapped external third phase is a layer of water in between the rough surface asperities such that the oil droplet remains suspended atop the water trapped surface features with apparent contact angle expressed as follows,[9]

$$cos\theta_{CB}^{oil} = f_W cos\theta_{OW} + f_W - 1$$

where, $\theta_{Oil}^{CB}$ is the apparent oil contact angle and $f_W$ is the fraction of solid surface in contact with the oil droplet, underwater.

Thus, for surfaces with static contact angles greater than 150°, the fraction of contact between the solid surface and the beaded liquid droplet is minimum. Considering the theory of the models of liquid wettability, a superhydrophobic or underwater superoleophobic surface can be formally defined as a surface with both static and advancing liquid (water/oil) contact angles greater than 150° as shown in Figure 1.4D.[9-10] The difference between the advancing contact angle and receding contact angle is known as the contact angle hysteresis that accounts for the adhesive interaction between the beaded liquid droplet and the solid surface. Based on the contact angle hysteresis, surfaces with contact angle hysteresis value below 10° display lotus-leaf inspired non-adhesive superhydrophobicity, whereas surfaces with contact angle hysteresis above 10° display rose-petal inspired adhesive superhydrophobicity. The same definitions are applicable for underwater superoleophobicity.

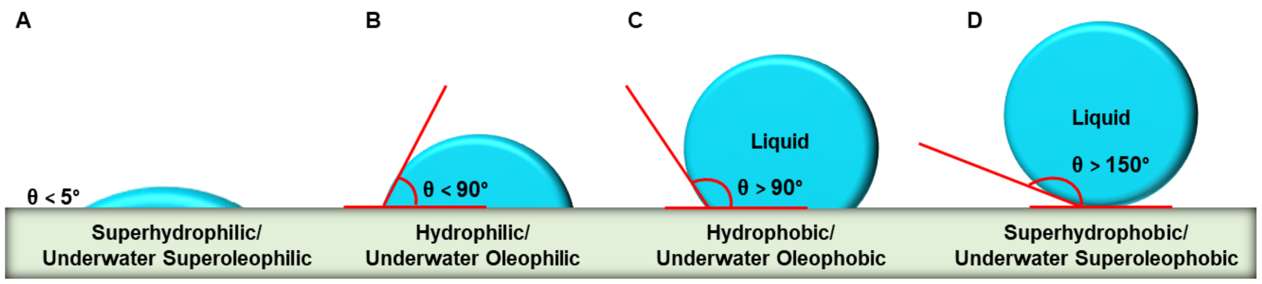

**Figure 1.4.** A-D) Schematic illustrating superhydrophilic (A), hydrophilic (B), hydrophobic (C) and superhydrophobic (D) surface.

## 1.4. Bio-Mimicked Anti-Wetting Interfaces: Assessing the Fundamental Requirements

The lotus-leaf with dual degree of surface roughness that exhibits non-adhesive superhydrophobicity with water contact angle ~161° and hysteresis ~2°, is a special case of the Cassie-Baxter heterogenous liquid wetting state.[22-23,38] It was experimentally proven that the presence of either micro or nano-structures individually created surfaces with large contact angle hysteresis.[23] In case of the micro-structures, the trapped external phase i.e. the metastable air layer is unstable, whereas the nano-structures itself are incapable of trapping enough metastable air that is required for displaying non-adhesive superhydrophobicity. Thus, only surfaces with both micro and nano features display the lotus-leaf inspired self-cleaning property as shown in Figure 1.5A-I.[10] The rose petal with water contact angle above 150º and contact angle hysteresis above 10º is an example of the transitional state between Wenzel and Cassie state.[24,38] The beaded water droplet impregnates only the microstructures of the rose petal (not the nano-folds) thus, creating surfaces with large hysteresis. Further, investigations on the lotus-leaf further revealed the presence of low surface energy coating i.e. a hydrophobic coating as the second essential parameter for exhibiting superhydrophobicity.[21-23] Thus, the presence of hierarchical topography and hydrophobic coating are the two essential parameters that need to be adapted for fabricating bio-mimicked non-adhesive superhydrophobicity.[10-19]

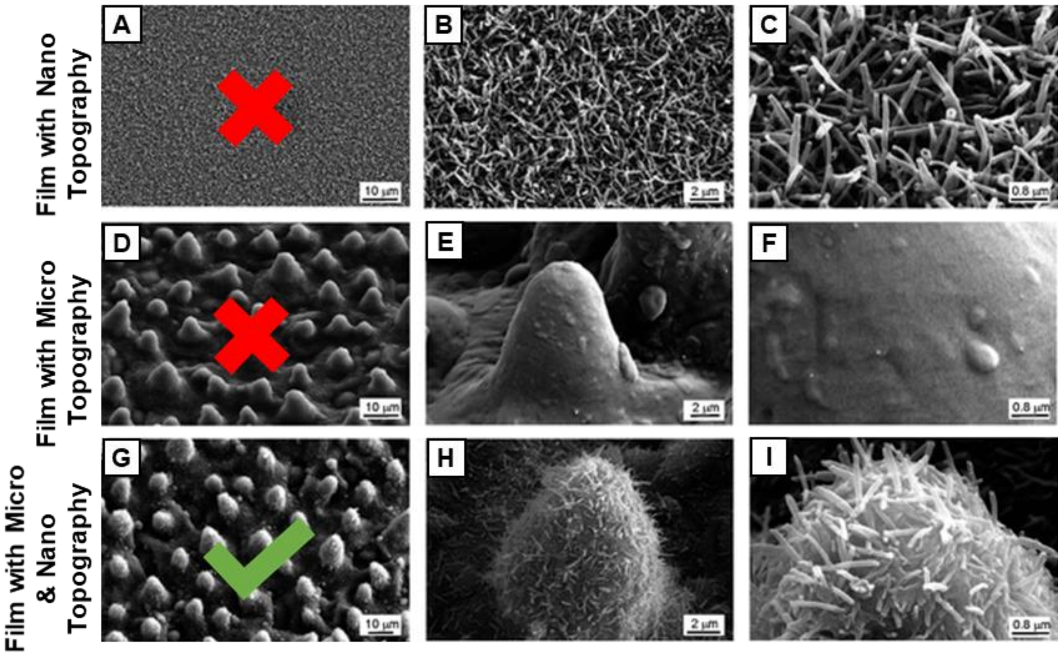

**Figure 1.5.** A-I) Scanning electron microscopy images of nano structures (A-C), micro-structures (D-F) and micro-nano structured G-I) surfaces developed using replicas of lotus leaf. Reprinted with permission from (*Soft Matter*, 2009, **5**, 1386-1393). Copyright 2009, The Royal Society of Chemistry.

Similarly, investigations on the underwater superoleophobic fish-scales (Figure 1.6A-B) revealed the essential presence of two vital parameters i.e., a) hierarchical topography (Figure 1.6C-F) and b)

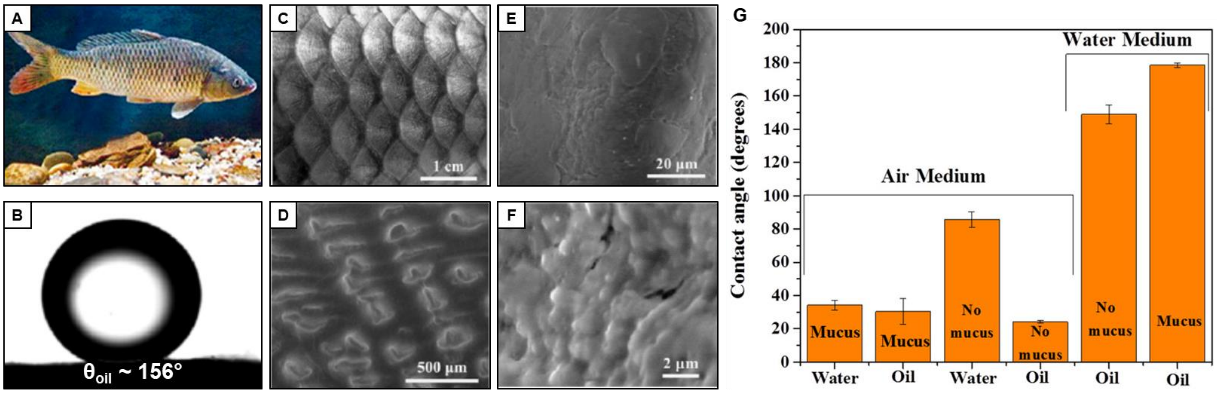

**Figure 1.6.** A-B) Underwater superoleophobic property of the fish-scales. C-F) Scanning electron microscopy images of the fish-scales. Reprinted with permission from (*Adv. Mater.*, 2009, **21**, 665-669). Copyright 2009, Wiley-VCH Verlag GmbH & Co. KGaA, Weinheim. G) Bar diagram illustrating the change in water and oil contact angles in 'air' and 'underwater' in the presence and absence of the mucus layer. Reprinted with permission from (*Sci. Rep.*, 2014, **4**, 7454-7459). Copyright 2014, Springer Nature.

hydrophilic surface coating (Figure 1.6G).[9,30] In an oil/water/solid system, a solid surface with micro/nano features aids in effectively trapping an external phase i.e. the impregnated water layer like the 'fish scales' forming a new composite interface that can extremely repel the oil phase . Further, to stabilize the trapped water layer in the hierarchal features, a high surface energy coating (hydrophilic) mimicking the mucus layer of fish scales is of utmost importance. Experimental evidences proved that the removal of the mucus layer altered the oil wettability of the fish-scales from underwater superoleophobicity (oil contact angle ~178°) to oleophobicity (oil contact angle ~148°) as shown in Figure 1.6G, thus, re-validating the need for the hydrophilic mucus layer to stabilize the trapped water layer for displaying extreme oil repellence.[39-40] Therefore, a combination of the aforementioned two criteria have been successfully deployed to fabricate bio-mimicked underwater superoleophobicity.

## 1.5. The Prospective Applications of Bio-Mimicked Anti-Wetting Interfaces

The main objective of mimicking the characteristic extremes of anti-wetting properties of the naturally existing species is for resolving the day-to-day problems afflicting mankind and the environment alike.[10-19] Over the years, the different types of superhydrophobic and underwater superoleophobic functional materials have been extended for widespread applications as shown in Figure 1.7.[9-19,30] A hydrophobic surface is incapable to clean the dust deposited on the surface as shown in Figure 1.8A. However, the hierarchically featured lotus-leaf, often considered as a symbol of purity has inspired the design of various superhydrophobic interfaces exhibiting the self-cleaning property similar to the lotus-leaf as shown in Figure 1.8B.[8,10-11] In 2020, Geyer *et al.* determined the removal of single particle contaminant from a silicone nanofilament coated, nano-porous superhydrophobic surface.[41] It was concluded that the presence of hydrophobic or hydrophilic contaminants doesn't affect the superhydrophobicity, however, the pore size of the superhydrophobic interfaces determines the

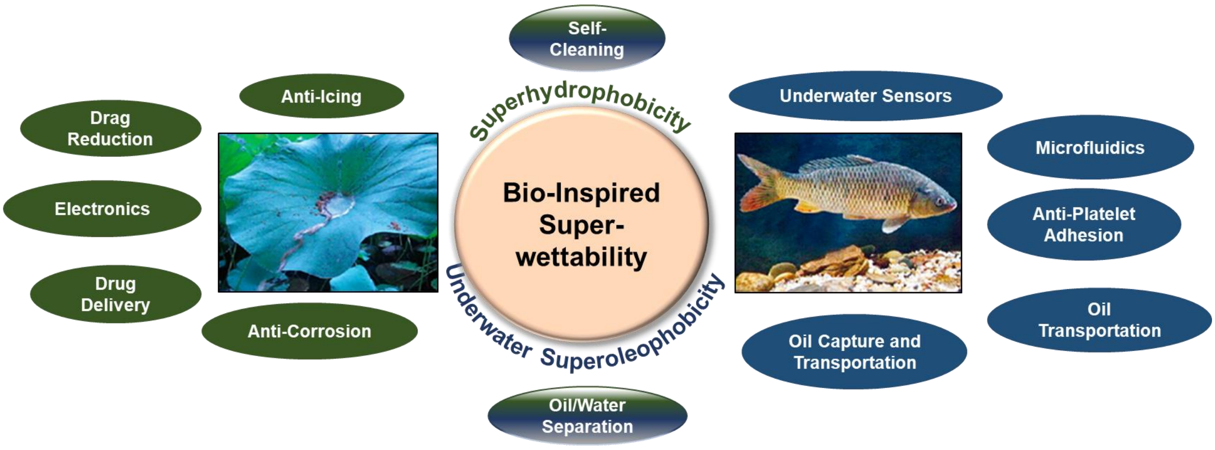

**Figure 1.7.** Schematic illustrating the various prospective applications of the superhydrophobic and underwater superoleophobic materials developed over the years following the mimicking of the characteristic water wettability of lotus-leaf and underwater oil repellence of fish-scales.

complete removal of the deposited contaminants from the solid interface. Superhydrophobicity also finds applications in sustained drug delivery,[42-44] water-proof textiles,[15,18,45] anti-icing interfaces,[46-47] anti-corrosion surfaces,[48-49] catalysis,[50] anti-bio-adhesion,[51-52] oil/water separation[10-19] etc. The association of superhydrophobicity with electrical devices increase the longevity and performance of such devices under aqueous exposure.[53] Wu *et al.* exploited branched poly(ethylenimine), silver nanoparticles and fluorinated decyl polyhedral oligomeric silsesquioxane to fabricate a colorful, self-healing superhydrophobic coating on a cotton fabric that exhibited anti-bacterial property.[45] The degradation of metals and its alloys on exposure to corrosive aqueous environments is another urgent issue that has been successfully tackled using various superhydrophobic interfaces.[48] Xiang *et al.* developed a porous Zn-Ni-Co coating on an underlying steel substrate followed by the modification with low surface energy molecule, myristic acid to obtain a superhydrophobic surface that displayed excellent anti-corrosion performance even after submersion in sodium chloride solution for 48 h.[49] The presence of the metastable air layer in the porous, superhydrophobic interface restricts the interaction between the corrosive liquids and the underlying metal-based solid interface.

Grinstaff *et al.* were the first to hypothesize that three-dimensional (3D) superhydrophobic materials entrap a robust air layer in comparison to a two-dimensional superhydrophobic material which results in the delayed impregnation of an aqueous phase into a 3D-superhydrophobic material as shown in Figure 1.8C.[54] This delayed infiltration of aqueous phase to displace the trapped air layer proved beneficial for prolonged drug release applications that holds potential utility in pain therapy and wound healing.[42] A 3D, porous, electrospun mesh of poly(Ɛ-caprolactone) and a hydrophobic dopant was developed which was pre-loaded with an anti-cancer drug molecule. The slow displacement of the metastable air layer from such 3D, porous meshes on exposure to phosphate buffer, generated a

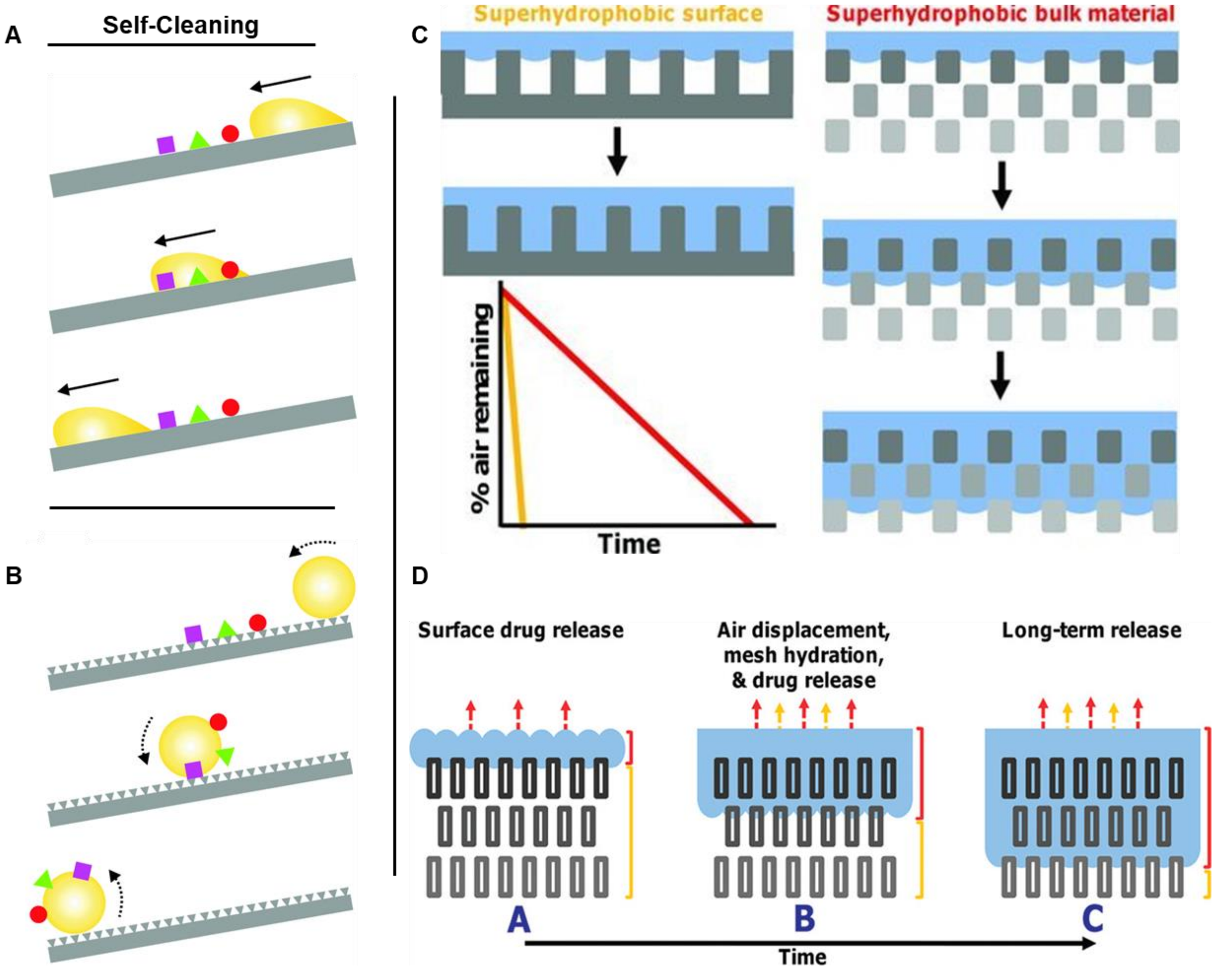

**Figure 1.8.** A-B) Schematic illustrating the sliding of a water droplet on a tilted hydrophobic surface that is incapable of cleaning the dust particles deposited on the surface (A), whereas a tilted superhydrophobic surface ensures the removal of the dust particles along with the rolling water droplet (B). Reprinted with permission from (*Chem. Soc. Rev.*, 2017, **46**, 4168-4217). Copyright 2017, The Royal Society of Chemistry. C) Schematic representing the rapid water wetting mechanism of a two-dimensional superhydrophobic interface and the delayed water wetting of a three-dimensional, bulk superhydrophobic material. Reprinted with permission from (*Adv Funct Mater.*, 2013, **23**, 3628-3637). Copyright 2013, Wiley-VCH Verlag GmbH & Co. KGaA, Weinheim. D) Schematic depicting the gradually water impregnation into a bulk superhydrophobic material that leads to the displacement of the metastable air layer and aids in the sustained release of the loaded drug molecules. Reprinted with permission from (*J. Am. Chem. Soc.*, 2012, **134**, 2016-2019). Copyright 2012, American Chemical Society.

sustained release profile over a period of 70 days as shown in Figure 1.8D. However, non-porous meshes that lacked the metastable air layer, released the entire loaded drug molecules in just 28 days. The vast practical utility of anti-wetting materials is not just limited to superhydrophobicity. Underwater superoleophobicity has been widely adopted for applications in anti-fouling of marine vessels,[9,55] underwater sensors,[56] oil droplet manipulation,[57-58] oil/water separation,[9,11,18], anti-platelet adhesion[59] etc. The underwater superoleophobic surfaces exhibit excellent self-cleaning property wherein, an oil contaminated surface on submerging underwater removes the oil phase owing to the rapid impregnation of a water layer into the hydrophilic, rough solid surface.[9,60] Pipe blockages due to

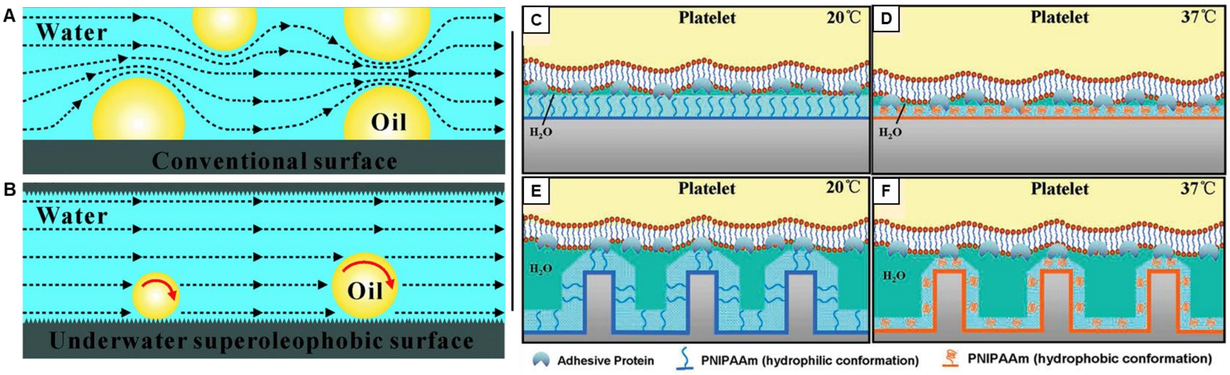

**Figure 1.9.** A) Schematic representing the flow of oil contaminated water through a conventional pipe. B) Schematic depicting the flow of oil contaminated water through a pipe coated with an underwater superoleophobic coating where, the black dotted arrows represent the water flow and the red arrow indicates the rolling of the oil droplet without pinning on the walls of the pipe. Reprinted with permission from (*Chem. Soc. Rev.*, 2017, **46**, 4168-4217). Copyright 2017, The Royal Society of Chemistry. C-F) Schematic representing the hydrated polymeric chains of a smooth PNIPAAm hydrogel restricting the platelet adhesion at low temperature (C). At higher temperature (D) the polymeric chains of a smooth PNIPAAm hydrogel crumble into a hydrophobic pocket and promotes platelet adhesion. However, a nanoscale structured PNIPAAm hydrogel the water entrapping ability of the hydrogel inhibits platelet adhesion at both low (E) and higher (F) temperatures. Reprinted with permission from (*J. Am. Chem. Soc.*, 2009, **131**, 10467-10472). Copyright 2009. American Chemical Society.

fouling by oil/oily phases present in a continuous water phase is a common problem around the globe (Figure 1.9A). The low oil adhesion of underwater superoleophobicity presents a facile way to prevent the pipe blockage in households and industries due to the discharge of oil contaminated water phase as shown in Figure 1.9B.[61]

The prolonged sustenance of the micro/nano structured, underwater superoleophobic interfaces (with a stable, trapped water layer) on aqueous exposure imparts its potential applicability in inhibiting platelet adhesion on the surface of medical implants to prevent thrombosis.[62-64] Chen *et al.* developed nanoscale topography on the surface of (poly(*N*-isopropylacrylamide), PNIPAAm) following the surface-initiated atom transfer radical polymerization of silicone nanowires, such that the nanoscale topography aided in trapping an increased water content by hydrophilic PNIPAAm generating underwater oil repellent interfaces that exhibited reduced platelet adhesion at temperatures both below and above the lower critical solution temperature of PNIPAAm as shown in Figure 1.9E-F.[59] However, the smooth, non-structured PNIPAAm surfaces with a reduced content of trapped water, exhibited anti-platelet adhesion property only at temperatures below the LCST as shown in Figure 1.9C-D. Self-repairable, underwater superoleophobic coating that displayed excellent protein anti-adhesion upto 30 days was developed by Chen *et al.* following the self-assembly of hydrophilic polymeric chains grafted onto silica nanoparticles to obtain hierarchical microgel spheres.[55] Thus, such self-healable, underwater superoleophobic surfaces with an ability to prevent the adhesion of proteins, bacteria, spores of micro-algae, diatoms etc, hold potential for remediating the marine vehicles and devices bio-fouling concerns. Later, various groups developed salt and harsh chemically contaminated aqueous conditions resistant underwater superoleophobic interfaces that holds potential for marine anti-biofouling applications.[35,65-66]

Furthermore, underwater superoleophobicity has also been extended for the no-loss transfer of oil droplets underwater that presents advanced applications for droplet derived micro-reactors, lab-on-chip devices thus, reducing the conventional operational costs and minimizing droplet loss due to pinning and wetting.[9,57-58]

Interestingly, the acute issue of oil spill remediation has been successfully tackled exploiting both superhydrophobicity and underwater superoleophobicity in different ways.[9-19] The progress of human civilization has led to an increase in the demand for energy, which in turn has escalated issues related to oil-spill incidents, industrial oily waste discharge affecting the industrial economy and environment.[67-69] The conventional ways of remediating oil spills from vast, open water bodies involve spraying chemical dispersants, *in-situ* burning, skimming etc, that suffers from the inherent drawbacks of generating secondary pollution, time and energy inefficient and cost-ineffective.[70-71] Moreover, these conventional methods lack selectivity towards a particular liquid phase that further limits its efficiency and recyclability. Bio-inspired super-wettability with extreme repellence towards either water or oil has received widespread attention over the years for its selectivity and efficiency in segregating the oil and water phases in an economic way without producing any additional secondary by-products.[9-19] In that context, bio-inspired superhydrophobicity with extreme repellence towards the

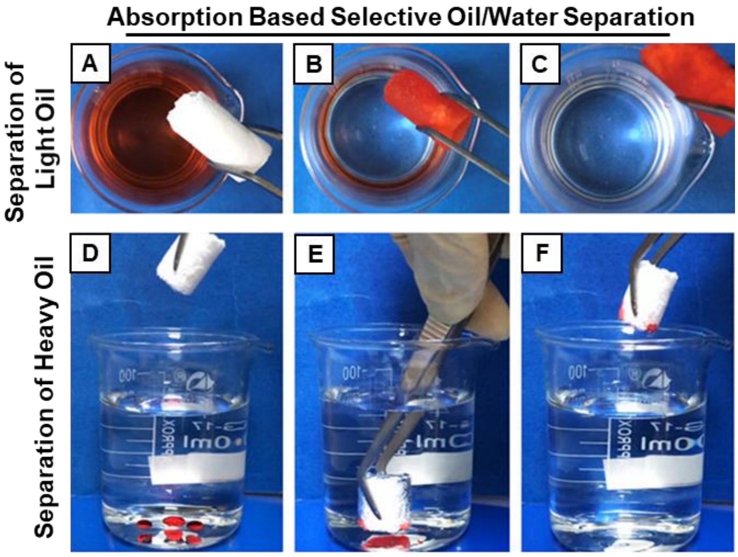

**Figure 1.10.** A-F) Digital images depicting the selective, absorption-based collection of both light (A-C) and heavy (D-F) oils from an oil/water interface using a poly(lactic) acid derived superhydrophobic foam. Reprinted with permission from (*ACS Appl. Mater. Interfaces*, 2019, **11**, 14362-14367). Copyright 2019, American Chemical Society.

water phase, exhibits an inherent affinity towards the oil phase.[72] Thus, superhydrophobic oil absorbents have been deployed over the years for the selective collection of both floating and heavy oil/oily phase from an oil/water interface as shown in Figure 1.10A-F.[10-19,72-76] Das *et al.* reported the absorption-based selective separation of both oil-in-water and water-in-oil emulsions using magnetically active, superhydrophobic graphene oxide powder.[77] Moreover, superhydrophobic membranes have also been fabricated for the selective filtration of both light and heavy oil phases from the respective oil/water mixtures as shown in Figure 1.11A-D and water-in-oil emulsion separation.[10-19,78-79] However, at conditions wherein the content of water phase in an oil/water mixture is higher, thus, demanding the selective filtration of only the water phase, underwater superoleophobicity plays an important role in this regard. At such scenarios, underwater superoleophobic membranes with extreme oil repellence property and an affinity for the water phase, allows the selective filtration of only the water phase while restricting the oil phase.[9-19,80-83] Such filtration-based separation of oil/water mixtures and oil-in-water emulsions can be performed even under harsh settings as shown in Figure 1.11E-H.[66]

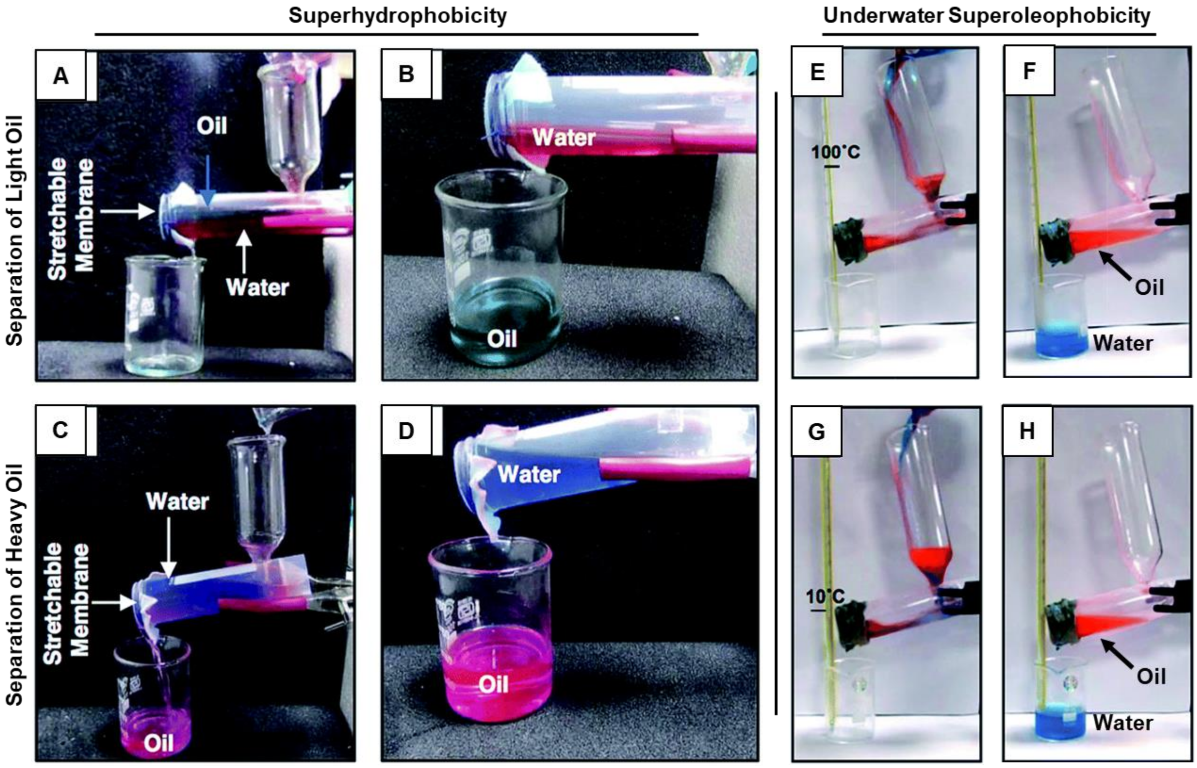

**Figure 1.11.** A-D) Digital images depicting the selective, gravity-driven filtration-based permeation of the oil phase from both light (A-B) and heavy (C-D) oil/water mixtures through a superhydrophobic membrane. Reprinted with permission from (*J. Mater. Chem. A*, 2017, **5**, 15208-15216). Copyright 2017, The Royal Society of Chemistry. E-H) Digital images depicting the selective, gravity-driven filtration-based permeation of the water phase from oil/water mixtures through an underwater superoleophobic membrane wherein the high (100°C, E-F) and low (10°C, G-H) temperature aqueous phases were taken for the demonstration. Reprinted with permission from (*J. Mater. Chem. A*, 2018, **6**, 22027-22036). Copyright 2018, The Royal Society of Chemistry.

## 1.6. Components and Chemistries Integrated to Develop Bio-Mimicked Anti-Wetting Interfaces

In the previous section, an elaboration about the various prospective applications of bio-inspired liquid wettability was provided, that pressed the urgent necessity for the development of bio-mimicked anti-wetting functional material. In the following sections, a detailed discussion on the various synthetic and naturally derived chemical components-based bio-mimicked anti-wetting interfaces are outlined. However, the basic challenges faced by the existing reports makes them less appropriate for practical applicability and tackling these shortcomings using facile fabrication approaches and chemical avenues is the motive of this thesis.

### 1.6.1. Synthetic Chemical Constituents Derived Bio-Mimicked Wettability

The construction of the various bio-inspired anti-wetting interfaces have generally adapted three routes, a) building the rough topography followed by appropriate surface chemical modification,[84-85] b) selection of appropriately chemically modified surface followed by construction of the adequate topography[86] or c) *in-situ* development of both topography and chemistry.[42,54,66] The appropriate topography and chemistry of bio-inspired interfaces have been developed following majorly the top-down and bottom up approaches.[10] Top-down approach involves the carving, moulding or machining into the bulk of a material to design the pre-defined topographical patterns or arrangement that aid in trapping the external third phase for conferring bio-inspired wettability.[87] Such approaches involve templation,[88-89] lithography,[90-91] plasma etching,[92-93] etc. Bottom up approaches involve the physical or covalent assembly of the basic building blocks to generate larger, macroscopic materials consisting of a porous, rough topography and desired chemistry that is appropriate for imparting bio-inspired wettability.[10] Such approaches involve sol-gel,[66,85,94] layer-by-layer assembly,[95-97] chemical vapour deposition,[98-99] electrospinning[100-101] etc.

Over the years, the topography and chemistry of lotus-leaf inspired artificial superhydrophobic interfaces have been developed using various synthetic components such as carbon materials (carbon nanotubes, carbon nanofibers, soot particles, graphene derivatives, Mxenes),[102-103] polymers (such as polydimethylsiloxane, polystyrene, polyacrylonitrile,),[42,46,48,54,104] organo-silicones (fluoroalkylsilane, octadecyltrichlorosilane),[15,45,85] metal oxides (zinc oxide, copper oxide),[46,49,84,] organic monomers (such as long chain thiols, hydrophobic amines) etc.[12,18,43,45,49] The deposition of carbon nanotubes,[105-106] soot particles[107-108] , polymeric nanoparticles[66] or the metal oxides nanoparticles[46,49,84] generate the required rough surface topography and the subsequent post modification with low surface energy molecules such as fluoro/alkyl silanes,[15,45,85] long chain amines/thiols[43,45,49] or hydrophobic polymers such as polydimethylsiloxane,[48,54,104] imparts the essential low surface energy coating to exhibit superhydrophobicity.[12,18]

Metal-thiol bonding (Figure 1.12A),[84,109] metal-ion interaction,[110-111] hydrogen bonding (Figure 1.12B),[112] electrostatic interactions (Figure 1.12C),[96-97] silane chemistry (Figure 1.12E),[85,113] etc are the dominant chemistries utilized for fabricating conventional superhydrophobic interfaces. However, the susceptibility of electrostatic multilayers, metal-ion interactions, brittle metal oxides etc to physical abrasions and prolonged exposure to chemically contaminated aqueous phases limits the practical

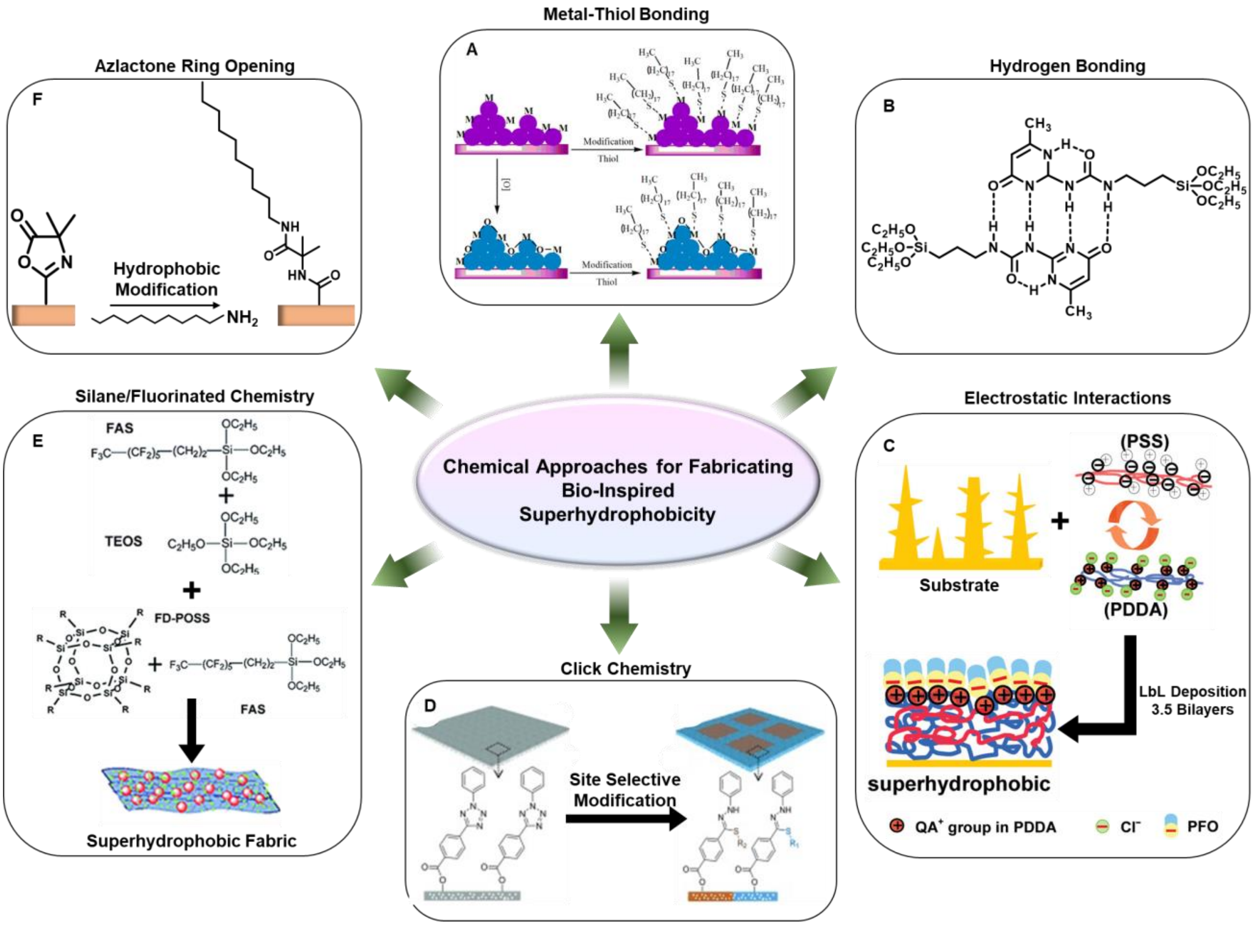

**Figure 1.12.** A) Schematic illustrating the fabrication of superhydrophobic fabric following the *in-situ* growth of transition-metal/metal oxide nanoparticles followed by post modification with thiols. Reprinted with permission from (*ACS Appl. Mater. Interfaces*, 2013, **5**, 1827-1839). Copyright 2013, American Chemical Society. B) Schematic depicting the development of a superhydrophobic surface following the quadruple hydrogen bonding of an organo-silane. Reprinted with permission from (*J. Am. Chem. Soc.*, 2004, **126**, 4796-4797). Copyright 2004, American Chemical Society. C) Schematic depicting the development of superhydrophobic multilayer coating following the layer-by-layer assembly of oppositely charged polyelectrolytes. Reprinted with permission from (*Langmuir*, 2010, **26**, 12203-12208). Copyright 2010, American Chemical Society. D) Schematic depicting the UV-assisted click chemistry for developing superhydrophobic-superhydrophilic patterned surface following the tetrazole ring opening reaction with thiols. Reprinted with permission from (*Angew. Chem. Int. Ed.*, 2015, **54**, 8732-8735). Copyright 2015, Wiley-VCH Verlag GmbH & Co. KGaA, Weinheim. E) Depiction of the fabrication of superhydrophobic fabric following silanization and post modification with fluorine chemistry. Reprinted with permission from (*ACS Appl. Mater. Interfaces*, 2013, **5**, 10221-10226). Copyright 2013, American Chemical Society. F) Schematic depicting the azlactone ring opening chemistry following the post modification with a hydrophobic alkylamine (decylamine) to obtain bio-inspired superhydrophobicity. Reprinted with permission from (*Adv. Mater.*, 2012, **16**, 4291-4295). Copyright 2012, Wiley-VCH Verlag GmbH & Co. KGaA, Weinheim.

utility of the earlier conventional superhydrophobic interfaces.[110-112] On exposure to harsh physical abrasions, the low surface energy coating on the top of the interface is easily eroded that exposes the underlying hydrophilic building blocks (such as metal oxides), thus, compromising the superhydrophobicity as shown in Figure 1.13A.[114] To tackle the durability concerns, post-repairing[115-116] and self-healing approaches[117-118] were introduced that involved the stimuli-assisted regeneration

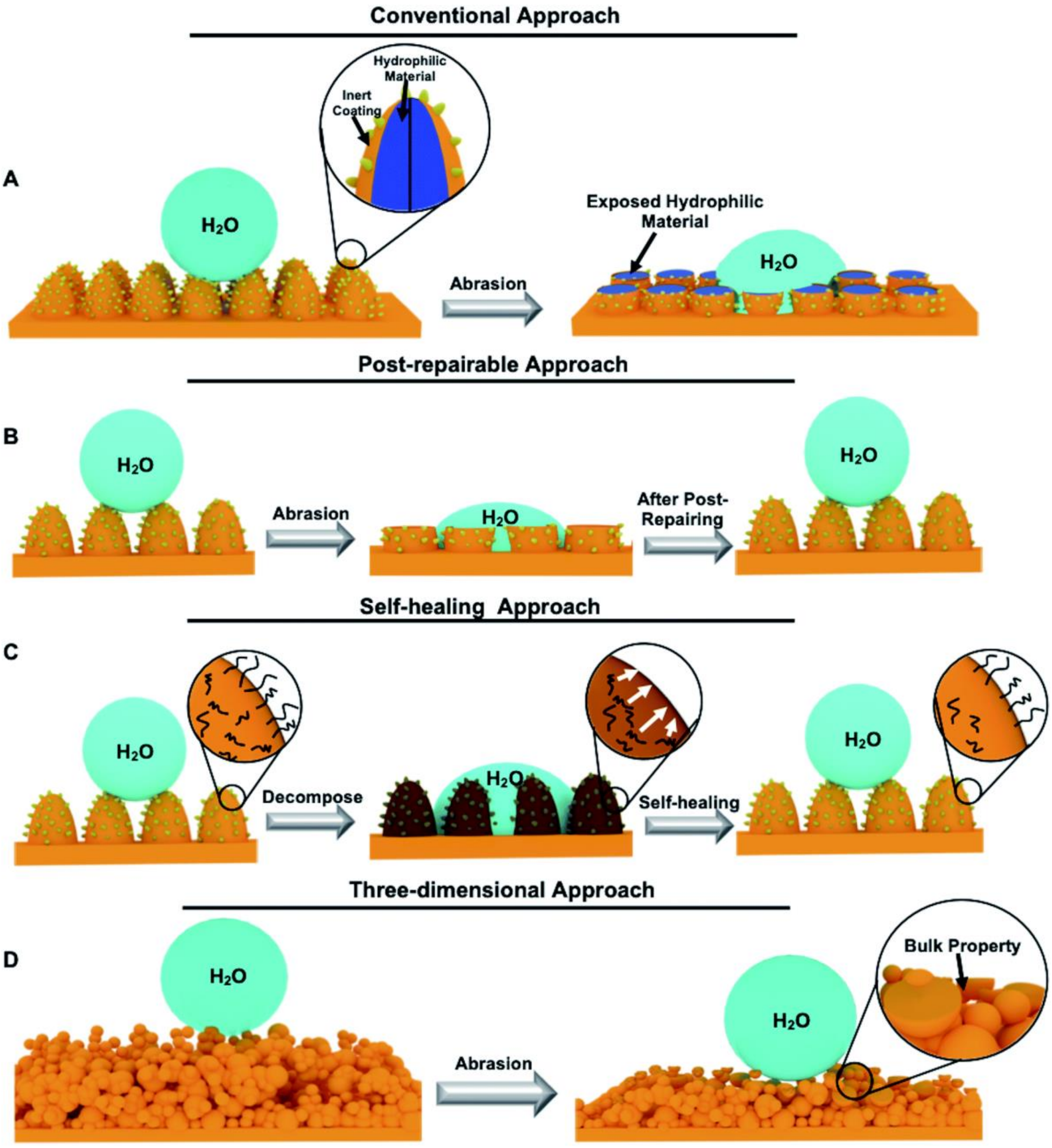

**Figure 1.13.** A) Schematic representing the conventional superhydrophobic surfaces that compromise the inert low surface energy coating on top during harsh physical abrasions, thus, exposing the hydrophilic building blocks and eventually compromising the embedded water-repellent property. B-C) Schematic illustrating the regeneration of topography through post repairing approach (B) and chemistry following self-healing pathway (C) to restore the compromised superhydrophobicity. D) Schematic illustrating the bulk superhydrophobicity wherein the topography and chemistry is co-optimised throughout the material i.e. three-dimensionally. Reprinted with permission from (*J. Mater. Chem. A*, 2021, **9**, 824-856). Copyright 2021, The Royal Society of Chemistry.

of the topography and chemistry at the site of damage as shown in Figure 1.13B-C. However, such stimuli-assisted regeneration restricts the scalability due to cost-ineffectiveness, need for external intervention and limited regeneration cycles.

Levkin *et al.* introduced the concept of three-dimensional or bulk superhydrophobicity that ensures the uniform co-optimization of the topography and chemistry throughout the material, thus, providing an abrasion-tolerant functional superhydrophobic material as shown in Figure 1.13D.[119] Subsequently, a few robust covalent chemistries were introduced that generated highly physically and chemically durable superhydrophobic materials for various practical applications.[120-125] In 2020, Wang *et al.* designed armoured microstructures that consisted of fragile nanostructures which collectively generated highly mechanical and physical abrasion tolerant superhydrophobicity.[126] However, such complex and expensive design processes would be less appropriate for practical applications. Table 1.1 summarizes a few superhydrophobic interfaces that were fabricated using different types of

**Table 1.1** Illustrating the various superhydrophobic functional materials developed using synthetic, chemically hazardous building blocks following different chemical pathways.

| Synthetic Chemical Components | Associated Chemistry | Eco-Friendly | Physical/Chemical Durability | Reference |
|---|---|---|---|---|
| Copper oxide-Stearic acid | Metal-Ion interactions | No | Not Performed | 110 |
| Supramolecular organosilane | Hydrogen bonding | No | Not Performed | 113 |
| Poly(butylmethyacrylate-co-ethylene dimethacrylate) | UV-initiated radical polymerization | No | Adhesive tape peeling test, outdoor exposure for 8 weeks, repels aqueous droplets of NaOH and HCl | 119 |
| Polyvinylidene fluoride | Phase inversion induced dehydrofluorination | No | Scratch test, thermal stability upto 150°C for 12 h, exposure to temperature range -25°C to 40°C and relative humidity 10-80% | 120 |
| Fluoropolymer/silica nanoparticles deposited on poly(diallyldimethylammonium chloride) surface | Electrostatic interactions | No | Not Performed | 121 |
| Copper Foam-N-dodecyl mercaptan | Metal-Thiol Bonding | No | Sand paper abrasion for 50 cycles, immersion in NaCl solution for 30 mins | 122 |
| Fluorinated epoxy resin, perfluoropolyether, perfluoropolymeric nanoparticles | Amidation, Epoxy ring opening | No | Cyclic tape test for 30 cycles, taber abrasion for 100 cycles, exposure to aqua regia for 60 mins and NaOH for 12 h | 123 |
| Surface modified silica nanoparticles-polyurethane nanoparticles | Hydrolysis, Condensation | No | UV irradiation for 9 days, immersion in non-polar and polar aprotic solvent for 20 days | 124 |
| Methyl-substituted Graphdiyne | Glaser-Hay Coupling reaction | No | Mechanical abrasion for 30 cycles, immersion in pH 5 and 9 for 800 days | 125 |
| Carboxyl ended polyester, triglycidyl isocyanurate, polytetrafluoroethylene | Epoxy ring opening, Electrostatic interactions | No | Sand paper abrasion for 100 cycles, tape peeling test for 100 cycles, immersion in pH 1 and 13 for 12 h, UV irradiation for 84 h | 126 |

synthetic building blocks following different chemical approaches and the details of the durability of these reported interfaces are also enlisted.

Similarly, fish-scale inspired underwater superoleophobic interfaces have been developed exploiting hydrogels,[55,59,128-130] electrostatic multilayers[9,65,131] and metal oxides.[32,57-58,132,133] Hydrogels have the tendency to entrap a large amount of aqueous phase that inclines with the hydrophilic mucus layer of fish-scales which aids in extremely repelling the oil phase underwater. Covalently cross-linked hydrogels of polyacrylamide,[59,82] polyvinyl alcohol (Figure 1.14A),[134] composite hydrogels[135] etc have been explored in the past for developing underwater superoleophobicity.[9,12,15,18] The electrostatic assembly of oppositely charged, hydrophilic polymers, metal oxides etc are other reported approaches for fabricating underwater superoleophobic interfaces that allows to have precise control over the

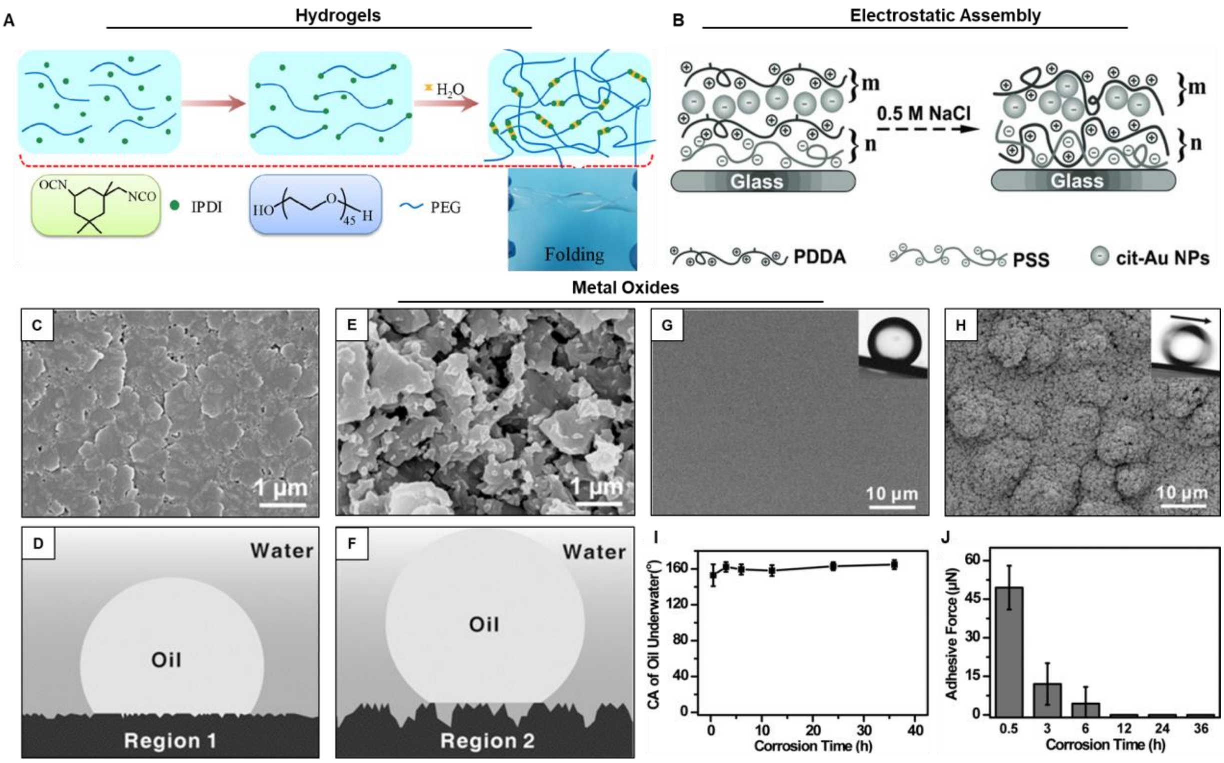

**Figure 1.14.** A) Schematic illustrating the cross-linking of diisocyanate with polyvinyl alcohol to obtain a polyurethane hydrogel. Reprinted with permission from (*ACS Appl. Mater. Interfaces*, 2020, **12**, 56530-56540). Copyright 2020, American Chemical Society. B) Schematic illustrating the ion-induced electrostatic assembly of polyelectrolytes to generate underwater superoleophobicity. Reprinted with permission from (*Adv. Mater.*, 2013, **25**, 606-611). Copyright 2013, Wiley-VCH Verlag GmbH & Co. KGaA, Weinheim. C-F) Scanning electron microscopic images of the outer (C) and inner (E) portion of clam's shell that exhibits oleophobicity (D) and underwater superoleophobicity (F) respectively. G-H) Scanning electron microscopic images of a smooth copper oxide film (G) and micro/nano featured copper oxide film (H) that exhibits oleophobicity and non-adhesive underwater superoleophobicity respectively. I-J) Graph depicting the variation in underwater oil contact angle (I) and adhesive force (J) with the change in corrosion time of the cooper sheets. Reprinted with permission from (*Adv. Mater.*, 2012, **24**, 3401-3405). Copyright 2012, Wiley-VCH Verlag GmbH & Co. KGaA, Weinheim.

thickness of the coating.[9,65,131] Xu *et al.* developed NaCl-induced, underwater superoleophobic multilayer coating following the layer-by-layer assembly of poly(diallyldimethyl-ammonium chloride), poly(styrenesulfonic acid) and Au nanoparticles as shown in Figure 1.14B.[65] The NaCl induced structural changes in the multilayer coating enhanced the underwater oil wettability. Liu *et al.* reported the distinct underwater oil wettability of the inner and outer regions Clam's shell.[133] The outer portion of the clam shell exhibited oleophobicity (Figure 1.14C-D) whereas the inner potion exhibited underwater superoleophobicity (Figure 1.14E-F) which was attributed to the presence of high surface energy building block of inorganic, calcium carbonate that imparted the hierarchical topography and hydrophilic surface coating. Inspired from the clam's shell, hydrophilic metal oxides have been widely explored in the past for building the hierarchal surface topography for displaying underwater oil repellence. [32,57-58,132,133] For instance, chemical etching of copper sheets generated hydrophilic, copper oxide films with micro-sized cauliflower structures topped with nano-meter branches exhibited non-adhesive underwater superoleophobicity as shown in Figure 1.14H.[133] The duration of corrosion time altered the underwater oil wettability and oil adhesion as shown in Figure 1.14I-J, from oleophobicity, adhesive underwater superoleophobicity to non-adhesive underwater superoleophobicity (Figure 1.14H), where smooth copper oxide films exhibited only underwater oleophobicity (Figure 1.14G). However, hydrogels are well-known to be fragile on swelling underwater and thus, hydrogel derived coatings are prone to fracture under applied mechanical stress and physical abrasions. Moreover, brittle metal oxides and electrostatic multilayers are susceptible to disintegration under prolonged exposure to chemically contaminated aqueous phases including extremes of pH, salt and surfactant contaminated water.

Recently, a few bio-inspired robust approaches reported the fabrication of mechanically tough, abrasion resistant, sea-water tolerant underwater superoleophobicity.[35,136] The strategic uses of covalent chemistries provided a basis for developing highly abrasion-tolerant, prolonged aqueous exposure tolerant underwater superoleophobicity.[66,137] However, the fabrication process of such approaches is tedious for practical applications. Table 1.2 summarizes the various types of underwater superoleophobic interfaces that were fabricated using different types of synthetic building blocks following different chemical approaches and durability of these interfaces are also accounted in the table. The vast applications of bio-inspired wettability have triggered its rapid advancement over the years. Even though, robust superhydrophobic and underwater superoleophobic coatings as well as bulk materials have been developed over the years following different chemical approaches, the major concern regarding the bio-degradability and toxicity of the basic chemical constituents hinders the industrial scalability owing to the health and environmental hazards.[143-144] Industrialization and

**Table 1.2** Illustrating the various underwater superoleophobic functional materials developed using synthetic, chemically hazardous building blocks following different chemical pathways.

| Synthetic Chemical Components | Associated Chemistry | Eco-Friendly | Physical/Chemical Durability | Reference |
|---|---|---|---|---|
| Poly(diallyldimethylammonium chloride)-poly(4-styrenesulfonic acid)-Ag nanoparticles | Electrostatic interactions | No | Immersion in artificial sea-water for 10 days | 65 |
| Poly(acrylamide) hydrogel | Photo-initiated polymerization | No | Not Performed | 82 |
| Pentaerythritol tetrakis (3-mercaptopropionate)-diethylene glycol diglycidyl ether hydrogel coated on alkali modified poly(vinylidene fluoride) membrane | Thiol-epoxy<br>Thiol-Ene | No | Soxhlet Extraction for 24 h to examine the stability of the hydrogel coating | 128 |
| Sodium polyacrylate grafted poly(vinylidene fluoride) poly-ionized hydrogel | Alkaline-induced phase inversion | No | Not Performed | 129 |
| Polyurethane hydrogel | Polycondensation | No | Silica abrasion and resistant to different pH contaminated aqueous phases | 130 |
| Polyacrylic acid-polyvinylidene fluoride-graphene nanosheet | Physical interaction | No | Immersion in artificial sea-water and extremes of pH for 30 days | 136 |
| Poly(ethyleneimine), poly(vinyl-4,4-dimethylazlactone) | Azlactone Ring Opening | No | Sand paper abrasion, sand drop test, tape test, boiling for 1 h, freezing/thawing for 10 cycles, immersion in pH conditions for 30 mins, surfactant contaminated water for 45 days and salt-contaminated water for 120 days | 137 |
| Polystyrene-Au nanoparticles/ carbon nanotubes membrane | Physical interaction | No | Not Performed | 138 |
| Graphite-polyurethane foam | Physical interaction | No | Emulsion separation after 25 cycles of abrasion and at different pH conditions | 139 |
| Graphene oxide-calcium carbonate | Physical interaction | No | Sand drop test, immersion in extremes of pH for 1 day and salt water for 10 days | 140 |
| Polyacrylonitrile grafted with poly(sulfobetaine methacrylate) brushes | Surface initiated atom transfer radical polymerization | No | Not Performed | 141 |
| Styrene-acrylate co-polymer filtration membrane | Hydrolysis assisted conversion of styrene-acrylonitrile co-polymer | No | Not Performed | 142 |

economic growth at the cost of the environment is not a desirable policy for a sustainable economy. Thus, in this context, the shift towards the substitution of synthetic components with naturally occurring, abundant, low-cost and eco-friendly alternatives for the development of bio-inspired anti-wetting interfaces has recently been explored.

### 1.6.2. Natural Derived Bio-Mimicked Wettability: Progress and Drawbacks

Well-known naturally derived, abundant, cheap and environment-friendly components such as cellulose, chitosan, nano-clay, phytic acid, phenolic acid, poly(lactic) acid etc, have been explored over in the recent years for the development of various bio-mimicked anti-wetting materials.[17,111,145-155]

Natural components are processed strategically to impart the essential rough surface topography followed by the chemical modification with low surface energy molecules to impart superhydrophobicity. [17,111,145-155] Table 1.3 summarizes a few superhydrophobic interfaces that were fabricated using different types of naturally derived components following different chemical approaches and the details of their durability examination are also provided.

Cellulose and its derivatives, abundantly found in nature, are the most explored natural components for achieving superhydrophobicity.[17,148-149,156-158] Badiya *et al.* spray deposited fluoroalkyl silane modified cellulose nanofibers on a commercial filter paper to generate a water-proof paper substrate, where the cellulose nanofibers provided the topography and the fluoroalkyl modification imparted the low surface energy as shown in Figure 1.15A-D.[158] The resultant superhydrophobic paper with water contact angle ~160°, exhibited self-cleaning property with tolerance towards physical abrasions such as knife scratch test, tape adhesion, finger wiping for 100 cycles, high temperature (200°C), low temperature (-80°C), direct sunlight and inertness towards organic solvent. Phytic acid, a naturally occurring, non-toxic component found in legumes, cereals, oil seeds etc, consists of six phosphate groups that bind the toxic minerals in the human body and help in excretion.[159] Zhou *et al*. explored

**Table 1.3** Illustrating the various superhydrophobic functional materials developed using naturally derived building blocks following different chemical pathways.

| Synthetic Chemical Components | Associated Chemistry | Physical/Chemical Durability | Reference |
|---|---|---|---|
| Phytic acid coordinated metal ions followed by polydimethylsiloxane post modification | Metal-ion interaction | Sand paper abrasion for 30 cycles, adhesive tape peeling for 300 cycles, UV irradiation for 24 h, heat treatment 2 h, immersion in organic solvent for 7 days | 111 |
| Wood modified with Vinyltrimethoxysilane followed by alkyl thiol post modification | Silanization, Thiol-Ene reaction | Water jet test, Scratch test, Scotch tape test | 145 |
| Hydroxyapatite and ketjen black paper modified with polydimethylsiloxane | Physical interactions | Repelled beaded aqueous droplets with pH 1-14, resistant to 50-90% relative humidity, thermal stability upto 300°C | 146 |
| Alkene substituted Resorcinarenes post modified with fluorothiol | Thiol-Ene reaction | Not Performed | 147 |
| Polydopamine modified nano-fibrillated cellulose post modified with octadecylamine | Self-Polymerization, Schiff-base reaction | Not Performed | 148 |
| Cellulose nanofibrils modified with polysiloxanes | TEMPO oxidation, condensation | Not Performed | 149 |
| Wood-Epoxy Composite | Physical interactions | Not Performed | 150 |
| Sepiolite powder modified with octadecyltrimethylammonium bromide and octadecyltrichlorosilane | Hydrolysis, Condensation | Immersion in pH 1,7,14 and sodium chloride solution for 24 h | 151 |
| Poly(lactic acid) foam | Physical interactions | Not Performed | 152 |
| Hexadecyltrimethoxysilane modified halloysite nanotubes | Hydrolysis, Condensation | Not Performed | 153 |
| DNA-Ag-Octadecyltriethoxysilane coated cotton fabric | Electrostatic interactions, polycondensation | Repelled beaded aqueous droplets with pH 1-14, detergent washing for 4 cycles | 154 |
| Silica nanoparticles coated Chitin nanoaerogel modified with trichlorooctadecyl silane | Hydrolysis, Condensation | Not Performed | 155 |

phytic acid as ligand to bind to metal ions ($Ag^{I}$, $Fe^{III}$, $Ce^{III}$, $Zr^{IV}$, $Sn^{IV}$) to produce the hierarchical topography on a wide range of substrates followed by post modification with polydimethylsiloxane (PDMS) to impart the low surface energy as shown in Figure 1.15E.[111] The superhydrophobic Phytic acid-$Fe^{III}$- polydimethylsiloxane coated fabric with water contact angle ~151°, retained the embedded water wettability even after 30 cycles of sand paper abrasion and adhesive tape peeling, UV irradiation for 24 h, heat treatment 2 h, immersion in organic solvents for 7 days. Thus, such a durable interface was extended for oil/water remediation. DNA was exploited as bio-viable flame retardant to develop a superhydrophobic, flame-retardant coating on cotton fabric.[154] The deposition of electrostatically bound silver nanoparticles-deoxyribonucleic acid on cotton fabric provided the essential surface topography whereas the further modification with octadecyltriethoxysilane following the polycondensation of silane provided the low surface energy framework. The resultant superhydrophobic fabric with water contact angle ~157° repelled the chemically contaminated, beaded aqueous droplets of pH 1-14 and retained the embedded water repellence property even after detergent washing for 4 cycles. Bio-degradable polylactic acid was exploited by Wang *et al.* to obtain lightweight, porous, superhydrophobic foams for selective and repetitive oil/water remediation.[152] The non-solvent induced phase separation approach introduced porosity into the foams while the subsequent skin peeling with an adhesive tape produced rough features on the surface of the foam. The as-obtained superhydrophobic foam repelled the beaded water droplet with water contact angle ~151°, however, the durability of the embedded water repellence property was not examined.

However, there exists major issues with the reported natural ingredients derived superhydrophobic interfaces. The use of fluorinated molecules for post modification to achieve durable superhydrophobicity limits its scalability due to the associated environmental hazards.[158,160] The metal-ion interactions,[111] electrostatic interactions[154] derived superhydrophobicity was demonstrated to retain the water repellence behaviour even after performing harsh physical abrasions and exposure to UV, organic solvents, however, the durability of such interfaces on prolonged exposure to chemically contaminated aqueous phases were not demonstrated. The prolonged durability of any superhydrophobic interface in harsh aqueous phases is of utmost importance since such severe settings are bound to be present at practical settings.

A few covalent chemistries such as Schiff base reaction (Figure 1.16A),[148] click-chemistry,[145,147] condensation reactions (Figure 1.16B)[151,153-155] were also associated to develop natural components derived superhydrophobic materials, but, the physical or chemical durability examination of these materials were not examined in the earlier reported studies. Importantly, there exists a dearth of reports in literature providing a facile, catalyst-free chemical pathway for tailoring the embedded water

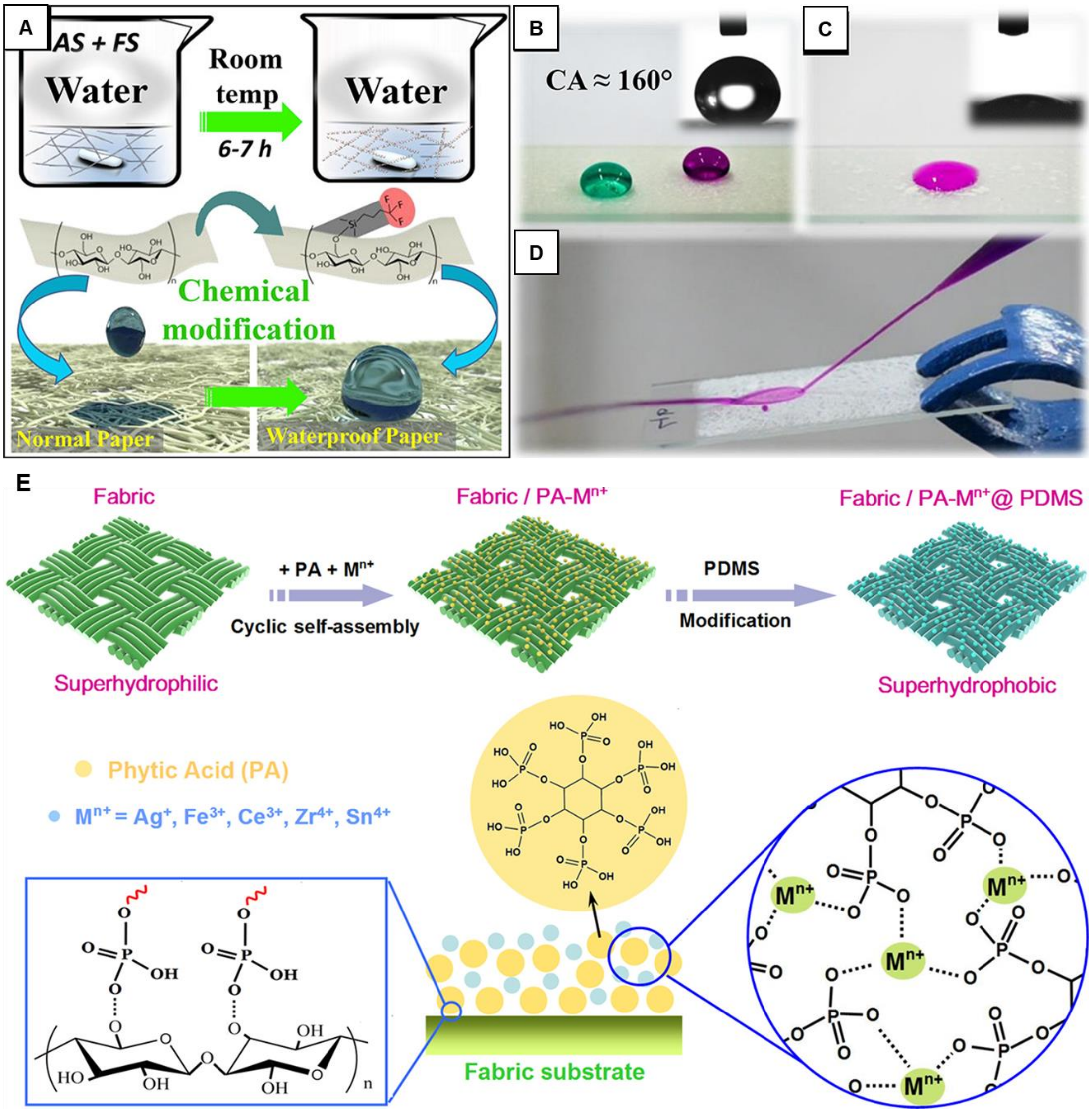

**Figure 1.15.** A) Schematic representing the silanization of cellulose nanofibers with an amine containing silane and a fluoro-silane followed by spray coating of the modified cellulose nanofibers on a filter paper to obtain a water-proof paper. B-C) Water wettability on the modified (B) and unmodified cellulose nanofibers coated filter paper (C). D) Digital image showing the bouncing of a water jet from the surface of the water proof-paper. Reprinted with permission from (*ACS Nano*, 2017, **11**, 11091-11099). Copyright 2017, American Chemical Society. E) Schematic representing the phytic acid coordinated metal ion complexes deposited on a fabric to obtain the essential topography followed by post modification with polydimethylsiloxane to obtain a superhydrophobic fabric. Reprinted with permission from (*ACS Appl. Mater. Interfaces*, 2017, **9**, 9184-9194). Copyright 2017, American Chemical Society.

wettability or other associated physical properties of the materials. Such an avenue to tailor the water wettability is useful for sustained drug delivery applications[42] and the integration of bio-viable natural components would prove useful for real-life applicability. In a rare demonstration, Behboodi *et al.* reported the dip coating of alkene substituted resorcinarene (plant derived phenolic compound) coatings on a wide range of substrates via hydrogen bonding, electrostatic interactions to provide the essential surface topography as shown in Figure 1.17A-B.[147] The UV-initiated thiol-ene reaction of the residual alkene groups with alkyl-thiol (perfluorodecanethiol) and hydrophilic thiol (2-hydroxy-1-

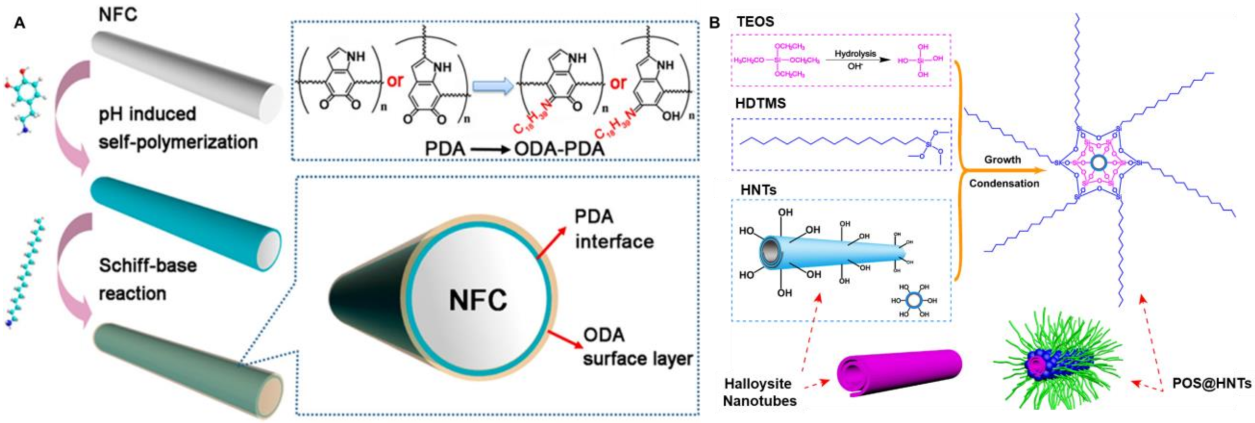

**Figure 1.16.** A) The self-polymerization of dopamine on nano-fibrillated cellulose followed by post modification with octadecylamine adopting Schiff base chemistry to obtain a superhydrophobic aerogel. Reprinted with permission from (*ACS Sustainable Chem. Eng.*, 2018, **6**, 9047-9055). Copyright 2018, American Chemical Society. B) Schematic depicting the condensation of the hydroxyl groups of halloysite nanotube with polysiloxanes, such that the dip coating of the modified halloysite nanotubes on a polyurethane foam produced a superhydrophobic foam. Reprinted with permission from (*ACS Appl. Mater. Interfaces*, 2019, **11**, 25445-25456). Copyright 2019, American Chemical Society.

ethane thiol) generated superhydrophobic/superhydrophilic patterns as shown in Figure 1.17C-D. The physical and chemical durability examination of this macrocycle derived superhydrophobic interface was not examined. Moreover, such catalyst-assisted embedment of water wettability is less likely feasible for large scale production and further, resorcinarene extraction, processing is an expensive approach. Moreover, most of the naturally derived superhydrophobic interfaces that lack both

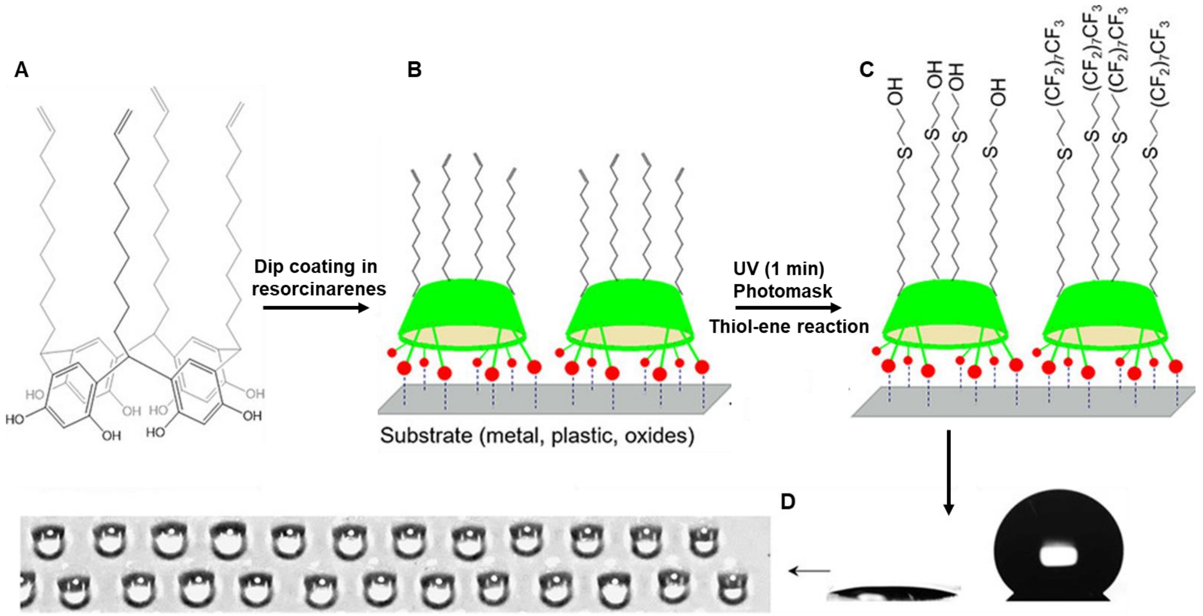

**Figure 1.17.** A-D) Schematic representing the hydrogen bonding of alkene-substituted resorcinarene onto various planar substrates (B) followed by UV-assisted thiol-ene post modification with alkyl-thiol (perfluorodecanethiol) and hydrophilic thiol (2-hydroxy-1-ethane thiol) (C) to produce superhydrophobic/superhydrophilic patterns (D). Reprinted with permission from (*ACS Appl. Mater. Interfaces*, 2018, **10**, 39268-39278). Copyright 2018, American Chemical Society.

durability and chemical reactivity have been developed following tedious, complicated and expensive fabrication processes that raises challenges related to scalability.[145,147,149-150,152,154]

Natural components have also been exploited to develop underwater superoleophobic interfaces for various prospective applications.[161-174] Table 1.4 summarizes a few underwater superoleophobic interfaces that were fabricated using different types of naturally derived components following different chemical approaches and the durability examinations of these interfaces. Processed, hydrophilic cellulose nanosheets,[162] sand layer,[164] wood,[165] walnut shell powder,[169] are some of the unconventional ingredients that exhibited underwater extreme oil repellence property on conversion into a membrane or physical deposition on the appropriately selected substrates.

**Table 1.4** Illustrating the various underwater superoleophobic functional materials developed using naturally derived building blocks following different chemical pathways.

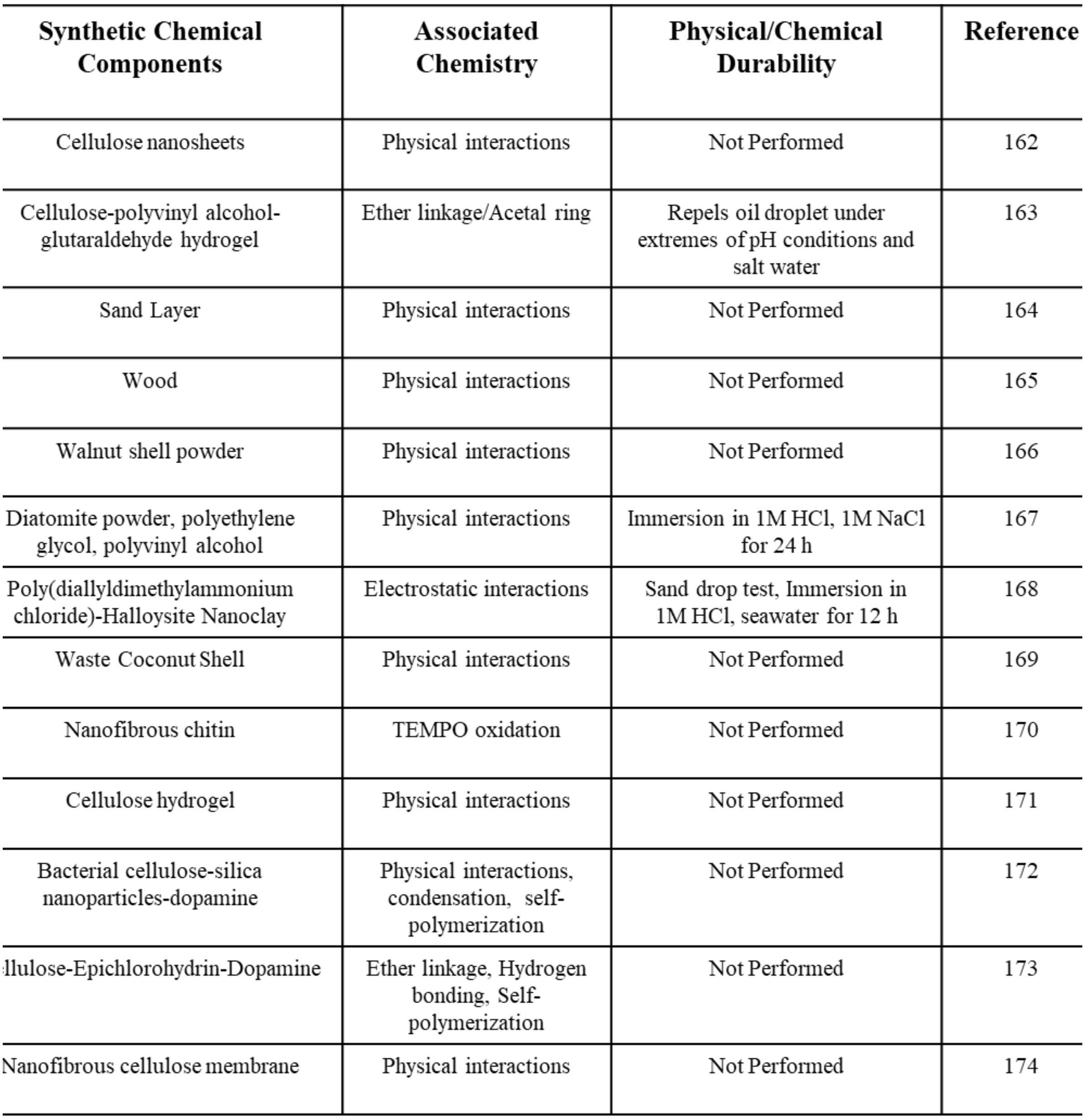

| Synthetic Chemical Components | Associated Chemistry | Physical/Chemical Durability | Reference |
|---|---|---|---|
| Cellulose nanosheets | Physical interactions | Not Performed | 162 |
| Cellulose-polyvinyl alcohol-glutaraldehyde hydrogel | Ether linkage/Acetal ring | Repels oil droplet under extremes of pH conditions and salt water | 163 |
| Sand Layer | Physical interactions | Not Performed | 164 |
| Wood | Physical interactions | Not Performed | 165 |
| Walnut shell powder | Physical interactions | Not Performed | 166 |
| Diatomite powder, polyethylene glycol, polyvinyl alcohol | Physical interactions | Immersion in 1M HCl, 1M NaCl for 24 h | 167 |
| Poly(diallyldimethylammonium chloride)-Halloysite Nanoclay | Electrostatic interactions | Sand drop test, Immersion in 1M HCl, seawater for 12 h | 168 |
| Waste Coconut Shell | Physical interactions | Not Performed | 169 |
| Nanofibrous chitin | TEMPO oxidation | Not Performed | 170 |
| Cellulose hydrogel | Physical interactions | Not Performed | 171 |
| Bacterial cellulose-silica nanoparticles-dopamine | Physical interactions, condensation, self-polymerization | Not Performed | 172 |
| llulose-Epichlorohydrin-Dopamine | Ether linkage, Hydrogen bonding, Self-polymerization | Not Performed | 173 |
| Nanofibrous cellulose membrane | Physical interactions | Not Performed | 174 |

Cai *et al.* reported that seaweed *S. japonica* made up of polysaccharides such as carrageenan, alginate and agar, exhibited salt-water tolerant underwater superoleophobicity as shown in Figure 1.18A-D.[35] Atomic force microscopy of dehydrated seaweed revealed a porous outer interface with reticular structures and microfibers, resembling a dehydrated hydrogel. However, atomic force microscopy performed underwater revealed the absence of reticular structures and confirmed the presence of randomly distributed micro-domains that in turn generated nanoscale roughness. The presence of polysaccharides ensured the trapping of a large amount of water, similar to a hydrogel that aided in exhibiting underwater oil repellence. Inspired from the seaweed, a hybrid hydrogel of calcium alginate with polyacrylamide was fabricated with doping of nano-clay, where the hydrogel entrapped the water phase to exhibit underwater oil repellence and the presence of nano-clay imparted mechanical stability to the otherwise fragile hydrogel.[35] The resultant double network-composite hydrogel with inherent nanoscale roughness exhibited underwater oil contact angles above 150° in saturated NaCl solutions and retained the anti-fouling property even after immersion in viscous oils for 30 days. Figure 1.18E shows the cleaning of the contaminated oil phase from the surface of the hydrogel coated glass using a splash of water whereas the oil phase sticks to the bare glass surface. Moreover, the immersion in distilled water, artificial sea-water for 5 days and consecutive drying and swelling of the hydrogel for 5 cycles failed to deter the embedded oil wettability. Fan *et al.* reported a cellulose-polyvinyl alcohol hydrogel cross-linked with glutaraldehyde following the ether/acetal formation reactions as shown in Figure 1.18F.[163] The covalently cross-linked hydrogel coating on a filter paper exhibited underwater superoleophobicity with oil contact angle above 150° that was extended for oil/water separation using hexane as the model oil and chemically contaminated aqueous phases such as 2 M $H_2SO_4$, 2 M NaOH, saturated NaCl and for surfactant stabilized oil-in-water emulsion separation. The hydrogel coated filter paper repelled the chemically contaminated beaded aqueous droplets (with pH 1-14) and different concentrations of NaCl.

Hou *et al.* exploited the electrostatic interactions between negatively charged halloysite nanotubes and positively charged poly(diallyldimethyl ammonium chloride) to build a hierarchically featured, underwater superoleophobic coating on a stainless-steel mesh (Figure 1.18G ) that was extended for selective and repetitive oil/water separation.[168] The clay derived underwater oil repellent interface retained its embedded wettability even after exposure to chemically aqueous acidic and salt contaminated environments for 12 h and after sand drop test.

Chen *et al.* reported transparent and mechanically durable underwater superoleophobicity inspired by the bio-mineralization assisted mechanically tough, hierarchical outer surface of nacre composed of 5% organic matrix and 95% inorganic aragonite, which protects the inner soft body.[175] Nacre-inspired mineralized, transparent films of chitosan as the organic component and aragonite platelet as the inorganic component was developed on a wide range of planar substrates that exhibited underwater oil repellence with oil contact angles above 150°. Primarily, methacrylic anhydride modified chitosan was photo-cross linked to form a thick film on the desired substrate followed by the deposition of amorphous calcium carbonate that reduced the mineralization time and acted as seed molecules for the growth of inorganic aragonite platelet as shown in Figure 1.19A-B. The chitosan derived underwater oil repellent coating retained its oil repellence property even after 30 days immersion in sea water and dropping from upto 60 cm height.

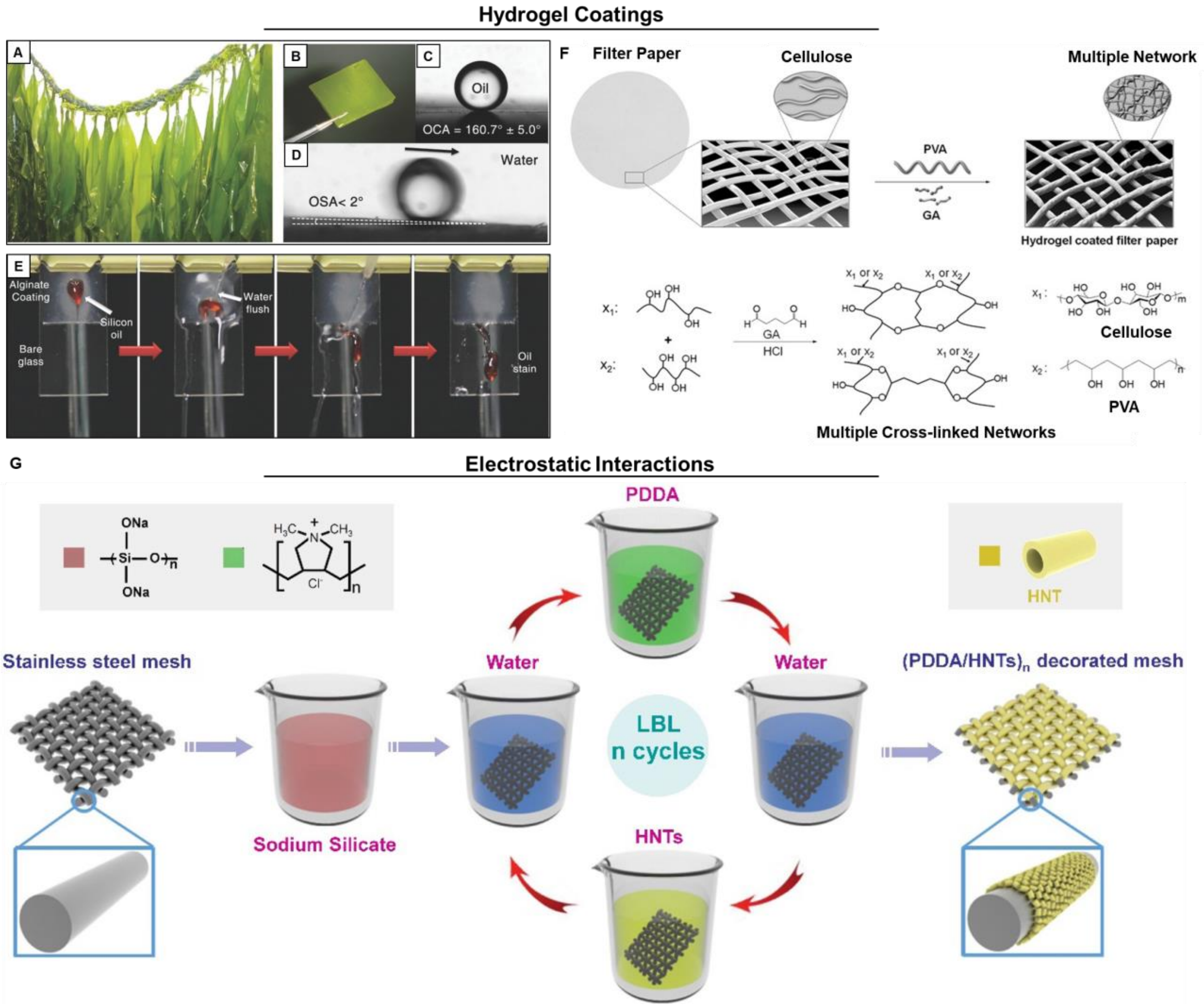

**Figure 1.18.** A-D) Underwater superoleophobic property of seaweed. E) Digital images depicting the anti-fouling property of the alginate hydrogel coated glass slide. The oil phase is easily washed off by water on the alginate coating whereas the uncoated glass slide is stained by the oil phase. Reprinted with permission from (*Adv. Mater.*, 2015, **27**, 4162-4168). Copyright 2015, Wiley-VCH Verlag GmbH & Co. KGaA, Weinheim. F) Schematic depicting the cross-linking of cellulose and polyvinyl alcohol with glutaraldehyde to obtain an underwater superoleophobic hydrogel coating on filter paper. Reprinted with permission from (*Adv. Funct. Mater.*, 2015, **25**, 5368-5375). Copyright 2015, Wiley-VCH Verlag GmbH & Co. KGaA, Weinheim. G) Schematic depicting the layer-by-layer electrostatic assembly of poly(diallyldimethyl ammonium chloride) with halloysite nanotubes to generate underwater superoleophobicity on a stainless-steel mesh. Reprinted with permission from (*Appl. Surf. Sci.*, 2017, **416**, 344-352). Copyright 2017, Elsevier B. V.

Zou *et al.* developed a polydopamine filled cellulose aerogel cross-linked via epichlorohydrin following ether formation, self-polymerization reactions to produce an underwater superoleophobic aerogel that was extended for solar-assisted dye separation from wastewater.[173] The durability of the reported oil-repellent aerogel was not examined.

Even though appreciable progress has been made in the area of natural components derived underwater superoleophobicity, there exists glaring loopholes in the reported approaches. For instance, the hydrogel-based coatings were not thoroughly demonstrated for its ability to withstand severe physical abrasions such as scratch test, tape peeling test, sand paper abrasion or subjection to mechanical stretching.[35,163] Hydrogels are extremely fragile on exposure to aqueous phase which renders their mechanical handling difficult. Moreover, the acetal ring/ether linkages oil-repellent coatings would be susceptible under acidic conditions due to hydrolysis of ether/acetal,[176-177] thus, such coatings would be unfit for practical applications. Even though a few approaches reported the salt-tolerant oil repellent

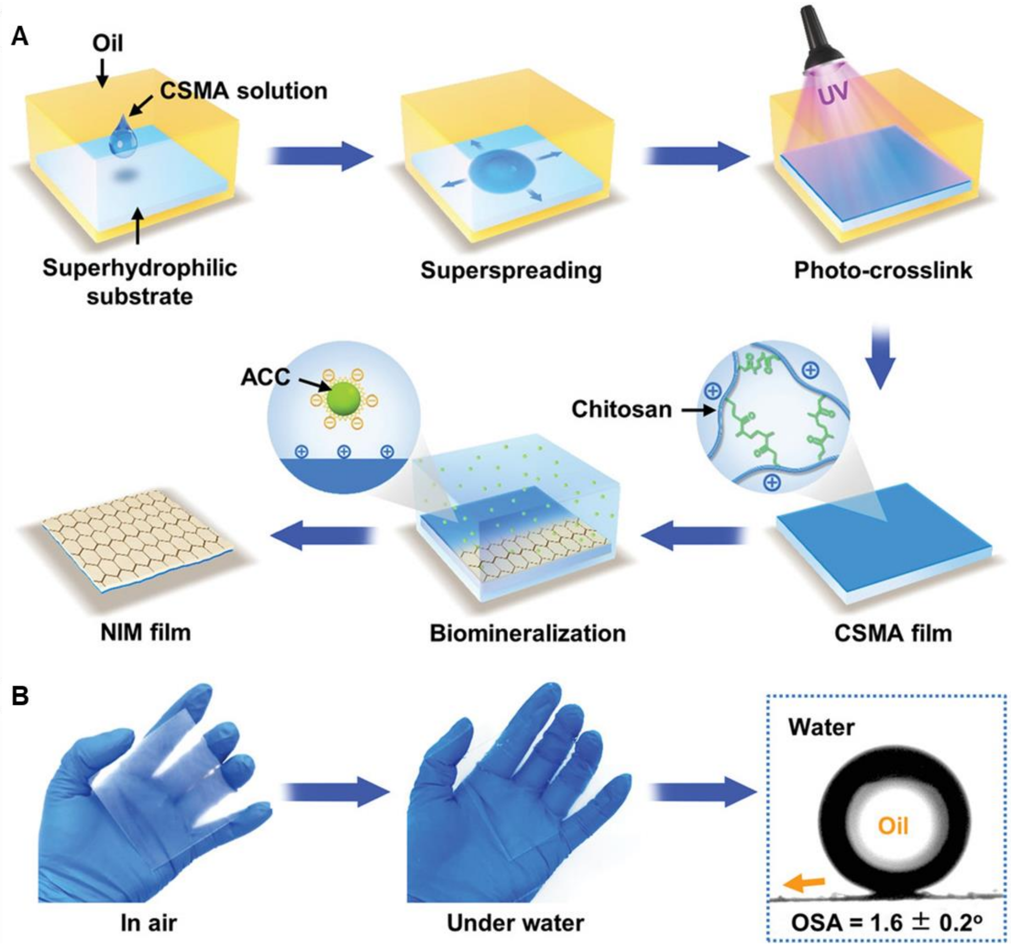

**Figure 1.19.** A-B) Schematic representing the photo-crosslinking of methacrylic anhydride modified chitosan to form a thick film followed by deposition of amorphous calcium carbonate that reduced the mineralization time of the chitosan film and also acted as seed molecules for the growth of aragonite platelets. The nacre-inspired mineralized (NIM) film exhibited underwater transparent, superoleophobicity. Reprinted with permission from (*Adv. Mater.*, 2020, **32**, 1907413-1907420). Copyright 2020, Wiley-VCH Verlag GmbH & Co. KGaA, Weinheim.

coatings upto 30 days of exposure to saturated NaCl ,[35,163,178] Most of the reports failed to examine the long duration sustainability of the oil-repellent coatings after exposure to chemically contaminated aqueous phases including extremes of pH, surfactant contaminated water etc. The halloysite derived oil-repellent multilayer coatings were exposed to acidic water and seawater for a mere 12 h duration,[168] whereas for practical applications, the prolonged durability examination is a necessity. Furthermore, most of the reported approaches involve the use of catalyst-assisted cross-linking or oxidation processes,[170,175] laborious layer-by-layer assembly[168] and multistep synthesis[167,172-175] which adds to the cost of production and thus, limits its scalability. Although mechanically tough coatings have been achieved,[133,175,178] however, none of the approaches till date have exploited natural components to obtain stretchable and durable underwater superoleophobicity. Importantly, natural components derived durable anti-wetting materials that allow to associate other relevant physical properties is rare in the literature.

Thus, to address the inadequacies of the reported approaches, I have adopted facile chemical pathways to fabricate bio-mimicked anti-wetting interfaces with impeccable long-term durability exploiting cheap, eco-friendly components.

## 1.7. Motivation and Objectives

The development of bio-inspired wettability has witnessed widespread advancement in the recent decade owing to its enormous practical applicability.[9-19] Various types of synthetic components have been utilized to develop both artificial superhydrophobic and underwater superoleophobic interfaces, however, the associated toxicity and non-biodegradability of the as-fabricated materials or the constituent building blocks of the synthetic counterparts pose a major hindrance for scalability and the related health, environmental hazards.[143-144] As already discussed in section 1.6.2, Table 1.3 and 1.4, recently, natural components derived anti-wetting interfaces have gained precedence owing to its low-cost, abundance and environment-friendliness.[145-155,161-174] However, the naturally derived anti-wetting material integrated together through weak physical interactions or susceptible covalent chemistries suffer from major durability issues that limits their practical applicability, where prolonged chemical, physical and mechanical durability of the materials is of utmost importance.[110-112,114] Moreover, the reported naturally derived anti-wetting interfaces lack a facile, catalyst-free chemical avenue to tailor the embedded liquid wettability and other physical parameters that would be useful for various relevant applications. Furthermore, most of the synthetic and naturally derived anti-wetting materials have been developed adopting expensive, tedious and complex fabrication processes that is non-viable for industrial scale-up. [65,113,139,145,147,149-150,152,154,167,172-175]

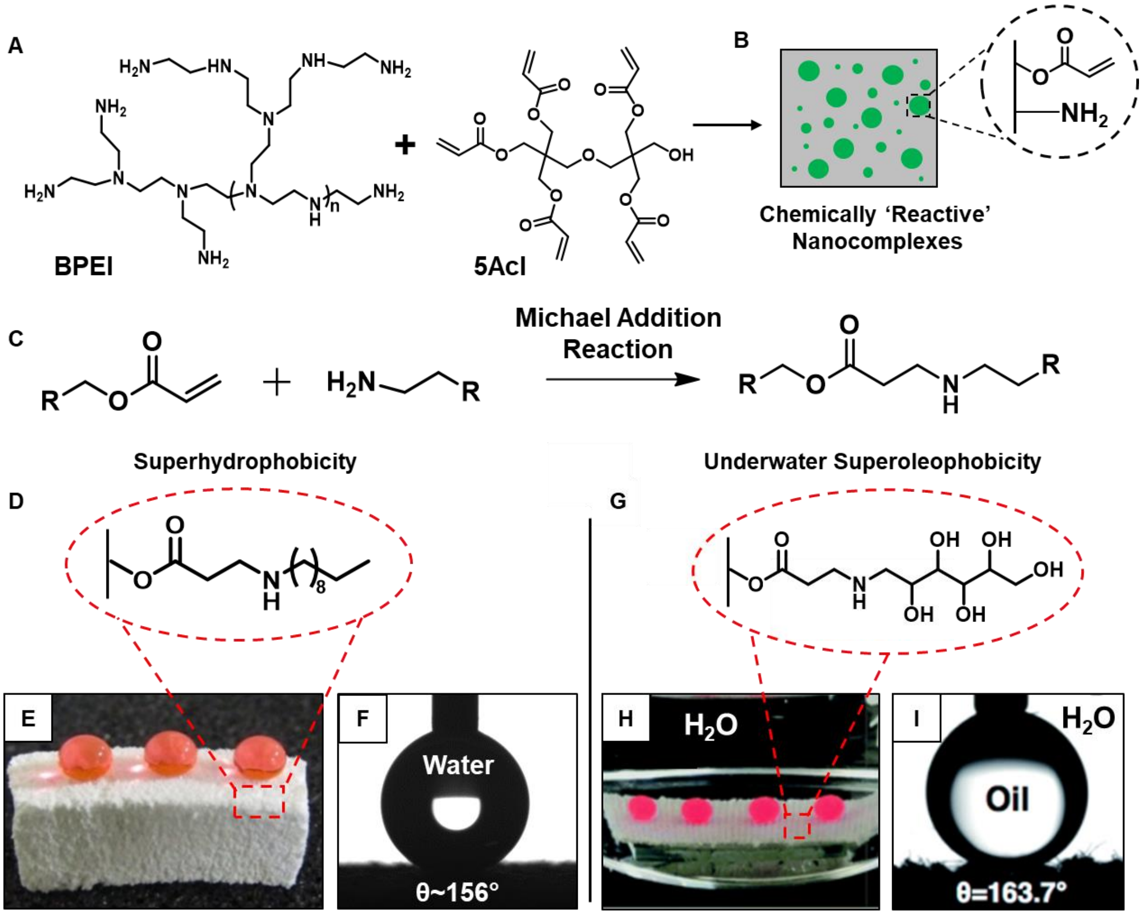

**Figure 1.20.** A-C) Schematic illustrating the formation of the chemically 'reactive' polymeric nanocomplexes following the catalyst-free Michael addition reaction between a branched amine containing polymer and multi-functional acrylate cross-linker. D-F) The growth of the 'reactive' polymeric nanocomplexes generate three-dimensional monoliths that produce bulk superhydrophobicity after post modification of the residual acrylate groups with decylamine. Reprinted with permission from (*Chem. Mater.*, 2016, **28**, 8689-8699). Copyright 2016, American Chemical Society. G-I) The deposition of a dispersion of 'reactive' polymeric nanocomplexes generate underwater superoleophobicity on a fibrous substrate following the post modification of the residual acrylate groups with glucamine. Reprinted with permission from (*J. Mater. Chem. A*, 2018, **6**, 22027-22036). Copyright 2018, The Royal Society of Chemistry.

To combat the durability challenges associated with the anti-wetting interfaces and the lack of chemical reactivity that would allow to tailor the embedded liquid wettability, a robust, readily reactive, covalent chemistry appears as a promising counter-tool.[114] For example, the catalyst-free Michael addition reaction between an amine containing branched polymer (BPEI) and a multi-functional acrylate cross-linker (5Acl) was exploited earlier to generate chemically 'reactive' nanocomplexes that imparted both the a) essential topography and b) residual chemical reactivity for post modification with the desired chemical functionalities to exhibit anti-wetting property.[114] The 'reactive' nanocomplexes derived free-standing, porous monoliths or thick polymeric coatings displayed superhydrophobicity on post modification with a hydrophobic alkylamine i.e. decylamine.[179]

Moreover, the post covalent modification of the 'reactive' polymeric coating with a high surface energy molecule i.e. glucamine, imparted underwater superoleophobicity.[66] Even though, robust superhydrophobic and underwater superoleophobic functional materials were obtained following Michael addition chemistry, but those materials were developed using synthetic and non-biodegradable polymer i.e. BPEI. [180] Moreover, BPEI is synthesized from aziridine which is widely known for its toxicity, hence, the industrial scalability is a major threat.[181]

Thus, the development of robust, functional anti-wetting interfaces exploiting low cost, abundant and widely known eco-friendly alternatives following facile Michael addition reaction and Schiff base reaction using an economical fabrication technique, is the motive of my thesis. The strategic association of Michael addition reaction at ambient conditions is expected to provide residual chemical reactivity to the naturally derived functional interfaces for the three-dimensional tailoring of the embedded liquid wettability. The tailoring of water wettability in a bulk superhydrophobic material would provide a facile avenue for the controlled and sustained release of the loaded drug molecules. Such prolonged drug release using naturally abundant components derived anti-wetting materials is unprecedented in literature, that can be extended for prospective bio-medical applications. Moreover, the tailoring of both liquid wettability and other physical parameters such as porosity, mechanical

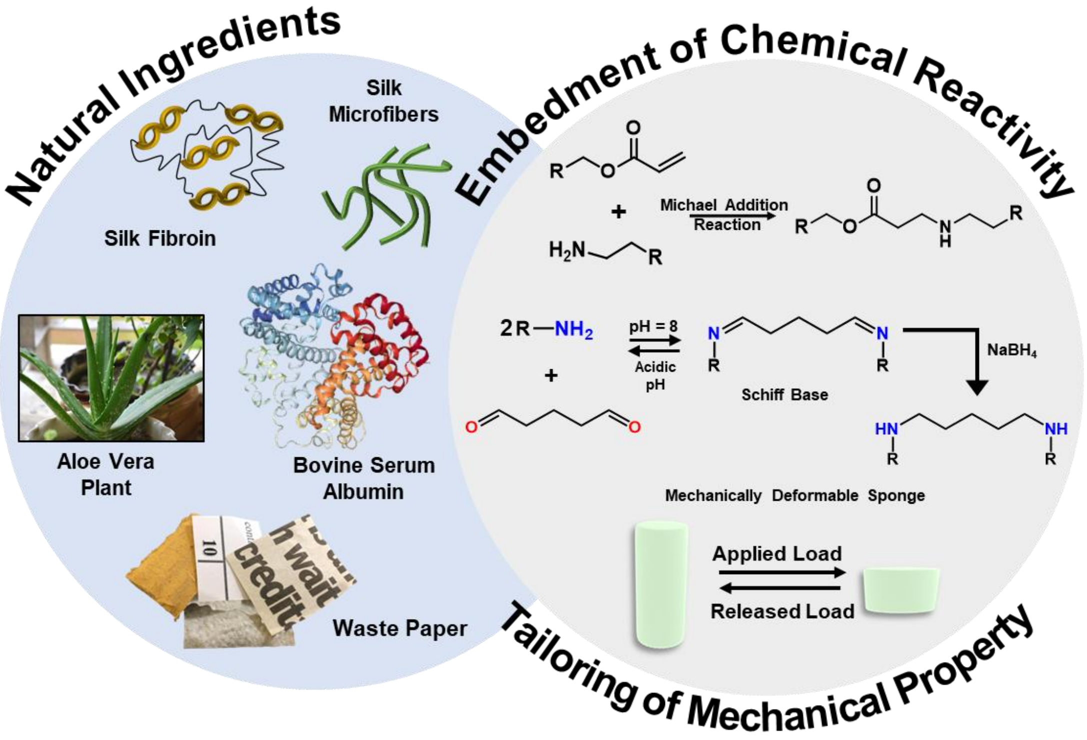

**Figure 1.21.** Schematic representing the exploitation of various naturally derived, abundant, eco-friendly ingredients for the fabrication of bio-mimicked anti-wetting interfaces following a facile chemical approach that would allow the induction of chemical reactivity to tailor the embedded liquid wettability. Furthermore, such natural ingredients associated chemical strategies can be explored to modulate the mechanical property.

property of the naturally derived functional materials is rare in the literature but would be useful for various real-world potential applications. Moreover, the uniform co-optimization of topography and chemistry is expected to produce physically and chemically durable, stretchable and mechanically deformable, eco-friendly, anti-wetting materials for extended applications in oil/water separation even at diverse severe settings.

## 1.8. References:

1. K. Verbrugge, *Harvard Review*, 2011, 16-19.
2. M. N. Hill and A. R. Robinson, *Harvard University Press*, 1962, 498.
3. F. E. Fish, P. W. Weber, M. M. Murray and L. E. Howle, *Integrative and Comparative Biology*, 2011, **51**, 203-213.
4. N. K. Katiyar, G. Goel, S. Hawi and S. Goel, *NPG Asia Mater.*, 2021, **13**, 56-72.
5. Wilbur and Orville Wright, U. S. Patent, 1906, **821**, 393-395.
6. G. D. Mestral, U. S. Patent, 1955, **717**, 437-439.
7. A. B. D. Cassie and S. Baxter, *Trans. Faraday Soc.*, 1944, **40**, 546-551.
8. Y. Si, Z. Dong and L. Jiang, *ACS Cent. Sci.*, 2018, **4**, 1102-1112.
9. J. Yong, F. Chen, Q. Yang, J. Huo and X. Hou, *Chem. Soc. Rev.*, 2017, **46**, 4168-4217.
10. X.-M. Li, D. Reinhoudt and M. Crego-Calama, *Chem. Soc. Rev.*, 2007, **36**, 1350-1368.
11. Y. Sunab and Z. Guo, *Nanoscale Horiz.*, 2019, **4**, 52-76.
12. Z. Chu, Y. Feng and S. Seeger, *Angew. Chem., Int. Ed.*, 2015, **54**, 2328-2338.
13. L. Wen, Y. Tian and L. Jiang, *Angew. Chem., Int. Ed.*, 2015, **9**, 3387-3399.
14. X. Tian, T. Verho and R. H. A. Ras, *Science*, 2016, **352**, 142-143.
15. Z. Lia and Z. Guo, *Nanoscale*, 2019, **11**, 22636-22663.
16. I. S. Bayer, *Adv. Mater. Interfaces*, 2020, **7**, 2000095-2000120.
17. J. Yong, J. Huo, F. Chen, Q. Yang and X. Hou, *Phys. Chem. Chem. Phys.*, 2018, **20**, 25140 25163.
18. S. Zhang, J. Huang, Z. Chen, S. Yang and Y. Lai, *J. Mater. Chem. A*, 2019, **7**, 38-63.
19. M. Liu, S. Wang and L. Jiang, *Nat. Rev. Mater.*, 2017, **2**, 17036-17053.
20. S. Shiri and J. C. Bird, *Proc. Natl. Acad. Sci. U. S. A.*, 2017, **114**, 6930-6935.
21. W. Barthlott and C. Neinhuis, *Planta*, 1997, **202**, 1-8.
22. K. Koch, B. Bhushan, Y. C. Jung and W. Barthlott, *Soft Matter*, 2009, **5**, 1386-1393.
23. L. Feng, S. Li, Y. Li, H. Li, L. Zhang, J. Zhai, Y. Song, B. Liu, L. Jiang and D. Zhu, *Adv. Mater.*, 2002, **14**, 1857-1860.

24. L. Feng, Y. A. Zhang, J. M. Xi, Y. Zhu, N. Wang, F. Xia and L. Jiang, *Langmuir*, 2008, **24**, 4114-4119.

25. A. R. Parker and C. R. Lawrence, *Nature*, 2001, **414**, 33-34.

26. Y. Zheng, H. Bai, Z. Huang, X. Tian, F.-Q. Nie, Y. Zhao, J. Zhai and L. Jiang, *Nature*, 2010, **463**, 640-643.

27. J. Ju, H. Bai, Y. Zheng, T. Zhao, R. Fang and L. Jiang, *Nat. Commun.*, 2012, **3**, 1247-1253.

28. K. Autumn, M. Sitti, Y. A. Liang, A. M. Peattie, W. R. Hansen, S. Sponberg, T. W. Kenny, R. Fearing, J. N. Israelachvili and R. J. Full, *Proc. Natl. Acad. Sci. U. S. A.*, 2002, **99**, 12252-12256.

29. X. Gao and L. Jiang, *Nature*, 2004, **432**, 36.

30. M. Liu, S. Wang, Z. Wei, Y. Song and L. Jiang, *Adv. Mater.*, 2009, **21**, 665-669.

31. Q. Cheng, M. Li, Y. Zheng, B. Su, S. Wang and L. Jiang, *Soft Matter*, 2011, **7**, 5948-5951.

32. X. Liu, J. Zhou, Z. Xue, J. Gao, J. Meng, S. Wang and L. Jiang, *Adv. Mater.*, 2012, **24**, 2869-3405.

33. S. Nishimoto and B. Bhushan, *RSC Adv.*, 2013, **3**, 671-690.

34. Y. Cai, L. Lin, Z. Xue, M. Liu, S. Wang and L. Jiang, *Adv. Funct. Mater.*, 2014, **24**, 809-816.

35. Y. Cai, Q. Lu, X. Guo, S. Wang, J. Qiao and L. Jiang, *Adv. Mater.*, 2015, **27**, 4162-4168.

36. T. Young, *Philos. Trans. R. Soc. London*, 1805, **95**, 65-87.

37. R. N. Wenzel, *Ind. Eng. Chem.*, 1936, **28**, 988-994.

38. S. Wang and L. Jiang, *Adv. Mater.*, 2007, **19**, 3423-3424.

39. G. D. Bixler and B. Bhushan, *Soft Matter*, 2012, **8**, 11271-11284.

40. P. R. Waghmare, N. S. K. Gunda and S. K. Mitra, *Sci. Rep.*, 2014, **4**, 7454-7459.

41. F. Geyer, M. D'Acunzi, A. Sharifi-Aghili, A. Saal, N. Gao, A. Kaltbeitzelk, T.-F. Sloot, R. Berger and D.Vollmer, *Sci. Adv.*, 2020, **6**, eaaw9727 (1-11).

42. S. T. Yohe, Y. L. Colson and M. W. Grinstaff, *J. Am. Chem.Soc.*, 2012, **134**, 2016-2019.

43. U. Manna, M. J. Kratochvil and D. M. Lynn, *Adv. Mater.*, 2013, **25**, 6405-6409.

44. A. M. Rather, S. Mahato, K. Maji, N. Gogoi and U. Manna, *Nanoscale*, 2017, **9**, 16154-16165.

45. M. Wu, B. Ma, T. Pan, S. Chen and J. Sun, *Adv. Funct. Mater.*, 2016, **26**, 569-576.

46. L. Wang, Q. Gong, S. Zhan, L. Jiang and Y. Zheng, *Adv. Mater.*, 2016, **28,** 7729-7735.

47. S. Zhang, J. Huang, Y. Cheng, H. Yang, Z. Chen and Y. Lai, *Small*, 2017, **13**, 1701867-1701887.

48. H. Qian, D. Xu, C. Du, D. Zhang, X. Li, L. Huang, L. Deng, Y. Tu, J. M. C. Mol and H. A. Terryn, *J. Mater. Chem. A*, 2017, **5**, 2355-2364.

49. T. Xiang, Y. Han, Z. Guo, R. Wang, S. Zheng, S. Li, C. Li and X. Dai, *ACS Sustainable Chem. Eng.*, 2018, **6**, 5598-5606.

50. S. Wu, H. Zhao, F. Dong, W. Ling, Z. Tang and J. Zhang, *ACS Appl. Mater. Interfaces*, 2021, **13**, 2610-2621.

51. J. Zhao, L. Song, J. Yin and W. Ming, *Chem. Commun.*, 2013, **49**, 9191-9193.

52. C. Hu, S. Liu, B. Li, H. Yang, C. Fan and W. Cui, *Adv. Healthc. Mater.*, 2013, **2**, 1314-1321.

53. L. Li, Y. Bai, L. Li, S. Wang and T. Zhang, *Adv. Mater.*, 2017, **29**, 1702517.

54. S. T. Yohe, J. D. Freedman, E. J. Falde, Y. L. Colson and M. W. Grinstaff, *Adv. Funct. Mater.*, 2013, **23**, 3628-3637.

55. K. Chen, S. Zhou and L. Wu, *ACS Nano*, 2016, **10**, 1386-1394.

56. X. Huang, B. Li, L. Wang, X. Lai, H. Xue and J. Gao, *ACS Appl. Mater. Interfaces*, 2019, **11**, 24533-24543.

57. E. Zhang, Z. Cheng, T. Lv, L. Li and Y. Liu, *Nanoscale*, 2015, **7**, 19293-19299.

58. Z. Cheng, H. Liu, H. Lai, Y. Du, K. Fu, C. Li, J. Yu, N. Zhang and K. Sun, *ACS Appl. Mater. Interfaces*, 2015, **7**, 20410-20417.

59. L. Chen, M. Liu, H. Bai, P. Chen, F. Xia, D. Han and L. Jiang, *J. Am. Chem. Soc.*, 2009, **131**, 10467-10472.

60. D. Wu, S. Z. Wu, Q. D. Chen, S. Zhao, H. Zhang, J. Jiao, J. A. Piersol, J. N. Wang, H. B. Sun and L. Jiang, *Lab Chip*, 2011, **11**, 3873-3879.

61. J. L. Yong, F. Chen, Q. Yang, D. Zhang, U. Farooq, G. Du and X. Hou, *J. Mater. Chem. A*, 2014, **2**, 8790-8795.

62. Y. Lee, S. H. Park, K. B. Kim and J. K. Lee, *Adv. Mater.*, 2007, **19**, 2330-2335.

63. E. P. Ivanova, J. Hasan, H. K. Webb, G. Gervinskas, S. Juodkazis, V. K. Truong, A. H. Wu, R. N. Lamb, V. A. Baulin, G. S. Watson, J. A. Watson, D. E. Mainwaring and R. J. Crawford, *Nat. Commun.*, 2013, **4**, 2838-2845.

64. J. Y. Huang, Y. K. Lai, F. Pan, L. Yang, H.Wang, K. Q. Zhang, H. Fuchs and L. F. Chi, *Small*, 2014, **10**, 4865-4873.

65. L. -P. Xu, J. Zhao, B. Su, X. Liu, J. Peng, Y. Liu, H. Liu, G. Yang, L. Jiang, Y. Wen, X. Zhang and S. Wang, *Adv. Mater.*, 2013, **25**, 606-611.

66. D. Parbat and U. Manna, *J. Mater. Chem. A*, 2018, **6**, 22027-22036.

67. W. Lei, D. Portehault, D. Liu, S. Qin and Y. Chen, *Nat. Commun.*, 2013, **4**, 1777-1783.

68. J. Lahann, *Nat. Nanotechnol.*, 2008, **3**, 320-321.

69. S. B. Joye, *Science*, 2015, **349**, 592-593.

70. S. Kleindienst, J. H. Paul and S. B. Joye, *Nat. Rev. Micro.*, 2015, **13**, 388-396.

71. J. F. Rasmussen, S. Wegeberg and K. Gustavson, *Water Air Soil Pollut.*, 2015, **226**, 329-340.

72. J. Ge, H. Y. Zhao, H. W. Zhu, J. Huang, L. A. Shi and S. H. Yu, *Adv. Mater.*, 2016, **28**, 10459-10491.

73. J. Zhang and S. Seeger, *Adv. Funct. Mater.*, 2011, **21**, 4699-4704.

74. D. D. Nguyen, N. H. Tai, S. B. Lee and W. S. Kuo, *Energy Environ. Sci.*, 2012, **5**, 7908.

75. P. Calcagnile, D. Fragouli, I. S. Bayer, G. C. Anyfantis, L. Martiradonna, P. D. Cozzoli, R. Cingolani and A. Athanassiou, *ACS Nano*, 2012, **6**, 5413-5419.

76. H. Zhu, D. Chen, W. An, N. Li, Q. Xu, H. Li, J. He and J. Lu, *Small*, 2015, 11, 5222-5229.

77. A. Das, K. Maji, S. Naskar and U. Manna, *Chem. Sci.*, 2020, **11**, 6556-6566.

78. L. Feng, Z. Y. Zhang, Z. H. Mai, Y. M. Ma, B. Q. Liu, L. Jiang and D. B. Zhu, *Angew. Chem., Int. Ed.*, 2004, **43**, 2012-2014.

79. Q. L. Ma, H. F. Cheng, A. G. Fane, R. Wang and H. Zhang, *Small*, 2016, **12**, 2186-2202.

80. Y. Liu, X. Chen and J. H. Xin, *J. Mater. Chem.*, 2009, **19**, 5602-5611.

81. P. Papadopoulos, L. Mammen, X. Deng, D. Vollmer and H.-J. Butt, *Proc. Natl. Acad. Sci. U. S. A.*, 2013, **110**, 3254-3258.

82. Z. Xue, S. Wang, L. Lin, L. Chen, M. Liu, L. Feng and L. Jiang, *Adv. Mater.*, 2011, **23**, 4270-4273.

83. J. Zhang, L. Wu, Y. Zhang and A. Wang, *J. Mater. Chem. A*, 2015, **3**, 18475-18482.

84. B. Wang, J. Li, G. Wang, W. Liang, Y. Zhang, L. Shi, Z. Guo and W. Liu, *ACS Appl. Mater. Interfaces*, 2013, **5**, 1827-1839.

85. H. Wang, H. Zhou, A. Gestos, J. Fang and T. Lin, *ACS Appl. Mater. Interfaces*, 2013, **5**, 10221-10226.

86. S. Li, J. Huang, Z. Chen, G. Chen and Y. Lai, *J. Mater. Chem. A*, 2017, **5**, 31-55.

87. M. -F. Wang, N. Raghunathan and B. Ziaie, *Langmuir*, 2007, **23**, 2300-2303.

88. M. Sun, C. Luo, L. Xu, H. Ji, Q. Ouyang, D. Yu and Y. Chen, *Langmuir*, 2005, **21**, 8978-8981.

89. M. Qu, G. Zhao, Q. Wang, X. Cao and J. Zhang, *Nanotechnology*, 2008, **19**, 055707-055711.

90. A. Pozzato, S. D. Zilio, G. Fois, D. Vendramin, G. Mistura, M. Belotti, Y. Chen and M. Natali, *Microelectron. Eng.*, 2006, **83**, 884-888.

91. L. Zhu, Y. Feng, X. Ye and Z. Zhou, *Sens. Actuators A*, 2006, **130**, 595-600.

92. C. Cardinaud, M. -C. Peignon and P. -Y. Tessier, *Appl. Surface Sci.*, 2000, **164**, 72-83.

93. S. Minko, M. Müller, M. Motornov, M. Nitschke, K. Grundke and M. Stamm, *J. Am. Chem. Soc.*, 2003, **125**, 3896-3900.

94. Y. Sia and Z. Guo, *Nanoscale*, 2015, **7**, 5922-5946.

95. G. Decher, *Science*, 1997, **277**, 1232-1237.

96. L. Zhai, F. Ç. Cebeci, R. E. Cohen and M. F. Rubner, *Nano. Lett.*, 2004, **4**, 1349-1353.

97. L. Wang, B. Peng and Z. Su, *Langmuir*, 2010, **26**, 12203-12208.

98. E. Ozkan, C. C. Crick, A. Taylor, E. Allan and I. P. Parkin, *Chem. Sci.*, 2016, **7**, 5126-5131.

99. S. Azlinda, A. Kamal, R. Ritikos and S. A. Rahman, *Appl. Surf. Sci.*, 2015, **328**, 146-153.

100. C. Ao, W. Yuan, J. Zhao, X. He, X. Zhang, Q. Li, T. Xia, W. Zhang and C. Lu, *Carbohydr. Polym.*, 2017, **175**, 216-222.

101. J. -J. Li, L. -T. Zhu and Z. -H. Luo, *Chem. Eng. J.*, 2016, **287**, 474-481.

102. J. Feng and Z. Guo, *Nanoscale Horiz.*, 2019, **4**, 339-364.

103. W. Y. Chen, S.-N. Lai, C. -C. Yen, X. Jiang, D. Peroulis and L. A. Stanciu, *ACS Nano*, 2020, **14**, 11490-11501.

104. S. Kim, J. -W. Lee and W. Hwang, *ACS Appl. Mater. Interfaces*, 2020, **12**, 28869-28875.

105. S. Srinivasan, V. K. Praveen, R. Philip and A. Ajayaghosh, *Angew. Chem., Int. Ed.*, 2008, **120**, 5834-5838.

106. A. Asthana, T. Maitra, R. Büchel, M. K. Tiwari and D. Poulikakos, *ACS Appl. Mater. Interfaces*, 2014, **6**, 8859-8867.

107. X. Deng, L. Mammen, H. -J. Butt and D. Vollmer, *Science*, 2012, **335,** 67-69.

108. R. Iqbal, B. Majhy and A. K. Sen, *ACS Appl. Mater. Interfaces*, 2017, **9**, 31170-31180.

109. B. Wang and Z. G. Guo, *Chem. Commun.*, 2013, **49**, 9416-9418.

110. Z. Han, B. Li, Z. Mu, S. Niu, J. Zhang and L. Ren, *Small*, 2017, **13**, 1701121-1701131.

111. C. Zhou, Z. Chen, H. Yang, K. Hou, X. Zeng, Y. Zheng and J. Cheng, *ACS Appl. Mater. Interfaces*, 2017, **9**, 9184-9194.

112. J. T. Han, D. H. Lee, C. Y. Ryu and K. Cho, *J. Am. Chem. Soc.*, 2004, **126**, 4796-4797.

113. Z. Wang, Y. Wang and G. Liu, *Angew. Chem., Int. Ed.*, 2016, **55**, 1291-1294.

114. A. Das, A. Shome and U. Manna, *J. Mater. Chem. A*, 2021, **9**, 824-856.

115. G. Kwak, M. Lee and K. Yong, *Langmuir*, 2010, **26**, 9964-9967.

116. X. Zhu, Z. Zhang, X. Men, J. Yang, K. Wang, X. Xu, X. Zhou and Q. Xue, *J. Mater. Chem.*, 2011, **21**, 15793-15797.

117. Y. Li, L. Li and J. Sun, *Angew. Chem., Int. Ed.*, 2010, 49, 6129-6133.

118. H. X. Wang, Y. H. Xue, J. Ding, L. F. Feng, X. G. Wang and T. Lin, *Angew. Chem., Int. Ed.*, 2011, **50**, 11433-11436.

119. P. A. Levkin, F. Svec and J. M. J. Fréchet, *Adv. Funct. Mater.*, 2009, **19**, 1993-1998.

120. W. Zhang, Z. Shi, F. Zhang, X. Liu, J. Jin and L. Jiang, *Adv. Mater.*, 2013, **25**, 2071-2076.

121. X. Zeng, L. Qian, X. Yuan, C. Zhou, Z. Li, J. Cheng, S. Xu, S. Wang, P. Pi and X. Wen, *ACS Nano*, 2017, **11**, 760-769.

122. Z. Wang, C. Xiao, Z. Wu, Y. Wang, X. Du, W. Kong, D. Pan, G. Guan and X. Hao, *J. Mater. Chem. A*, 2017, **5**, 5895-5904.

123. C. Peng, Z. Chen and M. K. Tiwari, *Nat. Mater.*, 2018, **17**, 355-360.

124. W. Luo, D. Sun, S. Chen, L. Shanmugam, Y. Xiang and J. Yang, *ACS Appl. Mater. Interfaces*, 2020, **12**, 57547-57559.

125. X. Li, N. Wang, J. He, Z. Yang, F. Zhao, K. Wang and C. Huang, *Small*, 2020, **16**, 1907013.

126. J. Huang, M. Yang, H. Zhang and J. Zhu, *ACS Appl. Mater. Interfaces*, 2021, **13**, 1323-1332.

127. D. Wang, Q. Sun, M. J. Hokkanen, C. Zhang, F. -Y. Lin, Q. Liu, S. -P. Zhu, T. Zhou, Q. Chang, B. He, Q. Zhou, L. Chen, Z. Wang, R. H. A. Ras and X. Deng, *Nature*, 2020, **582**, 55-59.

128. T. Yuan, J. Meng, T. Hao, Z. Wang and Y. Zhang, *ACS Appl. Mater. Interfaces*, 2015, **7**, 14896-14904.

129. S. Gao, J. Sun, P. Liu, F. Zhang, W. Zhang, S. Yuan, J. Li and J. Jin, *Adv. Mater.*, 2016, **28**, 5307-5314.

130. J. Huang, Z. Zhang, J. Weng, D. Yu, Y. Liang, X. Xu, Z. Qiao, G. Zhang, H. Yang and X. Wu, *ACS Appl. Mater. Interfaces*, 2020, **12**, 56530-56540.

131. N. Han, C. Yang, Z. Zhang, W. Wang, W. Zhang, C. Han, Z. Cui, W. Li and X. Zhang, *ACS Appl. Mater. Interfaces*, 2019, **11**, 35479-35487.

132. S. Xu, R. Sheng, Y. Cao and J. Yan, *Sci. Rep.*, 2019, **9**, 12486-12494.

133. X. Liu, J. Zhou, Z. Xue, J. Gao, J. Meng, S. Wang and L. Jiang, *Adv. Mater.*, 2012, **24**, 3401-3405.

134. J. -B. Fan, Y. Song, S. Wang, J. Meng, G. Yang, X. Guo, L. Feng and L. Jiang, *Adv. Funct. Mater.*, 2015, **25**, 5368-5375.

135. C. Teng, D. Xie, J. Wang, Y. Zhu and L. Jiang, *J. Mater. Chem. A*, 2016, **4**, 12884-12888.

136. X. Meng, M. Wang, L. Heng and L. Jiang, *Adv. Mater.*, 2018, **30**, 1706634-1706642.

137. U. Manna and D. M. Lynn, *Adv. Funct. Mater.*, 2015, **25**, 1672-1681.

138. L. Zhang, J. Gu, L. Song, L. Chen, Y. Huang, J. Zhang and T. Chen, *J. Mater. Chem. A*, 2016, **4**, 10810-10815.

139. L. Vasquez, L. Campagnolo, A. Athanassiou and D. Fragouli, *ACS Appl. Mater. Interfaces*, 2019, **11**, 30207-30217.

140. J. Dai, L. Wang, Y. Wang, S. Tian, X. Tian, A. Xie, R. Zhang, Y. Yan, and J. Pan, *ACS Appl. Mater. Interfaces*, 2020, **12**, 4482-4493.

141. L. Li, Y. Xiang, W. Yang, Z. Liu, M. Cai, Z. Ma, Q. Wei, X. Pei, B. Yu and F. Zhou, *J. Colloid Interface Sci.*, 2020, **575**, 388-398.

142. Z. Shami, S. M. Amininasab, S. A. Katoorani, A. Gharloghi, and S. Delbina, *Langmuir*, 2021, **37**, 12304-12312.

143. M. Nielsen, P. Jurasek, J. Hayashi and E. Furimsky, *J. Anal. Appl. Pyrolysis*, 1995, **35**, 43-51.

144. S. R. Allayarov, M. P. Confer, S. V. Demidov, U. Y. Allayarova, D. V. Mishenko, E. N. Klimanova and D. A. Dixon, *J. Fluor. Chem.*, 2021, **251**, 109885-109895.

145. S. Kostic, J. K. Berg, K. Casdorff, V. Merk, I. Burgerta and E. Cabane, *Green Chem.*, 2017, **19**, 4017-4022.

146. F. -F. Chen, Y. –J. Zhu, Z. –C. Xiong, L. –Y. Dong, F. Chen, B. –*Q. Lu and R. -L. Yang, ACS Appl. Mater. Interfaces*, 2017, **9**, 39534-39548.

147. F. Behboodi-Sadabad, V. Trouillet, A. Welle, P. B. Messersmith and P. A. Levkin, *ACS Appl. Mater. Interfaces*, 2018, **10**, 39268-39278.

148. R. Gao, S. Xiao, W. Gan, Q. Liu, H. Amer, T. Rosenau, J. Li and Y. Lu, *ACS Sustainable Chem. Eng.*, 2018, **6**, 9047-9055.

149. S. Chen, Y. Song and F. Xu, *ACS Sustainable Chem. Eng.*, 2018, **6**, 5173-5181.

150. Q. Fu, F. Ansari, Q. Zhou and L. A. Berglund, *ACS Nano*, 2018, **12**, 2222-2230.

151. S. Qiu, Y. Li, G. Li, Z. Zhang, Y. Li and T. Wu, *ACS Sustainable Chem. Eng.*, 2019, **7**, 5560-5567.

152. X. Wang, Y. Pan, X. Liu, H. Liu, N. Li, C. Liu, D. W. Schubert and C. Shen, *ACS Appl. Mater. Interfaces*, 2019, **11**, 14362-14367.

153. F. Wu, Ky. Pickett, A. Panchal, M. Liu and Y. Lvov, *ACS Appl. Mater. Interfaces*, 2019, **11**, 25445-25456.

154. T. Suryaprabha and M. G. Sethuraman, *J Mater Sci.*, 2020, **55**, 11959-11969.

155. J. Xu, Y. Zhang, J. He, J. Wu, W. Li, H. Zhang, H. Wang, J. Tu, Y. Zhou, Y. Dong and D. Zhu, *ACS Sustainable Chem. Eng.*, 2021, **9**, 5000-5009.

156. T. Keplinger, X. Wang and I. Burgert, *J. Mater. Chem. A*, 2019, **7**, 2981-2992.

157. E. Abraham, D. E Weber, S. Sharon, S. Lapidot and O. Shoseyov, *ACS Appl. Mater. Interfaces*, 2017, **9**, 2010-2015.

158. A. Baidya, M. A. Ganayee, S. J. Ravindran, K. C. Tam, S. K. Das, R. H. A. Ras and T. Pradeep, *ACS Nano*, 2017, **11**, 11091-11099.

159. Q. Chen, M. Li, F. Zhang, R. Li, G. Chen, S. H. Zhu and H. Wang, *Anal. Methods*, 2016, **8**, 6382-6387.

160. S. Guth, S. Hüser, A. Roth, G. Degen, P. Diel, K. Edlund, G. Eisenbrand, K.-H. Engel, B. Epe, T. Grune, V. Heinz, T. Henle, H. -U. Humpf, H. Jäger, H. -G. Joost, S. E. Kulling, A. Lampen, A. Mally, R. Marchan, D. Marko, E. Mühle, M. A. Nitsche, E. Röhrdanz, R. Stadler, C. van Thriel, S. Vieths, R. F. Vogel, E. Wascher, C. Watzl, U. Nöthlings and J. G. Hengstler, *Arch Toxicol.*, 2020, **94**, 1375-1415.

161. Z. -M. Zhang, Z. -Q. Gan, R. -Y. Bao, K. Ke, Z. -Y. Liu, M. -B. Yang and W. Yang, *J. Membr. Sci.*, 2020, **593**, 117420-117429.

162. K. Zhou, Q. G. Zhang, H. M. Li, N. N. Guo, A. M. Zhu and Q. L. Liu, *Nanoscale*, 2014, **6**, 10363-10369.

163. J. –B. Fan, Y. Song, S. Wang, J. Meng, G. Yang, X. Guo, L. Feng and L. Jiang, *Adv. Funct.Mater.,* 2015, **25**, 5368-5375.

164. J. Yong, F. Chen, Q. Yang, H. Bian, G. Du, C. Shan, J. Huo, Y. Fang and X. Hou, *Adv. Mater. Interfaces* **2016**, *3*, 1500650-1500657.

165. M. V. del Blanco, E. J. Fischer and E. Cabane, *Adv. Mater. Interfaces,* 2017, **4**, 1700584-1700592.

166. J. Li, Z. Zhao, D. Li, X. Tang, H. Feng, W. Qi and Q. Wang, *Appl. Surf. Sci.,* 2017, **419,** 869-874.

167. Y. -H. Lo, C. –Y. Yang, H. –K. Chang, W. –C. Hung and P. –Y. Chen, *Sci. Rep.,* 2017, **7**, 1426-1437.

168. K. Hou, Y. Zeng, C. Zhou, J. Chen, X. Wen, S. Xu, J. Cheng, Y. Lin and P. Pi, *Appl. Surf. Sci.,* 2017, **416**, 344-352.

169. J. Li, C. Xu, Y. Zhang, X. Tang, W. Qi and Q. Wang, *J. Colloid Interface Sci.,* 2018, **511**, 233-242.

170. L. Yan, P. Li, W. Zhou, Z. Wang, X. Fan, M. Chen, Y. Fang and H. Liu, *ACS Sustainable Chem. Eng.,* 2019, **7**, 2064-2072.

171. X. Xie, L. Liu, L. Zhang and A. Lu, *Carbohydr. Polym.,* 2020, **229,** 1154677-1154685.

172. F. Wahid, X. –J. Zhao, Y. –X. Duan, X. –Q. Zhao, S. –R. Jia and C. Zhong, *Carbohydr. Polym.*, 2021, **257,** 117611-117622.

173. Y. Zou, J. Zhao, J. Zhu, X. Guo, P. Chen, G. Duan, X. Liu and Y. Li, *ACS Appl. Mater. Interfaces,* 2021, **13**, 7617-7624.

174. S. K. Hong, S. Bae, H. Jeon, M. Kim, S. J. Cho and G. Lim, *Nanoscale*, 2018, **10**, 3037-3045.

175. W. Chen, P. Zhang, R. Zang, J. Fan, S. Wang, B. Wang and J. Meng, *Adv. Mater.*, 2020, **32**, 1907413-1907420.

176. L. Moity, A. Benazzouz, V. Molinier, V. Nardello-Rataj, M. K. Elmkaddem, P. de Caro, S. Thiébaud-Roux, V. Gerbaud, P. Marion and J. -M. Aubry, *Green Chem.*, 2015, **17**, 1779-1792.

177. M. D. Pluth, R. G. Bergman and K. N. Raymond, *J. Org. Chem.*, 2009, **74**, 58-63.

178. L. -P. Xu, J. Peng, Y. Liu, Y. Wen, X. Zhang Lei Jiang and S. Wang, *ACS Nano*, 2013, **7**, 5077-5083.

179. A. M. Rather and U. Manna, *Chem. Mater.*, 2016, **28**, 8689-8699.

180. V. Kafil and Y. Omidi, *BioImpacts*, 2011, **1**, 23-30.

181. T. Gleede, L. Reisman, E. Rieger, P. C. Mbarushimana, P. A. Rupar and F. R. Wurm, *Polym. Chem.*, 2019, **10**, 3257-3283.

# Chapter 2. Protein Derived Chemically 'Reactive' Interface for Obtaining Durable Superhydrophobicity*

Over the years, the conventional bio-mimicked extreme liquid-repellent interfaces that have been developed using synthetic/non-synthetic polymers adopting various chemistries generally failed to provide a facile avenue for tailoring the water wettability. Hence, chemically 'reactive' interfaces were extended to integrate and modulate different water wettability on the same interface, however, derivation of such interfaces from natural protein is rare in the literature. In this chapter, a naturally abundant, well-known biodegradable protein i.e. bovine serum albumin, was exploited to develop chemically 'reactive' protein nanoparticles following the catalyst-free Michael addition reaction between the amine residues of BSA and an acrylate cross-linker at ambient conditions. The deposition of chemically 'reactive' protein nanoparticles on a fibrous cotton substrate imparted the essential topography and residual chemical reactivity that allowed to associate the desired chemical functional groups. The appropriate post covalent modification of the 'reactive' coating with the selected alkylamines allowed to tailor the water wettability from hydrophobicity, adhesive superhydrophobicity to non-adhesive superhydrophobicity. This protein-derived 'bulk' superhydrophobicity could endure severe repetitive compression, physical abrasions and prolonged exposure (30 days) to chemically contaminated aqueous phases. Moreover, the chemically modulable water wettability was rationally utilized for the controlled and sustained release of the bioactive small molecules that were post loaded onto the fibrous substrate, from days to months. Moreover, the small molecules from the superhydrophobic cotton remained highly bioactive and prevented the proliferation of bacteria.

---

*****A. Shome *et al.*, *Nanoscale Adv.*, 2019, **1**, 1746-1753, A. Shome *et al.*, *ACS Sustainable Chem. Eng.*, 2019, **7**, 7502-7509.

## 2.1. Introduction

Superhydrophobic interfaces have been fabricated over the years through mimicking the structural features and chemical composition of the lotus-leaf for applications in drug delivery, oil/water separation, anti-counterfeiting, self-cleaning etc.[1-3] Superhydrophobicity guided prolonged drug delivery (upto 70 days) was first reported by Grinstaff and co-workers.[4] Electrospun, three-dimensional superhydrophobic meshes made up of a synthetic polymer i.e. poly(Ɛ-caprolactone) and a hydrophobic dopant were fabricated wherein, the drug molecules were pre-loaded into the meshes during fabrication. The presence of metastable trapped air in such 'bulk' superhydrophobic substrates (thickness ~300 µm) was revealed to be responsible for the prolonged drug release owing to the slow penetration of the aqueous phase into the bulk of the substrate. Moreover, it was proven that two-dimensional superhydrophobic interfaces with a 'thin' layer of metastable trapped air at the surface, allowed the rapid infiltration of the aqueous phase leading to the quick displacement of the metastable trapped air layer.[5] In such a scenario, the loaded drugs are expected to be released rapidly, hence, failing to provide a prolonged release profile. Moreover, the pre-loading of drugs limits the concentration of drug loaded without compromising the embedded water wettability and also restricts the loading of a wide range of drugs owing to solubility issues with the reaction solvent. Importantly, the superhydrophobic meshes reported by Grinstaff *et al.* allowed to control the embedded water wettability through optimizing the hydrophobic dopant concentration.[5] But, for practical applicability, a facile approach is required to control the rate of drug release and significantly enhance the drug loading capacity. In that context, chemically 'reactive' interfaces integrated with bio-inspired wettability can prove to be a turning point.

Over the last two decades, catalyst-free, chemically 'reactive' coatings have been explored for various relevant medical applications including patterning of proteins and mammalian cells, developing antibacterial coatings, tissue engineering, drug delivery etc.[6-9] In general, such chemically 'reactive' coatings have been developed through the uncontrolled polymerization of chemical vapor deposited monomers[10-11] and layer-by-layer deposition of non-biodegradable synthetic polymers.[12-14] Levkin *et al.* have exploited catalyst-assisted click chemistry for fabricating chemically 'reactive' interfaces using synthetic polymers for integrating extreme liquid-repellence properties for a wide range of biological applications.[15-18] Lynn *et al*, developed chemically 'reactive' polymeric multilayers of 80 µm thickness exploiting azlactone ring opening chemistry, that were embedded with superhydrophobicity and extended for the post loading and release of drug molecules/peptides for a prolonged (~400 days) period.[19] However, such earlier reported chemically 'reactive' coatings were mostly derived from synthetic and non-biodegradable polymers following complex and tedious fabrication processes that is likely to limit the practical bio-medical applicability. Thus, in this chapter, naturally abundant and well-known biodegradable protein,[20] bovine serum albumin (BSA) was strategically exploited for the facile and scalable synthesis of a durable, deformable, bulk superhydrophobic coating on a fibrous substrate adopting the catalyst-free Michael addition chemistry for the proof-of-concept prolonged drug release demonstrations.

In the recent past, BSA protein was successfully integrated with various nanomaterials for surfactant-free stabilization of colloidal dispersion, improving therapeutic properties, synergistic therapy of tumours, exfoliation of transition metal dichalcogenides, photothermal therapy of cancer cells etc.[21-28] Furthermore, BSA nanoparticles have been widely exploited for therapeutic applications.[25-28] However, reports on the ambient condition chemical modification of the amine residues of BSA to a) cross-link the protein network and b) induct chemical reactivity such that the further post functionalization would be possible, is scarce in literature. In this chapter, the economically feasible and naturally abundant serum protein was successfully exploited for the synthesis of covalently cross-linked and chemically 'reactive' BSA nanoparticles following the catalyst-free Michael addition reaction between the amine residues of BSA and an acrylate cross-linker at ambient conditions. The residual acrylate groups in the BSA nanoparticles were exploited to decorate an abundantly available fibrous substrate i.e. medical cotton, where the chemically 'reactive' BSA nanoparticles provided both the a) essential surface topography and b) residual chemical reactivity for the post covalent modification of the chemically 'reactive' coating on a fibrous substrate. The post modification of the residual acrylates with octadecylamine provided durable, bulk superhydrophobicity which remained unperturbed even after repetitive physical deformations, prolonged (30 days) exposure to UV radiation and chemically contaminated aqueous phases. Moreover, the presence of residual chemical reactivity allowed to tailor the embedded water wettability from hydrophobicity, adhesive superhydrophobicity to non-adhesive superhydrophobicity through the post covalent modification with the desired amine containing small molecules following the catalyst-free Michael addition reaction at ambient conditions. The tailorable water wettability allowed the controlled and sustained release of the drug molecules (aspirin and tetracycline) from days to months that were loaded onto the appropriately post modified fibrous substrates. The tailored water repellence in the appropriately post modified coating remained intact even after post loading with the hydrophilic dye molecules. The released tetracycline continued to display bioactivity against *E. coli* and *S. aureus*.

## 2.2. Experimental Section:

### 2.2.1. Materials Required:

Bovine serum albumin (BSA, MW~66.5 KDa, faction V), dipentaerythritol penta-acrylate (5Acl, MW = 524.51 g/mol), pentylamine, hexylamine, octylamine, decylamine, octadecylamine (ODA), sodium dodecyl sulfate (SDS), dodecyl trimethyl ammonium chloride (DTAB), octanol, fluorescein, tetracycline hydrochloride, aspirin, phosphate buffer saline (PBS) capsules (pH 7.4, 0.01 M), rhodamine 6G and methylene blue, were purchased from Sigma-Aldrich (Bangalore, India). Absolute ethyl alcohol (CAS 64-17-5, Lot No. 17030799) was purchased from TEDIA Company (United States of America). Methanol (CAS 67-56-1) was purchased from RANKEM (Maharashtra, India). Reagent grade THF was purchased from RANKEM (Maharashtra, India). Sodium chloride, magnesium chloride, calcium chloride, magnesium sulphate and sodium hydroxide were purchased from Merck Specialties Private Limited. Hydrochloric acid was purchased from Fischer Scientific (Hyderabad, India). Adhesive tape was purchased from Jonson Tapes Pvt Ltd. New Delhi, India. Calibration weights were procured from Amazon, India. Aluminium wire, tissue and sand paper used for submersion of loaded cotton in PBS buffer was purchased from a local shop in Guwahati city (Assam, India). Sand was collected from a local construction site in IIT Guwahati and rinsed with water, dried before use. River water was collected from Brahmaputra river, Guwahati, Assam.

### 2.2.2 General Considerations:

Glass vials used for preparing the solutions were washed thoroughly with water and acetone prior to use. The Zeta potential (ζ) and dynamic light scattering (DLS) analysis was carried out using Zetasizer Nano ZS90 (model no. ZEN3690). Contact angles were measured using KRUSS Drop Shape Analyser-DSA25 with an automatic liquid dispenser at ambient conditions. The contact angles were measured using 5 µl water droplet at three different locations for each sample. FTIR spectra was recorded with a Perkin Elmer instrument at ambient conditions using KBr pellets. Scanning electron microscope images were obtained using a Sigma Carl Zeiss scanning electron microscope (samples were coated with a thin layer of gold prior to imaging). Fluorescence microscopic images of the superhydrophobic cotton before and after loading of Rh-6G and fluorescein were acquired using an AX10 observer Z1 & AXio Cam MRCS, Carl Zeiss, Germany. Digital images were acquired using a Canon Powershot SX420 IS digital camera. Milli-Q grade water was used for all experiments.

### 2.2.3. Synthesis of Chemically ‘Reactive’ BSA-Protein Nanoparticles:

BSA nanoparticles were prepared by following the de-solvation method. Briefly, 3 mL of ethanol was added dropwise (at the rate of 1 mL/min) to 1 mL (30 mg/mL) of aqueous BSA solution, under constant stirring (600 rpm). Thereafter, the resulting solution was centrifuged down (at 12000 rpm for 15 mins), re-dispersed in 5Acl/methanol (1.325 g in 10 mL) and kept undisturbed for 2 hours. The resulting chemically ‘reactive’ covalently cross-linked nanoparticles were collected through centrifugation, and re-dispersed in methanol. The re-dispersion followed by centrifugation of the 'reactive' nanocomplexes was repeated multiple times (at 12000 rpm for 10 mins) to wash off the loosely bound 5Acl molecules. After washing, the obtained nanoparticles were re-dispersed in Milli-Q water. For the post covalent modification of the chemically 'reactive' covalently cross-linked nanoparticles, the nanoparticles were re-dispersed in a solution of octadecylamine denoted as ODA (5 mg/mL) in THF and kept for 5 hours. The size and surface potential of the nanoparticles was characterized using DLS and the morphology was examined using field emission scanning electron microscopy (FESEM). FTIR spectra were recorded for examining the residual chemical functionalities and post modification of the nanoparticles.

### 2.2.4. Bovine Serum Albumin (BSA) Derived Superhydrophobicity:

To develop a durable and highly compressible superhydrophobic material from a naturally existing ingredient, the following steps were followed: 1) fibrous medical cotton of dimension (1.5 cm × 1.5 cm × 0.5 cm) was dipped in 3 mL aqueous solution of BSA (10 mg/mL) and kept for continuous agitation for 3 hours. 2) To this aqueous BSA solution with the dipped fibrous substrate, 6 ml of ethanol was added dropwise till turbidity appeared indicating the formation of nanoparticles. The whole system was left undisturbed for 1 hour. Subsequently, the nanoparticles deposited cotton was washed thoroughly with ethanol. (3) The BSA nanoparticles deposited cotton was then further treated with 5Acl in methanol (1.325 g in 10 mL) for 3 hours to obtain a chemically 'reactive' fibrous substrate, which was further washed with methanol to remove the loosely adhered 5Acl molecules. (4) To achieve the extreme water repellence property, the BSA nanoparticles derived chemically 'reactive' cotton was treated with ODA solution (5 mg/mL) for 12 hours. Thereafter, the post modified fibrous substrate was washed thoroughly with ethanol and left to air dry. The residual chemical reactivity was characterized via FTIR analysis. For the appropriate and desired post chemical modulations, this chemically 'reactive' BSA coating on the fibrous substrate was exposed to primary amine containing selected small molecules with concentration (30 mg/mL), including pentylamine, hexylamine, octylamine and decylamine. The anti-wetting property of the fibrous substrate treated with amine containing small molecule was examined through visual inspections and contact angle measurements.

### 2.2.5. Physical and Chemical Durability Tests:

Various severe and practically relevant standard physical and chemical durability tests were imposed on the BSA derived superhydrophobic cotton to examine the durability of the embedded extreme water repellence. The details of each of these tests have been explained in detail below:

**2.2.5.1. Compressive Deformation:** The BSA derived superhydrophobic cotton was manually compressed by gradually increasing the strain from 0% to 80% wherein the fibrous substrate restored its shape after releasing the applied manual stress. The manual compressive strain (80%) was repetitively inflicted for 1000 times. The water wettability was examined at regular intervals to account for the durability of the embedded superhydrophobicity in the BSA derived superhydrophobic cotton.

**2.2.5.2. Adhesive Tape Test:** Adhesive tape was fixed onto the BSA derived superhydrophobic cotton and peeled out to arbitrarily expose the interior of the synthesized material. The contact angle and digital images were thereafter acquired to examine the anti-wetting property on the freshly exposed interior of the as-synthesized material.

**2.2.5.3. Sand Paper Abrasion :** Sand paper abrasion was executed by fixing the protein coated cotton (2 cm x 2 cm) onto a glass slide using adhesive tape and thereafter, the top interface was rubbed using an abrasive sand paper in back and forth motion with a 200 g load atop for 5 times. Subsequently, the anti-wetting property on the freshly exposed interior of the substrate was examined using contact angle measurement and digital images.

**2.2.5.4. Finger Wiping Test:** In this durability test, the BSA derived superhydrophobic cotton was immobilized on the microscopic glass slide using adhesive tape and rubbed with the right-hand index finger for multiple (10) times. Thereafter, the anti-wetting property was examined on the abraded surface through visual inspection and contact angle measurements.

**2.2.5.5. Tissue Paper Wiping Test:** Similar to the finger wiping test, the tissue paper wiping test was performed. Here, tissue paper was used instead of finger. Thereafter, the anti-wetting property was examined on the abraded surface through visual inspection and contact angle measurement.

**2.2.5.6. Scissor Cutting Test:** In this test, a thick piece of BSA derived superhydrophobic cotton was cut with a sharp-edged scissor at one end and which was considered as the first cycle of cutting. The anti-wetting property was examined after each cycle of cutting (that exposed a fresh interior interface) through visual inspection and contact angle measurement.

**2.2.5.7. Physical Manipulations:** Bending, creasing, twisting and winding was performed on the BSA coated superhydrophobic cotton for 25 times to examine the durability of the material. The anti-wetting property was further validated after these physical manipulations through contact angle measurements and digital images.

**2.2.5.8. UV Irradiation Test:** The protein derived superhydrophobic cotton was exposed to both short (254 nm) and long (365 nm) wavelengths UV radiation for 30 days. The water wettability was regularly examined through visual inspections and measuring the water contact angles (WCA).

**2.2.5.9. Chemical Durability Tests:** The BSA protein derived superhydrophobic cotton was exposed to various chemically contaminated aqueous media including acidic (pH 1), alkaline (pH 12), anionic (SDS, 1 mM)/cationic (DTAB, 1 mM) surfactant contaminated aqueous phases, artificial sea and river (Brahmaputra, Assam, India) water for 30 days. The artificial sea water was prepared by mixing $MgSO_4$ (0.325 g), $MgCl_2$ (0.226 g), $CaCl_2$ (0.112 g) and NaCl (2.673 g) in 100 mL deionized water in a volumetric flask. The water wettability was examined at regular intervals through visual inspections and measuring the WCA.

### 2.2.6. Post-Loading and Release of Drug Molecules:

Ethanol solvent assisted reversible switching of water wettability was strategically exploited for the post loading of various small molecules with different structures and functions. For the proof of concept demonstration of post loading of small molecules, Rhodamine 6G, fluorescein and methylene blue were the selected dye molecules loaded onto the BSA-derived superhydrophobic (ODA modified) cotton. Thereafter, the selected dye/drug loaded substrates were left to air dry in a dark place. Aspirin and tetracycline hydrochloride were the selected bio-active drug molecules that were loaded from its ethanolic solution onto the protein coated fibrous substrate that was embedded with various water wettability. The deposition of dye/drug molecules were examined through fluorescence images and the anti- wetting property was examined through digital images and contact angle measurements. To perform the release study of the post loaded drug molecules from the ‘reactive’ BSA nanoparticles coated fibrous substrate with tailored water wettability, the drug loaded functional cotton was incubated in PBS buffer (pH = 7.4) at 37°C. The aliquot was collected at different time intervals, and the UV/Vis absorption was recorded at wavelengths 265 nm and 385 nm for aspirin and tetracycline hydrochloride, respectively to determine the concentration of the drug released.

### 2.2.7. Disc-Diffusion Assay:

Disc diffusion method was performed to determine the antibacterial activity of released tetracycline from the matrix. Briefly, *Staphylococcus aureus* MTCC (gram +ve bacteria) 3160 and *Escherichia coli* MTCC 40 (gram -ve bacteria) (MTCC, IMTECH, India) were used for the anti-bacterial assessment. 100 µl of bacterial suspension (108 CFU/ml) was spread over the surface of solidified nutrient-agar plate (Himedia, India) using a sterile glass L-spreader followed by drying for 10 min under sterile laminar air flow. Prior to the test, the concentration of released tetracycline was adjusted to 180 μg/ml. Thereafter, sterile paper discs (6 mm) were soaked in released tetracycline solution followed by placing them on the bacterial lawn. On the other side, freshly added tetracycline having the same concentration (180 μg/ml) and sterile PBS (pH 7.4) were used as positive (+ve) and negative (-ve) control, respectively. Test plates were incubated at 37°C for 48 h. The antibacterial activity of the released tetracycline against the test bacteria was measured as “zone of inhibition” using a Vernier calipers.

## 2.3. Results and Discussions:

### 2.3.1. Synthesis of Chemically ‘Reactive’ BSA Nanoparticles

In the past, BSA nanoparticles were mostly synthesized following the standard de-solvation technique, where the protein nanoparticles were de-solvated from the respective aqueous solution by the addition of ethanol followed by covalent cross-linking of the amine residues with glutaraldehyde molecules.[25-28] However, the glutaraldehyde cross-linking approach limits the further chemical functionalization of the readily ‘reactive’ amines residues at ambient conditions. In this chapter, de-solvated BSA protein nanoparticles (10 mg/mL) were strategically exposed to di-pentaerythritol penta-acrylate (5Acl), instead of glutaraldehyde, to develop chemically ‘reactive’ and covalently cross-linked protein nanoparticles as shown in Figure 2.1A-C. The amine groups of BSA readily underwent Michael addition reaction with the acrylate groups of the cross-linker without the aid of any catalyst at ambient conditions,[29-31] as shown in Figure 2.1D. This cross-linking approach of de-solvated BSA nanoparticles using a multifunctional small molecule (5Acl) imparted residual chemical reactivity to the protein nanoparticles (average diameter: 487 nm ± 16.85 nm, Figure 2.1E). The appearance of the IR peaks at 1410 cm$^{-1}$ and 1736 cm$^{-1}$ corresponding to the asymmetric C-H stretching of β-carbon of the vinyl group and carbonyl stretching revealed the presence of unreacted acrylate groups in the prepared nanoparticles as shown in Figure 2.1F (black). Prior to 5Acl treatment, these IR signature peaks for acrylate were missing in the de-solvated BSA nanoparticles (Figure 2.1F, violet). Hence, these residual acrylate groups provided further scope for post-covalent modification with a primary amine containing small molecule i.e. octadecylamine (ODA). The covalent modification of these ‘reactive’ BSA nanoparticles with ODA resulted in the change of zeta potential from -10.9 mV to -5.03 mV at pH 7. The long hydrocarbon tail of the attached ODA molecules is likely to screen the surface charge of the BSA nanoparticles. Furthermore, the significant depletion in the IR peak intensity for the asymmetric C-H stretching at 1410 cm$^{-1}$ of β-carbon of the vinyl group with respect to the normalized carbonyl stretching at 1736 cm$^{-1}$ strongly suggested the covalent reaction between the chemically ‘reactive’ protein nanoparticles and ODA through the catalyst-free Michael addition reaction at ambient conditions as shown in Figure 2.1F (red). The stretching vibration of carbonyl groups provided an internal reference for the Michael addition reaction as the carbonyl moiety remained unaltered during the course of this mutual reaction between acrylate and amine groups. This FTIR characterization and zeta potential analysis unambiguously revealed the unprecedented synthesis of readily 'reactive' BSA nanoparticles.

### 2.3.2. BSA-derived Chemically 'Reactive' Coating on a Fibrous Substrate and its Post Covalent Modifications

This simple, catalyst-free approach of synthesizing covalently cross-linked and chemically 'reactive' protein nanoparticles was extended for developing nature-inspired durable superhydrophobicity. In the presence of a naturally abundant fibrous substrate i.e. medical cotton, the same de-solvation process was repeated for directly depositing the BSA nanoparticles on the selected fibrous substrate. The deposited BSA protein strongly adheres to the cotton fibres likely through hydrogen bonding, similar to the mussel inspired chemistry.[32] Upon addition of ethanol, (a) BSA nanoparticles were immediately deposited on the fibrous substrate, and (b) upon treatment with 5Acl molecules, a covalently cross-linked, chemically 'reactive', uniform coating of BSA on the selected fibrous substrate was obtained. The smooth fibres of the uncoated i.e. bare cotton (Figure 2.2A-B) were entirely decorated by the

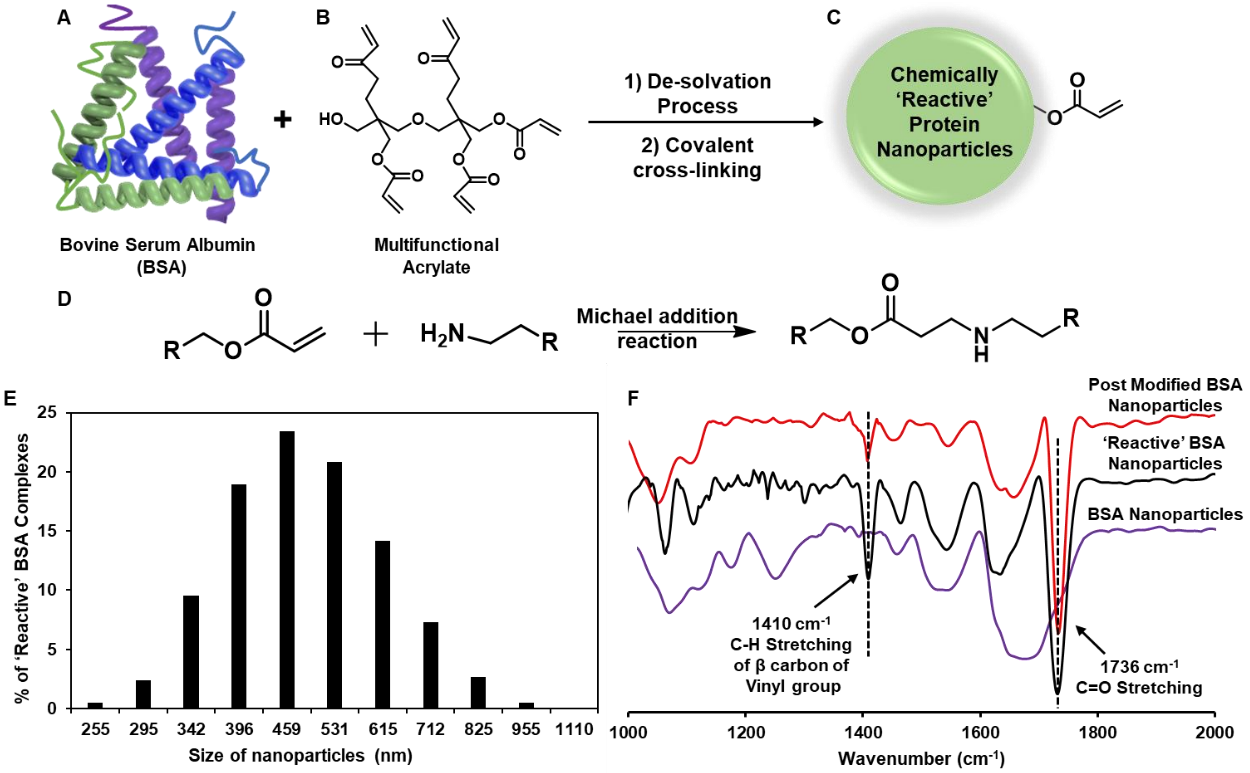

**Figure 2.1.** A-D) Schematic illustrating the formation of the chemically 'reactive' BSA nanoparticles (C) by de-solvating BSA protein (A) from aqueous media using ethanol followed by covalent cross-linking with an acrylate cross-linker (B) through Michael addition reaction (D). E) DLS data depicting the size of the 'reactive' BSA nanoparticles. D) FTIR spectra of BSA nanoparticles (violet) after covalent cross-linking (black) with 5Acl molecules, and after post-modification with ODA (red).

randomly aggregated granular domains of BSA nanoparticles that provided the essential hierarchical topography for achieving extreme water repellence as shown in Figure 2.2C-D. Moreover, this hierarchically featured, hydrophilic (Figure 2.2E-F), chemically 'reactive' BSA coating consists of residual acrylate groups that provided a facile basis for the post covalent modulation with the desired chemical functionalities to embed superhydrophobicity. The presence of residual acrylate groups and the post covalent modification of the chemically 'reactive' BSA coating with a selected alkylamine i.e. ODA were characterized through FTIR analysis as shown in Fig. 2.2G. The appearance of IR peaks at 1410 cm$^{-1}$ and 1710 cm$^{-1}$ that corresponds to the asymmetric C-H stretching of β-carbon of the vinyl group and the carbonyl stretching frequency, suggested the existence of residual acrylate functionalities in the BSA coating. The reduction in the IR peak intensity at 1410 cm$^{-1}$ with respect to the IR peak at 1710 cm$^{-1}$ upon treatment with ODA unambiguously proved the mutual covalent

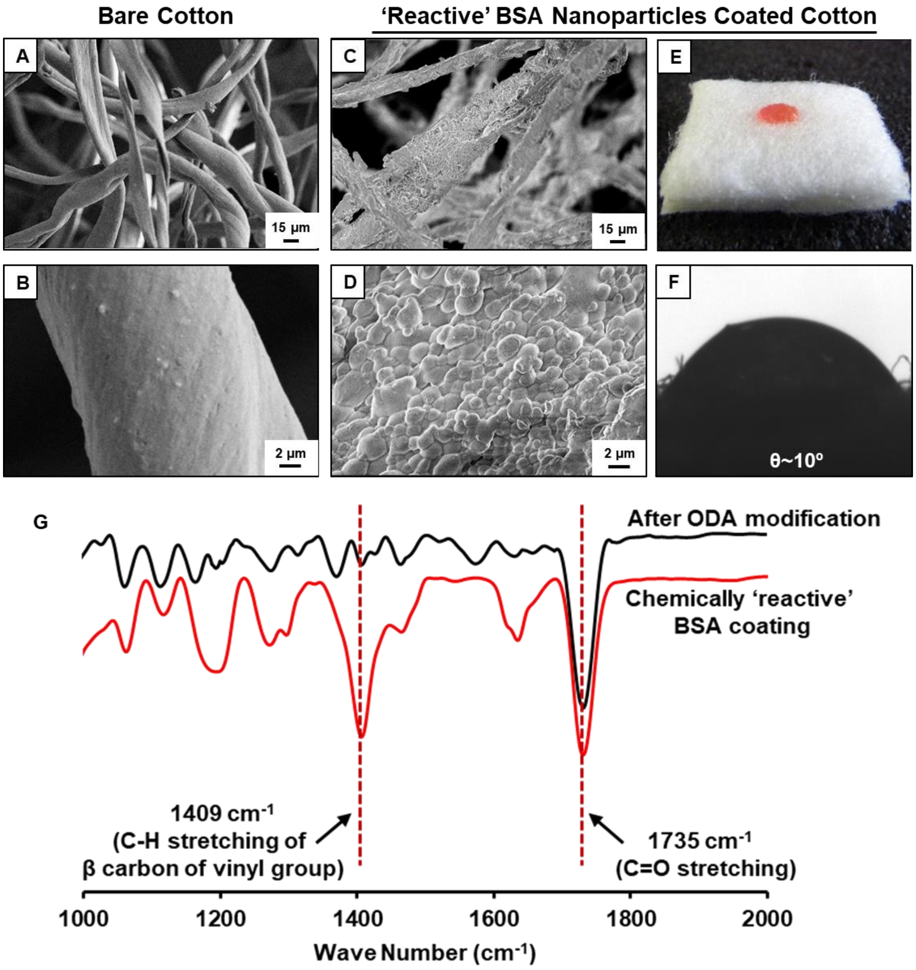

**Figure 2.2.** A-D) FESEM images of bare cotton fibres (A-B) and the 'reactive' BSA nanoparticles coated cotton fibres at low (A,C) and high (B,D) magnifications. E-F) Digital image (E) and static WCA image (F) of a beaded water droplet on the 'reactive' BSA nanoparticles coated cotton. G) FTIR spectra depicting the 'reactive' BSA nanoparticles coating on a fibrous substrate (red) and after its post covalent modification (black) with octadecylamine.

reaction between the primary amine groups of ODA and the residual acrylate groups of the BSA coating (Figure 2.2G, black). The carbonyl peak at 1735 cm$^{-1}$ remained unaffected during the course of the reaction thus, serving as an internal reference.

The water wettability on the ODA post modified ‘reactive’ fibrous coating was investigated wherein a dyed water droplet beaded on the interface with static water contact angle (WCA) ~157° as shown in Figure 2.3A-B. The appearance of a shiny interface (Figure 2.3C) in the superhydrophobic cotton after immersing underwater, suggested the presence of a metastable trapped air layer which contributed to the extreme heterogeneous water wettability. A stream of aqueous phase immediately bounced away from the interface of the BSA protein derived superhydrophobic cotton as shown in Figure 2.3D, revealing the presence of robust, non-adhesive superhydrophobicity. However, below a certain concentration of BSA (10 mg/mL), the deposited coating failed to provide extreme water repellence as showed in Figure 2.3E. The depositing solution with concentrations accounting to 3 mg/mL, 5 mg/mL and 7 mg/mL failed to impart superhydrophobicity as the percentage of ‘reactive’ BSA complexes deposition is exceedingly reduced. Only 1.56 wt%, 3.42 wt%, and 4.31 wt% of ‘reactive’ BSA complexes were deposited for concentrations corresponding to 3 mg/mL, 5 mg/mL and 7 mg/mL respectively, whereas 7% deposition was calculated for 10 mg/mL concentration of BSA. After post-chemical modification with ODA, the BSA derived coating that was prepared with a lower concentration (3 mg/mL) of BSA was found to be hydrophilic (WCA~80°) while the higher concentrations of BSA provided hydrophobic coatings with WCA~115° (5 mg/mL) and ~140° (7

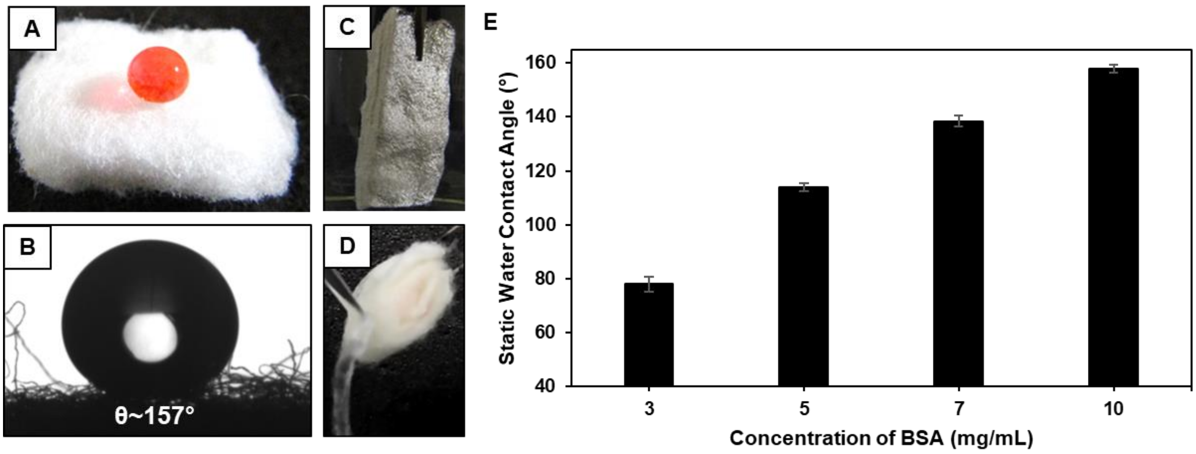

**Figure 2.3.** A-B) Digital images (A) and static WCA image (B) of the beaded water droplet on the ‘reactive’ BSA complexes coated cotton that post modified with ODA to achieve superhydrophobicity. C) Digital image showing a shiny interface on submerging the superhydrophobic cotton under water. D) Digital image illustrating the bouncing of a stream of water from the superhydrophobic cotton. E) Bar diagram accounting for the static WCA of ‘reactive’ BSA nanoparticles coated cotton after post modification with ODA wherein varying concentrations of BSA (3,5,7,10 mg/mL) was used to examine the impact of protein concentration on the resultant water wettability.

mg/mL) as shown in Figure 2.3E. Thus, the concentration of BSA in the deposition solution played an important role for achieving extreme water repellence.

The presence of residual reactivity in the chemically ‘reactive’ BSA coating paved an opportunity to embed a wide range of water wettability following the appropriate post covalent functionalization with the selected amine containing small molecule adopting the Michael addition pathway (Figure 2.4A-B). The post covalent modification of the hydrophilic, chemically ‘reactive’ BSA coating with pentylamine, hexylamine, octylamine and decylamine embedded hydrophobicity (pentyl WCA~125°, hexyl WCA~134°), adhesive superhydrophobicity (octyl WCA~145°) and non-adhesive superhydrophobicity (decyl WCA~151°, ODA WCA~155°) respectively in the BSA derived coating on the fibrous substrate as shown in Figure 2.4C-G and Table 2.1. FTIR analysis confirmed the successful post modification of the ‘reactive’ coating with the various amine containing small

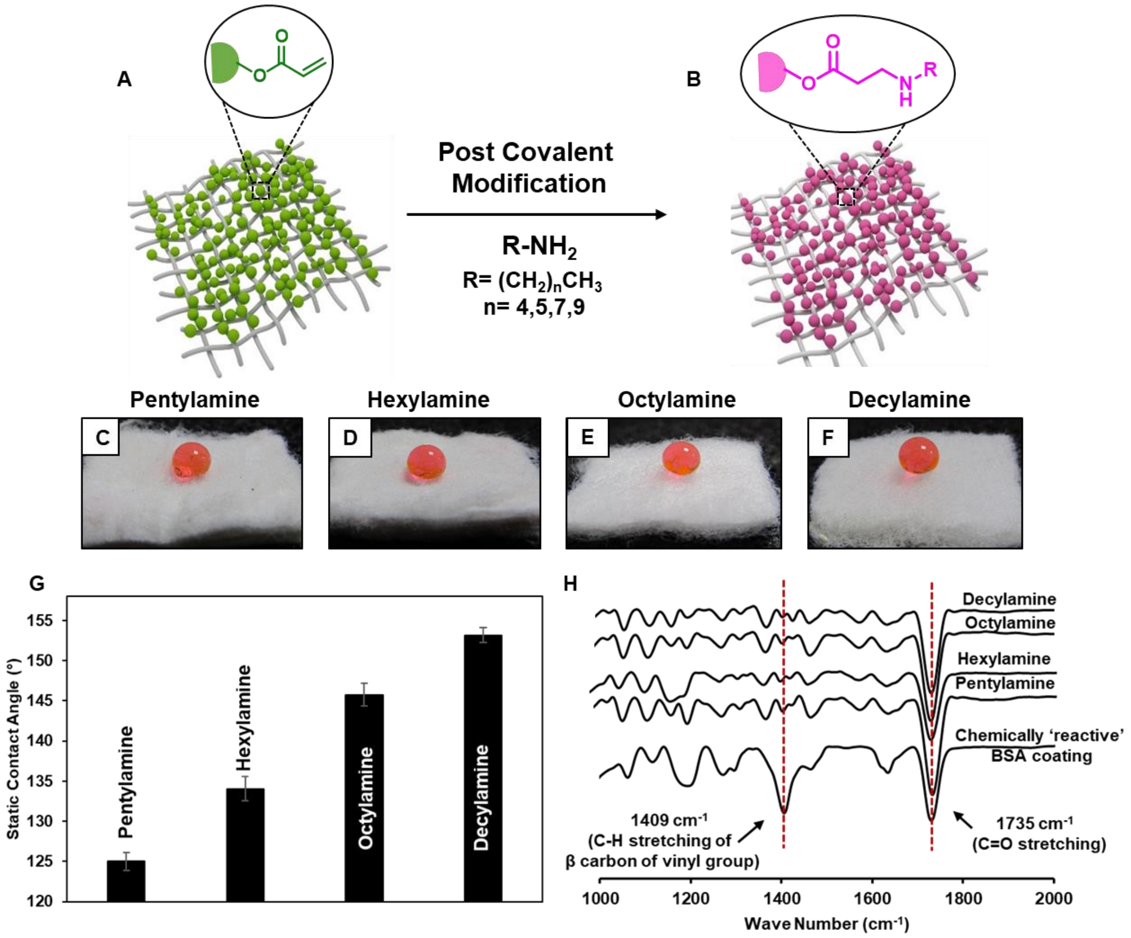

**Figure 2.4.** A-B) Schematic illustrating the post covalent modulation of the chemically ‘reactive’ BSA coating through Michael addition reaction with the selected alkylamines. C-F) Digital images depicting the beaded water droplet on the pentylamine (C), hexylamine (D), octylamine (E) and decylamine (F) post modified ‘reactive’ BSA cotton. G) Bar diagram representing the static WCA on the chemically ‘reactive’ BSA coated cotton after post modification with different alkylamines. N) FTIR spectra of the chemically ‘reactive’ BSA nanoparticles coated cotton after post covalent modification with pentylamine, hexylamine, octylamine and decylamine.

**Table 2.1.** Accounts for the advancing WCA and contact angle hysteresis of the 'reactive' BSA complexes coated cotton after post modification with different alkylamines.

| Different Amine Modifications | Advancing Contact Angle (°) | Contact Angle Hysteresis (°) |
|---|---|---|
| Pentylamine | 130.1 ± 0.5 | 23.4 ± 0.5 |
| Hexylamine | 137.4 ± 0.8 | 19.8 ± 1.1 |
| Octylamine | 145.3 ± 0.6 | 13.5 ± 0.8 |
| Decylamine | 158.6 ± 0.7 | 8.1 ± 0.3 |
| Octadecylamine | 160.3 ± 1.1 | 6.4 ± 0.4 |

molecules. The 'reactive' BSA coating exhibited IR peaks at 1410 cm$^{-1}$ and 1710 cm$^{-1}$ that corresponds to the asymmetric C-H stretching of β-carbon of the vinyl group and the carbonyl stretching frequency as shown in Figure 2.4H. The reduction of the residual acrylate IR peak intensity at 1410 cm$^{-1}$ with respect to the normalized IR peak at 1710 cm$^{-1}$ after modification with the alkylamines, unambiguously suggested the successful post covalent reaction of the chemically 'reactive' acrylates present in the BSA coating with the primary amine groups of the selected alkylamines as shown in Figure 2.4H.

### 2.3.3. Physical and Chemical Durability of the Protein Derived Superhydrophobicity

Various practically relevant, standard physical and chemical durability tests were performed for investigating the robustness of the embedded extreme water repellence in the BSA derived superhydrophobic cotton. First, different physical manipulations, i.e. bending, creasing, twisting and winding, were performed for 25 times on this nature-inspired protein derived fibrous substrate and it was found that the embedded superhydrophobicity remained intact with static WCA above 150° and

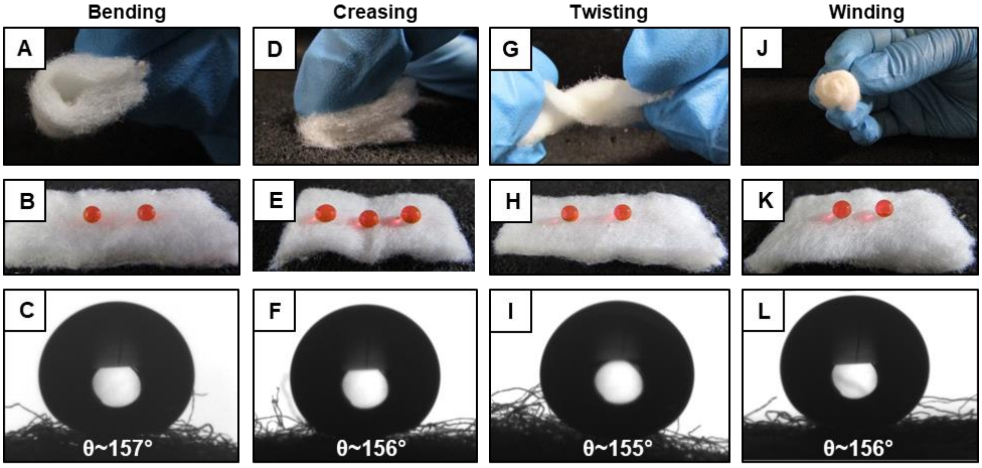

**Figure 2.5.** Digital Images (A-B, D-E, G-H, J-K) and static WCA images (C, F, I, L) demonstrating the impact of various physical manipulations—including bending (A-C), creasing (D-F), twisting (G-I) and winding (J-L) on the BSA coated superhydrophobic cotton.

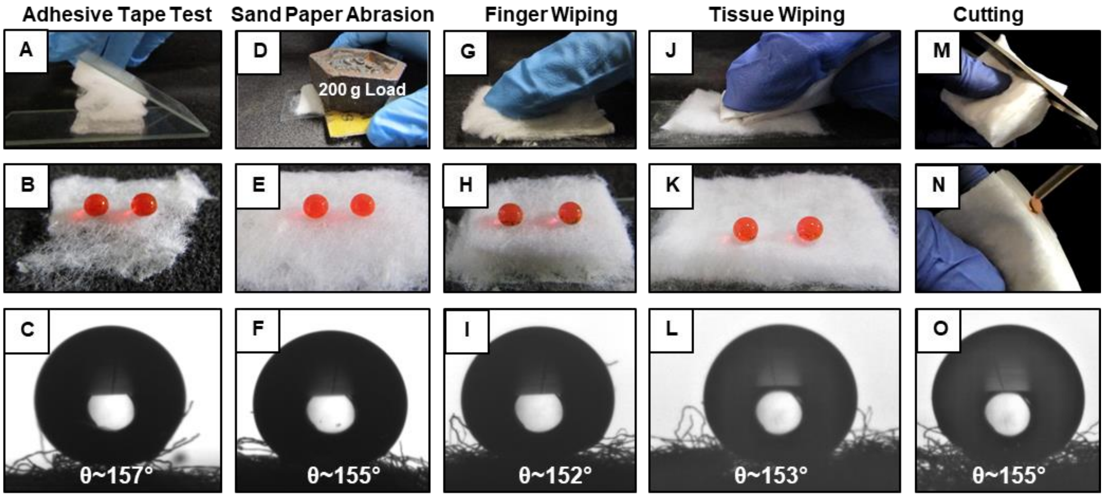

**Figure 2.6.** A-O) Digital images and static WCA images revealing the impact of different physical abrasions on the protein derived superhydrophobic cotton including—adhesive tape test (A-C), sand paper abrasion test (D-F), finger wiping test (G-I), tissue wiping test (J-L) and randomly cutting the substrate (M-O).

contact angle hysteresis below 10° as shown in Figure. 2.5A-L and Table 2.2 (the dynamic water contact angles are provided in table 2.2). Furthermore, severe physical abrasion tests, i.e. adhesive tape test, sand paper abrasion, finger wiping test, tissue wiping test and scissor cutting were also imposed on the synthesized superhydrophobic substrate (Figure 2.6A,D,G,J,M). The random peeling of the adhesive tape from the surface of the cotton exposed the bulk of the substrate (Figure 2.6A-B). During sand paper abrasion, the continuous to and fro rubbing of the sand paper over the fibrous substrate (for 5 times) exposed the interiors of the cotton (Figure 2.6D-E). Moreover, rubbing the protein derived superhydrophobic substrate with the finger (Figure 2.6G-H) and a tissue paper (Figure 2.6J-K) for 10 times exposed a fresh interface for examining the sustenance of the water wettability. Further, during

**Table 2.2.** Accounts for the advancing WCA and contact angle hysteresis of the BSA derived superhydrophobic cotton after various physical abrasions.

| Physical Abrasions | Advancing Contact Angle (°) | Contact Angle Hysteresis (°) |
|---|---|---|
| Bending | 160.6 ± 0.3 | 6.3 ± 0.9 |
| Creasing | 159.2 ± 0.7 | 6.8 ± 1.4 |
| Twisting | 157.1 ± 1.0 | 7.5 ± 0.5 |
| Winding | 158.5 ± 0.8 | 7.1 ± 0.5 |
| Adhesive Tape Test | 157.6 ± 0.9 | 8.1 ± 1.2 |
| Sand Paper Abrasion | 158.3 ± 0.2 | 8.6 ± 0.2 |
| Finger Wiping Test | 159.0 ± 1.3 | 7.4 ± 0.8 |
| Tissue Wiping Test | 157.6 ± 1.1 | 7.7 ± 0.3 |
| Scissor Cutting | 158.8 ± 0.8 | 6.6 ± 0.7 |

scissor cutting test, every cycle of scissor cutting exposed a fresh layer of the bulk (Figure 2.6M-N). Interestingly, even after inflicting these severe physical abrasions, the freshly exposed interiors (bulk) of the fibrous substrate continued to exhibit unperturbed superhydrophobicity with static WCA above 150° and contact angle hysteresis below 10° as shown in Figure 2.6B-C,E-F,H-I,K-L,N-O and Table 2.2. Thus, these demonstrations undoubtedly revealed the presence of abrasion tolerant three-dimensional or bulk superhydrophobicity. The uniformly co-optimized essential topography and chemistry of the BSA derived coating, three-dimensionally was responsible for exhibiting the robust nature-inspired bulk superhydrophobicity.

Next, the as-synthesized superhydrophobic cotton was subjected to manually imposed varying compressive strain and the impact of compressive deformation on the nature-inspired water wettability was examined in detail. The applied compressive strain on the synthesized material could be increased from 0% to 80% gradually without compromising the embedded non-adhesive superhydrophobicity

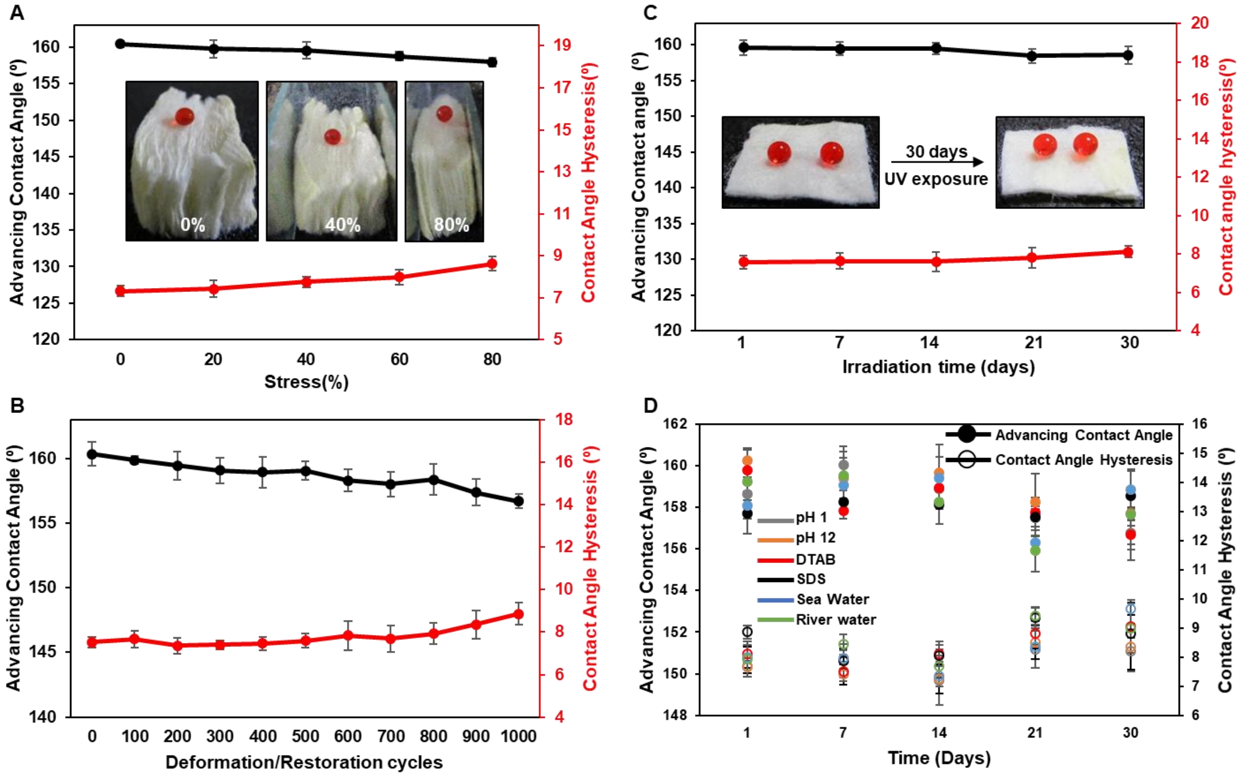

**Figure 2.7.** A) Plot depicting the advancing WCA (black) and the contact angle hysteresis (red) of a beaded water droplet on the superhydrophobic cotton that was manually and gradually deformed up to 80% compressive strain. The inset digital images show the superhydrophobic cotton after applying 0% (left), 40% (middle) and 80% (right) compressive strains. B) Plot illustrating the advancing WCA (black) and contact angle hysteresis (red) of the protein coated superhydrophobic cotton after repetitively squeezing with 80% deformation for 1000 cycles. C) Plot depicting the advancing WCA (black) and contact angle hysteresis (red) of the superhydrophobic cotton that was exposed to UV radiation for 30 days. Inset images of the beaded water droplets on the substrate before and after prolonged UV irradiation. D) Plot showing the impact of various chemically contaminated aqueous phases on the superhydrophobic cotton upto 30 days of exposure.

with advancing WCA above 155° and contact angle hysteresis below 10° as shown in Figure. 2.7A. This BSA protein derived superhydrophobic, spongy cotton was successively squeezed with 80% compressive strain for 1000 times, however, the spongy cotton remained capable of displaying uninterrupted superhydrophobicity with advancing WCA above 155° and contact angle hysteresis below 10° as shown in Figure. 2.7B.

Another important durability test was performed, where the superhydrophobic cotton was kept under UV radiation (at λ ~ 254 nm and 365 nm) for 30 days and the water wettability examined at regular time intervals revealed the presence of unperturbed embedded superhydrophobicity with advancing WCA above 158° and contact angle hysteresis below 10° as shown in Figure 2.7C. The superhydrophobic cotton was also exposed to various practically relevant chemically challenging conditions, i.e. extremes of pH, artificial sea water, river water and surfactant contaminated aqueous phases for 30 days. However, the embedded superhydrophobicity remained intact with advancing WCA above 155° and contact angle hysteresis below 10° as elucidated in Figure. 2.7D. Thus, the unperturbed bio-mimicked water wettability was attributed to the covalent cross-linking and modification of BSA based coating through Michael addition reaction between amines and acrylates.

### 2.3.4. Michael Addition Reaction Assisted Controlled and Sustained Drug Release

In the past, the metastable trapped air that was deemed responsible for conferring the extreme heterogeneous water wettability[34] was smartly exploited for the long-term and sustained release of small molecules, where the external trapped air phase controlled the rate of infiltration of the aqueous phase into the small, hydrophilic molecules loaded superhydrophobic materials.[4-5, 19, 33] However, the past demonstrations on prolonged release of the encapsulated small molecules were performed using synthetic polymers derived bulk superhydrophobic substrates, wherein the drug molecules were preloaded onto the superhydrophobic substrates while material fabrication.[4,33] This pre-loading approach limits the drug loading capacity of the material. Moreover, many of the reported approaches failed to offer a facile, catalyst-free, robust avenue for tailoring the water wettability.[4,19,33] In this context, the protein derived three-dimensional superhydrophobicity with an advanced avenue for tailoring the embedded water wettability, holds potential for the post loading and controllable release of bio-active drug molecules.

For the proof-of-concept demonstration, the superhydrophobic fibrous substrate (Figure 2.8A-B) was post loaded with cationic (Figure 2.8D,J) and anionic dye (Figure 2.8G) molecules from the respective ethanolic solutions with concentrations upto 45 mg of the dye per gram of cotton. This concentration is notably higher than the concentration of dye loaded previously using the pre-loading approach (10

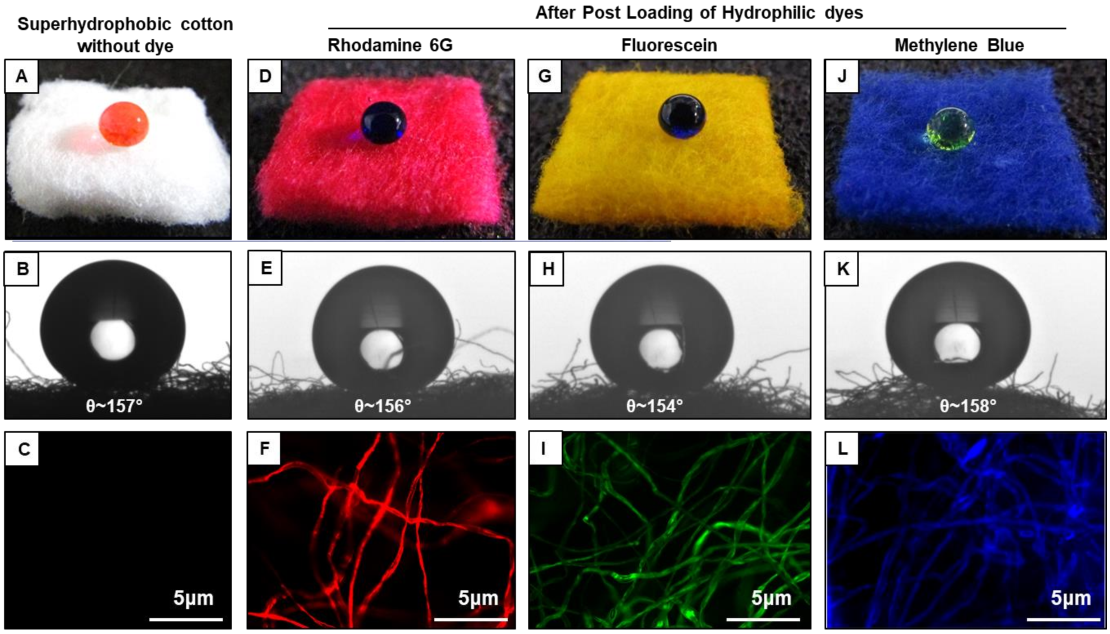

**Figure 2.8.** A-C) Digital image (A) and static WCA image (B) of a non-fluorescent (C) superhydrophobic cotton without any loaded dye. D-L) Digital images and static WCA images of the superhydrophobic cotton that was post loaded with various hydrophilic dyes including rhodamine 6G (D-E), fluorescein (G-H), methylene blue (J-K) and subsequently, the fibres of the cotton exhibited fluorescence as viewed under the fluorescence microscope (F,I,L).

mg/g).[4] Interestingly, even after loading such a high amount of the hydrophilic dye, the embedded superhydrophobicity remained unperturbed with WCA above 150° and contact angle hysteresis less than 10° as shown in Figure 2.8D-E,G-H,J-K and Table 2.3. Fluorescence microscopic image further confirmed the uniform deposition of the selected dye molecules in each and every individual fibre of the fibrous substrate as shown in Figure 2.8F,I,L. Thus, this superhydrophobic fibrous substrate capable of post loading hydrophilic small molecules was utilized for demonstrating the release of bio-active molecules following the same post loading approach.

**Table 2.3.** Accounts for the advancing WCA and contact angle hysteresis of the BSA derived superhydrophobic cotton after loading of various hydrophilic dye/drugs.

| Selected Small Molecules | Advancing Contact Angle (°) | Contact Angle Hysteresis (°) |
|---|---|---|
| Rhodamine 6G | 158.2 ± 0.6 | 6.7 ± 1.2 |
| Fluorescein | 156.6 ± 1.2 | 7.1 ± 0.5 |
| Methylene Blue | 158.9 ± 0.8 | 7.6 ± 1.4 |
| Tetracycline | 159.4 ± 0.4 | 6.8 ± 0.8 |
| Aspirin | 160.7 ± 0.2 | 7.3 ± 0.6 |

Tetracycline, which is a widely used antibiotic,[35] was post-loaded onto the superhydrophobic fibrous substrate following the ethanol assisted reversible switching of extreme water repellence. Loading tetracycline from its ethanolic solution turned the colour of cotton from white to pale yellow, however, the embedded water repellence was restored after air-drying the solvent with static WCA~158° as shown in Figure 2.9A,B and Table 2.3. For every gram of cotton, 15 mg tetracycline could be loaded without affecting the embedded superhydrophobicity which is a) higher than the concentration of drug loaded adopting the pre-loading approach and b) sufficient to exhibit bio-activity. Further, the fluorescence microscopic images revealed the successful and uniform deposition of tetracycline as shown in Figure 2.9C,D. Similarly, aspirin, a well-known anti-inflammatory agent[36] was post loaded onto the medical cotton (15 mg aspirin per gram of cotton) without affecting the embedded superhydrophobicity with static WCA~157° as shown in Figure 2.9E,F and Table 2.3. Thereafter, the tetracycline and aspirin post loaded superhydrophobic cotton was separately exposed to PBS buffer at pH 7.4 and 37 °C for monitoring the release rate of the encapsulated small molecules from the protein derived superhydrophobic cotton. Both tetracycline and aspirin, which are widely different with respect to their structures and functionalities, continued to release over 100 days. Initially, around 30% of the loaded drug was released over 2 days for both tetracycline (Figure 2.9H) and aspirin (Figure 2.9J). Subsequently, this release was sustained for a prolonged duration and it required 110 days for releasing ~90% of the total loaded drug molecules from the as-synthesized superhydrophobic cotton as shown in Figure 2.9G,I. The initial burst release was attributed to the drug molecules present at the

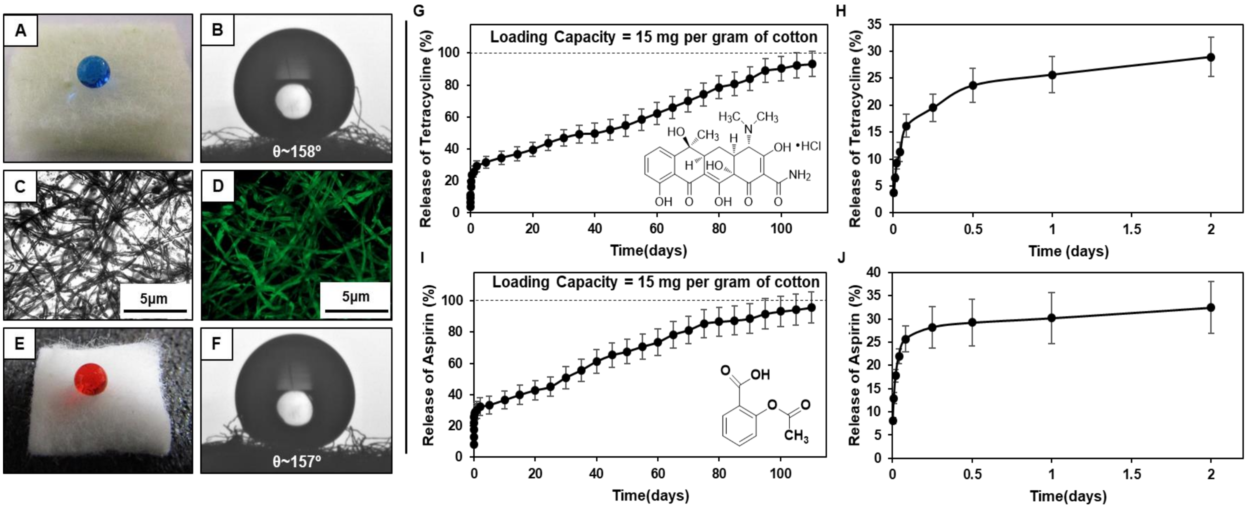

**Figure 2.9.** A-B) Digital image (A) and static WCA image (B) of beaded water droplet on the protein derived superhydrophobic cotton after post loading with tetracycline. C-D) Bright field (C) and fluorescence (D) microscopic images of tetracycline loaded superhydrophobic cotton. E-F) Digital and static WCA image illustrating the beading of water droplet on aspirin loaded superhydrophobic cotton. G-J) Plots illustrating the release of tetracycline (G-H) and aspirin (I-J) from the BSA derived superhydrophobic cotton after 2 days (H,J) and 110 days (G,I) in phosphate buffer at pH 7.4 and 37 °C.

less compact, exposed outer surface, thus leading to the rapid release. However, the slow displacement of the metastable trapped air layer from the bulk of the substrate was responsible for the delayed release profile.

The protein derived chemically ‘reactive’ coating that provided a unique avenue to tailor the water wettability through appropriate post covalent modulation was rationally exploited for controlling the release rate of the encapsulated drug molecules. The pentylamine post modified coating with moderate hydrophobicity (static WCA~125°), released ~64% of the total encapsulated tetracycline over 2 days as shown in Figure 2.10A, and this extent of release was observed to have gradually decreased on increasing the hydrophobicity of the selected fibrous substrate through strategic post modification of the ‘reactive’ coating with hexylamine and octylamine. However, the extent of release over the same duration (2 days) was significantly reduced to ~36% after modifying the chemically ‘reactive’ coating with decylamine molecules. Moreover, only ~62% of the total drug was released over 50 days for the decylamine modified coating as shown in Figure 2.10A,B, whereas the pentylamine modified coating released ~90% of the loaded tetracycline. The pentylamine and hexylamine modified protein derived hydrophobic coatings represent the homogenous model of water wettability that facilitates the faster

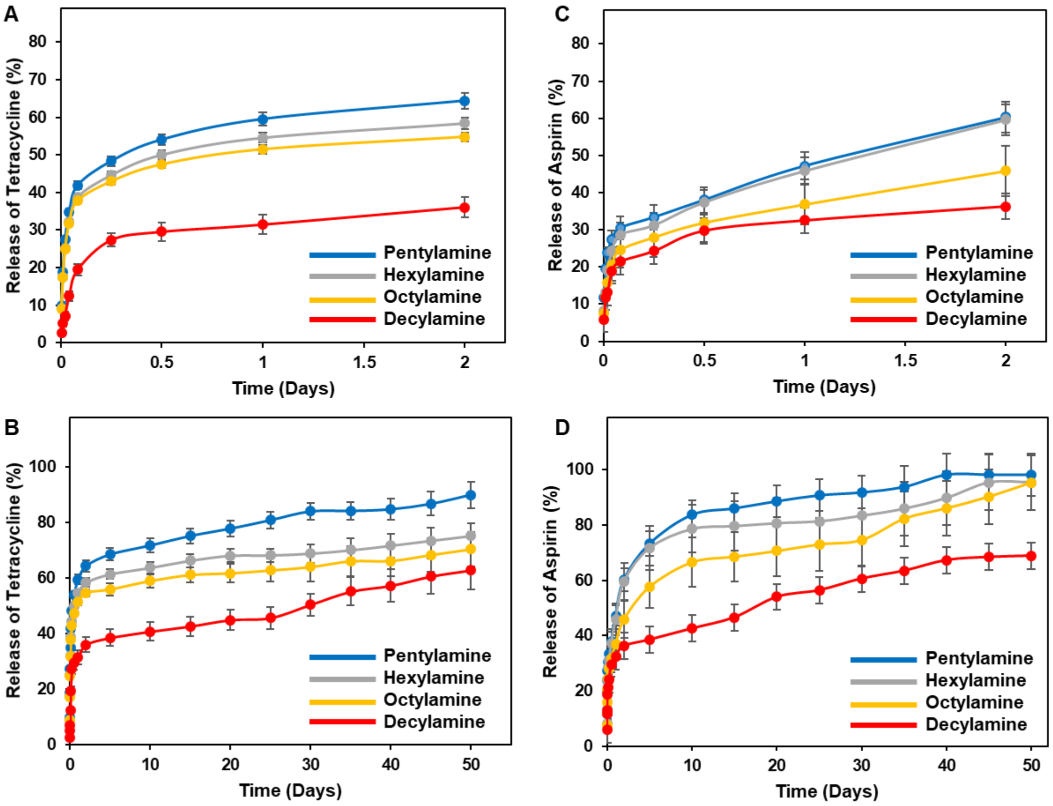

**Figure 2.10.** A-D) Plots illustrating the controlled release of tetracycline (A,B) and aspirin (C,D) from the chemically ‘reactive’ BSA coated cotton after the post modification with selected alkylamines, including pentylamine (blue), hexylamine (grey), octylamine (yellow) and decylamine (red) respectively upto 2 days (A,C) and 50 days (B,D).

ingression of the aqueous phase and subsequently the rapid displacement of the trapped air layer to release the loaded drug molecules in comparison to the octylamine modified substrate present in the Cassie-Wenzel transitional state. However, the decylamine modified substrates represent the heterogeneous model of water wettability where sufficient trapped air is stabilized to a greater extent, thus, inhibiting the rapid ingression of the aqueous phase. Hence, the delayed displacement of the trapped air layer is likely to lead to the prolonged rate of drug release. Similar trend for the release of aspirin was observed for the different alkylamines post modified protein derived coatings as shown in Figure 2.10C,D. Therefore, a facile and catalyst-free post covalent modification approach allowed to alter the water wettability at ambient conditions which subsequently bestowed a novel way to tailor the rate of drug release.

### 2.3.5. Anti-Bacterial Analysis of the Released Drug Molecule

In the previous reports, the drug molecules collected after release from the superhydrophobic substrates continued to exhibit bioactivity. Thus, we also aimed to examine the released drug for its bio-activity in the current work. The antibacterial study of the released tetracycline from the BSA derived superhydrophobic cotton was performed against two different types of bacteria, i.e. *S. aureus*, a Gram-positive bacteria and *E. coli*, a Gram-negative bacteria. To determine the activity of released

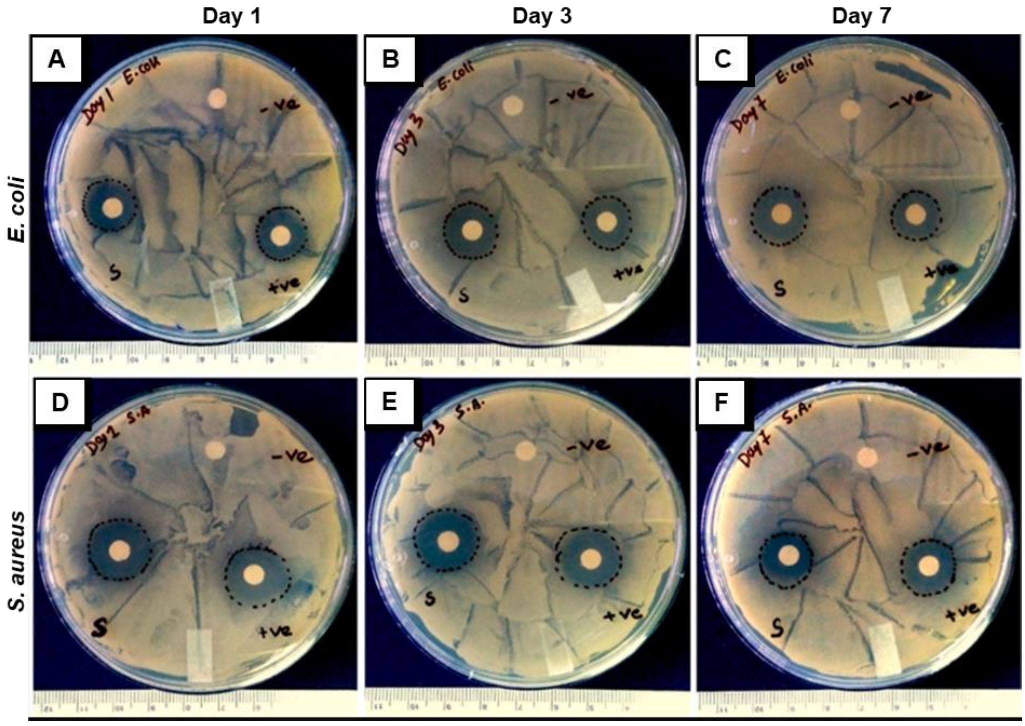

**Figure 2.11.** A-F) Digital images of disc-diffusion assay of released tetracycline (180 µg/mL) from the BSA derived superhydrophobic cotton at different time intervals including 1 day (A,D), 3 days (B,E) and 7 days (C,F) against *E. coli* (A−C) and *S. aureus* (D-F). +ve and −ve control represent as freshly added tetracycline (180 µg/mL) and sterile PBS impregnated discs, respectively. In the digital images, "S" represents "released tetracycline" from BSA derived superhydrophobic cotton.

**Table 2.4.** Measurement of Antibacterial Activity (zone of inhibition) of Releasate Tetracycline against the Test Bacteria (S. aureus and E. coli) Following Disc-Diffusing Method[a]

| Average Diameter of Zone of Inhibition (mm) | | | | | | | | | |
|---|---|---|---|---|---|---|---|---|---|
| | Day 1 | | | Day 3 | | | Day 7 | | |
| **Bacteria** | **Released** | **+ve Control** | **-ve Control** | **Released** | **+ve Control** | **-ve Control** | **Released** | **+ve Control** | **-ve Control** |
| **S. aureus** | **17.5 ± 0.49** | **17.4 ± 0.44** | **N.D.** | **17.5 ± 0.56** | **17.2 ± 0.46** | **N.D.** | **14.9 ± 0.86** | **15.1 ± 0.23** | **N.D.** |
| **E. coli** | **14.4 ± 0.32** | **14.6 ± 0.86** | **N.D.** | **15.5 ± 0.48** | **14.6 ± 0.77** | **N.D.** | **15.42 ± 0.51** | **14.2 ± 0.61** | **N.D.** |

[a] +ve control = tetracycline (180 μg/mL), −ve control = sterile PBS (pH 7.4) and N.D. = not detected.

tetracycline from the superhydrophobic cotton, an inhibition zone of bacterial growth surrounding the discs on nutrient-agar plate was estimated and its activity was compared to the activity of the freshly added tetracycline molecules. In both the cases, the concentration of the tetracycline was 180 μg/mL. In the case of *E. coli*, around 14 mm of inhibition zone was measured, whereas a similar anti-bacterial activity (~17 mm of inhibition zone) in *S. aureus* was recorded for both the released tetracycline and freshly added tetracycline (Figure 2.11A,D). The sterile PBS (negative control) did not show any anti-bacterial activity against the both bacteria. Moreover, the released tetracycline over 3 days and 7 days remained efficient in inhibiting the bacterial growth as shown in Figure 2.11B-F. The overall results indicated that there was no significant difference in inhibition zones by both the released tetracycline and freshly added tetracycline against both bacteria. The details of inhibition zone by both released tetracycline and freshly added tetracycline against both bacteria have been presented in Table 2.4.

## 2.4. Conclusion

In this chapter, a facile and scalable chemical process was introduced for embedding the nature-inspired extreme water repellence on a naturally abundant fibrous substrate utilizing a well-known bio-degradable protein macromolecule. Bovine serum protein was rationally utilized to develop chemically ‘reactive’ nanoparticles following Michael addition reaction that were subsequently deposited on a fibrous substrate for inducting the essential topography and achieving a chemically ‘reactive’ coating. The further post covalent modulation of the ‘reactive’ coating with ODA conferred bio-inspired, bulk superhydrophobicity that sustained repetitive (1000 times) and high (80%) compressive strain, different physical manipulations (e.g. bending, creasing, twisting etc), various physical abrasions (adhesive tape test, abrasive sand paper abrasion etc.), prolonged exposure (30 days) to UV radiation and subjection to various chemically contaminated aqueous phases i.e. extremes of pH, surfactant contaminated aqueous phases, artificial sea water and river water. Furthermore, the residual chemical ‘reactivity’ of the protein coating allowed to tailor the embedded water wettability from hydrophobicity, adhesive superhydrophobicity to non-adhesive superhydrophobicity, following the strategic post covalent modulations with the selected alkylamines. This Michael addition reaction assisted controllable water wettability was successfully extended for the controlled and sustained release of bioactive small molecules. Thus, the current approach has advanced potential for utility as durable coatings on medical implants for inhibiting platelet adhesion, bacterial growth and thrombosis through strategic selection of bio-active molecules.

## 2.5. References

1. Y. Si, Z. Dong and L. Jiang, *ACS Cent. Sci.*, 2018, **4**, 1102-1112.

2. X.-M. Li, D. Reinhoudt and M. Crego-Calama, *Chem. Soc. Rev.*, 2007, **36**, 1350-1368.

3. Y. Sunab and Z. Guo, *Nanoscale Horiz.*, 2019, **4**, 52-76.

4. S. T. Yohe, Y. L. Colson and M. W. Grinstaff, *J. Am. Chem. Soc.*, 2012, **134**, 2016-2019.

5. S. T. Yohe, J. D. Freedman, E. J. Falde, Y. L. Colson and M. W. Grinstaff, *Adv. Funct. Mater.*, 2013, **23**, 3628-3637.

6. B. Sun, X. Liu, M. E. Buck and D. M. Lynn, *Chem. Commun.*, 2010, **46**, 2016-2018.

7. J. Lahann, M. Balcells, H. Lu, T. Rodon, K. F. Jensen and R. Langer, *Anal. Chem.*, 2003, **75**, 2117-2122.

8. R. Manova, T. A. Van-Beek and H. Zuilhof, *Angew. Chem. Int. Ed.*, 2011, **50**, 5428-5430.

9. J. M. Spruell, M. Wolffs, F. A. Leibfarth, B. C. Stahl, J. Heo, L. A. Connal, J. Hu and C. J. Hawker, *J. Am. Chem. Soc.*, 2011, **133**, 16698-16706.

10. H. Nandivada, H.-Y. Chen and J. Lahann, *Macromol. Rapid Commun.*, 2005, **26**, 1794-1799.

11. J. Lahann, M. Balcells, T. Rodon, J. Lee, I. S. Choi, K. F. Jensen and R. Langer, *Langmuir*, 2002, **18**, 3632-3638.

12. M. E. Buck, J. Zhang and D. M. Lynn, *Adv. Mater.*, 2007, **19**, 3951-3955.

13. P. Liu, H. Zhang, W. He, H. Li, J. Jiang, M. Liu, H. Sun, M. He, J. Cui, L. Jiang and X. Yao, *ACS Nano*, 2017, **11**, 2248-2256.

14. A. H. Broderick, S. M. Azarin, M. E. Buck, S. P. Palecek and D. M. Lynn, *Biomacromolecules*, 2011, **12**, 1998-2007.

15. W. Feng, L. Li, X. Du, A. Welle and P. A. Levkin, *Adv. Mater.*, 2016, **28**, 3202-3208.

16. J. Li, L. Li, X. Du, W. Feng, A. Welle, O. Trapp, M. Grunze, M. Hirtz and P. A. Levkin, *Nano Lett.*, 2015, **15**, 675-681.

17. W. Feng, L. Li, C. Yang, A. Welle, O. Trapp and P. A. Levkin, *Angew. Chem., Int. Ed.*, 2015, **54**, 8732-8735.

18. A. I. Neto , K. Demir , A. A. Popova, M. B. Oliveira , J. F. Mano and P. A. Levkin, *Adv. Mater.*, 2016, **28**, 7613-7619.

19. U. Manna, M. J. Kratochvil and D. M. Lynn, *Adv. Mater.*, 2013, **25**, 6405-6409.

20. X. Ma, X. Sun, D. Hargrove, J. Chen, D. Song, Q. Dong, X. Lu, T.-H. Fan, Y. Fu and Y. Lei, *Sci. Rep.*, 2016, **6**, 19370-19382.

21. Y. Yong, L. Zhou, Z. Gu, L. Yan, G. Tian, X. Zheng, X. Liu, X. Zhang, J. Shi, W. Cong, W. Yin and Y. Zhao, *Nanoscale*, 2014, **6**, 10394-10403.

22. M. Tebbe, C. Kuttner, M. Männel, A. Fery and M. Chanana, *ACS Appl. Mater. Interfaces*, 2015, **7**, 5984-5991.

23. A. Aires, S. M. Ocampo, D. Cabrera, L. Cueva, G. Salas, F. J. Teran and A. L. Cortajarena, *J. Mater. Chem. B*, 2015, **3**, 6239-6247.

24. Z. Guo, S. Zhu, Y. Yong, X. Zhang, X. Dong, J. Du, J. Xie, Q. Wang, Z. Gu and Y. Zhao, *Adv. Mater.*, 2017, **29**, 1704136-1704148.

25. L. Xie, W. Tong, Y. Dahai, J. Xu, J. Li and C. Gao, *J. Mater. Chem.*, 2012, **22**, 6053-6060.

26. Y. Huang, Y. Luo, W. Zheng and T. Chen, *ACS Appl. Mater. Interfaces*, 2014, **6**, 19217-19228.

27. P.-L. Lam, S. H.-L. Kok, R. Gambari, T.-W. Kok, H.-Y. Leung, K.-L. Choi, C.-S. Wong, D. K.-P. Hau, W.-Y. Wong, K. H. Lam, Z.-X. Bian, K. K.-H. Lee and C.-H. Chui, *Green Chem.*, 2015, **17**, 1640-1646.

28. H. J. Lee, H. H. Park, J. A. Kim, J. H. Park, J. Ryu, J. Choi, J. Lee, W. J. Rhee and T. H. Park, *Biomaterials*, 2014, **35**, 1696-1704.

29. S. L. Bechler and D. M. Lynn, *Biomacromolecules*, 2012, **13**, 1523-1532.

30. M. R. Weatherspoon, M. B. Dickerson, G. Wang, Y. Cai, S. Shian, S. C. Jones, S. R. Marder and K. H. Sandhage, *Angew. Chem., Int. Ed.*, 2007, **46**, 5724-5727.

31. J. Cao, D. Wang, P. An, J. Zhang and S. Feng, *J. Mater. Chem. A*, 2018, **6**, 18025-18030.

32. H. Lee, S. M. Dellatore, W. M. Miller and P. B. Messersmith, *Science*, 2007, **318**, 426-430.

33. S. T. Yohe, V. L. M. Herrera, Y. L. Colson and M. W. Grinstaff, *J. Controlled Release*, 2012, **162**, 92-101.

34. A. B. D. Cassie and S. Baxter, *Trans. Faraday Soc.*, 1944, **40**, 546-551.

35. E. Scholar, *xPharm: The Comprehensive Pharmacology Reference*, 2007, 1-4.

36. T. Morris, M. Stables, A. Hobbs, P. de Souza, P. Colville-Nash, T. Warner, J. Newson, G. Bellingan and D. W Gilroy, *J Immunol.*, 2009, **183**, 2089-2096.

# Chapter 3. Silk Cocoon derived Superhydrophobicity with Tailorable Mechanical Property*

Naturally derived components have lately gained widespread attention for the eco-friendly design of durable, bio-inspired superhydrophobic interfaces for relevant applications. However, reports on the simultaneous tailoring of the mechanical property as well as the embedded water wettability of the functional materials made out of protein bio-polymers is rare in the literature. Silk fibroin and silk microfibers, both derived from silk cocoon, have been used in the past for prospective biomedical, energy, and environmental applications. However, the chemical modification of silk fibroin-based materials for association of various functionalities has mostly been reported following catalyst-based and complex chemical approaches. In this chapter, both mechanical property and water wettability were tailored in silk microfiber reinforced silk fibroin sponges (SMFRSFSs) through the strategic introduction of β-sheets and a catalyst-free chemical reaction at ambient conditions. The ethanol assisted controlled induction of β-sheets in the silk fibroin skeletal framework of the sponges allowed to modulate the compressive modulus whereas Michael addition reaction between the amine residues of silk and acrylate groups of a multifunctional cross-linker imparted residual chemical reactivity to the sponges. The additional silk microfibre reinforcements aided in self-recovery of the sponges on subjection to compressive deformation. The presence of chemical 'reactivity' in the sponges provided a facile basis for post modification with selected alkylamines to embed a wide range of water wettability from hydrophobicity, adhesive superhydrophobicity to non-adhesive superhydrophobicity without affecting the tailored mechanical property. Furthermore, the embedded 'three-dimensional' superhydrophobicity in the silk-cocoon derived sponges remained intact even after subjection to repetitive compressive deformations for 500 cycles, UV irradiation (for 28 days) and severe physical abrasions. Moreover, the sponges were capable of extremely repelling various chemically contaminated beaded aqueous phases. Thus, such silk cocoon-derived mechanically tailorable and chemically 'reactive' sponges could be useful for various biomedical and energy and environment related applications.

---

***A. Shome *et al.*, *ACS Appl. Mater. Interfaces*, 2021, **13**, 24258-24271.

## 3.1. Introduction

Naturally abundant proteins have emerged as the new greener and sustainable solution for fabricating functional materials to combat the existing challenges related to healthcare, bioengineering, water transport, energy harvesting, etc.[1-13] For instance, silk fibroin derived from silk cocoon has been utilized for applications in anisotropic thermal transport, water transport, bioengineering, energy harvesting, wearable sensors and so on.[1,2,4-6,12] In the previous chapter, ‘reactive’ protein nanoparticles derived controllable water wettability was introduced through the catalyst-free Michael addition reaction at ambient conditions for modulable drug release demonstrations, however, in the previous work, the simultaneous tailoring of the mechanical property and the embedded water wettability was not a feasible option. Thus, in this chapter, the aim was to introduce a distinct approach for tailoring both the mechanical property as well as the water wettability exploiting the different ingredients of silk cocoon.

It has been widely established that the controlled tailoring of chemistry is an important parameter for integrating various functionalities for applications, including association of bioinspired liquid wettability,[14-16] regulation of cellular attachment,[17-19] proliferation and survival,[20] tunable drug delivery, etc.[21-23] In that context, the covalent chemical modification of the amino acid residues of silk fibroin has generally followed the diazonium coupling reaction, copper-catalyzed “click chemistry” to tailor the chemistry of silk fibroin-derived functional materials.[20,24-27] For example, Raynal *et al.* controlled the water wettability of a silk fibroin-derived membrane from ~34 to ~85° through the strategic use of catalyst-assisted click chemistry between azide and alkyne, where the silk membrane was functionalized with alkyne groups following the coupling reaction of diazonium with the tyrosine residues of the protein.[26] In another approach, Zheng *et al.* performed the targeted oxidation of the serine residues of silk fibroin using sodium hypochlorite in a basic environment to investigate the impact of human bone marrow-derived mesenchymal stem cell proliferation and differentiation on the oxidized silk scaffolds.[28] But a catalyst-free approach to optimize the chemistry of silk protein-derived materials at ambient conditions is rare in the literature.

Recently, a few silk-based hybrid materials exhibiting water-repellent behavior have been introduced.[29,30] For example, Maleki *et al.* successfully embedded silk fibroin (SF) into a homogeneous interpenetrated (IPN) network of poly-(methylsilsesquioxane) (PMSQ)−SF to develop a hybrid hydrophobic (water contact angle, WCA~145°) sponge for oil-spill remediation.[29] In another approach, Zhou *et al.* integrated silk fibroin with graphene oxide (GO) for fabricating a hydrophobic coating on the commercially available, synthetic melamine sponge that exhibited WCA~130°.[30] However, these synthetic components-intertwined hybrid designs lack any residual ‘reactive’ functionalities for tailoring the embedded water wettability for relevant applications. Furthermore, entirely silk cocoon-derived 'reactive' spongy/porous materials with an avenue to tailor both the mechanical property and water wettability for realistic, durable applications is yet to be introduced in the literature.

Inspired from the earlier reports, a fundamentally different design has been introduced in this chapter, where the strategic integration of silk fibroin and silk microfibers generated a mechanically tailorable sponge facile while the catalyst-free Michael addition reaction between the amine residues of silk and acrylates of a cross-linker at ambient conditions, allowed to induct chemical 'reactivity' in the silk cocoon-derived functional material as shown in Figure 3.1. The ethanol-assisted controlled tailoring of β-sheets in the silk fibroin skeletal framework allowed to tune the compressive modulus from 90-290 kPa, while the silk microfiber reinforcement further enhanced the mechanical durability of the silk

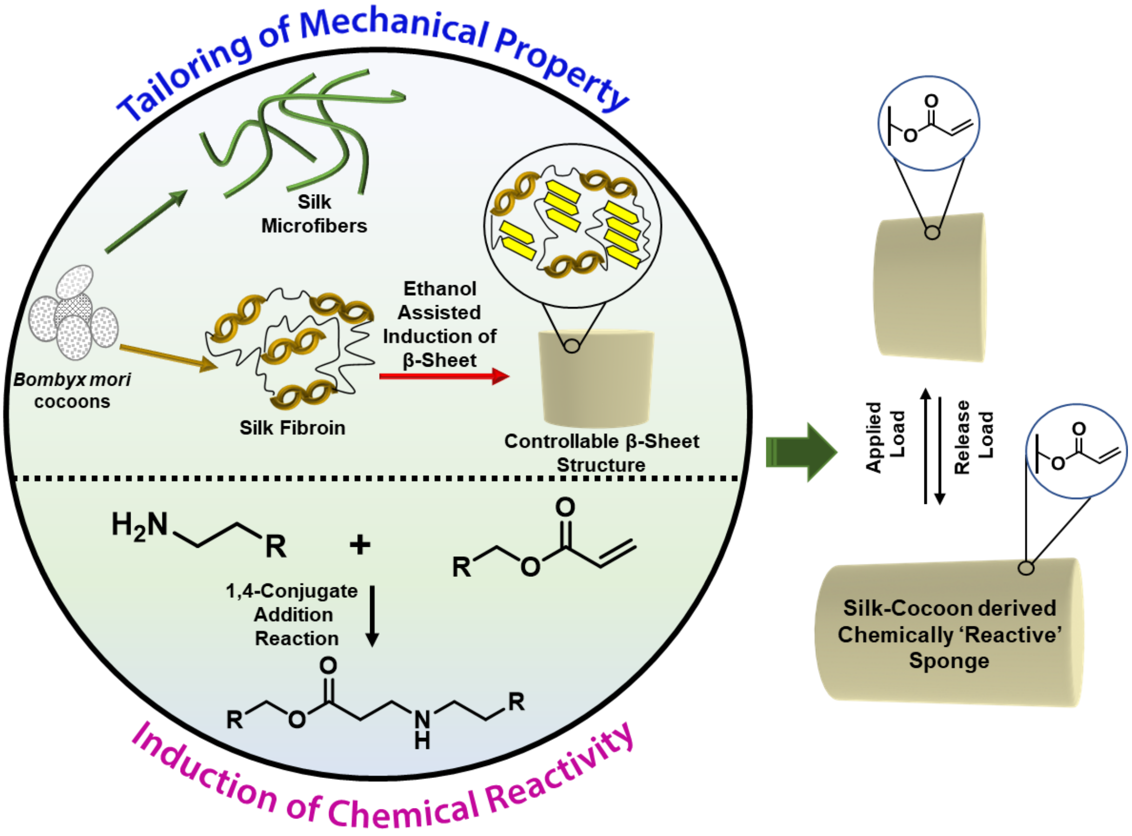

**Figure 3.1.** Silk fibroin, which is predominantly present in α-helical and random coil structures, can undergo transformation to β-sheet structures on exposure to ethanol, thus providing a facile basis to tailor the mechanical property by varying the ethanol concentration. Moreover, the silk microfibers act as reinforcements to enhance the mechanical durability of the fabricated sponges. The presence of amine residues in silk paves way for associating chemical reactivity following the facile, catalyst-free Michael addition reaction between amine residues of silk and a multifunctional acrylate crosslinker at ambient conditions. Thus, variation of the ethanol content provided an avenue to obtain a silk cocoon-derived sponge with tailorable mechanical property, and the existence of unreacted acrylate groups resulted in a chemically 'reactive' sponge. Further, an appropriate post-covalent modification of the residual acrylate groups with selected alkylamines allowed to tailor the embedded water wettability keeping the mechanical property unaltered.

cocoon-derived sponges. The residual 'reactive' acrylate functionalities that rendered the sponges chemically 'reactive' paved an avenue for the facile and rapid covalent post functionalization with different primary amine-containing molecules to embed a wide range of water wettability, including rose petal-inspired adhesive superhydrophobicity (WCA~145°, contact angle hysteresis~13°) and lotus leaf-inspired non-adhesive superhydrophobicity (WCA~160°, contact angle hysteresis~7°). Moreover, the silk cocoon derived superhydrophobic sponges retained the embedded water-repellent property even after exposure to various challenging settings, including repetitive compressive deformation, sand paper abrasion, sand drop test, contaminated aqueous phases (e.g. pH 1 and 12, surfactant water, river water and artificial seawater) and UV irradiation.

## 3.2. Experimental Section:

### 3.2.1. Materials Required:

*Bombyx mori* silk cocoons obtained from local silk farms. Dipentaerythritol penta-acrylate (5Acl, MW=524.51g/mol), rhodamine 6G (CAS No. 989-38-8), sodium dodecyl sulfate (SDS), dodecyl trimethyl ammonium chloride (DTAB), octadecylamine, decylamine, octylamine, hexylamine, pentylamine, butylamine, lithium bromide, sodium carbonate, ethyl alcohol, 12 kDa cut-off dialysis membrane were procured from Sigma-Aldrich (Bangalore, India). Tetrahydrofuran was procured from FINAR. Sodium Chloride, magnesium chloride, calcium chloride, magnesium sulphate, sodium hydroxide was purchased from Merck Specialties Private Limited. Hydrochloric acid was purchased from Fischer Scientific (Hyderabad, India). Calibration weights were purchased from Amazon, India. Sand paper purchased from a local grocery shop in Guwahati. River water was obtained from Brahmaputra river Guwahati, Assam, India. Sand were acquired from a neighboring construction site at IIT, Guwahati and washed thoroughly with water, dried before use.

### 3.2.2. General Considerations:

Glass vials used for preparing the solutions were washed thoroughly with water and acetone prior to use. Contact angles were measured using KRUSS Drop Shape Analyser-DSA25 with an automatic liquid dispenser at ambient conditions. The contact angles were measured using 5 µl water droplet at three different locations for each sample. Digital images were acquired using a Canon Powershot SX420 IS digital camera. Milli-Q grade water was used for all experiments.

#### 3.2.2.1. Field Emission Scanning Electron Microscopy and Pore Size Analysis:

The surface features and microarchitecture of the fabricated sponges were visualized using field emission electron microscope (FESEM, ∑IGMA, Carl Zeiss). The pore size distribution analysis was performed from the acquired micrographs (n = 3) following previous reports[31,32] using ImageJ software

(Wayne Rasband, National Institute of Health (NIH), USA) using nearest distances (ND) plugin by marking at least 35 measurements. ND plugin's algorithm[31,32] is equipped to calculate pore size from 2D cross sections of electron micrographs by defining pore boundaries from 8-bit images using image processing toolkit.

### 3.2.2.2. Infrared Spectroscopy:

Attenuated total reflectance sampling through infrared spectrometer (PerkinElmer Spectrum Two) for the sponges were performed and the spectral measurements averaging 30 scans were recorded between 4000 to 400 $cm^{-1}$ with a resolution of 2 $cm^{-1}$. To understand the secondary structural conformational changes, the Amide-I spectra between 4000 to 400 $cm^{-1}$ were deconvoluted (n = 3) following second order derivatization based on previous reports,[33] and gaussian peaks were fitted and the area under the curve was referenced to quantify the secondary structures of proteins. The band assignments for the fitted peaks were referenced as follows: β- sheets ranging between 1620-1640 $cm^{-1}$; anti-parallel β-sheets ranging between 1670-1695 $cm^{-1}$; α-helices ranging between 1650-1658 $cm^{-1}$; and disordered structures ranging between 1640-1650 $cm^{-1}$.

### 3.2.2.3. Wide angle X-ray Diffraction:

To ascertain the degree of crystallinity of samples, wide angle X-ray diffraction studies (WAXD) were performed using an X-ray diffractometer (Rigaku TTRAX III) with Cu Kα radiation source operating at 50 kV/ 100 mA, where data was recorded between 5° to 50° (2θ angles), with a step size of 0.5° and scan speed of 1°/min.

### 3.2.2.4. Characterization of Mechanical Property:

Unconfined uniaxial compressive loading tests of the sponges were performed using a universal testing machine (UTM, Instron 5944) with a 100 N load cell under non-hydrated ambient conditions. Compressive strength and Young's modulus were evaluated by adopting American Society for Testing and Materials (ASTM) standard - D1621-04a meant for testing rigid cellular foams.[34] Briefly, cylindrical specimens (20 mm height and 20 mm diameter, n = 5) with a crosshead displacement (1 mm/min) and corresponding load values were recorded till 70 % deformation. The stress-strain curves were plotted and compressive strength at 70% strain, Young's modulus (tangential slope of the linear region of the effective stress–strain curves) was determined through Bluehill software (Instron). Similarly, unconfined cyclic loading tests of the cylindrical specimens were carried out for 100 cycles corresponding to 50% deformation strain at loading/ unloading displacements of 10 mm/min. The Young's modulus, effective from the linear region of stress- strain curve from each loading cycle was recorded using the Bluehill software. For tensile testing, ASTM standard ASTMD882−02 was followed, where membrane like formats (rectangular strips (width, length, thickness) 1 cm x 3 cm x 0.1; n = 5) were used and measurements were performed at a displacement rate of 1mm/min until yield. The corresponding stress-strain curves were recorded and the effective tensile modulus, tensile stress at yield and tensile strain yield were calculated using Bluehill software.

### 3.2.2.5. Porosity Measurements:

The porosities of the sponges were calculated using the following widely accepted standard formula,

$$\textbf{Porosity}\ (\%) = \left(1 - \frac{\rho}{\rho_s}\right) \text{x}\ 100$$

where, $\rho$ and $\rho_s$ is the volumetric mass density of the dry sponge and wet sponge respectively.[35,36]

### 3.2.2.6. Statistical Analysis:

The experiments were performed in triplicates unless and otherwise mentioned, and the results are represented as mean ± standard deviation. The data obtained where analyzed for statistical significance using analysis of variance (ANOVA) through Tukey's test (OriginPro8 software) and groups with datasets with $p \leq 0.05$ were considered statistically significant, whereas with $p \leq 0.01$ were considered highly significant.

### 3.2.3. Silk Cocoon derived Sponge Fabrication Process:

### 3.2.3.1. Obtaining Microfibers and Regeneration of Silk Fibroin Solution:

*Bombyx mori* silk cocoons were processed following our reported procedure.[31,33,37] Briefly, cut silk cocoons were degummed in boiling 0.02 M $Na_2CO_3$ aqueous solution for 15 min to remove silk sericin, rinsed thoroughly in ultrapure water and dried to obtained silk fibroin (SF) fibers. SF microfibers were obtained through manual comminution [37-38] which were used as reinforcements for sponge fabrication. Concurrently, dissolution of dried silk fibers was done in 9.3 M LiBr and dialyzed thoroughly against

**Table 3.1.** Illustrates the composition of silk fibroin solution, silk microfibers and volume percent of ethanol used for fabrication of the different variants of silk-cocoon derived sponges.

| Sample | Aqueous regenerated silk fibroin (SF) solution used (w/v)% | SF Microfiber used per mL of SF solution (w/v)% | Ethanol For beta sheet induction (v/v)% |
|---|---|---|---|
| $\mathbf{SMFRSFS_{40}}$ | 1 | 0.02 | 40 % ethanol for 2 h |
| $\mathbf{SMFRSFS_{60}}$ | 1 | 0.02 | 60 % ethanol for 2 h |
| $\mathbf{SMFRSFS_{80}}$ | 1 | 0.02 | 80 % ethanol for 2 h |
| $\mathbf{SMFRSFS_{100}}$ | 1 | 0.02 | 100 % ethanol for 2 h |
| $\mathbf{SFS_{Control}}$ | 1 | - | 100 % ethanol for 2 h |

ultrapure water at ambient conditions using a 12 kDa cut-off dialysis membrane to obtain the regenerated aqueous SF solution.

#### 3.2.3.2. Fabrication of Silk Microfiber Reinforced Silk Fibroin Sponges (SMFRSFS):

The SF microfibers were packed in custom teflon molds and SF fibroin solution was added to fabricate the sponges/membranes. The composition of microfiber and fibroin is listed in Table 3.1. Briefly, for every mL of aqueous regenerated SF solution, 20 mg SF microfiber was packed in cylindrical teflon molds (for sponges/ membranes alike) and the regenerated aqueous SF solution was added on top of the packed column. For fabrication of one cylindrical sponge, 5 mL of the SF solution was used and 100 mg microfiber. Similarly, for preparation of membrane, 3 mL of SF solution and 60 mg microfiber was used. The packing densities were maintained to ascertain uniformity throughout the fabrication process. As control groups, sponge without SF microfiber reinforcements were molded wherein only SF solution was added to these molds denoted as $SFS_{control}$ (Table 3.1).

After addition of silk fibroin solution, the molds were frozen at -20°C overnight and lyophilized using a freeze drier. The content of β-sheet in the freeze-dried sponges were subsequently modulated by varying controlling the ethanol exposure as listed in Table 3.1. After the β-sheet induction, the sponges/membranes were washed thoroughly with ultrapure water and lyophilized again to be used further.

### 3.2.4. Chemically ‘Reactive’ Silk-Cocoon derived Sponge and Post Covalent Modification:

The silk microfiber reinforced silk fibroin sponges were subjected to covalent modification with dipentaerythritol penta-acrylate (5Acl), wherein, the sponges were dipped in an ethanolic solution of 5Acl (1.325 g in 10 mL ethanol) and kept undisturbed for 6 hours followed by thorough washing with ethanol and THF. Thereafter, the covalent post modification of the chemically ‘reactive’ sponges/membranes were carried out with different alkylamines (30 mg/mL) i.e. pentylamine, hexylamine, octylamine, decylamine and octadecylamine (5 mg/mL) in THF and kept for 12 hours undisturbed. Subsequently, the sponges were transferred in THF for washing for half an hour and air dried.

**3.2.5. Physical and Chemical Durability Tests:** Various severe and practically relevant standard physical and chemical durability tests were imposed on the silk cocoon derived superhydrophobic sponges to examine the durability of the embedded extreme water repellence. The details of each of these tests have been explained in detail below:

**3.2.5.1. Compressive Deformation:** The silk microfiber reinforced silk fibroin superhydrophobic sponge ($SCDSHS_{40}$) was manually compressed by gradually increasing the strain from 0% to 50%

wherein the spongy substrate restored its shape after releasing the applied manual stress. The manual compressive strain (80%) was repetitively inflicted for 500 times. The water wettability was examined at regular intervals to account for the durability of the embedded superhydrophobicity in the silk cocoon derived superhydrophobic sponge.

**3.2.5.2. Sand Paper Abrasion :** In sand paper abrasion, a part of the silk microfiber reinforced silk fibroin superhydrophobic sponge ($SCDSHS_{40}$) was manually rubbed with a sand paper in back and forth motion with a 500 g load on top to inflict severe damage to the sponge. Thereafter, the embedded water-repellent property was examined through digital images and contact angle measurements.

**3.2.5.3. Sand Drop Test:** Here, 150 g sand grains were poured from the height of 25 cm onto the surface of the silk microfiber reinforced silk fibroin superhydrophobic sponge ($SCDSHS_{40}$) which was pre-tilted at an angle 45°. Thereafter, the embedded water-repellent property was examined through digital images and contact angle measurements.

**3.2.5.4. Bulk Superhydrophobicity:** The superhydrophobic sponge ($SCDSHS_{40}$) was arbitrarily cut into pieces to expose the interiors of the substrate and subsequently, the embedded water repellence property was examined through digital images and contact angle measurements.

**3.2.5.5. UV Irradiation Test:** *:* $SCDSHS_{40}$ was subjected to both short (254 nm) and long (365 nm) wavelength UV irradiation for 28 days. The embedded extreme water-repellent behavior was examined at regular intervals through digital images and contact angle measurements.

**3.2.5.6. Chemical Durability Tests:** $SCDSHS_{40}$ was subjected to various severe, chemically contaminated aqueous media including acidic water (pH 1), basic water (pH 12), surfactant contaminated water (SDS, 1 mM and DTAB, 1 mM), river water (Brahmaputra river, Guwahati, Assam) and seawater. The artificial sea water was prepared by mixing $MgSO_4$ (0.325 g), $MgCl_2$ (0.226 g), $CaCl_2$ (0.112 g) and NaCl (2.673 g) in 100 mL deionized water in a volumetric flask. The water wettability was examined at regular intervals through visual inspections and measuring the water contact angles.

## 3.3. Results and Discussions:

### 3.3.1. Facile Tailoring of Mechanical Property in the Silk Cocoon-Derived Sponges

The naturally abundant silk cocoon derived silk fibroin and microfibers have been used individually to develop various functional materials for achieving smart solutions to the existing challenges related to environment, energy, and health.[1,2,4-6,12] In the past, different sources of silk fibroin and composites of silks were introduced to tailor the mechanical property.[39-41] It is pertinent to note here that the liquid

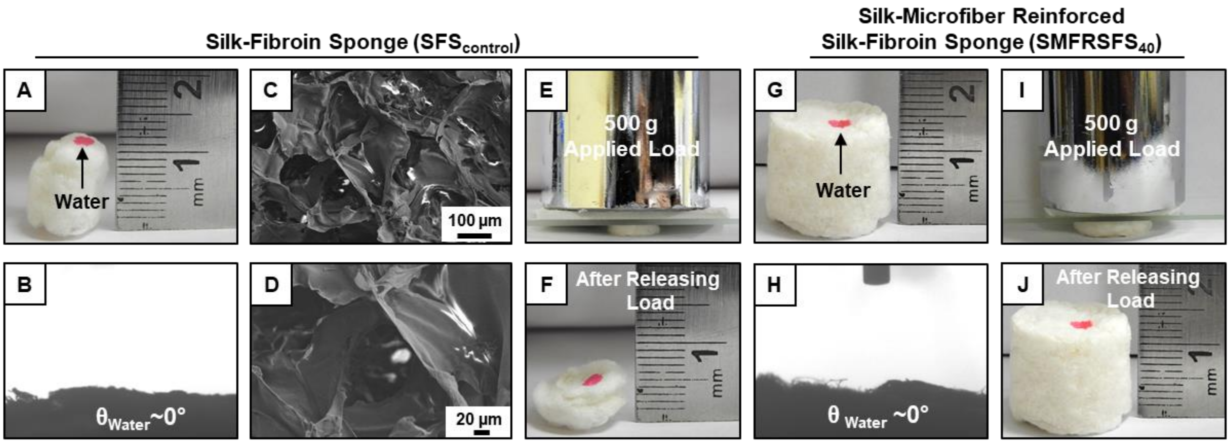

**Figure 3.2.** A-F) Digital images (A,E,F), WCA image (B) of the silk fibroin-derived sponge without any silk microfiber reinforcement (SFS$_{control}$) that exhibits an interconnected porous microarchitecture (C,D). On applying a 500 g external load (E), the sponge underwent permanent deformation and failed to recover its original shape (F). G-J) Digital image (G) and WCA image (H) of the silk microfiber reinforced silk fibroin sponge, SMFRSFS$_{40}$, which was subjected to 500 g external load (I). On releasing the load, the deformed sponge self-recovered its shape (J).

silk fibroin present predominantly in α-helical and random coil conformations, experiences immense shear when spun by silkworms that causes β-sheet crystallization and provides stable microfibers.[42,43] Inspired from this concept of β-sheet microfibers spun by silkworms, the current report on silk microfiber reinforced silk fibroin sponges (SMFRSFSs) involves the controlled tailoring of β-sheet in the silk fibroin skeletal framework to modulate the mechanical property while the additional silk microfiber reinforcement was hypothesized to provide mechanical durability. The silk cocoon-derived sponges were prepared following a facile fabrication strategy, where silk microfibers (0.02 (w/v) %) packed in Teflon molds were cast with 1 (w/v) % aqueous silk fibroin solution, followed by freeze-drying. The ice crystals (acting as porogens) developed during slow freezing (−20°C) sublimate to leave behind pores that were templated around the spaces occupied by ice crystals[44] in the silk microfiber reinforced silk fibroin sponge (SMFRSFS). The controlled exposure of freeze-dried SMFRSFSs to different (40, 60, 80, and 100 v/v%) concentrations of ethanol allowed the tailoring of the β-sheet content (and thereby the mechanical property) in SMFRSFS, which were classified into four different sponges (SMFRSFS$_{40}$, SMFRSFS$_{60}$, SMFRSFS$_{80}$, SMFRSFS$_{100}$), where the subscript denotes the content of ethanol exposure (refer to Table 3.1 for detailed sponge composition).

The porous and highly hydrophilic silk fibroin sponge that was fabricated without any fiber reinforcement (denoted as SFS$_{control}$, Figure 3.2A,B) was compressed with a 500 g external load and it subsequently underwent permanent deformation after removing the applied load, as depicted in Figure 3.2E-F. Field emission scanning electron microscopic (FESEM) images further revealed the existence of a porous microarchitecture without any fibrous morphology (Figure 3.2C,D). However, silk

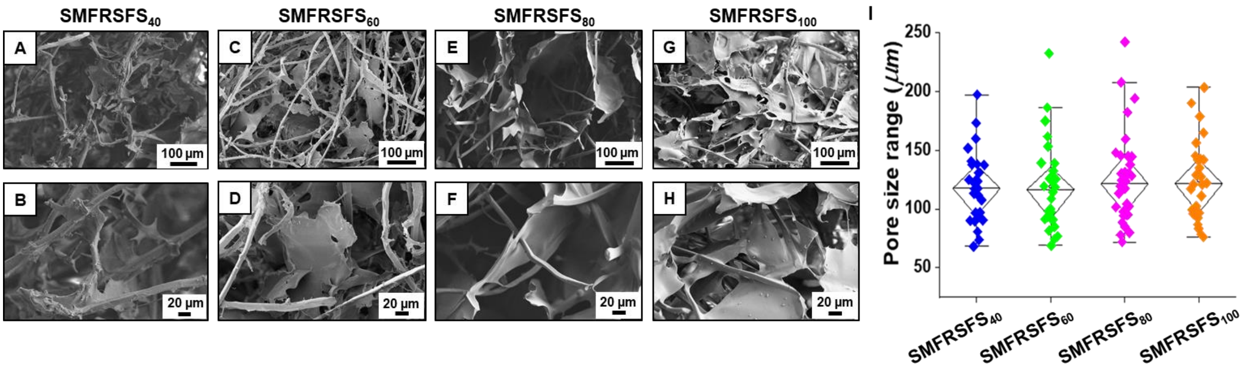

**Figure 3.3.** A-H) FESEM images exhibiting the porous interconnected fibrous network of the sponges including SMFRSFS$_{40}$ (A-B), SMFRSFS$_{60}$ (C-D), SMFRSFS$_{80}$ (E-F), SMFRSFS$_{100}$ (G-H). I) Plot depicting the pore size analysis data for the different beta sheet containing silk-cocoon derived sponges using Image-J plug in.

microfiber (0.02 w/v%) reinforcement provided a mechanically stable and hydrophilic sponge (Figure 3.2G,H), which underwent reversible deformation on compressing with a 500 g load as shown in Figure 3.2I,J. Further, the FESEM images of SMFRSFS revealed a porous interconnected network with fibrous morphology. With an increase in the ethanol content, the pore boundaries appeared to be more defined as in the case of SMFRSFS$_{100}$ while the pore boundaries of SMFRSFS$_{40}$ had fibrillar protrusions, as shown in Figure 3.3A-H, which is plausibly due to the difference in the β sheet content. The average pore size ranged between 120-140 μm (Figure 3.3I), and the porosity of the sponges was found to be 95-96% (Table 3.4). Such topography is important to adopt bioinspired super-water-repellence.

The incorporation of β-sheet conformation was further characterized through attenuated total reflectance Fourier transform infrared (ATR-FTIR) spectral analysis, which revealed that the controlled ethanol treatment caused a secondary conformational change in the silk fibroin skeletal framework. On increasing the content of ethanol exposure, a red shift in amide-I peak from ~1610 to 1640 cm$^{-1}$ was observed, which is indicative of secondary structural transition (from silk-I to silk-II conformation) as shown in Figure 3.4A.[45–47] Further, to get a better insight, these amide-I spectra were deconvoluted (Figure 3.5A-D), band assignments were made, and the secondary structures were quantified from the area-normalized fitted peaks. It was seen that with an increase in the ethanol content (from 40% to 100%), the β-sheet content increased (SMFRSFS$_{100}$>SMFRSFS$_{80}$>SMFRSFS$_{60}$>SMFRSFS$_{40}$), where the total β-sheet content for SMFRSFS$_{40}$ and SMFRSFS$_{100}$ were estimated to be ~20 and ~84%, respectively (Table 3.2). It is important to note here that even though SFS$_{control}$ exhibited a higher percentage of β-sheet (~58%, exposure to 100 v/v% ethanol) compared to SMFRSFS$_{40}$ (~20%) as tabulated in 3.2, the absence of microfiber reinforcement led to poor mechanical recovery of the sponge as discussed already in Figure

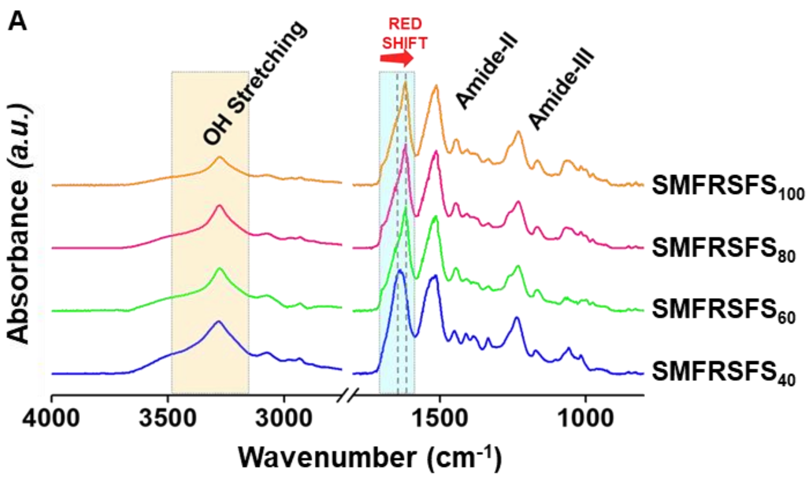

**Figure 3.4.** A) ATR-FTIR spectra of the silk microfiber reinforced silk fibroin sponges (SMFRSFS) that were fabricated following exposure to different concentrations of ethanol, where the subscript in SMFRSFS depicts the v/v % ethanol.

3.2E-F. Thus, the controlled tailoring of β-sheet would allow to modulate the mechanical property, but the fiber reinforcement is important for the mechanical recovery of the sponges. Moreover, when SFS$_{control}$ is untreated with ethanol (Figure 3.6A,C), then it exhibits predominantly α-helical/disordered structures, as tabulated in Table 3.2. The presence of only α-helical/disordered structures is similar to liquid SF present in silkworms prior to spinning in the glands.[43] The spinning of this α-

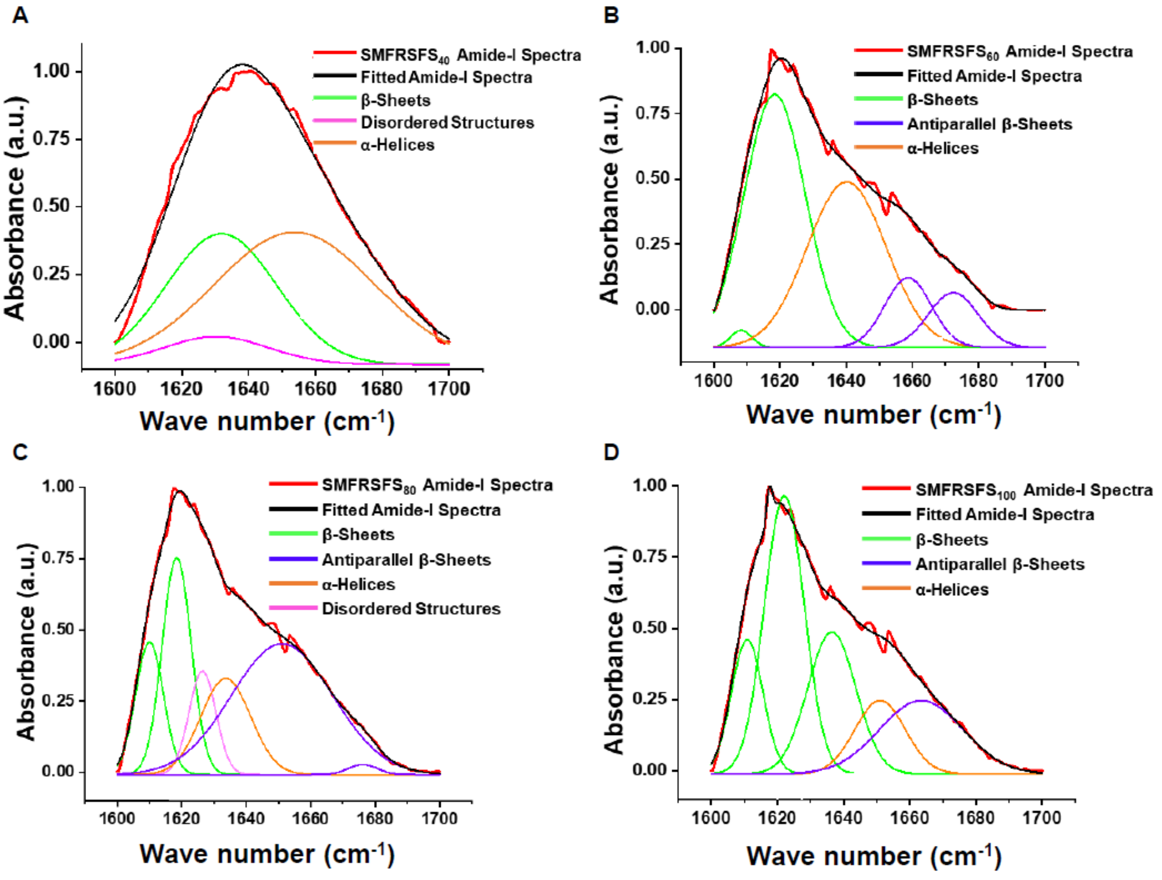

**Figure 3.5.** A-D) Deconvoluted secondary spectra of Amide-I peaks of SMFRSFS$_{40}$ (A), SMFRSFS$_{60}$ (B), SMFRSFS$_{80}$ (C) and SMFRSFS$_{100}$ (D).

**Table 3.2.** Accounts for the percentage of secondary structures present in the silk-cocoon derived sponges determined through the deconvoluted spectra.

| Secondary structures | Percentage (%) | | | | | |
|---|---|---|---|---|---|---|
| | SMFRSFS$_{40}$ | SMFRSFS$_{60}$ | SMFRSFS$_{80}$ | SMFRSFS$_{100}$ | SFS$_{Control}$ | SFS$_{Control}$ w/o Ethanol Treatment |
| α-helices | 60 ± 1.6 | 35.4 ± 2.1 | 22 ± 1.1 | 16.1 ± 0.7 | 32.8 ± 1.4 | 20 ± 0.8 |
| Disordered structures | 20 ± 0.8 | - | 7.7 ± 0.6 | - | 9.1 ± 0.5 | 68 ± 2.0 |
| Total Beta Sheet Content | 20 ± 1.5 | 65.0 ± 0.7 | 70.3 ± 2.4 | 83.9 ± 1.4 | 58.1 ± 1.1 | 12 ± 1.3 |

helical/disordered conformational liquid SF generates stable microfibers with β-sheet conformation. Thus, it can be concluded that ethanol treatment indeed induces the β-sheet conformational changes. To reaffirm the β sheet crystallinity within the sponges, wide-angle X-ray diffraction analysis was performed (Figure 3.7A) to assess the crystallinity (imparted due to β-sheets) of the sponges. Ethanol treatment induced a conformational change to silk-II, where the β-sheets are predominated as characterized by the appearance of two broad peaks in the range of 2θ (angles) from 5 to 35° (Figure 3.7A).[46] It was seen that with an increase in ethanol treatment, from SMFRSFS$_{40}$ to SMFRSFS$_{100}$,

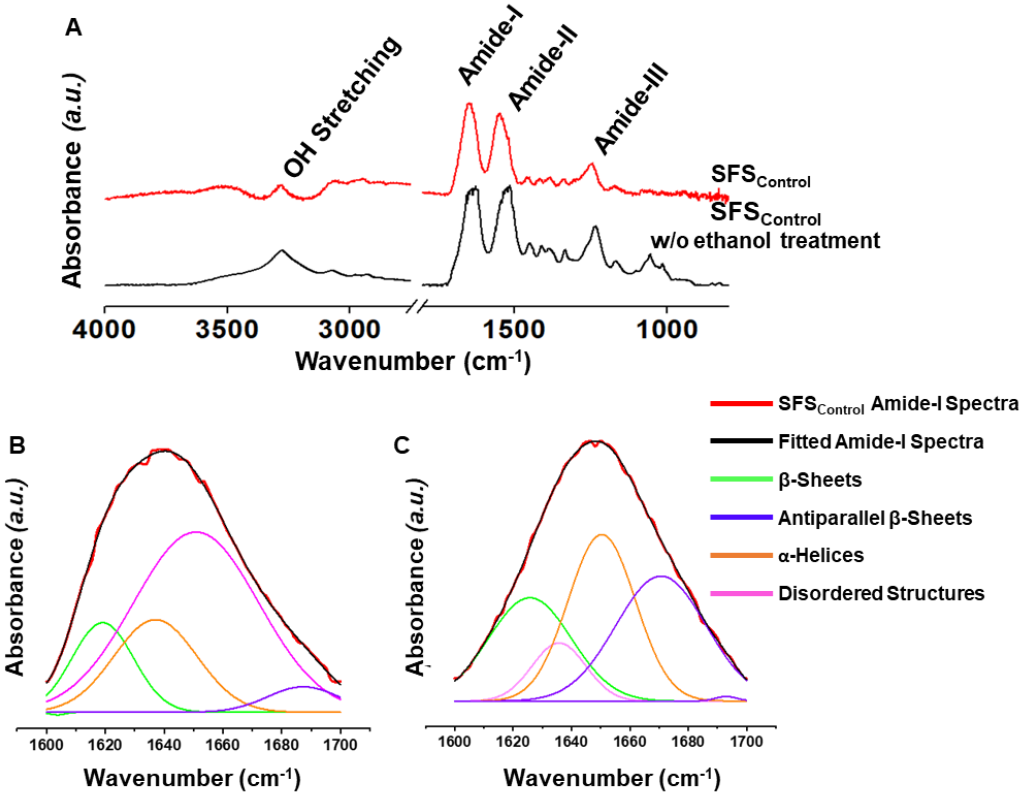

**Figure 3.6.** A) ATR-FTIR Spectra of the silk fibroin sponge control group (SFS$_{control}$) which is devoid of any fibre reinforcement (red) and SFS$_{control}$ which was untreated with ethanol (black). B-C) Deconvoluted secondary spectra of Amide-I peaks of SFS$_{control}$ (B) and SFS$_{control}$ which was untreated with ethanol (C).

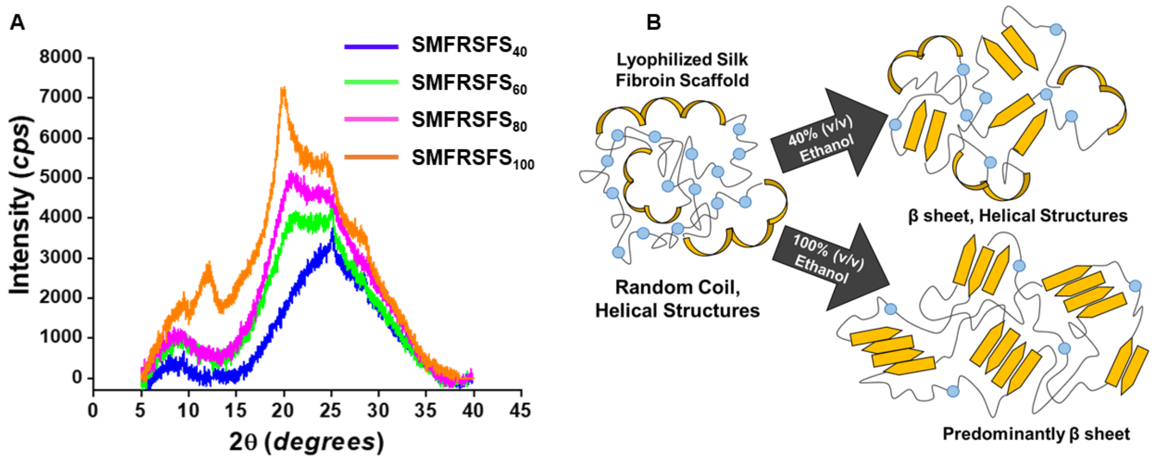

**Figure 3.7.** A) Wide-angle X-ray diffraction analysis showing increasing crystallinity in the order SMFRSFS$_{100}$ > SMFRSFS$_{80}$ > SMFRSFS$_{60}$ > SMFRSFS$_{40}$. B) Schematic representing the effect of increasing ethanol treatment on removing water molecules (which acts as plasticizers, depicted as blue spheres) and promoting helix-helix interaction, thus increasing the β-sheet content from SMFRSFS$_{40}$ to SMFRSFS$_{100}$.

these peaks became more intense suggesting the increase in crystallinity attributed to the increase in β-sheet structures. The ethanol exposure altered the hydration state in the sponges, where bound water molecules acting as plasticizers between the silk fibroin chains are displaced (Figure 3.7B). This displacement of water molecules helps in helix−helix interaction and promotes β-sheet crystallization,[46,48] thus, an increased ethanol content drives this structural transition by altering the hydration state.

The compressive stress/strain analysis revealed two important aspects of the current design: (1) the ethanol assisted controlled modulation of β-sheet conformation in the silk fibroin skeletal framework allowed to tailor the mechanical properties of the sponges, as shown in Figure 3.8A, (2) the incorporation of silk microfibers within the silk fibroin network improved the mechanical stability (self-recovery) as compared to the control sponge, SFS$_{control}$ that is devoid of fiber reinforcement as shown in Figure 3.8B-F. The increase in the β-sheet content led to an increase in the compressive modulus as observed for the prepared sponges in the order SMFRSFS$_{40}$< SMFRSFS$_{60}$< SMFRSFS$_{80}$<SMFRSFS$_{100}$. Thus, the ethanol assisted induction of β-sheet allowed to tailor the compressive modulus from 90-290 kPa as shown in Figure 3.12A (red bar). Furthermore, the ability to retain the tailored mechanical properties after repeated compressive deformations (100 cycles with 50% strain) was investigated (Figure 3.8B-F). It was found that all the fiber-reinforced sponges retained their elastic region with good recovery throughout the 100 cycles (under the applied 50% compressive strain) as illustrated in Figure 3.8C-F. However, recovery for SFS$_{control}$ was poor (as indicated by the red arrow, Figure 3.8B), indicative of plastic deformation under the subjected strain. Thus, both fiber reinforcement and controlled modulation of β-sheet conformation are important

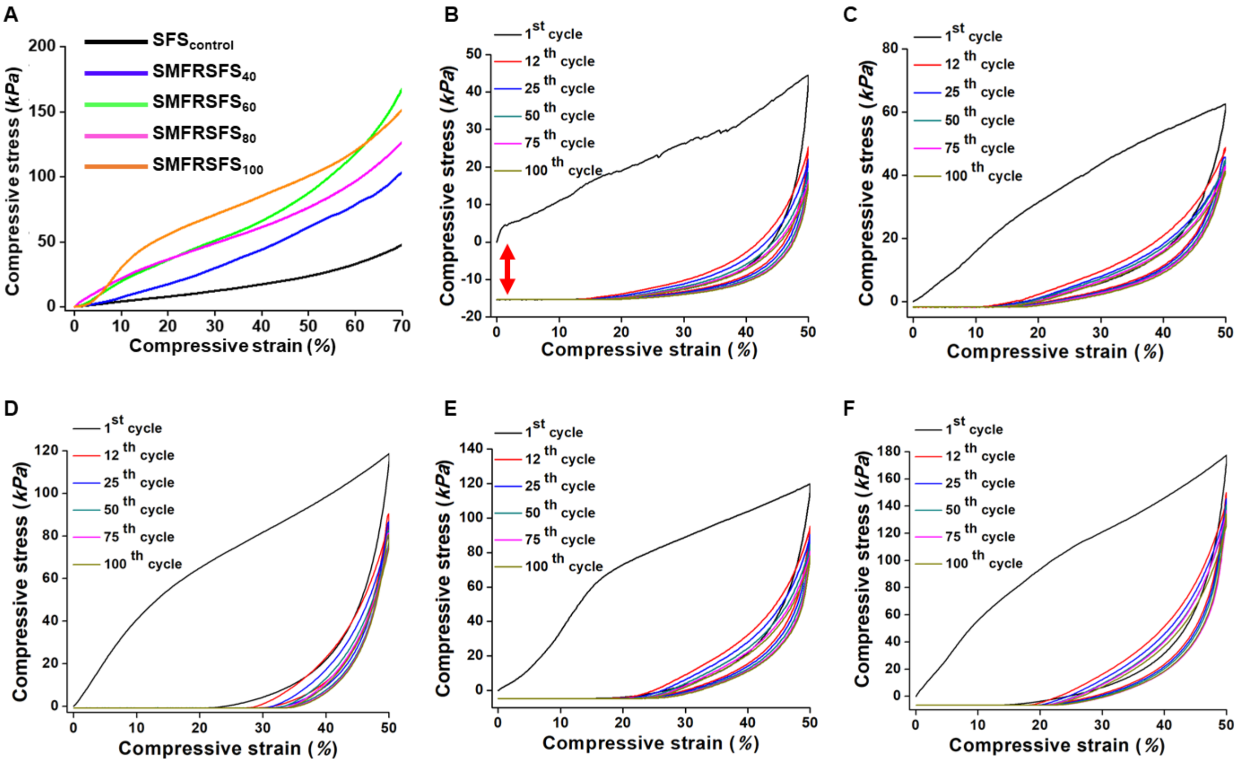

**Figure 3.8.** A) Compressive stress-strain plot for the silk microfiber reinforced silk fibroin-derived sponges. B) Cyclic mechanical properties of the silk fibroin control sponge, where the red arrow denotes the permanent deformation of the sponge after the 1st compression cycle. C-F) Cyclic stress-strain analysis of the silk microfiber reinforced silk fibroin sponges $SMFRSFS_{40}$ (C), $SMFRSFS_{60}$ (D), $SMFRSFS_{80}$ (E), $SMFRSFS_{100}$ (F) conducted for 1st, 12th, 25th, 75th and 100th cycles.

parameters to obtain the desired mechanical property and recovery of the shape of the sponges after incurring physical deformation.

### 3.3.2. Design of Chemically 'Reactive' Silk Cocoon-Derived Sponges Followed by Integration of Various Water Wettability

In the past, the covalent chemical modification of silk fibroin has been strategically performed adopting various chemistries. The process of altering the chemical functionalities of silk fibroin is mostly achieved through modification of the tyrosine amino acid residues following the diazonium coupling reaction,[20,25–27] oxidation of serine,[28] and condensation of the hydroxyl residues of silk.[29] Furthermore, the diazonium salt modification approach was adopted to impart reactivity to the silk fibroin substrates, which were further exploited for post modification following the catalyst-assisted azide–alkyne click chemistry.[25,26] Recently, Sun *et al*. exploited the amine and hydroxyl residues of a silk fibroin derived nanofibrous membrane for modification with pyro-mellitic dianhydride following the acid-catalyzed anhydride ring-opening reaction.[49]

In this chapter, the catalyst-free Michael addition reaction at ambient conditions[50-51] was exploited for the facile tailoring of chemistry in a silk cocoon-derived functional material while keeping the mechanical property of the substrate unaltered. In the current design, the amine residues of the silk cocoon-derived sponges were covalently modified with 5Acl, a penta-acrylate cross-linker following the Michael addition as depicted in Figure 3.9A-B. The progress of the reaction was monitored through ATR-FTIR analysis, as shown in Figure 3.9D. The ATR-IR spectrum of 5Acl (blue) displayed the characteristic acrylate signatures at 1408 cm$^{-1}$ and 1726 cm$^{-1}$, which corresponds to the C-H deformation of β carbon of the vinyl group and carbonyl stretching, respectively (Figure 3.9D, blue). Prior to 5Acl treatment, such IR signatures for acrylates were not observed for the silk cocoon-derived sponge (Figure 3.9D, green). During the Michael addition reaction between the amine residues of silk sponge with the acrylate cross-linker (5Acl), the IR signature at 1408 cm$^{-1}$ underwent depletion (Figure 3.9D, red), suggesting the selective consumption of the vinyl moiety (~29%) with respect to the carbonyl signature at 1726 cm$^{-1}$, which served as an internal standard to examine the progress of

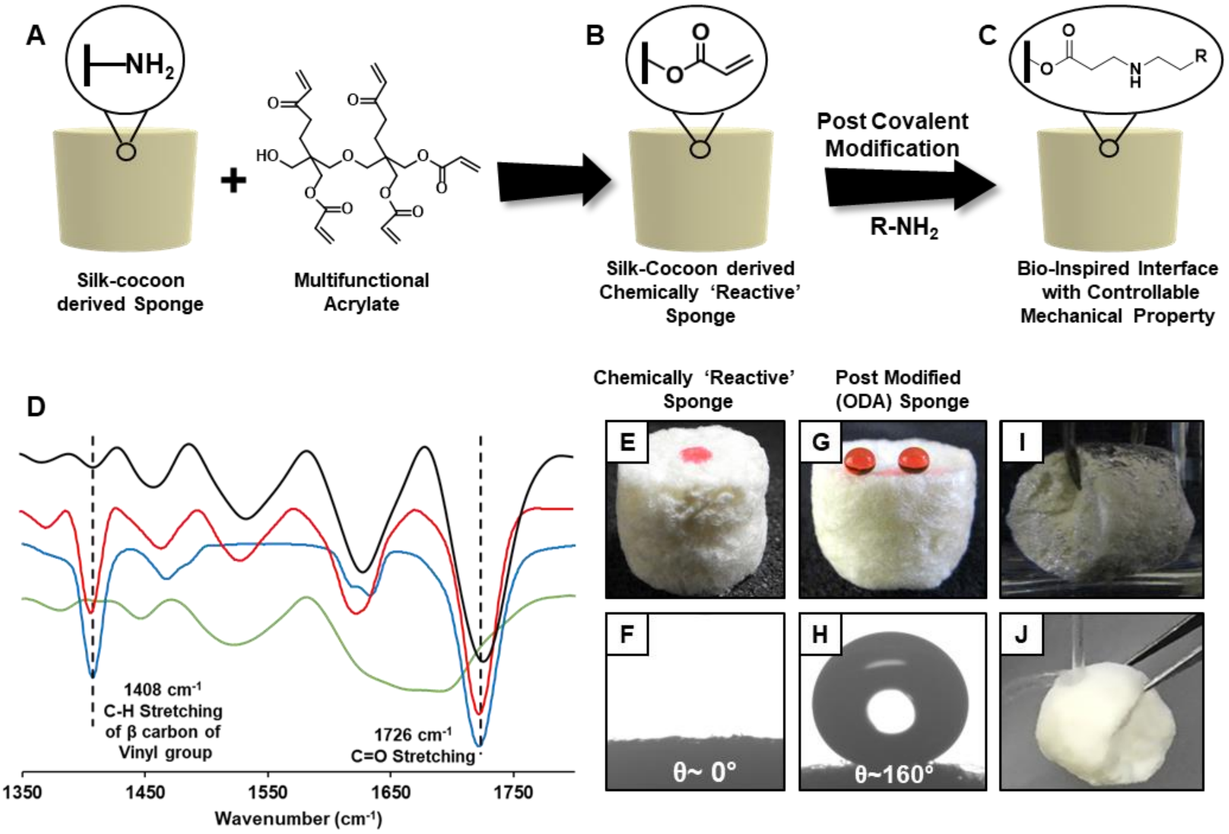

**Figure 3.9.** A-C) Schematic illustrating the Michael addition reaction between the amine residues of silk cocoon-derived sponge and 5Acl to obtain a chemically 'reactive' sponge (B). The residual acrylate reactivity of the sponge allowed the post modification with amine-containing molecules following the facile Michael addition reaction to obtain an interface with tailorable wettability (C). D) ATR-FTIR spectra of the unmodified silk cocoon-derived sponge (green), multifunctional acrylate cross-linker, 5Acl (blue), CRSCDS (red) and after covalent post modification of CRSCDS with ODA (black). E-F) Digital image (E) and WCA image (F) of CRSCDS. G-H) Digital image (G) and WCA image (H) of the beaded droplet on the silk cocoon-derived sponge that was post modified with ODA, denoted as SCDSHS$_{40}$. I) Digital image exhibiting the presence of a shiny interface on submerging SCDSHS$_{40}$ underwater, thus revealing the presence of a trapped metastable air layer. J) Digital image demonstrating the bouncing of a stream of water from the surface of SCDSHS$_{40}$.

the reaction.[50-51] After the 5Acl treatment, the IR intensity for the vinyl group remained significantly high in the silk derived sponge, indicating the presence of unreacted acrylate functionalities in the prepared spongy material (Figure 3.9D, red). Thus, the chemically 'reactive' silk cocoon-derived sponge (denoted as CRSCDS) with residual acrylate groups, which was observed to be hydrophilic with WCA~0° as depicted in Figure 3.9E-F, provided a general avenue for post-covalent functionalization with the desired amine containing small molecules at ambient conditions (Figure 3.9C). The successful post modification of CRSCDS with a hydrophobic alkylamine i.e. ODA was confirmed through the ATR-FTIR analysis, where the characteristic peak at 1408 $cm^{-1}$ underwent significant depletion (~91% residual acrylates were consumed) with reference to the normalized IR signature for carbonyl group at 1726 $cm^{-1}$, as shown in Figure 3.9D (black). Digital images further revealed that the post modification of CRSCDS (previously $SMFRSFS_{40}$) with ODA conferred superhydrophobicity to the sponge wherein, a dyed water (red) droplet beaded with static WCA~160° and contact angle hysteresis ~7° as shown in Figure 3.9G-H and Table 3.3. It is worth to mention that the previously reported silk-based materials barely displayed WCA ≥ 150°.[27,28] Both static and dynamic water contact angles (Table 3.3) were measured to examine the superhydrophobicity. The post-modified sponge was denoted as the silk cocoon-derived superhydrophobic sponge ($SCDSHS_{40}$; subscript 40 specifying the ethanol treatment). A characteristic shiny interface was observed on submerging the silk cocoon-derived superhydrophobic sponge underwater, due to the existence of a metastable trapped air layer that imparts the heterogeneous extreme water repellence, as depicted in Figure 3.9I. Further, a water stream immediately bounced off from the synthesized $SCDSHS_{40}$, indicating the presence of non-adhesive superhydrophobicity (Figure 3.9J).

Furthermore, to examine the impact of the concentration of cross-linker, the sponges were exposed to different concentrations (15 mM-250 mM) of the multi-acrylate cross-linker, however, the extent of reaction between amines and acrylates remained very similar, as depicted through the ATR-IR analysis in Figure 3.10A. Varying the acrylate concentration led to changes in the intensity of the IR peak at 1408 $cm^{-1}$ in comparison to the normalized IR signature for the carbonyl group at 1726 $cm^{-1}$. With respect to the 5Acl spectrum (blue), ~28, 32, and 34% of the IR peak intensities depleted during the reaction between amines and 5Acl with concentrations corresponding to 0.25 M (red), 0.0625 M (yellow) and 0.015 M (green), respectively, as shown in Figure 3.10A. This minimal variation in the depletion of the IR peak for acrylate groups indicated insignificant changes in the cross-linking density of the sponges on varying the concentration of the multi-functional acrylate. Thereafter, a decrease in the IR peak intensity at 1408 $cm^{-1}$ with respect to the normalized carbonyl stretching frequency at

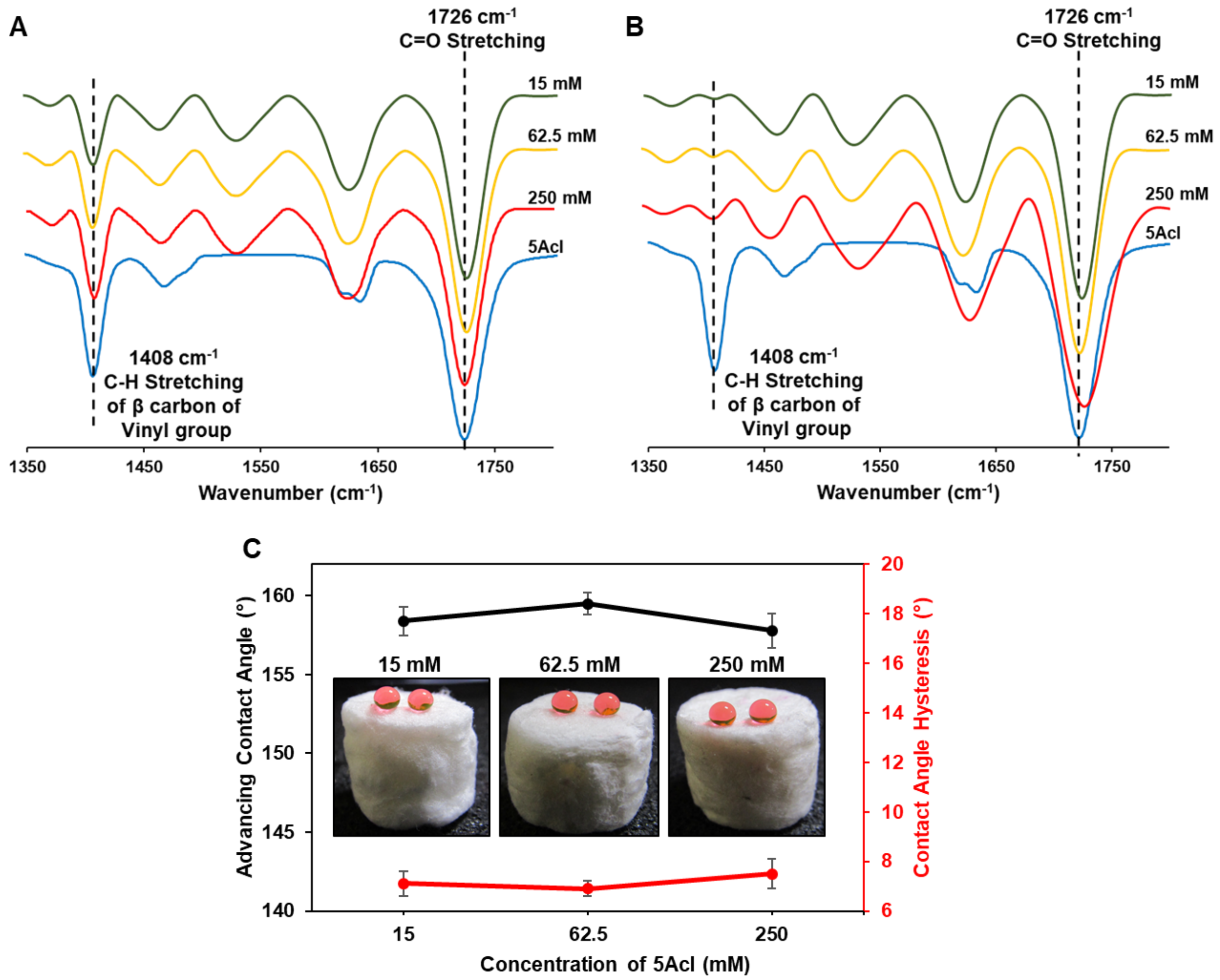

**Figure 3.10.** A) ATR-FTIR analysis of the silk-cocoon derived sponges that were subjected to covalent cross-linking with varying concentrations of 5Acl i.e. 250 mM (red), 62.5 mM (yellow) and 15 mM (green) for embedment of chemical reactivity. B) ATR-FTIR analysis of the silk cocoon derived sponges that were modified with varying concentrations of the multi-functional acrylate followed by post covalent modification with ODA. C) Plot illustrating the advancing WCA (black), contact angle hysteresis (red) and inset digital images of the silk-cocoon derived sponges that were subjected to cross-linking with different concentrations of 5Acl followed by post modification with ODA.

1726 cm$^{-1}$ was observed after post modification of the prepared sponges with ODA which indicated the successful covalent functionalization of the residual acrylates as shown in Figure 3.10B, to embed superhydrophobic behavior as shown in Figure 3.10C.

The presence of residual acrylate reactivity in CRSCDS was further exploited to embed a wide range of water wettability. CRSCDS was post modified independently with different alkylamines through the Michael addition reaction to tune the water wettability. The moderate increase in the hydrocarbon chain length of the selected alkylamines from butylamine to decylamine led to modulation of the water wettability corresponding to hydrophilicity (butylamine, WCA~36°), hydrophobicity (pentylamine, WC ~120°; hexylamine, WCA~136°), adhesive superhydrophobicity (octylamine, WCA~145°) to non-adhesive superhydrophobicity (decylamine, WCA~155°), as characterized by measuring the static

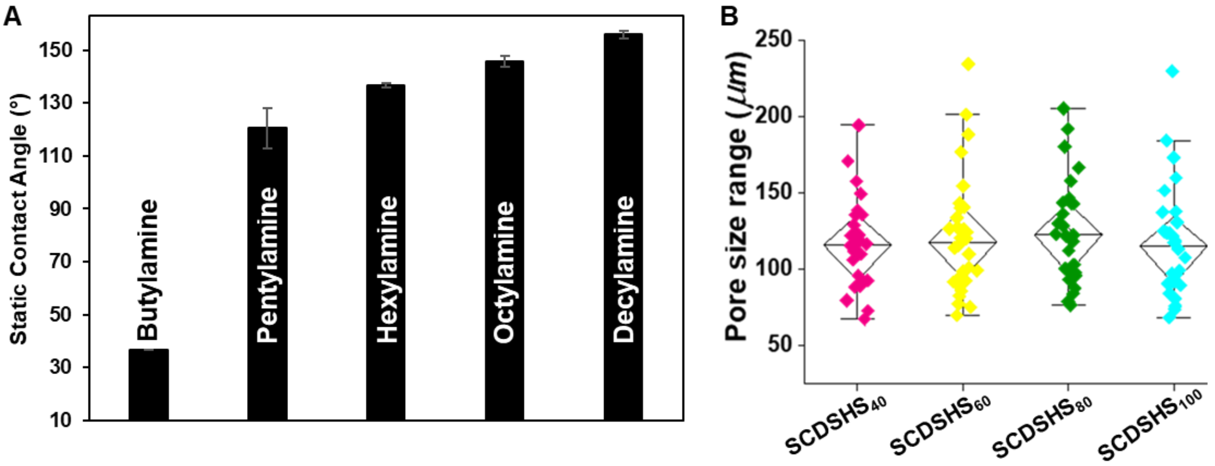

**Figure 3.11**. Bar diagram illustrating the static WCA of the silk cocoon-derived chemically 'reactive' sponge after post-covalent-modification with different amine-containing small molecules, including butylamine, pentylamine, hexylamine, octylamine and decylamine. B) Plot depicting the pore size analysis data for the different silk-cocoon derived superhydrophobic sponges using Image-J plug in.

WCA (Figure 3.11A) and dynamic WCA (Table 3.3). The porosity of the sponges barely changed before after the covalent cross-linking and the subsequent post modification with ODA as shown in Figure 3.11B and Table 3.4.

**Table 3.3.** Illustrates the advancing WCA and contact angle hysteresis of the beaded water droplet on the silk cocoon-derived chemically 'reactive' sponge that was post modified with different alkylamines

| Post Modification with Alkylamines | Advancing Contact Angle (°) | Contact Angle Hysteresis (°) |
|---|---|---|
| **Butylamine** | 35.7 ± 0.6 | - |
| **Pentylamine** | 121.3 ± 1.0 | 22.2 ± 0.5 |
| **Hexylamine** | 135.2 ± 1.3 | 19.8 ± 0.7 |
| **Octylamine** | 144.7 ± 0.7 | 13.6 ± 1.4 |
| **Decylamine** | 155.8 ± 1.1 | 7.8 ± 0.6 |
| **Octadecylamine** | 162.6 ± 0.9 | 7.2 ± 1.0 |

The compressive modulus of the as prepared sponges remained very similar before (i.e. $SMFRSFS_{40}$, $SMFRSFS_{60}$, $SMFRSFS_{80}$, $SMFRSFS_{100}$) and after post modification with ODA (i.e. $SCDSHS_{40}$, $SCDSHS_{60}$, $SCDSHS_{80}$, $SCDSHS_{100}$), as shown in Figure 3.12A. This indicates that the covalent cross-linking with the multifunctional acrylate cross-linker in ethanolic solution followed by covalent post modification of the residual acrylates with ODA barely impacted the mechanical property of the as-

**Table 3.4.** Summarizes the porosity of the different silk-cocoon derived sponges calculated experimentally before (SMFRSFS) and after covalent post modification with ODA (SCDSHS).

| Sample | Porosity (%) |
|---|---|
| **SMFRSFS$_{40}$** | 96.85 ± 0.8 |
| **SMFRSFS$_{60}$** | 95.81 ± 1.2 |
| **SMFRSFS$_{80}$** | 96.93 ± 0.7 |
| **SMFRSFS$_{100}$** | 96.35 ± 0.4 |
| **SCDSHS$_{40}$** | 95.90 ± 1.1 |
| **SCDSHS$_{60}$** | 96.18 ± 0.6 |
| **SCDSHS$_{80}$** | 95.76 ± 0.8 |
| **SCDSHS$_{100}$** | 96.92 ± 1.3 |

prepared sponges. Thus, the current design provided a rare opportunity to covalently embed and tailor the chemical functionality of the substrate while keeping the mechanical property intact.

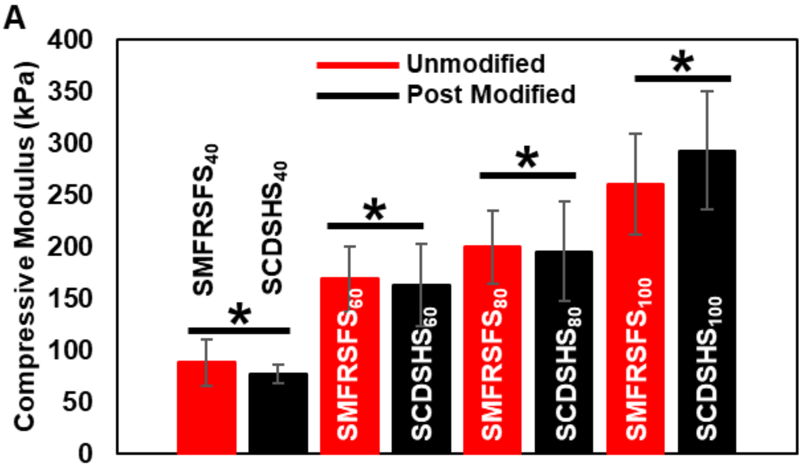

**Figure 3.12**. A) Comparative plot representing the compressive modulus of the silk microfiber reinforced silk fibroin sponges before (red) any covalent modification and after post modification with ODA (black) that indicates that the mechanical property of the sponges remained unaffected by the covalent chemical modification of the sponges .

### 3.3.3. Examining the Durability of the Silk Cocoon-Derived Superhydrophobic Sponges

The silk cocoon-derived highly compressible and chemically ‘reactive sponge’ embedded with superhydrophobicity (SCDSHS$_{40}$) was subjected to various harsh and practically relevant physically abrasive tests to investigate the robustness of the covalently embedded bio-mimicked extreme water wettability. First, the embedded anti-wetting property of the silk cocoon-derived sponge was investigated after physical deformation, wherein the compressive strain on the sponge was gradually

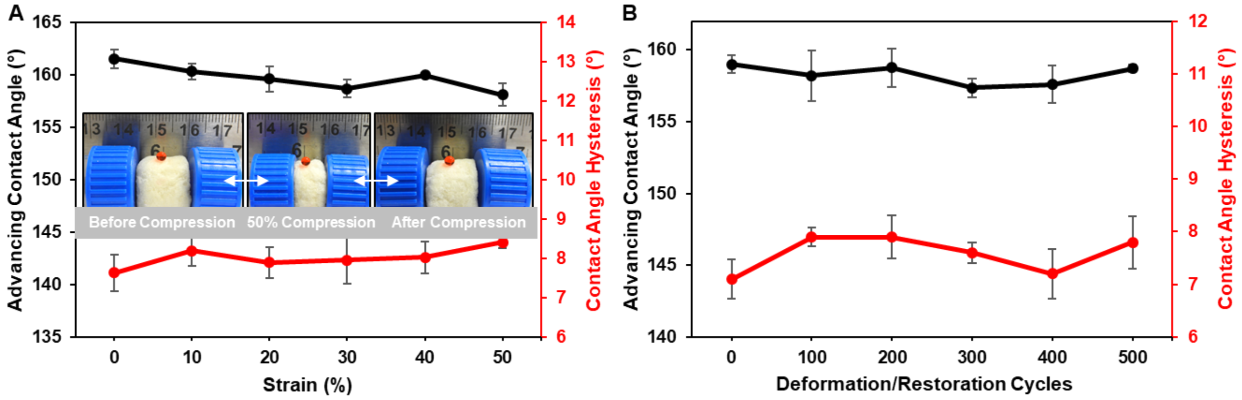

**Figure 3.13.** A) Plot representing the advancing WCA (black) and contact angle hysteresis (red) of the beaded water droplet on the silk cocoon-derived superhydrophobic sponge ($\text{SCDSHS}_{40}$) that was subjected to 50% manual compression. Inset images show the embedded extreme antiwetting property on the superhydrophobic sponge before (left), during 50% compression (middle), and after strain release (right). B) Plot representing the advancing WCA (black) and contact angle hysteresis (red) of a beaded water droplet on $\text{SCDSHS}_{40}$ that was repetitively deformed under 50% strain for 500 cycles.

increased from 0 to 50%. It was observed that the extreme water repellence remained intact with advancing WCA above 150° and contact angle hysteresis below 10°, as shown in Figure 3.13A. On removal of the applied strain, $\text{SCDSHS}_{40}$ recovered its dimensions and retained the water repellence as depicted in Figure 3.13A (inset). Furthermore, investigation of the anti-wetting property on the synthesized sponge after every 100 cycles of repetitive compression for 500 cycles with an applied compressive strain of 50% revealed that the embedded superhydrophobicity persisted with advancing WCA above 150° and contact angle hysteresis below 10° throughout all the cycles, as shown in Figure 3.13B. To examine the existence of three-dimensional water-repellent behavior, $\text{SCDSHS}_{40}$ was sliced into multiple pieces arbitrarily to expose the interiors and it was observed that the water droplet beaded on the freshly exposed interiors of the sponge with static WCA~157° and contact angle hysteresis ~7°, as shown in Figure 3.14A-B, thus revealing the presence of non-adhesive three-dimensional superhydrophobicity.

A few standard and widely accepted physical abrasion tests were strategically imposed to examine the sustenance of the silk cocoon-derived superhydrophobic sponge at practically harsh and relevant scenarios. In the sand drop test (Figure 3.14C), 150 g of sand grains was dropped onto $\text{SCDSHS}_{40}$ from a 25 cm height. The static WCA~156° and contact angle hysteresis ~ 7° revealed that such an abrasive exposure failed to perturb the embedded bio-mimicked antiwetting property, as shown in Figure 3.14D-E and Table 3.5. In another physically harsh test, an abrasive sand paper was manually rubbed in a back and forth motion multiple times on $\text{SCDSHS}_{40}$ with a 500 g load atop (Figure 3.14G), followed by investigation of the embedded anti-wetting property on the abraded surface of the silk

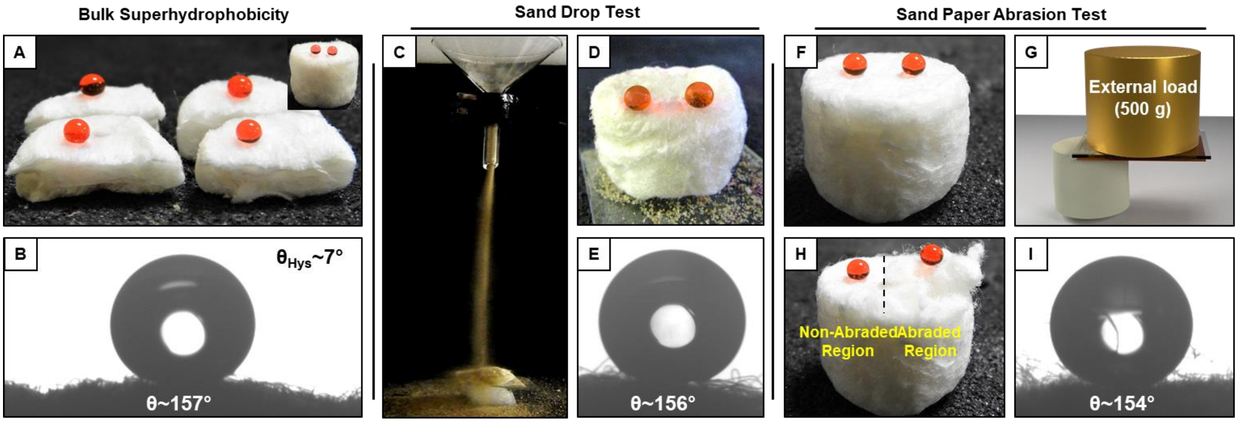

**Figure 3.14.** A-B) Digital image (B) and static WCA (B) on SCDSHS40 that was arbitrarily cut into small pieces to examine the water-repellent property in the bulk of the substrate. The inset image is the original sponge before slicing. C-E) Digital images (C, D) and static WCA (E) illustrating the sand drop test (C) and retention of the extreme water-repellent property (D, E) by the silk cocoon derived superhydrophobic sponge after the harsh physical abrasion. F-G) Digital image (F) of SCDSHS40 before sandpaper abrasion. Abrasive sandpaper was rubbed on one side of the sponge with an applied load of 500 g on top (G) such that the top surface was completely abraded, exposing the interiors. H-I) Digital image (H) and static WCA (I) on the abraded sponge area, which continued to display impeccable water repellence.

cocoon-derived superhydrophobic sponge which revealed that the water droplet beaded with static WCA~154° and contact angle hysteresis ~8°, as shown in Figure 3.14H-I and Table 3.5. Such demonstrations unambiguously implied the existence of impeccable three-dimensional durability of the implanted water wettability. Furthermore, exposure of SCDSHS$_{40}$ to UV radiation (254 and 365 nm) for 28 days failed to perturb the superhydrophobic property, where the water droplet beaded with advancing water WCA above 150° and contact angle hysteresis below 10° as depicted in Figure 3.15A.

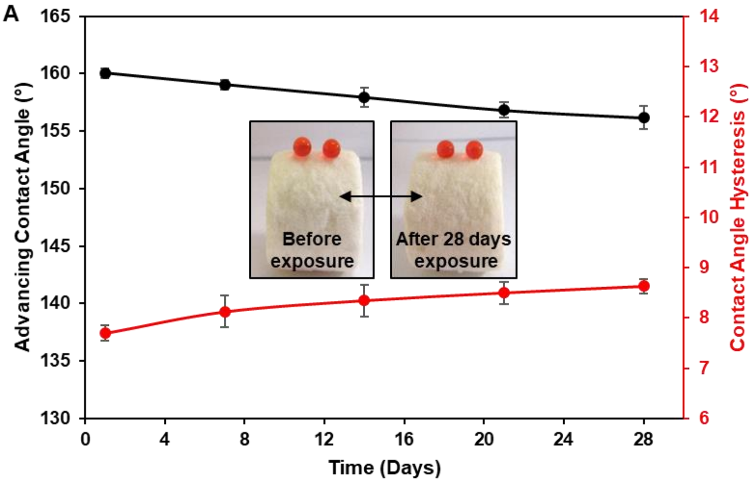

**Figure 3.15.** A) Plot depicting the change in advancing WCA (black) and contact angle hysteresis (red) of the beaded water droplet after exposing the silk-cocoon derived superhydrophobic sponge, SCDSHS40 to both long (365 nm) and short (254 nm) UV irradiation for 28 days. Inset images illustrates the embedded anti-wetting property of the sponge before and after 28 days of UV exposure.

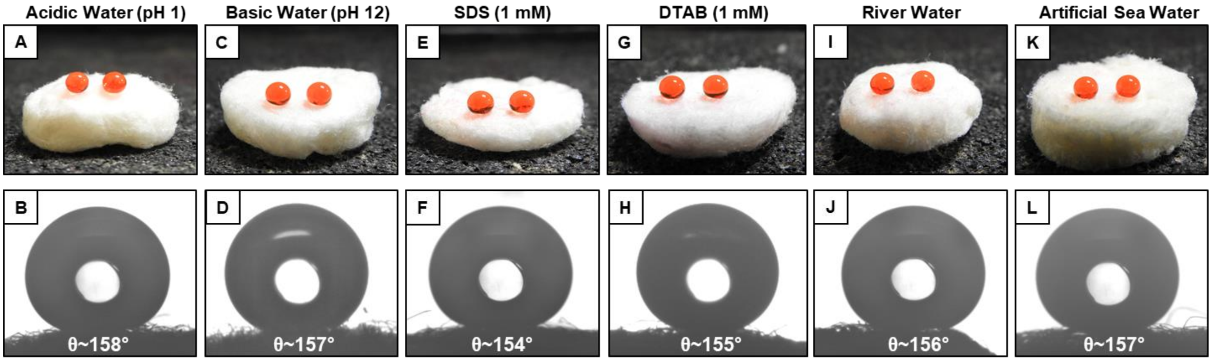

**Figure 3.16.** A-L) Digital images and WCA images of the water droplet on the silk-cocoon derived superhydrophobic sponge, $SCDSHS_{40}$ where the water droplet was chemically contaminated i.e. acidic water (A-B), basic water (C-D), surfactant contaminated water (E-H), river water (I-J) and artificial sea water (K-L).

Chemical durability is a vital parameter to examine the relevance of any substrate for practical utility. In this context, exposure of $SCDSHS_{40}$ to various severe aqueous chemical settings, i.e. basic water (pH 12), acidic water (pH 1), river water, surfactant-contaminated water (SDS and DTAB) and artificial seawater, revealed that the water droplet beaded with advancing WCA above 150° and contact angle hysteresis below 10°, as shown in Figure 3.16A-L and Table 3.5. Hence, the silk cocoon-derived superhydrophobic sponge survived various harsh physically abrasive and chemically contaminated aqueous phases and thus, can be deemed appropriate for outdoor applications even at diverse and challenging conditions.

**Table 3.5.** Accounts for the advancing WCA and contact angle hysteresis of the beaded water droplet on the silk-cocoon derived superhydrophobic sponge ($SCDSHS_{40}$) after various physical and chemical exposures.

| Physical/Chemical Exposures | Advancing Contact Angle (°) | Contact Angle Hysteresis (°) |
|---|---|---|
| Sand Paper Abrasion | 158.3 ± 0.8 | 8.2 ± 1.2 |
| Sand Drop Test | 159.5 ± 1.1 | 7.5 ± 0.9 |
| Acidic Water (pH 1) | 158.4 ± 0.4 | 7.2 ± 0.5 |
| Basic Water (pH 12) | 159.1 ± 0.8 | 6.9 ± 1.1 |
| SDS (1mM) | 157.5 ± 1.4 | 7.2 ± 0.8 |
| DTAB (1mM) | 156.8 ± 0.9 | 7.9 ± 0.7 |
| River Water | 158.8 ± 0.7 | 6.5 ± 1.2 |
| Artificial Sea Water | 156.0 ± 1.3 | 7.5 ± 0.6 |

## 3.4. Conclusion

In this chapter, the controlled tailoring of the mechanical property and water wettability in a silk cocoon-derived sponge (denoted as silk microfiber reinforced silk fibroin sponge, SMFRSFS), was introduced following a green and eco-friendly synthetic route. The ethanol-assisted modulation of β-sheet content in the silk fibroin network allowed to tailor the compressive modulus, while the rational integration of 'reactive' residual acrylate groups with the amine residues of silk, bestowed a pathway for modulating the water wettability adopting the catalyst-free Michael addition reaction at ambient conditions. The micro-fiber reinforcements further imparted mechanical durability to the sponges. The induction of residual acrylates allowed the embedment of various water wettability (WCA~ 36°-161°), including adhesive to non-adhesive superhydrophobicity, without perturbing the tailored mechanical property. The embedded bio-inspired superhydrophobicity could sustain various severe physical abrasive tests including sand paper abrasion and sand drop test, UV irradiation (for 28 days), repetitive (500 cycles) exposure to 50% compressive strain and repel the beaded chemically contaminated aqueous droplets including acidic water, basic water, river water, surfactant water and artificial seawater.

## 3.5. References

1. R. Xiong, H. S. Kim, S. Zhang, S. Kim, V. F. Korolovych, R. Ma, Y. G. Yingling, C. Lu, V. and V. Tsukruk, *ACS Nano*, 2017, **11**, 12008-12019.
2. P. Tseng, B. Napier, S. Zhao, A. N. Mitropoulos, M. B. Applegate, B. Marelli, D. L. Kaplan and F. G. Omenetto, *Nat. Nanotechnol.*, 2017, **12**, 474-480.
3. Y. Zhang, Z. Zhou, L. Sun, Z. Liu, X. Xia and T. H. Tao, *Adv. Mater.* 2018, **30**, 1805722-1805731.
4. Z. Zhou, S. Zhang, Y. Cao, B. Marelli, X. Xia and T. H. Tao, *Adv. Mater.*, 2018, **30**, 1706983-1707013.
5. W. Xin, Z. Zhang, X. Huang, Y. Hu, T. Zhou, C. Zhu, X. -Y. Kong, L. Jiang and L. Wen, *Nat. Commun.*, 2019, **10**, 3876-3886.
6. D. -L. Wen, X. Liu, H. -T. Deng, D. -H. Sun, H. -Y. Qian, J. Brugger and X. -S. Zhang, *Nano Energy*, 2019, **66**, 104123-104133.
7. S. Zhu, W. Zeng, Z. Meng, W. Luo, L. Ma, Y. Li, C. Lin, Q. Huang, Y. Lin and X. Y. Liu, *Adv. Mater.*, 2019, **31**, 1900870-1900877.
8. L. Gustafsson, C. P. Tasiopoulos, R. Jansson, M. Kvick, T. Duursma, T. C. Gasser, W. van der Wijngaart and M. Hedhammar, *Adv. Funct. Mater.*, 2020, **30**, 2002982-2002991.

9. X. Liu, H. Gao, J. E. Ward, X. Liu, B. Yin, T. Fu, J. Chen, D. R. Lovley and J. Yao, *Nature*, 2020, **578**, 550-554.

10. S. Acosta, L. Quintanilla-Sierra, L. Mbundi, V. Reboto and J. C. Rodríguez-Cabello, *Adv. Funct. Mater.*, 2020, **30**, 1909050-1909071.

11. L. Cheng, Z. Cai, T. Ye, X. Yu, Z. Chen, Y. Yan, J. Qi, L. Wang, Z. Liu, W. Cui and L. Deng, *Adv. Funct. Mater.*, 2020, **30**, 2001196-2001218.

12. W. Xin, H. Xiao, X. -Y. Kong, J. Chen, L. Yang, B. Niu, Y. Qian, Y. Teng, L. Jiang and L. Wen, *ACS Nano*, 2020, **14**, 9701-9710.

13. L. Cera, G. M. Gonzalez, Q. Liu, S. Choi, C. O. Chantre, J. Lee, R. Gabardi, M. C. Choi, K. Shin and K. K. Parker, K. K. *Nat. Mater.*, 2021, **20**, 242-249.

14. X. M. Li, D. Reinhoudt and M. Crego-Calama, M. *Chem. Soc. Rev.*, 2007, **36**, 1350-1368.

15. S. Wang, K. Liu, X. Yao and L. Jiang, *Chem. Rev.*, 2015, **115**, 8230-8293.

16. A. Das, A. Shome and U. Manna, *J. Mater. Chem. A*, 2021, **9**, 824-856.

17. M. Mrksich, *Chem. Soc. Rev.*, 2000, **29**, 267-273.

18. N. P. Reynolds, M. Charnley, M. N. Bongiovanni, P. G. Hartley and S. L. Gras, *Biomacromolecules*, 2015, **16**, 1556-1565.

19. L. Chen, C. Yan and Z. Zheng, *Mater. Today*, 2018, **21**, 38-59.

20. A. R. Murphy, P. S. John and D. L. Kaplan, *Biomaterials*, 2008, **29**, 2829-2838.

21. S. L. Bechler and D. M. Lynn, *Biomacromolecules*, 2012, **13**, 1523-1532.

22. K. Xiao, T. Y. Lin, K. S. Lam and Y. Li, *Nanoscale*, 2017, **9**, 7765-7770.

23. H. S. El-Sawy, A. M. Al-Abd, T. A. Ahmed, K. M. El-Say and V. P. Torchilin, *ACS Nano*, 2018, **12**, 10636-10664.

24. A. R. Murphy and D. L. Kaplan, *J. Mater. Chem.*, 2009, **19**, 6443- 6450.

25. S. Das, D. Pati, N. Tiwari, A. Nisal and S. Sen Gupta, *Biomacromolecules*, 2012, **13**, 3695-3702.

26. L. Raynal, B. J. Allardyce, X. Wang, R. J. Dilley, R. Rajkhowa and L. C. Henderson, *J. Mater. Chem. B*, 2018, **6**, 8037-8042.

27. I. S. Romero, M. L. Schurr, J. V. Lally, M. Z. Kotlik and A.R. Murphy, *ACS Appl. Mater. Interfaces*, 2013, **5**, 553-564.

28. K. Zheng, Y. Chen, W. Huang, Y. Lin, D. Kaplan and Y. Fan, *ACS Appl. Mater. Interfaces*, 2016, **8**, 14406-14413.

29. H. Maleki, L. Whitmore and N. Husing, *J. Mater. Chem. A*, 2018, **6**, 12598-12612.

30. J. Zhou, Y. Zhang, Y. Yang, Z. Chen, G. Jia and L. Zhang, *Appl. Surf. Sci.*, 2019, **497**, 143762-143770.

31. J. C. Moses, S. K. Nandi and B. B. Mandal, *Adv. Healthc. Mater.*, 2018, **7**, 1701418.

32. M. Haeri and M. Haeri M, *J. Open Res. Softw.*, 2015, **3**, Art e1.

33. J. C. Moses, M. Dey, K. B. Devi, M. Roy, S. K. Nandi and B. B. Mandal, *ACS Biomater. Sci. Eng.*, 2019, **5**, 1462-1468.

34. B. B. Mandal, A. Grinberg, E. S. Gil, B. Panilaitis and D. L. Kaplan, *Proc. Natl. Acad. Sci. USA*, 2012, **109**, 7699-7704.

35. Z. Zhang, G. Sèbe, D. Rentsch, T. Zimmermann and P. Tingaut, *Chem. Mater.*, 2014, **26**, 2659-2668.

36. S. Zhou, P. Liu, M. Wang, H. Zhao, J. Yang and F. Xu, *ACS Sustainable Chem. Eng.*, 2016, **4**, 6409-6416.

37. Y. P. Singh, J. C. Moses, B. K. Bhunia, S. K. Nandi and B. B Mandal, *J. Mater. Chem. B*, 2018, **6**, 5671-5688.

38. P. Gupta , M. Adhikary, J. C. Moses, M. Kumar, N. Bhardwaj and B. B. Mandal, *ACS Appl. Mater. Interfaces*, 2016, **8**, 30797-30810.

39. H. Tu, R. Yu, Z. Lin, L. Zhang, N. Lin, W. D. Yu and X. Y. Liu, *Adv. Funct. Mater.*, 2016, **26**, 9032-9043.

40. E. Ko, J. S. Lee, H. Kim, S. Y. Yang, D. Yang, K. Yang, J. Lee, J. Shin, H. S. Yang, W. Ryu, and S. -W. Cho, *ACS Appl. Mater. Interfaces*, 2018, **10**, 7614-7625.

41. Y. Feng, X. Li, M. Li, D. Ye, Q. Zhang, R. You and W. Xu, *ACS Sustainable Chem. Eng.*, 2017, **5**, 6227-6236.

42. C. Holland, K. Numata, J. Rnjak-Kovacina and F. P. Seib, *Adv. Healthcare Mater.*, 2019, **8**, 1800465-1800486.

43. G. Janani, M. Kumar, D. Chouhan, J. C. Moses, A. Gangrade, S. Bhattacharjee and B. B. Mandal, *ACS Appl. Bio Mater.*, 2019, **2**, 5460-5491.

44. B. B. Mandal and S. C. Kundu, *Biomaterials*, 2009, **30**, 2956-2965.

45. X. Wu, X. Wu, B. Yang, M. Shao and G. Feng, *Appl. Spectrosc.*, 2017, **71**, 1785-1794.

46. Q. Lu, X. Hu, X. Wang, J. A. Kluge, S. Lu and P. Cebe, *Acta Biomater.*, 2010, **6**, 1380-1387.

47. P. Gupta, J. C. Moses and B. B. Mandal, *ACS Biomater. Sci. Eng.*, 2019, **5**, 933-941.

48. K. Yazawa, K. Ishida, H. Masunaga, T. Hikima and K. Numata, *Biomacromolecules*, 2016, **17**, 1057-1066.

49. S. Yi, f. Dai, Y. Ma, T. Yan, Y. Si and G. Sun, *ACS Sustainable Chem. Eng.*, 2017, **5**, 8777-8784.

50. M. R. Weatherspoon, M. B. Dickerson, G. Wang, Y. Cai, S. Shian, S. C. Jones, S. R. Marder and K. H. Sandhage, *Angew. Chem. Int. Ed.*, 2007, **46**, 5724-5727.

51. J. Ford, S. R. Marder and S. Yang, *Chem. Mater.*, 2009, **21**, 476-483.

# Chapter 4. Conversion of Waste Products into Robust Functional Materials*

Controlled tailoring of mechanical property and water wettability is important for designing various functional materials. The integration of these characteristics with waste materials is unprecedented in literature, however, it can provide economically and environmentally sustainable solutions to combat relevant environmental pollutions. In this chapter, the strategic conversion of discarded and abundant waste paper into functional products has been introduced following a catalyst-free chemical approach to tailor both the mechanical property and water wettability at ambient conditions for sustainable waste management and remediation of another important environmental pollution. The controlled and appropriate silanization of waste paper allowed to modulate the a) porosity b) compressive modulus of the paper-derived sponges and c) induct the labile amine functionality. Further, the strategic association of Michael addition reaction between the amine and acrylate groups allowed to obtain an unconventional waste paper-derived chemically 'reactive' sponge. The appropriate covalent modification of the residual 'reactive' acrylate groups with the selected alkylamines at ambient conditions provided a facile basis to tailor the water wettability from moderate hydrophobicity, adhesive superhydrophobicity to non-adhesive superhydrophobicity, without altering the mechanical property of the sponges. The embedded superhydrophobicity in the waste paper-derived sponge was capable of sustaining large physical deformations, severe physical abrasions, prolonged exposure to harsh aqueous conditions, etc. Further, the waste paper-derived, extremely water-repellent sponges were successfully extended for proof-of-concept demonstration of selective oil/water separation, where the repetitive separation of oil phases were demonstrated following selective absorption of oils (for 25 repetitive cycles). The analogous waste paper derived superhydrophobic membranes were extended for gravity-driven filtration-based separation of oils (for 50 repetitive cycles) from various oil/water mixtures even under practically relevant aqueous settings, without compromising the embedded water repellence property.

---

*A. Shome *et al.*, *Chem Asian J.*, 2021, **16**, 1988-2001.

## 4.1. Introduction

In the past, mechanically durable materials embedded with superhydrophobicity have been fabricated extensively for various prospective energy and health related applications through the strategic integration of carbon nanotubes,[1-2] graphene derivatives,[3-4] cellulose nanocrystals,[5] elastomers, MXenes, electrodeposited nano-alloys etc.[6-8] However, such approaches utilizing synthetic components are inadequate to simultaneously tailor the mechanical property and water wettability using a single chemical approach due to the lack of any residual chemical reactivity. Chemically 'reactive' interfaces have been designed adopting click chemistry,[9-10] azlactone ring opening reaction,[11] for modulating the chemical functionalities of the interface and subsequently tailor the water wettability,[12-13] however, such reported approaches are unable to provide a common avenue to tune the mechanical property. In the previous chapter, silk-cocoon derived microfibers were used as reinforcements in a silk fibroin network wherein, the ethanol assisted induction of β-sheets into the silk fibroin network allowed to modulate the mechanical property and the microfibers reinforcements imparted mechanical durability to the sponges.[14] Moreover, the catalyst-free Michael addition reaction between the amine residues of silk and an acrylate cross-linker imparted chemical reactivity to the silk sponges to tailor the water wettability, keeping the mechanical property unaltered. However, such modulation of mechanical property through varying the β-sheet content is specific to proteins. Thus, in this chapter, the aim was to introduce a facile and separate chemical approach that would allow the consecutive tailoring of mechanical property and water wettability of a waste material to ensure its conversion into a robust functional material.

In the past, discarded plant bio-mass was transformed into functional materials to combat potential environmental pollutions.[15-16] In that context, waste paper that poses major concerns including deforestation, water consumption and pollution, landfills, air pollution,[17-18] was transformed into paper based functional materials for example, rewritable and functional chromogenic interfaces,[19] electrochemical devices for on-site bio-sensing,[20] energy storage devices,[21] combating electro-magnetic pollution[22] etc. Recently, a few water-repellent papers were developed through the strategic association of bio-inspired wettability for demonstrating controlled droplet manipulation, microbial resistance, self-cleaning performances etc.[23-29] For example, Li *et al.* oxidized office paper with sodium chlorite followed by carbonization at 1000°C under inert atmosphere to develop a compressible, superhydrophobic carbon aerogel.[25] In another report, Yue *et al.* developed a banana peel/waste paper derived hydrophobic, compressible hybrid aerogel with WCA~149° by adopting the pyrolysis approach (900°C).[29] However, the direct transformation of waste paper into durable and functional materials following a facile and scalable synthesis process is yet to be introduced in the literature.[24-29]

The existing approaches for deriving functional superhydrophobic materials from waste paper primarily depends on the high temperature pyrolysis process,[24-27,30-33] which is an energy consuming approach.[34] Furthermore, the previously reported approaches lacked the ability to modulate the compressive modulus of the synthesized materials, which could prove beneficial for obtaining the ideal substrate for oil/water separation and spongy thermal insulators.[30-31,35] Hence, a facile, economic design for converting waste paper into chemically 'reactive', durable sponges with the scope to tailor both the mechanical property and water wettability for practical applications has been introduced in chapter 4.

Different types of waste papers (i.e. tissue paper, office paper, newspaper, cardboard paper) were reconstructed into porous, highly compressible, covalently integrated, chemically 'reactive' sponges with tailorable mechanical property and water wettability. The strategic covalent integration of waste

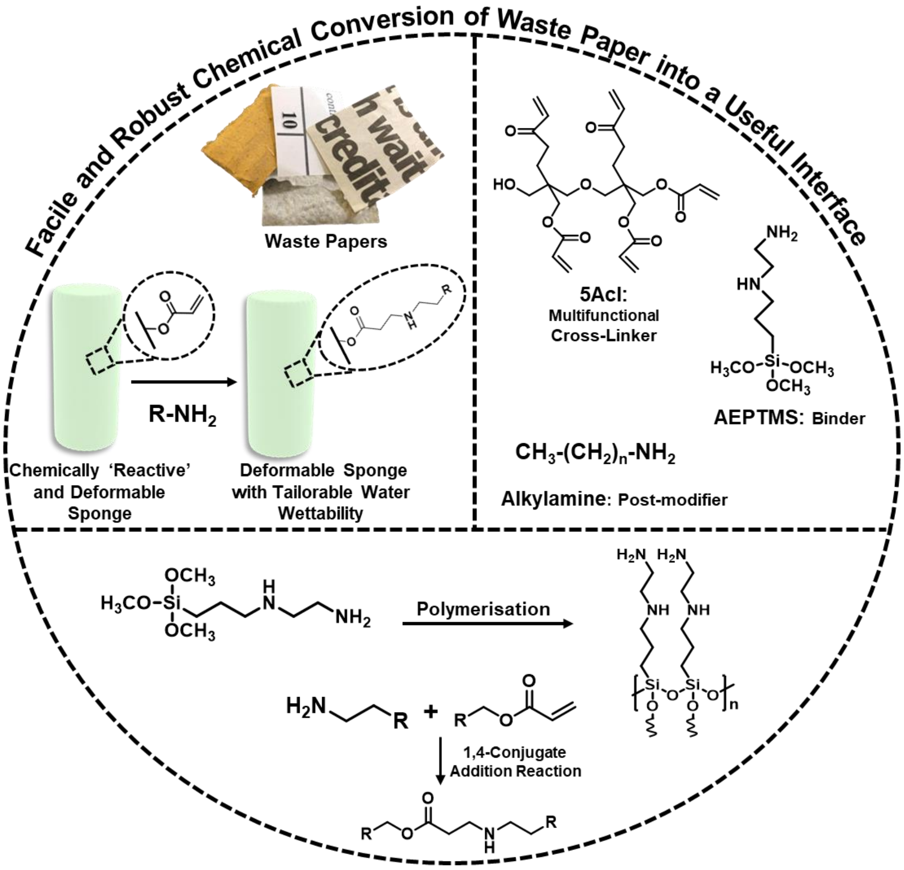

**Figure 4.1.** Schematic illustrating the facile and robust conversion of waste papers into a deformable and chemically 'reactive' sponge. The covalent association of an amine modified silane i.e. 3-(2-aminoethylamino)-propyltrimethoxysilane (AEPTMS) with waste paper paved an avenue to tailor the mechanical property of the sponge by varying the concentration of AEPTMS used. The catalyst-free Michael addition reaction between the amines of the silanized paper sponge with a multi-functional cross-linker provided a facile basis to induce residual chemical 'reactivity' in the waste paper derived sponge. The residual acrylate reactivity was exploited to alter the water wettability of the sponge following the Michael addition reaction with alkylamines of varying chain lengths.

paper with an amine functionalized silane molecule provided a facile basis for modulating the a) porosity, b) compressive modulus of the paper sponges and c) integrating a multi-functional acrylate cross-linker following the catalyst-free Michael addition reaction (Figure 4.1). This simple cross-linking process induced the desired chemical 'reactivity' in the waste paper derived sponge that allowed to modulate the embedded water wettability from hydrophobic, adhesive superhydrophobic to non-adhesive superhydrophobic (~25° to 161°) through the post covalent modification of the chemically 'reactive' paper sponge with the appropriate alkylamines following the same Michael addition reaction at ambient conditions. The embedded superhydrophobicity in the waste-paper derived spongy material withstood various harsh physical abrasions, repetitive manual compression (1000 times), prolonged (30 days) exposure to UV radiation, organic solvents and chemically contaminated aqueous phases. Such a durable and highly compressible superhydrophobic sponge was extended for proof of concept oil/water separation, wherein selective absorption based repetitive (25 times) cleaning of a wide range of oil phases at chemically harsh aqueous settings with high oil absorption capacities (upto 4000 wt%) was successfully demonstrated without compromising the physical integrity of the sponge and the embedded water wettability. The analogous waste paper derived membranes were also extended for repetitive (50 times) gravity-driven filtration-based separation of various oils from the respective oil/water mixtures with oil separation efficiency above 95% even at chemically contaminated aqueous environments without compromising the associated anti-wetting property. Thus, such strategic association of a facile and robust chemistry with the valueless waste paper at ambient conditions could be further useful for developing smart bio-interfaces, thermal insulators, open-microfluidic devices etc.

## 4.2. Experimental Section:

### 4.2.1. Materials Required:

Dipentaerythritol penta-acrylate (5Acl, MW=524.51 g/mol), silicone oil (CAS No. 63148-58-3), methylene blue (CAS No. 122965-43-9), rhodamine 6G (CAS No. 989-38-8), nile red (CAS No. 7385-67-3), octadecylamine, decylamine, octylamine, hexylamine, pentylamine, butylamine, 3-(2-aminoethylamino)-propyltrimethoxysilane (CAS No. 1760-24-3), sodium dodecyl sulfate (SDS), dodecyl trimethyl ammonium chloride (DTAB) were obtained from Sigma-Aldrich (Bangalore, India). Chloroform, tetrahydrofuran, dichloromethane was procured from FINAR. Ethyl acetate was procured from RANKEM (Maharashtra, India). Sodium chloride, magnesium chloride, calcium chloride, magnesium sulphate, and sodium hydroxide were purchased from Merck Specialties Private Limited. Hydrochloric acid was purchased from Fischer Scientific (Hyderabad, India). Ethanol was purchased from Changshu Hongsheng Fine Chemical Co. Ltd. Adhesive tape, calibration weights, vegetable oil, tissue paper, sand paper were purchased from Amazon, India. Motor Oil (Castrol GTX 20 W-50), kerosene oil, petrol and diesel were purchased from Indian Oil petrol pump. Newspaper, cardboard paper, office paper was purchased from a local store in IIT Guwahati. Sand grains were collected from a construction site at IIT Guwahati and rinsed with water, dried prior to use. River water was collected from Brahmaputra River, Guwahati (Assam, India)

### 4.2.2. General Considerations:

All the glass wares were washed with acetone prior to use. Contact angle measurements were carried out using a KRUSS Drop Shape Analyzer-DSA25 with an automatic liquid dispenser at ambient conditions. The contact angles were measured using 5 µl water droplet at three different locations for each sample. Labconco Freezone Freeze Dryer was used for lyophilization of the paper sponges. Scanning electron microscope images were acquired using the Sigma Carl Zeiss scanning electron microscope. The samples were sputtered with gold prior to imaging. ATR-FTIR spectra was recorded using the Perkin Elmer instrument at ambient conditions. To identify the chemical oxidation states of the elements, XPS was performed by using an ESCA probe TPD spectrometer, Omicron Nanotechnology with a polychromatic Al Kα (hν = 1486.6 eV) X-ray source with a step size of 0.1 eV per second. The binding energy (B.E) of all the elements was calibrated with respect to C 1s (284.8 eV). Compressive and tensile measurements were carried out using a 5 kN electromechanical Universal Testing Machine. Digital images were acquired using a Canon Power shot SX420 IS digital camera. Milli-Q grade water was used for all experiments.

The porosity measurements were calculated using the widely adapted standard formula,

$$\mathbf{Porosity}\ (\%) = (\mathbf{1} - \boldsymbol{\rho}/\boldsymbol{\rho}_{\mathbf{s}})$$

where, $\rho$ and $\rho_s$ is the volumetric mass density of the dry sponge and wet sponge respectively.[36-37]

### 4.2.3. Fabrication of Chemically 'Reactive' Waste Paper Sponges and Post Chemical Modification:

To fabricate the waste-paper derived sponges, 1.96 wt% of waste paper was shredded into pieces and dispersed in 30 mL of water under constant stirring for 1 hour followed by addition of 3-(2-amino-ethylamino)-propyltrimethoxysilane (AEPTMS) in the desired amounts and the resultant sponges were denoted as $WPDS_{0.5}$, $WPDS_1$, $WPDS_2$, $WPDS_3$ respectively. Refer to Table 4.1 for detailed sponge composition.

Here, tissue paper was selected as the model waste paper for performing all the experiments. The AEPTMS added waste paper mixture was kept under continuous stirring at room temperature for 6

**Table 4.1** Accounting for the concentration of waste paper and AEPTMS used for developing the different waste paper derived sponges.

| Sample | Concentration of Waste Paper (wt%) | AEPTMS added (wt%) |
|---|---|---|
| **$WPDS_{0.5}$** | 1.96 | 1.65 |
| **$WPDS_1$** | 1.96 | 3.25 |
| **$WPDS_2$** | 1.96 | 4.79 |
| **$WPDS_3$** | 1.96 | 6.29 |

hours to ensure uniform mixing. Thereafter, the mixture was poured into cylindrical molds and glass petri-dish for fabricating the sponges and membranes respectively. The molds were frozen in liquid nitrogen and subsequently, lyophilized at -101°C for 36 hours. Afterwards, the dried sponges/membranes were further treated with an ethanolic solution of dipentaerythritol penta-acrylate (1.325 g 5Acl in 10 mL ethanol) for 3 hours followed by thorough washing in ethanol and THF for 15 mins each. Thereafter, the sponges were subjected to post covalent modification with amine containing small molecules with concentrations (30 mg/mL) i.e. butylamine, pentylamine, hexylamine, octylamine, decylamine and octadecylamine (5 mg/mL) for 12 hours. The samples were thoroughly washed with THF after the post modification and subsequently dried at ambient conditions.

**4.2.4. Physical and Chemical Durability Tests:** To examine the durability of the embedded anti-wetting property of the waste paper derived superhydrophobic sponges, various harsh physical and chemical challenges were imposed as described in detail below.

**4.2.4.1. Sand Paper Abrasion:** In this test, the waste paper derived compressible, superhydrophobic sponge, $WPDSHS_1$ (length ~ 5 cm) was rubbed manually with a sand paper for 20 times back and forth with a 500 g load on top to inflict severe damage to the sponge. Thereafter, the embedded anti-wetting property on the freshly exposed interior of the sponge was examined through contact angle measurements and digital images.

**4.2.4.2. Bulk Superhydrophobicity:** The presence of three-dimensional water wettability in the waste paper derived sponge ($WPDSHS_1$) was examined by arbitrarily slicing the sponge into pieces to expose the interiors. Subsequently, the anti-wetting property was examined using contact angle measurements.

**4.2.4.3. Sand Drop Test:** In this test, 150 g of sand grains were poured from a height of 25 cm on the waste paper derived superhydrophobic sponge, $WPDSHS_1$ (length ~ 4 cm) which was pre-tilted at 45°. Thereafter, the embedded anti-wetting property was examined on the abraded surface of the sponge via contact angle measurements and digital images.

**4.2.4.4. UV Irradiation:** The waste paper derived superhydrophobic sponge, $WPDSHS_1$ was subjected to both short (254 nm) and long (365 nm) UV irradiation for 30 days. The embedded water-repellent property was examined at regular intervals through contact angle measurements and digital images.

**4.2.4.5. Chemical Durability:** The waste paper derived superhydrophobic sponge, $WPDSHS_1$ was exposed to various harsh chemically complex aqueous phases including acidic water (pH 1), basic water (pH 12), surfactant contaminated water (SDS, 1 mM and DTAB, 1 mM), river water (Brahmaputra River, Assam, India) and artificial seawater. Artificial seawater was prepared by mixing $MgCl_2$ (0.226 g), MgSO4 (0.325 g), NaCl (2.673 g) and $CaCl_2$ (0.112 g) in 100 mL of de-ionized water in a volumetric flask. Similarly, the waste paper derived superhydrophobic sponge, $WPDSHS_1$ was exposed to various polar and non-polar organic solvents including methanol, ethanol, tetrahydrofuran, dimethyl sulfoxide, acetone, chloroform, hexane, dichloromethane for 30 days and subsequently, the embedded water repellence was examined at regular intervals through contact angle measurements.

**4.2.5. Absorption Based Oil/Water Separation:** The waste paper derived compressible superhydrophobic sponges were exploited successfully for absorption-based collection of oils of varying densities and viscosities from an oil/water interface. Briefly, 1 mL of the oil (dyed with Nile red for petrol, diesel, silicone and vegetable oil for visual inspection) was placed in a petri-dish filled with water. Then, the waste paper derived superhydrophobic sponge was placed at the oil/water interface such that it selectively absorbed only the oil phase. The absorbed oil was recovered by manually squeezing the sponge. Furthermore, this absorption-based selective separation was extended for model heavy oil i.e. dichloromethane, DCM (dyed with Nile red). Briefly, 5 mL of DCM was poured in a beaker filled with 15 mL of water followed by immersion of the superhydrophobic sponge into the oil/water mixture such that sediment oil phase was selectively absorbed. The absorbed oil was recovered by manual squeezing of the sponge.

**4.2.6. Gravity-Driven Filtration Based Oil/Water Separation:** The waste paper derived superhydrophobic membranes were extended for gravity-driven selective filtration of various light and heavy oils from the respective oil/water mixtures. A lab made proto-type was developed using a 50 mL falcon tube where one end of the tube was tied with the waste paper derived superhydrophobic membrane and a hole was made at the closed end of the tube to pour the oil/water mixture with the help of a funnel. Water was dyed with methylene blue and rhodamine 6G as required and dichloro-methane (model heavy oil) was dyed with Nile red. To demonstrate the gravity-driven filtration-based oil/water separation, an equal amount of oil and water (20 mL each) was poured through the funnel at the closed end such that the oil phase selectively permeated through the superhydrophobic membrane, while the water phase remained restricted by the water-repellent membrane.

## 4.3. Results and Discussions:

### 4.3.1. Fabrication of Waste Paper Derived Mechanically Tailorable Sponges

In this chapter, waste paper was converted into a functional material with the ability to tailor both the 1) mechanical property and 2) chemistry following a catalyst-free, facile chemical approach. In the recent past, Baidya *et al*. developed a fluorinated cellulose nanofiber based superhydrophobic coating, where perfluoro-octyltriethoxysilane and AEPTMS were covalently integrated with the hydroxyl groups of cellulosic nanofibers.[23] The polymerization of AEPTMS imparted mechanical stability to the silane modified cellulose nanofibers in comparison to the unmodified one. Inspired from this report, in the current chapter, the association of AEPTMS and chemically 'reactive' cross-linking with waste paper allowed to tailor the mechanical property and water wettability respectively. Shredded pieces of a model waste paper (i.e. tissue paper) in aqueous media were stirred under room temperature for 6 hours and thereafter, this mixture was poured into cylindrical molds followed by freeze drying to obtain an inherently hydrophilic sponge (with WCA of 0°), denoted as $\text{WPS}_{\text{control}}$ as shown in Figure 4.2A-B. On application of an external load (500 g), $\text{WPS}_{\text{control}}$ underwent permanent deformation and failed to regain its original shape as shown in Figure 4.2C-D. FESEM images of $\text{WPS}_{\text{control}}$ revealed compact and fibrous domains as shown in Figure 4.2E-F, the compact network is attributed to the distortion of the skeletal framework of the fragile $\text{WPS}_{\text{control}}$ while manual handling. However, the

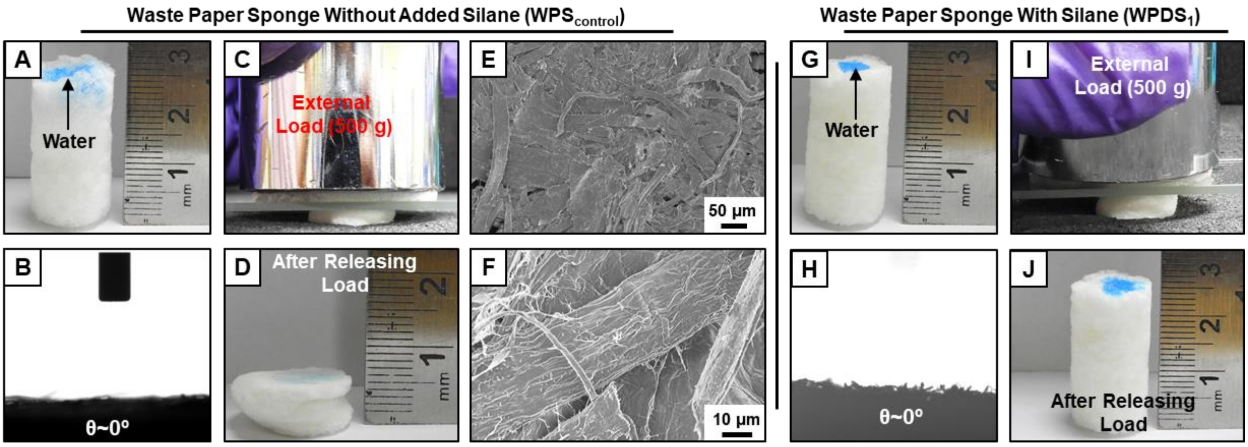

**Figure 4.2.** A-D) Digital image (A) and WCA image (B) illustrating the hydrophilic waste paper sponge ($\text{WPS}_{\text{control}}$) that was compressed with an external load of 500 g (C) such that $\text{WPS}_{\text{control}}$ underwent permanent deformation on releasing the load (D). E-F) FESEM images at low (E) and high (F) magnifications revealing the morphology of $\text{WPS}_{\text{control}}$. G-J) Digital image (G) and WCA image (H) illustrating a waste paper derived sponge that was developed by *in situ* covalent modification of waste paper with an amine modified silane moiety (AEPTMS). On compressing the silane modified waste paper derived sponge, ($\text{WPDS}_1$ where 1 denotes the concentration of AEPTMS) with an external load of 500 g (I) followed by load release (J) led to complete recovery of the sponge dimensions thus, validating the role of AEPTMS in imparting mechanical durability to the sponge.

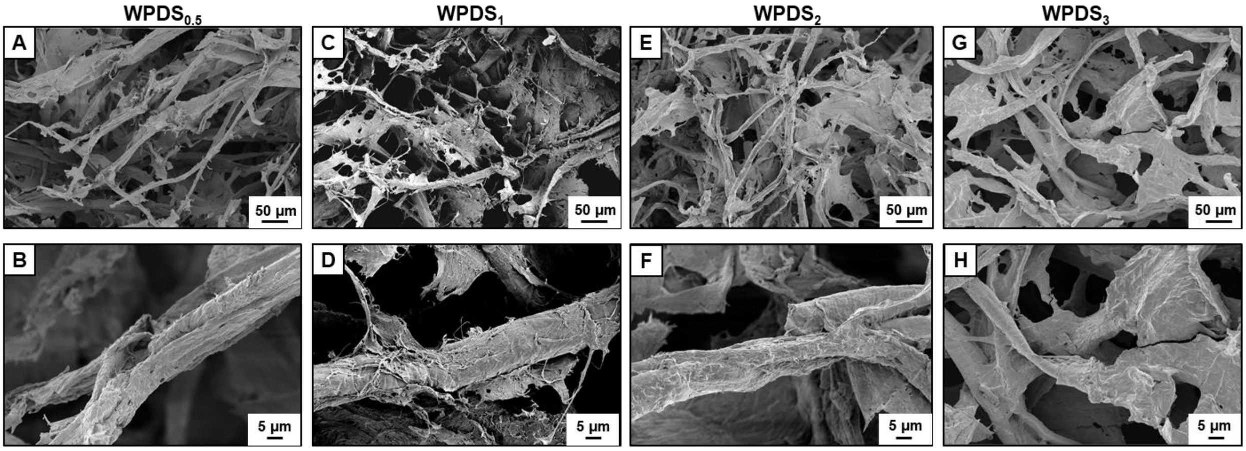

**Figure 4.3.** A-H) FESEM images at low (A, C, E, G) and high (B, D, F, H) magnifications exhibiting the interconnected, fibrous and porous morphology of the waste paper derived sponges doped with different concentrations of AEPTMS.

strategic *in situ* association of AEPTMS with this disintegrated waste paper fibers in aqueous media followed by freeze drying yielded a hydrophilic and spongy material that can regain its original shape after removal of the external load (500 g) as shown in Figure 4.2G-J. Thus, the addition of AEPTMS to waste paper denoted as waste paper derived sponge $WPDS_1$ (where the subscript denotes the concentration of AEPTMS added, refer to Table 4.1), resulted in a highly porous interconnected spongy network as shown in Figure 4.3C-D. Varying the concentration of AEPTMS further led to change in the morphology and porosity of the as prepared sponges as shown in Figure 4.3A-H and Table 4.2. Increasing the AEPTMS concentration decreased the porosity of the sponges as tabulated in 4.2. This change in morphology was attributed to the polymerization of AEPTMS resulting in a polymeric network.

The integration of AEPTMS with the waste paper sponge was validated through XPS analysis as shown in Figure 4.4D, where the additional peaks corresponding to N and Si were exhibited after AEPTMS modification. These peaks were absent in the waste paper sponge without any added AEPTMS as shown in Figure 4.4A. De-convoluted XPS for C 1s of waste paper sponge ($WPS_{control}$) is shown in Figure 4.4B, where the peaks at 284.5, 286.5 and at 287.6 eV corresponds to C-C, C-O

**Table 4.2** Accounting for the porosity of the waste paper derived sponges with varying concentrations of AEPTMS.

| Sample | Porosity (%) |
|---|---|
| **$WPDS_{0.5}$** | 99.1 ± 1.2 |
| **$WPDS_1$** | 98.4 ± 0.8 |
| **$WPDS_2$** | 96.8 ± 1.6 |
| **$WPDS_3$** | 95.1 ± 0.7 |

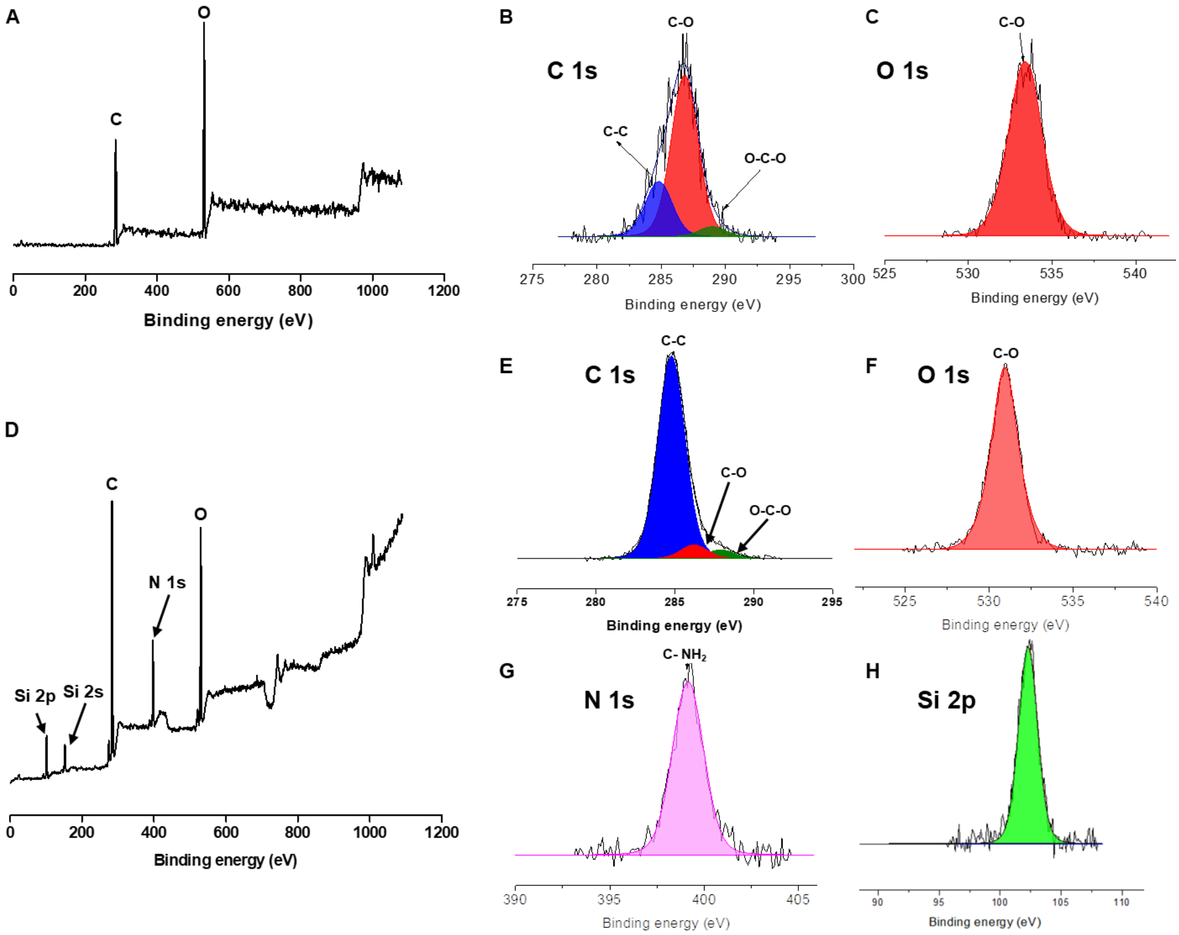

**Figure 4.4.** A) XPS spectra of waste paper sponge, $WPS_{control}$. B-C) De-convoluted XPS spectra of C 1s (B) and O 1s (C) of $WPS_{control}$ respectively. D) XPS spectra of waste paper derived sponge, $WPDS_1$. E-H) De-convoluted XPS spectra of C 1s (E), O 1s (F), N 1s (G) and Si 2p (H) of $WPDS_1$ respectively.

and O-C-O respectively. After the association of AEPTMS, the relative peak intensity corresponding to C-O depleted and slightly shifted (to 286.1 eV) as shown in Figure 4.4E, which was attributed to the covalent bonding between Si of (AEPTMS) with the hydroxyl groups of cellulose.[23] Further, the polymerization of AEPTMS in aqueous media was confirmed through the standard FTIR analysis. The AEPTMS monomer exhibited the characteristic Si-O-C stretching peak at 1078 $cm^{-1}$ as shown in Figure 4.5A (black). On polymerization of AEPTMS, the peak at 1078 $cm^{-1}$ diminished and a new peak at 1020 $cm^{-1}$ appeared which corresponds to the Si-O-Si stretching as shown in Figure 4.5A(red). Moreover, Energy Dispersive X-ray (EDX) analysis of the paper sponge confirmed the doping of AEPTMS, where the peaks corresponding to N and Si elements were exhibited in addition to the C and O peaks of cellulose as shown in Figure 4.5B. The uniform and varying distribution of C, O, N, Si was confirmed with elemental mapping for the AEPTMS associated sponge as shown in Figure 4.5C-G. Hence, EDX analysis confirmed the homogenous integration of AEPTMS with the waste paper mixture, providing a uniform skeletal network of AEPTMS all throughout the sponge.

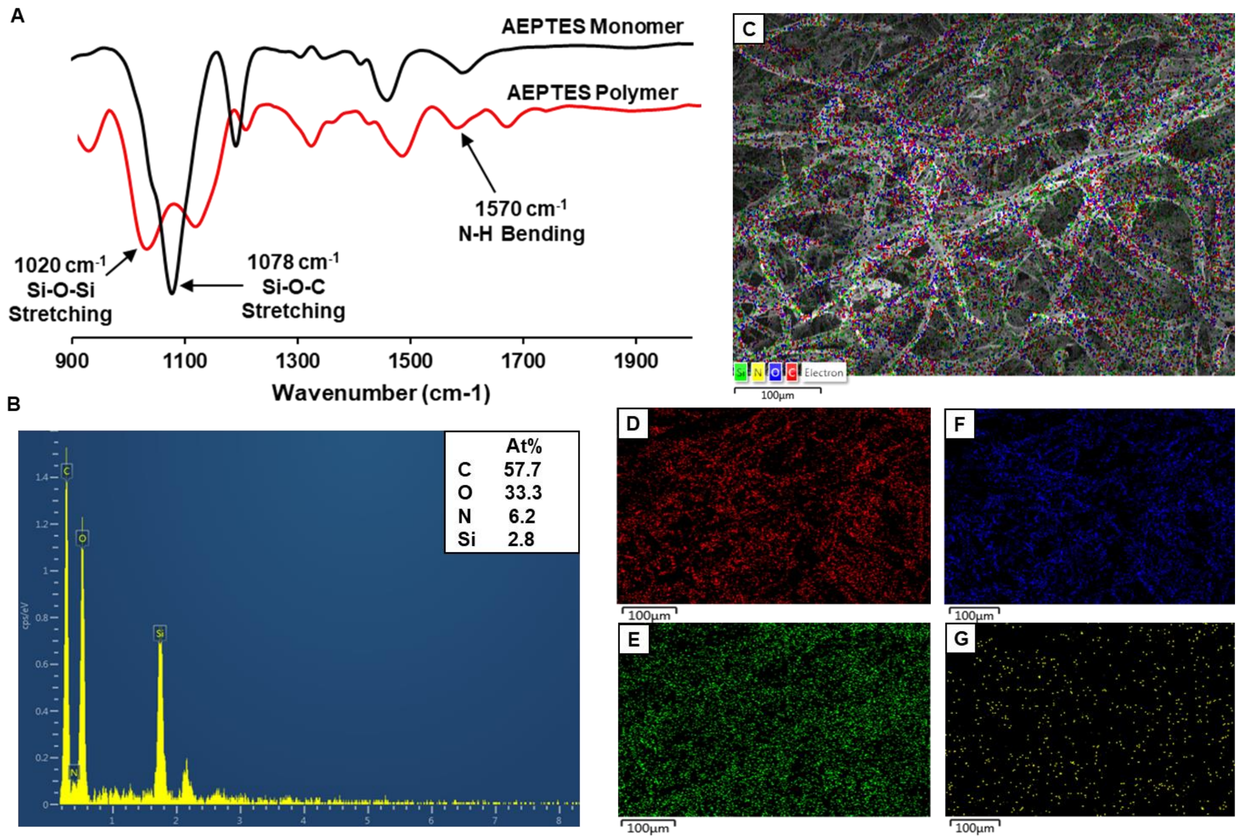

**Figure 4.5.** A) ATR-FTIR analysis of AEPTMS monomer exhibits a peak at 1078 cm$^{-1}$ corresponding to the Si-O-C bond of the monomer (black) which depleted entirely on polymerization and a new peak at 1028 cm$^{-1}$ corresponding to the Si-O-Si bond appeared for the AEPTMS polymer, thus, confirming the silane polymerization process (red). B-G) Energy dispersive X-ray spectral analysis (B) and mapping images (C-G) of WPDS$_1$.

The compressive stress-strain analysis further revealed that the AEPTMS modification played the major role in tailoring the compressive modulus of the sponges as shown in Figure 4.6A. Varying the AEPTMS concentration provided a facile avenue to modulate the mechanical property of the sponges. The compressive modulus values decreased in the order as WPDS$_3$ >WPDS$_2$ >WPDS$_1$ >WPDS$_{0.5}$

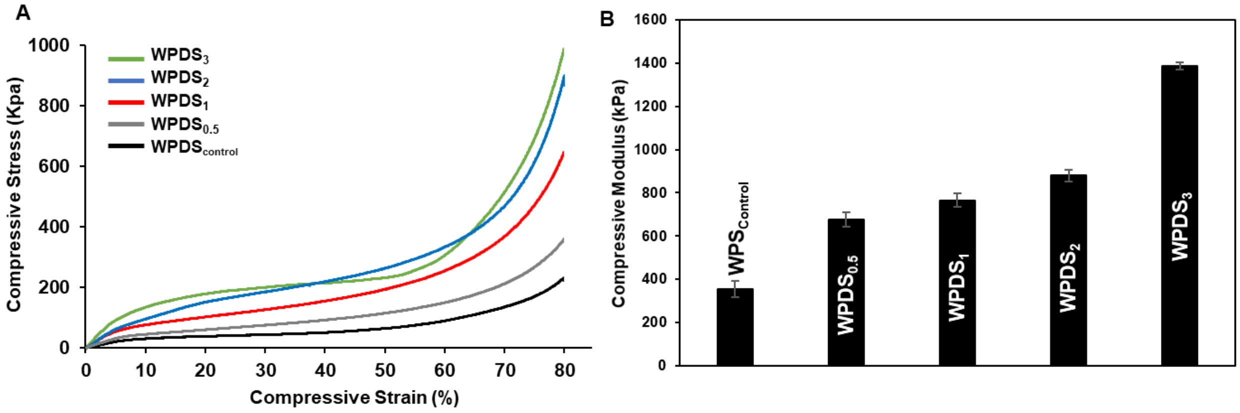

**Figure 4.6.** A) Plot depicting the stress-strain analysis of the different sponges derived from waste paper. B) Bar diagram accounting for the varying compressive modulus values of the sponges developed using waste paper doped with different concentrations of AEPTMS.

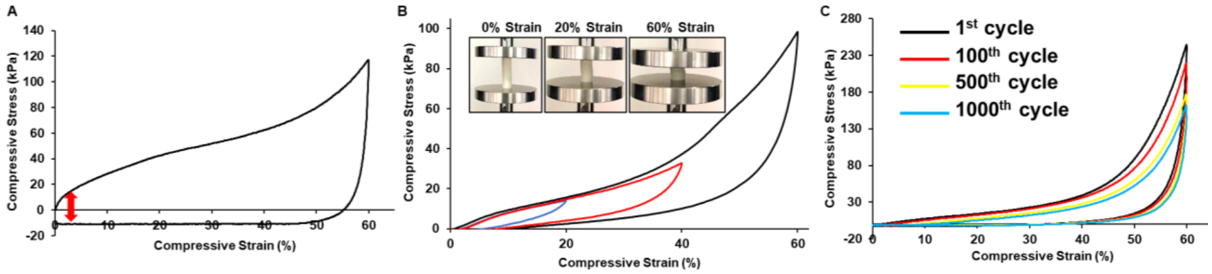

**Figure 4.7.** A) Plot accounting for the cyclic compression analysis of the waste paper derived sponge, $WPS_{control}$. B) Plot illustrating the cyclic stress-strain analysis of $WPDS_1$ under different percentage of strain. C) Plot accounting for the cyclic compression analysis of the waste paper derived sponge, $WPDS_1$.

>$WPS_{control}$ as shown in Figure 4.6B. Thus, the lower concentration of AEPTMS yielded a highly compressible sponge whereas higher concentration generated a comparatively stiffer sponge. In-plane compression test was further performed to evaluate the shape recovery of the AEPTMS associated sponges after application of external strain. In case of $WPS_{control}$, a permanent physical deformation was observed after the 1st cycle of compression as shown in Figure 4.7A. However, the physically deformable $WPDS_1$, which was subjected to 20%, 40% and 60% compressive strain, recovered its original shape, once the applied load was released as evident from the hysteresis curve as shown in Figure 4.6B. Moreover, the cyclic compressive study of $WPDS_1$ revealed that the as fabricated sponge exhibited satisfactory recovery even after 1000 cycles of compression (Figure 4.6C), unlike $WPS_{control}$. Thus, the controlled association of AEPTMS with waste paper allowed to adopt a route for tailorable and durable mechanical property.

### 4.3.2. Induction of Chemical 'Reactivity' in the Waste Paper Derived Highly Compressible Sponges

Over the years, various waste paper derived functional substrates have been developed for a wide range of applications.[18-26,29-33] However, the reported materials lack the covalent cross-linking network and none of the reported approaches provides an avenue to associate diverse and the desired chemical functionalities.[18-26,29-33] In this chapter, the catalyst-free Michael addition reaction between amine and acrylate was adopted to induct readily 'reactive' residual acrylate groups for post covalent modification with different nucleophiles at ambient conditions.[38-39] The XPS analysis of the deconvoluted N 1s peak (at ~400 eV, Figure 4.8A) of $WPDS_1$ revealed the presence of amine moiety in the paper sponge after addition of AEPTMS. The induction of chemical reactivity in the paper sponge was achieved through the reaction of the amine groups of the AEPTMS modified paper sponge with a multifunctional acrylate cross-linker (5Acl) following the catalyst-free Michael addition reaction between amine and acrylate groups at ambient conditions (Figure 4.1). The presence of 'reactive' acrylate groups in the waste paper sponge rendered it chemically 'reactive' at ambient conditions towards amine containing

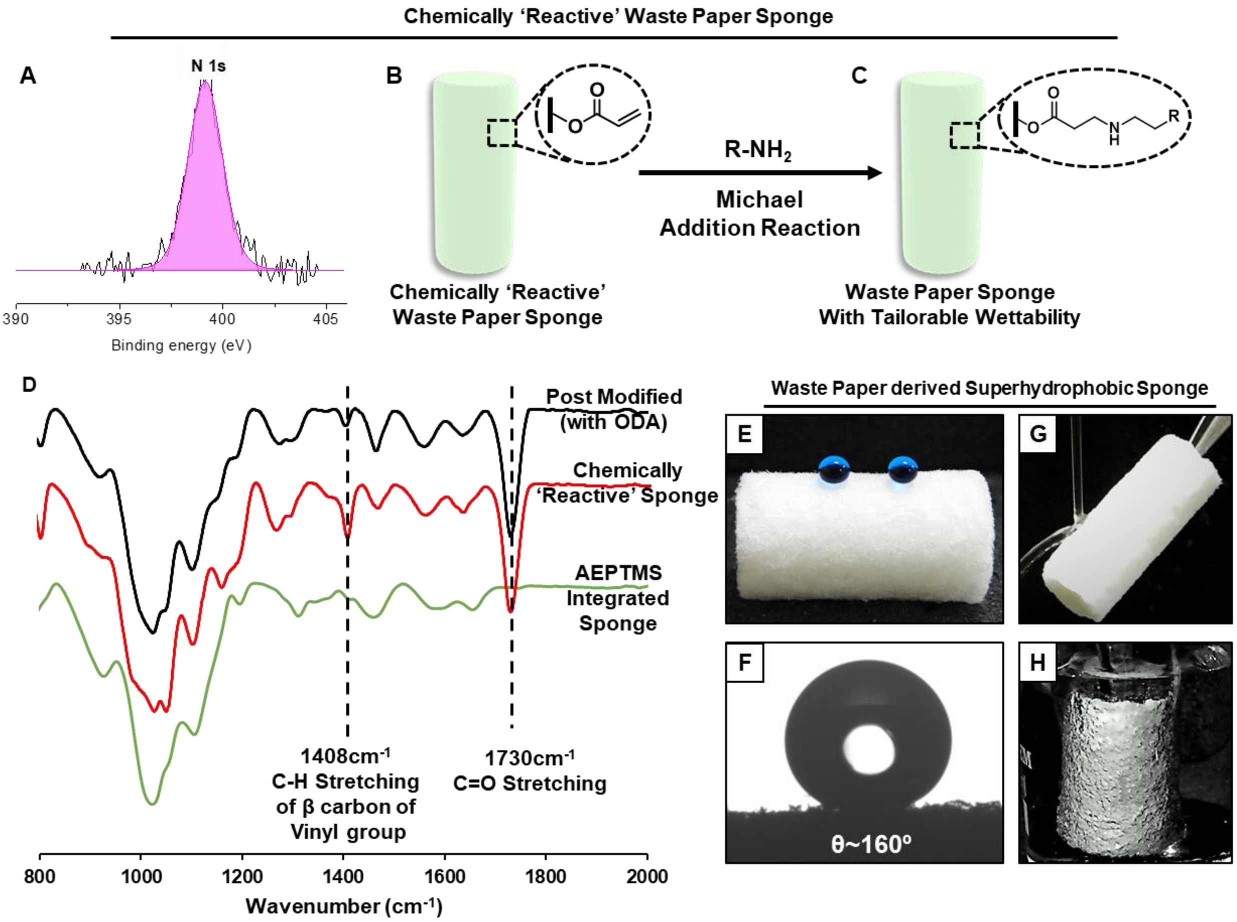

**Figure 4.8.** A) De-convoluted XPS spectra of N 1s of the waste paper derived sponge that was covalently associated with AEPTMS. The peak at 400 eV indicates the presence of amines in the fabricated sponge owing to the presence of AEPTMS. B-C) Schematic depicting the Michael addition reaction of the chemically 'reactive' waste paper derived sponge with amine containing small molecules that provides an avenue to tailor the water wettability. D) ATR-FTIR analysis of the chemically 'reactive' waste paper derived sponge (red) revealed the presence of peaks at 1408 cm$^{-1}$ and 1730 cm$^{-1}$ which corresponds to the symmetric deformation of the C-H bond of β carbon of the vinyl group and carbonyl stretching frequency respectively. However, the AEPTMS modified waste paper derived sponge did not exhibit the mentioned peaks (green). The reduction in the peak intensity at 1408 cm$^{-1}$ with respect to the normalized carbonyl peak at 1730 cm$^{-1}$ confirmed the covalent linkage of the residual acrylate functionalities with ODA (black). E-F) Digital image (E) and static WCA image (F) of the beaded water droplet on the waste paper derived sponge, WPDSHS$_1$ that was post modified with ODA. G) Digital image demonstrating the bouncing of a stream of water from the surface of WPDSHS$_1$. H) WPDSHS$_1$ on submerging underwater, displayed a shiny interface that confirmed the presence of a metastable air layer responsible for conferring heterogeneous water wettability.

nucleophiles (Figure 4.8B-C). The successful covalent incorporation of acrylate groups in the AEPTMS modified paper sponge was characterized. The appearance of the characteristic IR peaks for acrylate groups in the AEPTMS functionalized waste paper derived sponge was further confirmed through standard FTIR analysis.[38-39] The appearance of the peaks at 1408 cm$^{-1}$ and 1730 cm$^{-1}$ corresponding to the C-H stretching of β carbon of the vinyl group and the carbonyl stretching respectively confirmed the presence of the residual presence of the groups in the paper sponge (Figure 4.8D, red) due to the integration of 5Acl with the paper derived sponge. These FTIR signatures were

**Table 4.3** Accounting for the advancing WCA and contact angle hysteresis of the beaded water droplet on the waste paper derived sponges after post covalent modification with ODA.

| Sample | Advancing Contact Angle (°) | Contact Angle Hysteresis (°) |
|---|---|---|
| **WPDSHS$_{0.5}$** | 146.4±1.1 | 15.3±1.5 |
| **WPDSHS$_1$** | 159.4±1.2 | 7.3±0.4 |
| **WPDSHS$_2$** | 158.7±0.6 | 7.5±0.6 |
| **WPDSHS$_3$** | 157.2±0.6 | 7.6±1.4 |

not observed in WPDS$_1$ prior to treatment with 5Acl as shown in Figure 4.8D (green). Interestingly, the existence of residual acrylate groups render the paper derived sponge chemically 'reactive' and after post modification of the chemically 'reactive' waste paper derived sponge with an amine containing nucleophile i.e. ODA, the FTIR peak intensity at 1408 cm$^{-1}$ decreased with respect to the normalized carbonyl peak at 1730 cm$^{-1}$ (which serves as the internal standard) as shown in Figure 4.8D (black). Hence, the FTIR analysis confirmed the successful post modification of the residual acrylates of the paper sponge with an amine containing nucleophile. The post covalent modification of the chemically 'reactive' waste paper sponge with ODA transformed the hydrophilic sponge into a superhydrophobic sponge with static WCA ~160° as shown in Figure 4.8E-F and Table 4.3. A stream of water readily bounced off from the surface of WPDSHS$_1$ thus, displaying non-adhesive superhydrophobicity as shown in Figure 4.8G. Moreover, on submerging WPDSHS$_1$ underwater, a shiny interface was observed which validated the presence of a metastable trapped air layer that is responsible for the existence of heterogeneous wettability as shown in Figure 4.8H. As shown in Table 4.3, the concentration of another reactant i.e. AEPTMS also influenced the water wettability where,

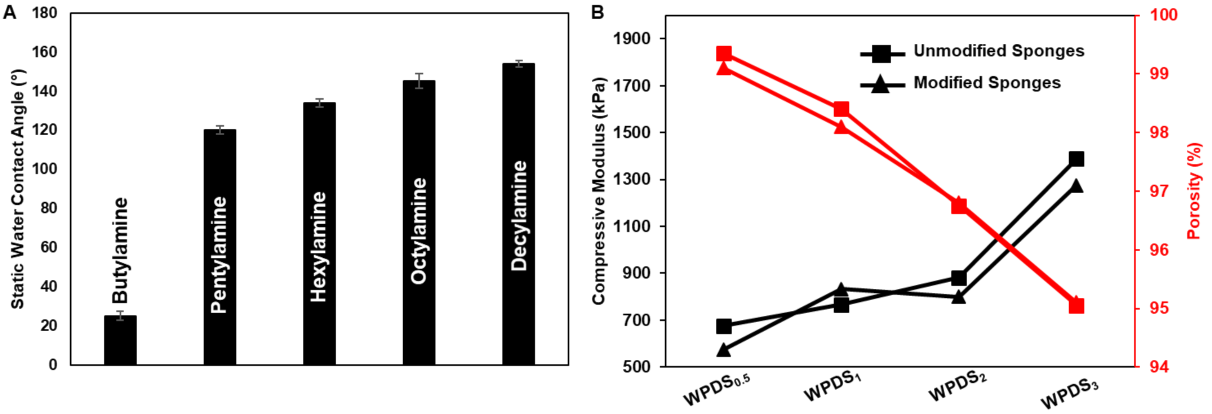

**Figure 4.9.** A) Bar diagram representing the static WCA of the beaded water droplet on WPDS$_1$ that was modified with different amine containing small molecules. B) Plot illustrating the compressive modulus (black) and porosity (red) of the waste paper derived superhydrophobic sponges before 5Acl treatment and after post covalent modification with ODA.

**Table 4.4** Accounting for the advancing WCA and contact angle hysteresis of the beaded water droplet on $WPDS_1$ after post covalent modification with different amine containing small molecules.

| Post Modification with Alkylamines | Advancing Contact Angle (°) | Contact Angle Hysteresis (°) |
|---|---|---|
| **Butylamine** | 33.3 ± 1.0 | - |
| **Pentylamine** | 123.5 ± 0.5 | 21.6 ± 0.7 |
| **Hexylamine** | 136.0 ± 0.8 | 18.3 ± 1.0 |
| **Octylamine** | 146.2 ± 1.3 | 12.1 ± 0.6 |
| **Decylamine** | 156.7 ± 0.4 | 7.9 ± 0.3 |
| **Octadecylamine** | 161.0 ± 0.7 | 7.3 ± 0.5 |

3.25 wt% AEPTMS w.r.t. 1.96 wt% of waste paper (denoted as waste paper derived superhydrophobic sponge, $WPDSHS_1$) is the minimum concentration of AEPTMS required to display superhydrophobicity. However, the waste paper derived chemically 'reactive' sponge with 1.65 wt% AEPTMS (denoted as $WPDSHS_{0.5}$) after post modification displayed only hydrophobicity with advancing WCA~146° as shown in Table 4.3. The sponges developed with concentrations above 3.25 wt% of AEPTMS (denoted as $WPDSHS_2$ and $WPDSHS_3$) successfully displayed the extreme anti-wetting property with advancing WCA above 150° and contact angle hysteresis below 10° as shown in Table 4.3.

Moreover, the presence of residual acrylate based chemical reactivity provided a facile basis to tune the wettability from ~25° to ~161° i.e. moderate hydrophobicity, adhesive superhydrophobicity to non-adhesive superhydrophobicity following the Michael addition reaction between residual acrylates and selected various amine containing small molecule as shown in Figure 4.9A and Table 4.4. Moreover, the covalent modification with 5Acl and post modification with ODA did not alter the mechanical property of the sponge as confirmed from the study on the compressive modulus of the sponge before and after chemical modification as shown in Figure 4.9B (black line). Thus, AEPTMS is responsible for modulating the mechanical property of the sponges, however, the tailored mechanical property remains unchanged during further chemical modification of the sponges. Also, the porosity of the sponges remained unaltered after post covalent modification as shown in Figure 4.9B (red line).

Irrespective of the type of waste paper, this facile fabrication procedure could be further extended for developing compressible superhydrophobic sponges using different types of waste papers, including office paper (A4 paper), newspaper and cardboard paper as shown in Figure 4.10A-F. The water droplets beaded with WCA above 150° and contact angle hysteresis below 10° as shown in Table 4.5. Even the mixture (1:1:1:1 weight ratio) of all the different types of waste papers (tissue paper,

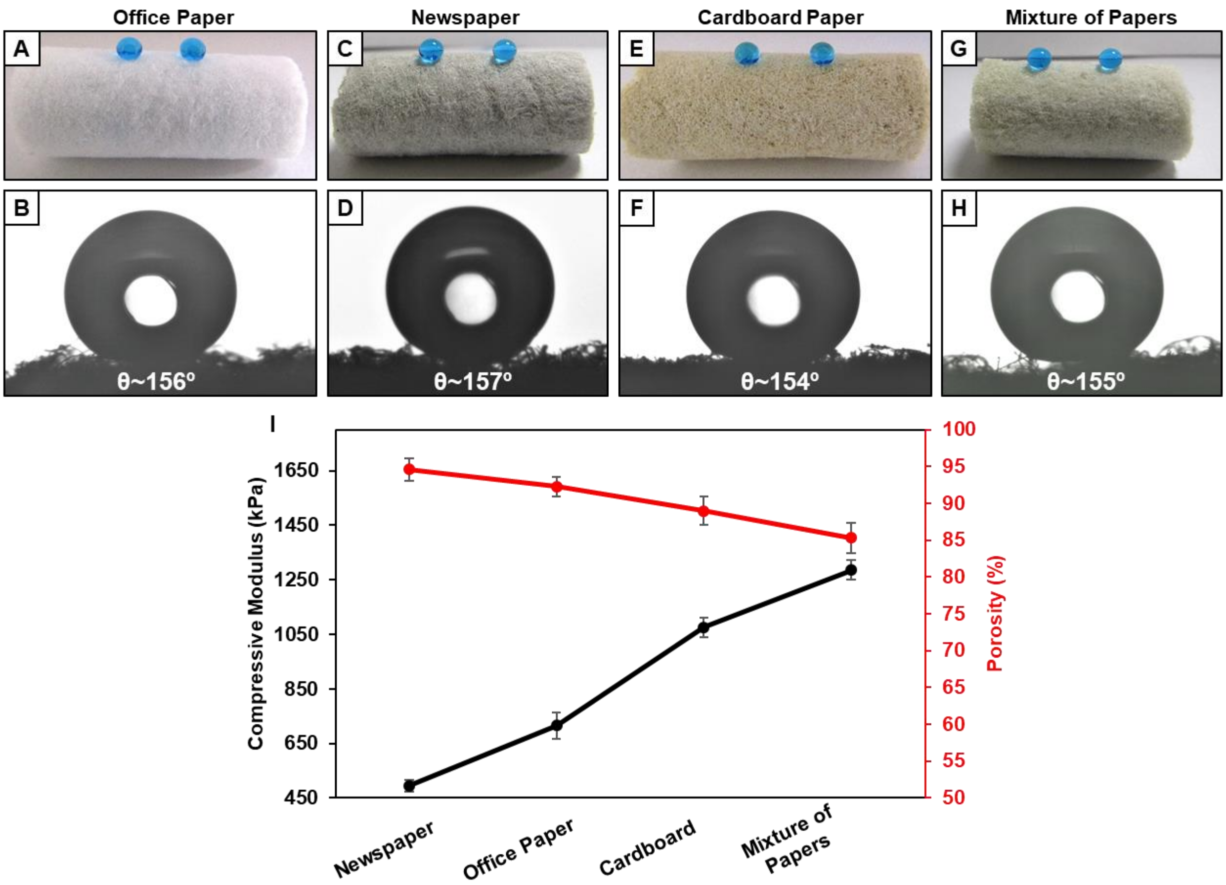

**Figure 4.10.** A-H) Digital images (A,C,E,G) and WCA images (B,D,F,H) of the superhydrophobic sponges that were developed using different types of waste papers i.e. office paper (A, B), newspaper (C, D), cardboard paper (E, F) and a mixture of the mentioned papers (G, H). I) Plot illustrating the compressive modulus (black) and porosity (red) of the different types of waste paper derived superhydrophobic sponges.

cardboard, newspaper and office paper) generated a superhydrophobic sponge as shown in Figure 4.10G-H and Table 4.5. The compressive modulus and porosity of the synthesized superhydrophobic sponges varied based on the nature of the waste paper used, even though the silanization and post-covalent modification process remains unchanged. Interestingly, the maximum compressive modulus (1285 kPa) and minimum porosity (85%) was observed for the sponge derived from the mixture of

**Table 4.5** Accounting for the advancing WCA and contact angle hysteresis of the beaded water droplet on the different types of waste paper derived superhydrophobic sponges.

| Sample | Advancing Contact Angle (°) | Contact Angle Hysteresis (°) |
|---|---|---|
| **Office Paper** | 158.4 ± 0.6 | 7.5 ± 1.3 |
| **Newspaper** | 159.2 ± 1.1 | 7.3 ± 0.9 |
| **Cardboard Paper** | 157.8 ± 1.2 | 7.8 ± 1.1 |
| **Mixture of Papers** | 156.7 ± 0.8 | 8.21± 1.4 |

different papers as shown in Figure 4.10I. The order of porosity and compressive modulus followed a completely opposite order as shown in Figure 4.10I, since increased porosity reduces the cross-sectional area for stress tolerance.

### 4.3.3. Examining the Durability of the Embedded Water Repellence in the Waste Paper Derived Sponge

The sustainability of the waste paper derived superhydrophobic sponges at severe challenging physical and chemical environments is of utmost importance for real life applicability. WPDSHS$_1$ displaying superhydrophobicity and appreciable compressibility was chosen to investigate the durability of the embedded water repellence. To examine the impact of physical deformation, WPDSHS$_1$ was gradually compressed upto 60% compressive strain and on releasing the applied strain the sponge regained its original shape without perturbing the embedded superhydrophobicity as shown in Figure 4.11A. Further, imposing repetitive, 60% compressive strain for 1000 consecutive cycles failed to perturb the embedded anti-wetting property in the sponge (WPDSHS$_1$) with advancing WCA above 150° and contact angle hysteresis below 10° as shown in Figure 4.11B.

The superhydrophobic property is not just limited to the surface of the sponge but was exhibited by the bulk of the prepared sponge as well as shown in Figure 4.12A-B, where WPDSHS$_1$ (inset image) was arbitrarily sliced into pieces to randomly expose the interior of the sponge. The freshly exposed interiors of the waste paper derived superhydrophobic sponge continued to repel the beaded water droplet with static WCA~158° as shown in Figure 4.12A-B. Next, a standard and widely accepted abrasive test, 150 g of sand grains were poured onto the surface of WPDSHS$_1$ (tilted at 45°) from a height of 25 cm (Figure 4.12C). The sand grains exposed interface of WPDSHS$_1$ displayed extreme

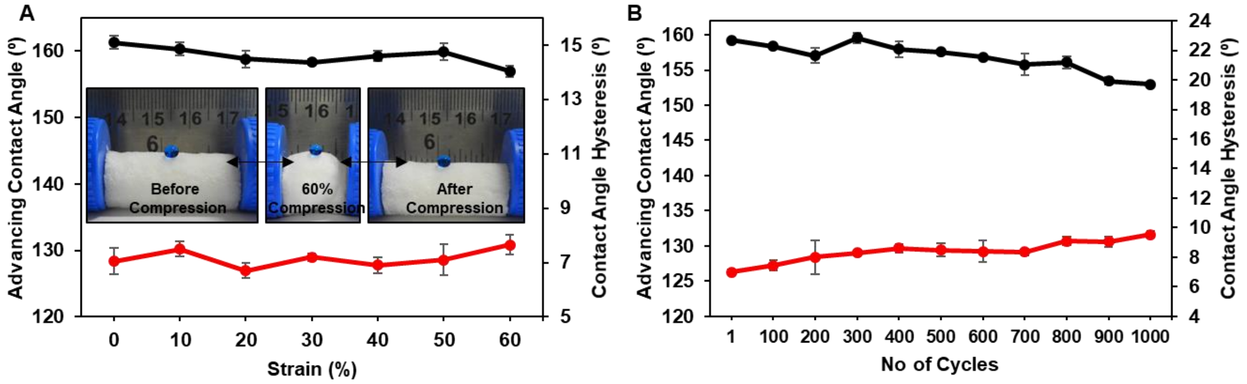

**Figure 4.11.** A) Plot accounting for the advancing WCA (black) and contact angle hysteresis (red) of the beaded water droplet on WPDSHS$_1$ that was subjected to 60% manual compression. The inset images exhibit that the embedded water repellence behaviour remains intact before (left), during (middle) and after (right) compression. B) Plot representing the advancing WCA (black) and contact angle hysteresis (red) of the beaded water droplet on WPDSHS$_1$ that was repetitively deformed for 1000 cycles under 60% manual compression.

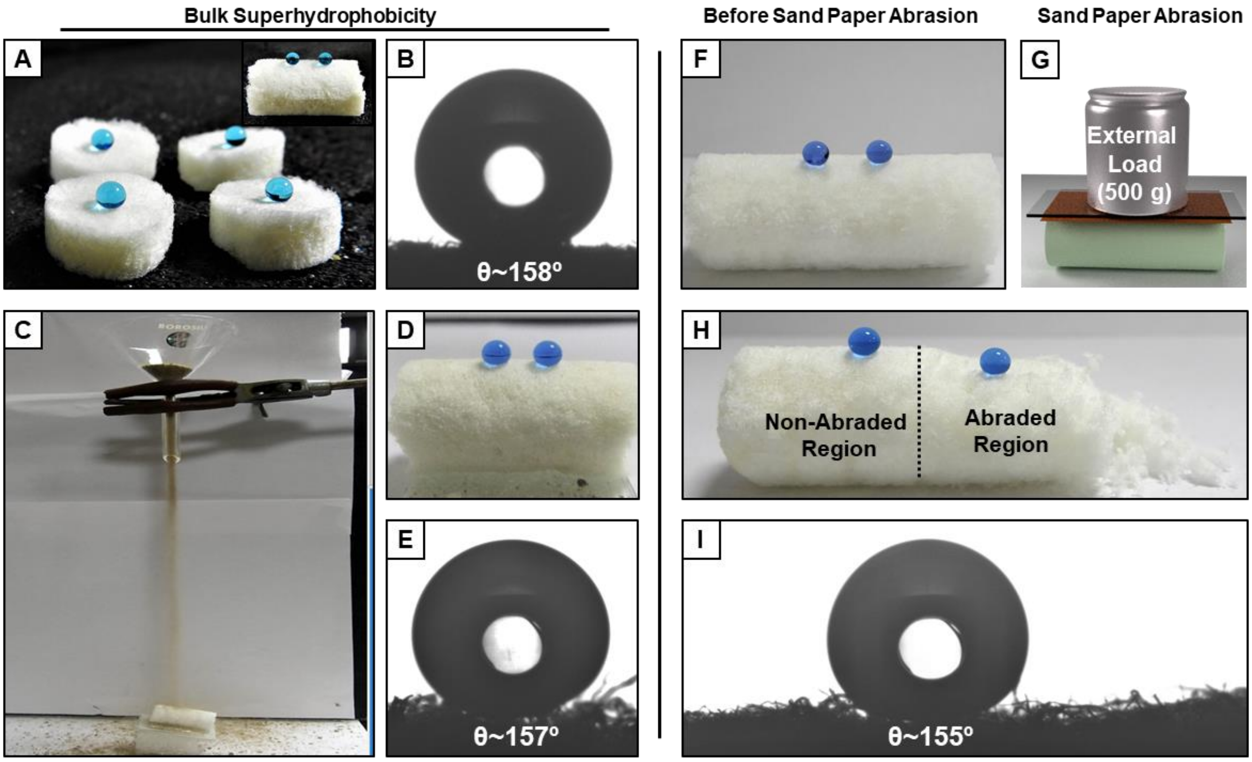

**Figure 4.12.** A-B) Digital image (A) and static WCA image (B) of WPDSHS$_1$ (inset image) that was arbitrarily sliced into pieces to investigate the presence of bulk superhydrophobicity. C-E) Digital image (C,D) and static WCA image (E) illustrating the sand drop test (C) on WPDSHS$_1$ followed by examination of water repellence (D-E). F-I) Digital images illustrating the rubbing of a sand paper on the surface of WPDSHS$_1$ (F) with a 500 g load on top (G). The freshly exposed interior of the superhydrophobic sponge continued to display unperturbed water repellence behaviour (H-I).

water repellence with static WCA~157° and contact angle hysteresis ~ 6° as shown in Figure 4.12D-E and Table 4.6. Next, an abrasive sand paper was rubbed with an applied load of 500 g in back and forth direction multiple (~20) times (Figure 4.12G) on WPDSHS$_1$. Although the physical integrity of the sponge was compromised (Figure 4.12H), the embedded water repellence on the physically abraded interface remained intact with static WCA~155° and contact angle hysteresis ~8° as shown in Figure 4.12H-I and Table 4.6. In addition to various severe physical abrasions, chemical durability is also vital for practical applications. In that context, WPDSHS$_1$ was exposed to severe harsh and practically relevant complex aqueous media including acidic water (pH 1), basic water (pH 12), surfactant water (SDS, DTAB), river water and seawater for a prolonged duration (30 days). The anti-

**Table 4.6** accounting for the advancing WCA and contact angle hysteresis of the beaded water droplet on WPDSHS$_1$ after performing san paper abrasion and sand drop test.

| Sample | Advancing Contact Angle (°) | Contact Angle Hysteresis (°) |
|---|---|---|
| **Sand Paper Abrasion** | 156.7±1.3 | 8.0±1.5 |
| **Sand Drop Test** | 158.5±1.1 | 6.4±0.9 |

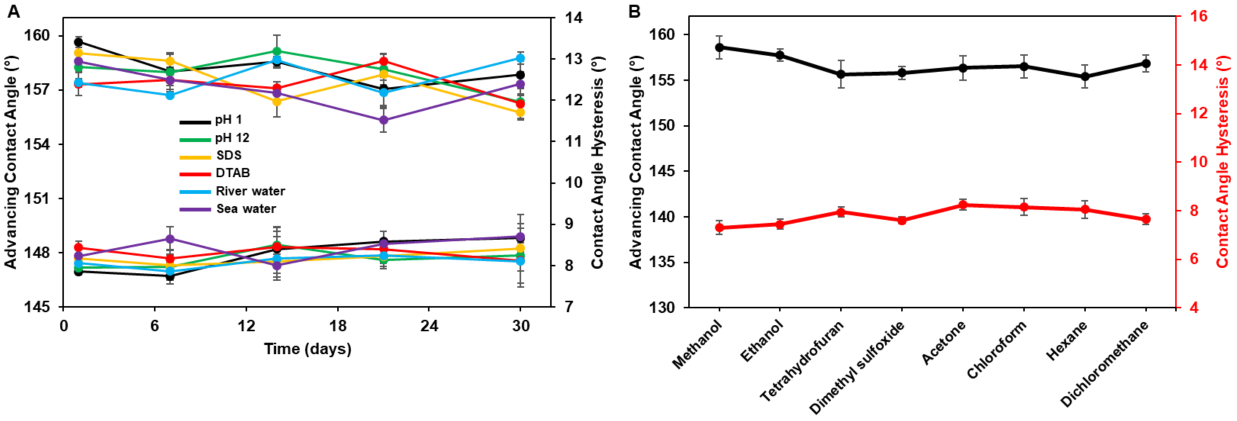

**Figure 4.13.** A) Plot accounting for the advancing WCA and contact angle hysteresis of the beaded water droplet on the WPDSHS$_1$ that was exposed to chemically contaminated, harsh aqueous phases for 30 days. B) Plot accounting for the advancing WCA (black) and contact angle hysteresis (red) of the beaded water droplet on WPDSHS$_1$ after 30 days exposure to different polar and non-polar organic solvents.

wetting property was examined at regular intervals and it was concluded that the embedded superhydrophobicity remained intact with advancing WCA above 150° and contact angle hysteresis below 10° as shown in Figure 4.13A. Moreover, WPDSHS$_1$ was exposed to various polar and non-polar organic solvents for 30 days, however, the embedded water repellence remained unaltered as shown in Figure 4.13B. Furthermore, the prolonged (30 days) exposure to both short (254 nm) and long (365 nm) UV radiation failed to perturb the embedded water repellence, which is evident with advancing WCA above 150° and contact angle hysteresis below 10° as shown in Figure 4.14A. Hence, the abundant and valueless waste paper was successfully reconstructed into a highly compressible superhydrophobic spongy material with extremely durable embedded water repellence property that would be appropriate for practical utility even at harsh and hostile practical settings.

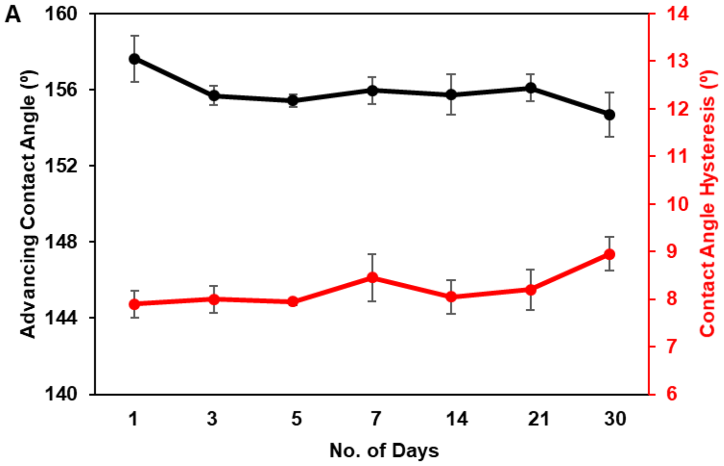

**Figure 4.14.** A) Plot accounting for the advancing WCA (black) and contact angle hysteresis (red) of the beaded water droplet on WPDSHS$_1$ after 30 days exposure to UV radiation.

### 4.3.4. Absorption Based, Selective Oil/Water Separation at Challenging Environments

In the past, a few approaches were introduced to convert the valueless and highly abundant waste paper into functional materials for various applications.[18-26,29-33] However, most of the earlier approaches failed to demonstrate the physical and chemical durability of the waste paper derived functional materials. Some of the waste paper derived bio-inspired materials that were prepared following the carbonization process at very high temperatures were successfully extended for oil/water separation, however, tolerance of such materials at harsh physical and chemical settings was not examined.[31-32,35] The highly compressible waste paper derived sponge with an interconnected porous network exhibited high porosity (above 95%, Figure 4.9B) and contrasting water/oil wettability (Figure 4.15A, inset) was exploited to demonstrate the energy efficient and environment friendly separation of oils from the aqueous phase. The embedded superhydrophobicity allowed the selective infiltration of the oil phase, while higher porosity facilitated the absorption and gravity-driven filtration of the oily phase. The oil

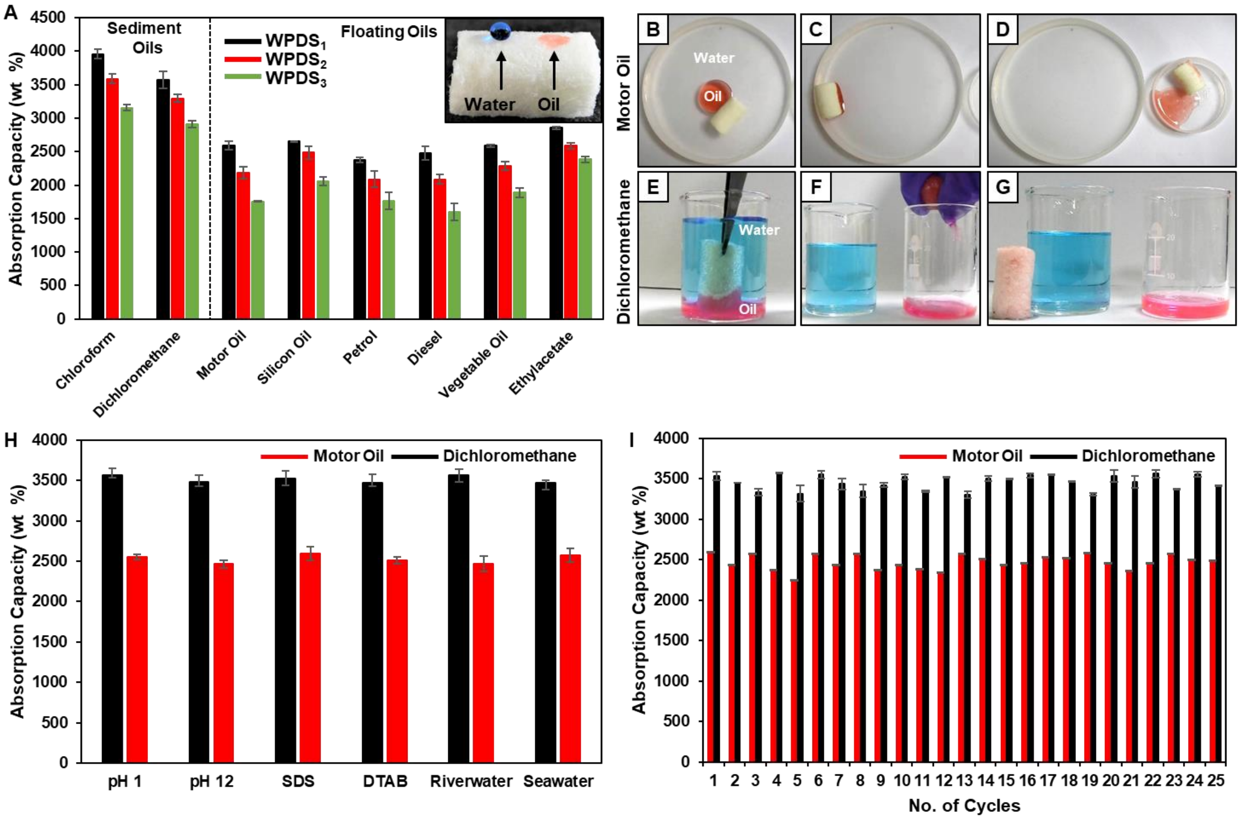

**Figure 4.15.** A) Plot accounting for the oil absorption capacities of the different waste paper derived compressible, superhydrophobic sponges i.e. WPDSHS$_1$, WPDSHS$_2$, WPDSHS$_3$ for a wide range of oils with varying densities and viscosities. Inset digital image displaying the presence of contrasting oil and water wettability on WPDSHS$_1$. B-G) Digital images illustrating the absorption based selective oil absorption of light oil i.e. motor oil (B-D) and model heavy oil i.e. dichloromethane (E-G) by WPDSHS$_1$ from an oil/water interface, such that the absorbed oil can be re-collected by manually squeezing the sponge (D, G). H) Plot illustrating the selective oil absorption capacity of WPDSHS$_1$ for both light (red) and heavy (black) oils under chemically contaminated aqueous phases. I) Plot illustrating the repetitive oil absorption capacity of WPDSHS$_1$ upto 25 cycles for both light (red) and heavy (black) oils.

absorption capacities were calculated for all the waste paper derived superhydrophobic sponges ($WPDSHS_1$, $WPDSHS_2$, $WPDSHS_3$) having different porosities using the formula given below,

$$Q = (M_2 - M_1)/M_1$$

where, $M_1$ and $M_2$ is the weight of the sponge before and after oil absorption. The oil absorption capacities were noted to be proportional to the porosity of the sponges. The oil absorption capacity of $WPDSHS_1$ was found to be maximum (~4000 wt% for chloroform) in comparison to $WPDSHS_2$ and $WPDSHS_3$ as shown in Figure 4.15A. The presence of high compressibility in a material which allows the easy compressive deformation, is appropriate for repetitive absorption/desorption of oil/oily phase without compromising the physical integrity of the substrate. Compressive modulus and cyclic compressibility analysis revealed that $WPDSHS_1$ is the most compressible, superhydrophobic variant with unperturbed embedded water repellence even after 1000 cycles of compression (as shown in Figure 4.11B). Therefore, the highly porous, durable and compressible $WPDSHS_1$ proved to be the ideal candidate for repetitive collection of the oil phase selectively from the water phase with high oil absorption capacities.

To demonstrate the selective collection of floating oil, motor oil was placed in a petri-dish filled with water and subsequently, $WPDSHS_1$ was placed at the oil/water interface and it rapidly, selectively absorbed only the oil phase while repelling the water phase as shown in Figure 4.15B-D. The absorbed oil was collected by manual squeezing of the sponge as shown in Figure 4.15D. Moreover, $WPDSHS_1$ was also extended for the selective collection of model sediment oil i.e. dichloromethane (DCM; dyed

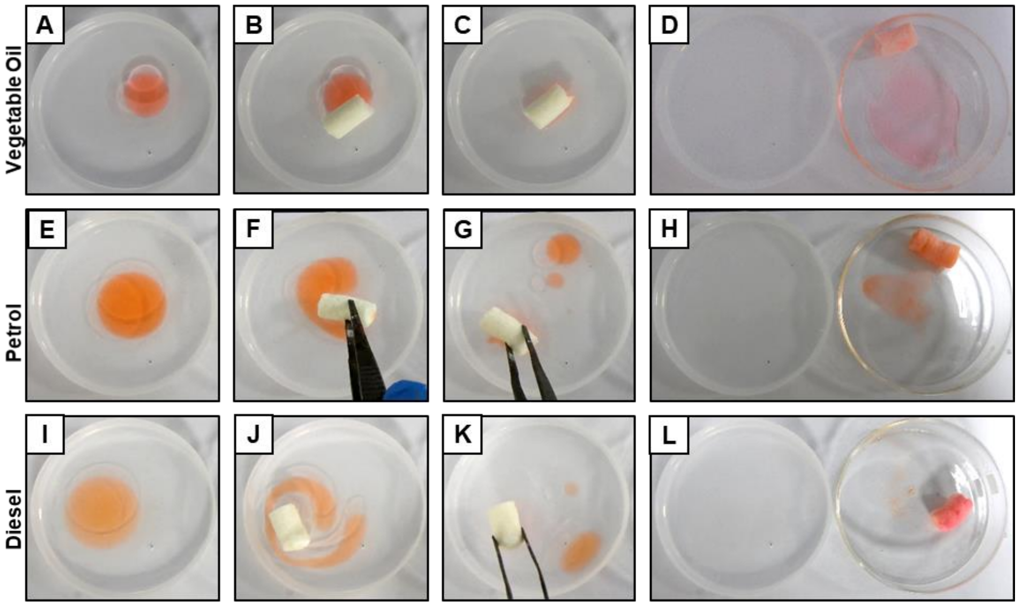

**Figure 4.16.** A-L) Digital images illustrating the absorption based selective separation of vegetable oil (A-D), petrol (E-H) and diesel (I-L) using $WPDSHS_1$ from the respective oil/water interfaces.

pink for visual inspection) as shown in Figure 4.15E-G. The absorbed oil was collected, and no trace of water was observed even though the sponge was first in contact with the aqueous phase prior to absorption of the model heavy oil phase as shown in Figure 4.15G. Furthermore, the same sponge was extended for the selective removal of various other floating oils including vegetable oil, petrol and diesel as shown in Figure 4.16A-L. The oil absorption capacity of $WPDSHS_1$ was further calculated for motor oil and dichloromethane in chemically harsh aqueous environments including acidic water (pH 1), basic water (pH 12), surfactant contaminated water (SDS, DTAB), river water and seawater. Remarkably, the oil absorption capacity remained unperturbed (i.e. ~2500 wt% for motor oil and ~3500 wt% for DCM) even at such extreme environments as shown in Figure 4.15H. Recyclability of the oil absorbents is an essential factor for practical applications. The repetitive absorption-desorption ability of $WPDSHS_1$ was examined with motor oil and DCM for 25 cycles and it was observed that

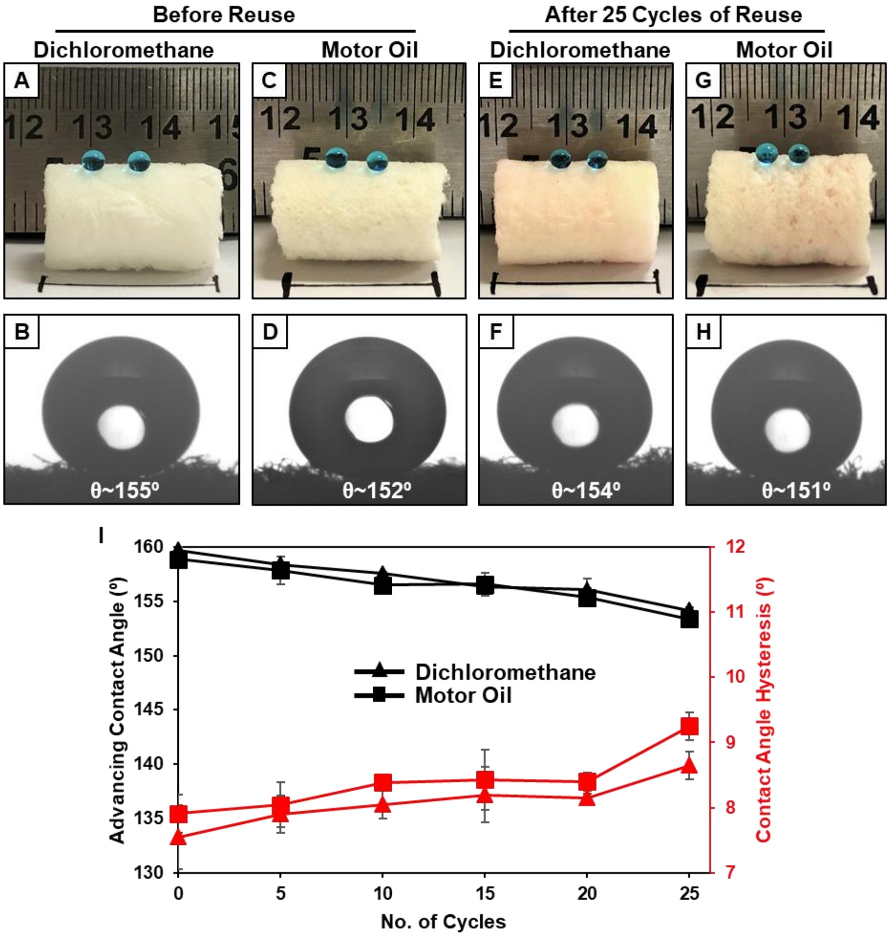

**Figure 4.17.** A-H) Digital images (A, C, E, G) and static WCA images (B, D, F, H) of $WPDSHS_1$ before (A-D) and after (E-H) 25 times reuse for selective absorption of light (motor oil) and heavy oils (dichloromethane) from an oil/water mixture. I) Plot accounting for the advancing WCA (black) and contact angle hysteresis (red) of the beaded water droplet on $WPDSHS_1$ that was used repetitively for 25 times of selective absorption of both light (motor oil) and heavy (dichloromethane) oils from the respective oil/water mixtures.

the oil absorption capacities remained unaltered as shown in Figure 4.15I. Even after repetitive use of WPDSHS$_1$ for selective collection of the oil phase, the physical integrity and embedded extreme water wettability of the sponges remained intact as shown in Figure 4.17A-H. The extreme water repellence was examined after every 5 cycles of absorption-desorption for both floating and sediment oils and it was found that the anti-wetting property remained intact with advancing WCA above 150° and contact angle hysteresis below 10° as shown in Figure 4.17I.

### 4.3.5. Gravity-Driven Filtration-Based, Selective Oil/water Separation Under Harsh Settings

Furthermore, this design provided a single strategy to fabricate waste paper derived superhydrophobic membranes of varying tensile strengths with compositions analogous to the sponges as shown in Figure 4.18A-B. The waste paper derived superhydrophobic membranes (WPDSHM$_1$, WPDSHM$_2$, WPDSHM$_3$) with varying compositions of AEPTMS displayed bio-mimicked extreme water repellence with advancing WCA above 150° and contact angle hysteresis below 10° as shown in Table 4.7. The tensile strength of the membranes revealed that the increase in AEPTMS content led to an increase in the tensile modulus in the order WPDSHM$_3$ > WPDSHM$_2$ > WPDSHM$_1$ as shown in Figure

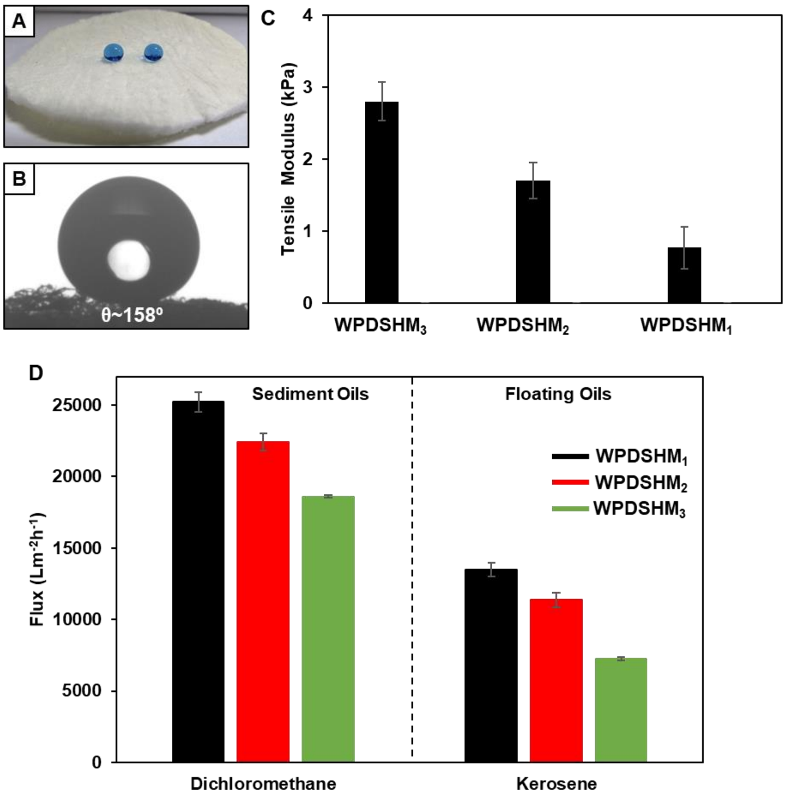

**Figure 4.18.** A-F) Digital images (A) and static WCA image (B) of the beaded water droplet on the waste paper derived superhydrophobic membrane, WPDSHM$_1$. C) Bar diagram accounting for the tensile modulus of the waste paper derived superhydrophobic membranes. D) Plot accounting for the rate of flux of model sediment and floating oils through the waste paper derived superhydrophobic membranes with varying porosities.

**Table 4.7** Accounts for the advancing WCA, contact angle hysteresis and porosity of the waste paper derived superhydrophobic membranes that were developed with different concentrations of AEPTMS.

| Sample | Advancing Contact Angle (°) | Contact Angle Hysteresis (°) | Porosity (%) |
|---|---|---|---|
| **WPDSHM$_1$** | 158.4 ± 1.3 | 7.3 ± 0.7 | 99.3 ± 1.2 |
| **WPDSHM$_2$** | 156.6 ± 1.5 | 7.5 ± 0.8 | 97.5 ± 0.9 |
| **WPDSHM$_3$** | 157.9 ± 0.7 | 7.4 ± 1.1 | 96.1 ± 0.5 |

4.18C. To maximize the utilization of the current design, the waste paper derived superhydrophobic membranes were extended for gravity-driven filtration-based oil/water separation. All three superhydrophobic membranes were individually tied to the open end of a lab made prototype followed by pouring of the respective oil/water mixtures to allow the selective filtration of the oil phase.

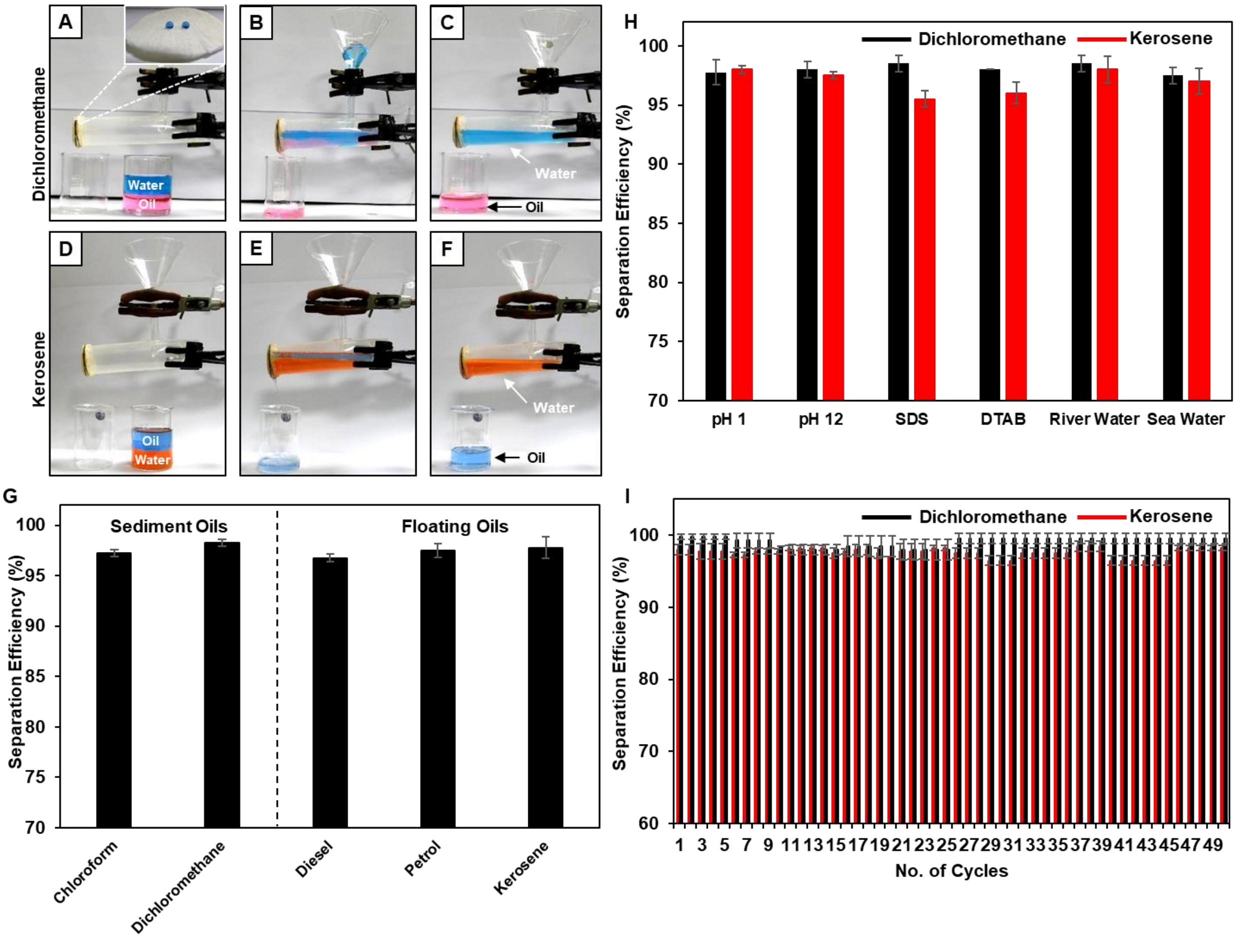

**Figure 4.19.** A-F) Digital images illustrating the gravity-driven filtration based selective passage of model sediment oil phase i.e. dichloromethane (A-C) and light oil i.e. kerosene (D-F) from the respective oil/water mixtures through WPDSHM$_1$ (inset image in A). G) Plot illustrating the oil separation efficiency of WPDSHM$_1$ for a wide range of oils with varying densities. H) Plot depicting the oil separation efficiency of WPDSHM$_1$ for both light (red) and heavy (black) oils under chemically contaminated aqueous phases. I) Plot illustrating the repetitive oil separation efficiency of WPDSHM$_1$ upto 50 cycles for both light (red) and heavy (black) oils.

However, the flux of oils through WPDSHM$_1$ was found to be maximum for both light and heavy oils compared to the other membranes as shown in Figure 4.18D. The oil flux rate was noted to be directly proportional to the porosity of the membranes which decreases in the order WPDSHM$_1$> WPDSHM$_1$>WPDSHM$_1$ as shown in Table 4.7. Thus, WPDSHM$_1$ was chosen as the ideal substrate for further demonstrations of gravity-driven filtration-based oil water separation. First, model sediment oil i.e. dichloromethane (dyed pink for visual inspection)/water (dyed blue for visual inspection) mixture was poured through the funnel of the lab-based prototype as shown in Figure 4.19A. The oil phase selectively permeated through the WPDSHM$_1$ while the water phase remained suspended and restricted by the superhydrophobic membrane as shown in Figure 4.19B-C. Furthermore, the same approach was extended for separation of floating oil i.e. kerosene/water (dyed red for visual inspection) mixture where the oil phase selectively permeated through the membrane as shown in Figure 4.19D-F. This energy efficient separation technique was also used for separation of other floating oil/water mixtures including petrol and diesel (Figure 4.20A-H). The oil separation efficiency of WPDSHM$_1$ was calculated for a wide range of oils including petrol, diesel, kerosene, dichloromethane and chloroform using the formula given below,

$$\eta = \left(\frac{V_f}{V_i}\right) X\ 100$$

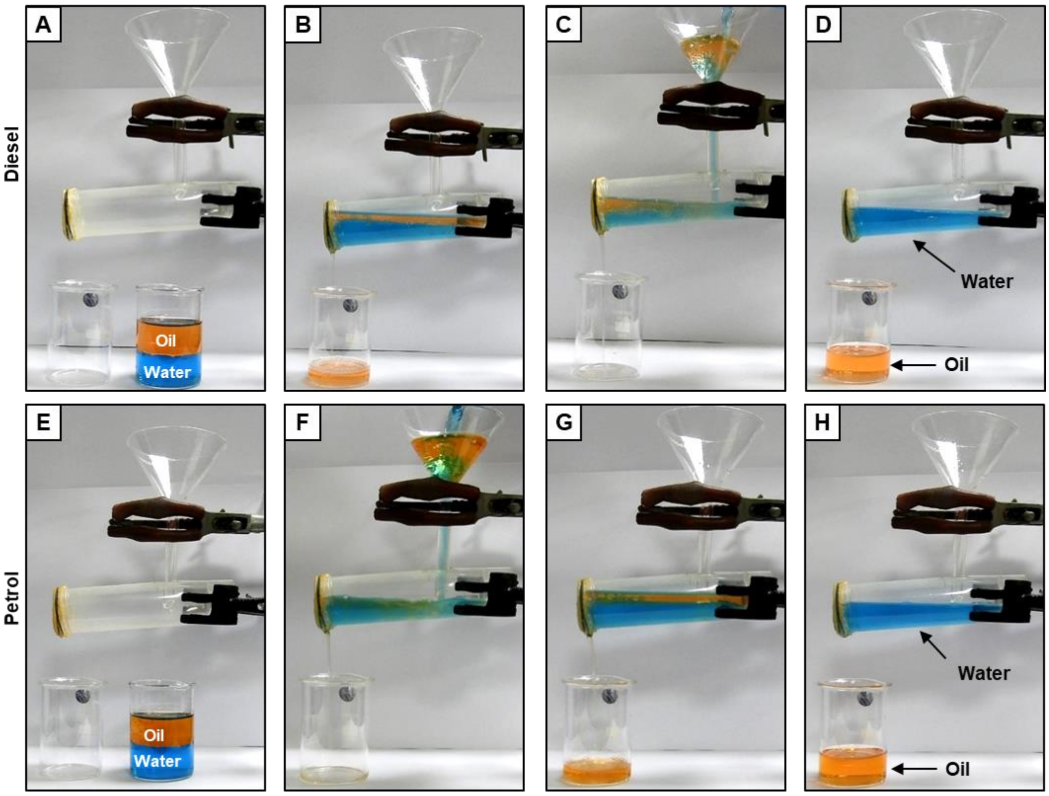

**Figure 4.20.** A-H) Digital images illustrating the gravity-driven filtration based selective separation of diesel (A-D) and petrol (E-H) using WPDSHM$_1$ from the respective oil/water mixtures.

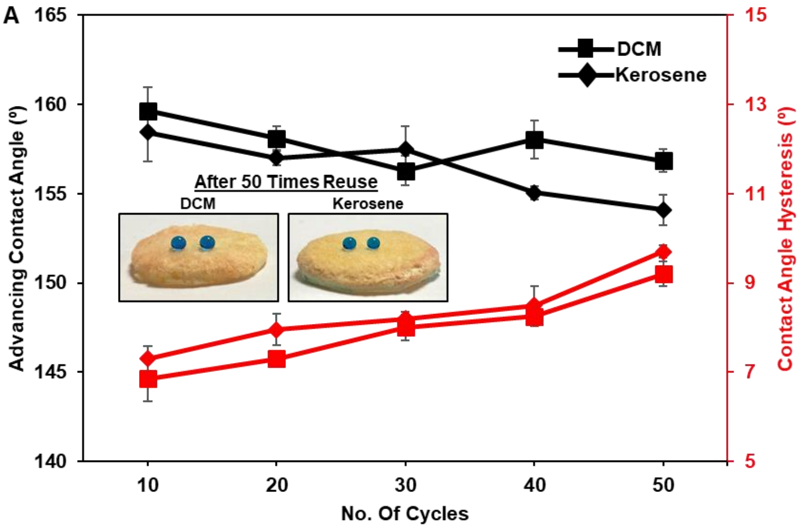

**Figure 4.21.** A) Plot accounting for the advancing WCA (black) and contact angle hysteresis (red) of the beaded water droplet on WPDSHM$_1$ that was repetitively used (50 times) for separation of both light (kerosene) and heavy (dichloromethane) oils from the respective oil/water mixtures. Inset images exhibit the intact water repellence property and physical integrity of the membrane after reuse.

where, $V_i$ and $V_f$ is the volume of the oil before and after separation respectively. The oil separation efficiency remained above 97% irrespective of the densities of the oils used as shown in Figure 4.19G. Moreover, the separation efficiency was calculated at extremes of harsh aqueous media including acidic water (pH 1), basic water (pH 12), surfactant contaminated water (SDS, DTAB), river water and seawater for oil/water mixtures using both heavy (i.e. dichloromethane) and light (i.e. kerosene) oils as shown in Figure 4.19H, where oil separation efficiency remained unperturbed. The recycling ability of the membrane was also examined for 50 cycles of separation for both sediment (dichloromethane) and floating (kerosene) oils and the oil separation efficiency remained above 95% for 50 consecutive cycles as shown in Figure 4.19I. Moreover, the embedded water repellence of the membrane was examined after every 5 cycles of separation for both dichloromethane and kerosene and the anti-wetting property was observed to remain intact with advancing WCA above 150° and contact angle hysteresis below 10° as shown in Figure 4.21A. Thus, such a robust and highly durable material that was prepared following a facile fabrication process displayed impeccable recyclability would be appropriate for applications at practical context.

## 4.4. Conclusion

In this chapter, the unconventional restructuring of discarded and valueless waste paper into a highly porous, compressible and chemically 'reactive' sponges embedded with extreme water repellence behaviour was reported. The varying concentration of the covalently integrated amine functionalized silane with the waste paper provided a basis to tailor the mechanical property. Further, the catalyst-free Michael addition reaction at ambient conditions between the labile amines of the silanized waste paper and a multi-functional acrylate cross-linker allowed to induce chemical ‘reactivity’ in the waste paper derived sponge. The strategic post covalent modification of the residual acrylate functionalities in the waste paper derived sponge was extended to tailor the water wettability from hydrophobicity to 3D-superhydrophobicity, without perturbing the tailored mechanical property. The as developed waste paper based superhydrophobic sponges could sustain repetitive compression (60% compressive strain) for 1000 cycles, severe physical abrasions including sand paper abrasion, sand drop test, prolonged (30 days) exposure to harsh chemical aqueous conditions including extremes of pH (1, 12), surfactant contaminated water (SDS, DTAB), river water, seawater, various organic solvents and UV irradiation for 30 days without compromising the embedded water-repellent property. These highly compressible, physically and chemically durable waste paper derived sponges were successfully extended for repetitive (25 times) absorption-based separation of various oils from the aqueous phase with oil absorption capacities upto 4000 wt%, without compromising the embedded water repellence and physical integrity even at chemically harsh aqueous settings. Furthermore, the waste paper derived membranes were utilized for repetitive (50 times) gravity-driven filtration-based oil/water remediation at chemically harsh aqueous settings with oil separation efficiency above 95%, without compromising the embedded lotus-leaf inspired anti-wetting property. Such an approach of converting waste paper into functional materials could be further useful for developing various other functional interfaces.

## 4.5. References

1. M. Jian, K. Xia, Q. Wang, Z. Yin, H. Wang, C. Wang, H. Xie, M. Zhang and Y. Zhang, *Adv. Funct. Mater.*, 2017, **27**, 1606066-1606074.

2. L. Han, K. Liu, M. Wang, K. Wang, L. Fang, H. Chen, J. Zhou and X. Lu, *Adv. Funct. Mater.*, 2018, **28**, 1704195-1704206.

3. D. Jiang, J. Zhang, S. Qin, Z. Wang, K. A. S. Usman, D. Hegh, J. Liu, W. Lei and J. M. Razal, *ACS Nano*, 2021, **15**, 5000-5010.

4. C. Li, J. Yang, P. Pachfule, S. Li, M.-Y. Ye, J. Schmidt and A. Thomas, *Nat. Commun.*, 2020, **11**, 4712-4719.

5. H. Zhuo, Y. Hu, Z. Chen, X. Peng, L. Liu, Q. Luo, J. Yi, C. Liu and L. Zhong, *J. Mater. Chem. A*, 2019, **7**, 8092-8100.

6. D. Brochetti, J. Kanczler, J. Feng, W. Li, Y. Shi, V. Farafonov, Y. Wang, R. F. Thompson, M.-M. Titirici, D. Nerukh, S. Karabasov, R. O. C. Oreffo, J. C. Rodriguez-Cabello, G. Vozzi, H. S. Azevedo, N. M. Pugno, W. Wang and A. Mata, *Nat. Commun.*, 2020, **11**, 1182-1193.

7. X. Cao, J. Zhang, S. Chen, R. J. Varley and K. Pan, *Adv. Funct. Mater.*, 2020, **30**, 2003618-2003627.

8. Y. Hu, Z. Chen, H. Zhou, L. Zhong, X. Peng and R.-C. Sun, *Adv. Funct. Mater.*, 2019, **29**, 1904472-1904499.

9. X. Du, M. Wang, A. Welle, F. Behboodi-Sadabad, Y. Wang, P. A. Levkin and Z. Gu, *Adv. Funct. Mater.*, 2018, **28**, 1803765-1803772.

10. W. Feng, L. Li, C. Yang, A. Welle, O. Trapp and P. A. Levkin, *Angew. Chem. Int. Ed.*, 2015, **54**, 8732-8735.

11. M. E. Buck and D. M. Lynn, *Adv. Mater.*, 2010, **22**, 994-998.

12. U. Manna, M. C. D. Carter and D. M. Lynn, *Adv. Mater.*, 2013, **25**, 3085-3089.

13. F. Behboodi-Sadabad, V. Trouillet, A. Welle, P. B. Messersmith and P. A. Levkin, *ACS Appl. Mater. Interfaces*, 2018, **10**, 39268-39278.

14. A. Shome, J. C. Moses, A. M. Rather, B. B. Mandal and U. Manna, *ACS Appl. Mater. Interfaces*, 2021, **13**, 24258-24271.

15. Z. Xia, J. Li, J. Zhang, X. Zhang, X. Zheng and J. Zhang, *J. Bioresour. Bioprod.*, 2020, **5**, 79-95.

16. X. Miao, J. Lin and F. Bian, *J. Bioresour. Bioprod.*, 2020, **5**, 26-36.

17. K. Pivnenko, D. Laner and T. F. Astrup, *Environ. Sci. Technol.*, 2016, **50**, 12302-12311.

18. J. Y. Keränen and E. Retulainen, *BioResources*, 2016, **11**, 10404-10418.

19. M. I. Khazi, W. Jeong and J.-M. Kim, *Adv. Mater.*, 2018, **30**, 1705310-1705332.

20. H. Yu, Z. Chen, Y. Liu, O. Alkhamis, Z. Song and Y. Xiao, *Angew Chem. Int. Ed.*, 2020, **60**, 2993-3000.

21. F. Brunetti, A. Operamolla, S. Castro-Hermosa, G. Lucarelli, V. Manca, G. M. Farinola and T. M. Brown, *Adv. Funct. Mater.*, 2019, **29**, 1806798-1806831.

22. Z. Wang, X. Fu, Z. Zhang, Y. Jiang, M. Waqar, P. Xie, K. Bi, Y. Liu, X. Yin and R. Fan, *J. Cleaner Prod.*, 2019, **234**, 588-596.

23. A. Baidya, M. A. Ganayee, S. J. Ravindran, K. C. Tam, S. K. Das, R. H. A. Ras and T. Pradeep, *ACS Nano*, 2017, **11**, 11091-11099.

24. Z. Xia, J. Li, J. Zhang, X. Zhang, X. Zheng and J. Zhang, *J. Bioresour. Bioprod.*, 2020, **5**, 79-95.

25. X. Miao, J. Lin and F. Bian, *J. Bioresour. Bioprod.*, 2020, **5**, 26-36.

26. K. Pivnenko, D. Laner and T. F. Astrup, *Environ. Sci. Technol.*, 2016, **50**, 12302-12311.

27. J. Y. Keränen and E. Retulainen, *BioResources*, 2016, **11**, 10404-10418.

28. M. I. Khazi, W. Jeong and J.-M. Kim, *Adv. Mater.*, 2018, **30**, 1705310-1705332.

29. H. Yu, Z. Chen, Y. Liu, O. Alkhamis, Z. Song and Y. Xiao, *Angew. Chem. Int. Ed.*, 2020, **60**, 2993-3000.

30. Y. Kobayashi, T. Saito and A. Isogai, *Angew. Chem. Int. Ed.*, 2014, **53**, 10394-10397.

31. C. Jia, L. Li, Y. Liu, B. Fang, H. Ding, J. Song, Y. Liu, K. Xiang, S. Lin, Z. Li, W. Si, B. Li, X. Sheng, D. Wang, X. Wei and H. Wu, *Nat. Commun.*, 2020, **11**, 3732-3745.

32. G. Zhang, G. Chen, F. Yang and Z. Guo, *Nanoscale Adv.*, 2020, **2**, 4813-4821.

33. Y.-Q. Li, W.-B. Zhu, X.-G. Yu, P. Huang, S.-Y. Fu, N. Hu and K. Liao, *ACS Appl. Mater. Interfaces*, 2016, **8**, 33189-33196.

34. W. -J. Liu, W. -W. Li, H. Jiang and H. -Q. Yu, *Chem. Rev.*, 2017, **117**, 6367-6398.

35. W. Sakuma, S. Yamasaki, S. Fujisawa, T. Kodama, J. Shiomi, K. Kanamori and T. Saito, *ACS Nano*, 2021, **15**, 1436-1444.

36. Z. Zhang, G. Sèbe, D. Rentsch, T. Zimmermann and P. Tingaut, *Chem. Mater.*, 2014, **26**, 2659-2668.

37. S. Zhou, P. Liu, M. Wang, H. Zhao, J. Yang and F. Xu, *ACS Sustainable Chem. Eng.*, 2016, **4**, 6409-6416.

38. M. R. Weatherspoon, M. B. Dickerson, G. Wang, Y. Cai, S. Shian, S. C. Jones, S. R. Marder and K. H. Sandhage, *Angew. Chem. Int. Ed.*, 2007, **46**, 5724-5727.

39. J. Ford, S. R. Marder and S. Yang, *Chem. Mater.*, 2009, **21**, 476-483.

# Chapter 5. Protein Derived Sustainable Underwater Superoleophobicity*

Similar to superhydrophobicity, nature has furnished ample examples of underwater superoleophobic interfaces that has been the source of inspiration for fabricating its artificial counterparts. However, inspired by fish-scales, direct utilization of proteins for designing durable underwater superoleophobicity is rare in literature. In this chapter, Bovine serum albumin (BSA) derived, dynamic and stable chemical cross-linkages integrated coatings were strategically introduced to obtain durable underwater superoleophobicity. *In-situ* modification of the amine residues of the deposited BSA protein on a fibrous substrate with glutaraldehyde (at pH 8) provided an imine-based cross-linked and the fluorescent coating following the Schiff Base reaction, that exhibited uninterrupted underwater superoleophobicity even after prolonged (30 days) exposure to alkaline (pH 12), surfactant-contaminated aqueous phases, river water and artificial sea water. However, the accelerated hydrolysis of imines under acidic conditions led to the compromise of the embedded underwater superoleophobicity. To restrict the dynamic nature of the imine bond, the reductive conversion of imine to secondary amine was adopted to generate a BSA-derived stably cross-linked underwater superoleophobic coating. The resultant coating on the fibrous substrate preserved the embedded oil repellence even under various challenging settings, including prolonged (30 days) exposure to different aqueous phases i.e. extremes of pH (1, 12), artificial seawater, river water and surfactant contaminated water, different physical abrasions, 150% tensile stretching and UV irradiation (for 30 days). Thus, this simple and scalable chemical approach provided a platform for developing highly sustainable underwater superoleophobicity, which holds potential for applicability under challenging scenarios.

---

*A. Shome *et al.*, *J. Mater. Chem. A*, 2020, **8**, 15148-15156.

## 5.1. Introduction

As I discussed earlier, the appropriate optimization of both topography and chemistry is essential for developing interfaces embedded with bio-inspired liquid wettability.[1-3] The fish scale-inspired extremely oil-repellent interfaces known as underwater superoleophobicity, have been commonly designed through association of a high surface energy coating along with hierarchical topography for a wide range of applications.[4-10] The infiltrated external third phase (i.e. aqueous phase), which is held within the hierarchal topography and stabilized by the presence of high surface energy chemistry, ensures minimized contact of the beaded oil phase with the bio-inspired interface under water.[2,3] However, the uninterrupted performance of the artificially synthesized underwater superoleophobic interfaces at diverse and severe settings is highly essential for its prospective applications. In the past, deformable polymeric hydrogels, brittle metal oxides and electrostatic multilayer coatings have been exploited to achieve artificial underwater superoleophobicity.[11-25] However, such reported interfaces fail to sustain severe physical abrasions and prolonged exposure to chemically contaminated aqueous phases. A few unique designs were introduced to achieve salt-tolerant underwater superoleophobicity and mechanically stable underwater superoleophobicity,[6,10,26-28] however, their prolonged durability and performance at other diverse and severe settings was not investigated in detail.

Chemically ‘reactive’ multi-layered coatings were introduced using synthetic, non-biodegradable polymers to achieve highly durable underwater superoleophobicity,[29,30] but the reported fabrication approaches are relatively laborious and time consuming. In the previous chapter, bovine serum albumin (BSA) was exploited to develop BSA nanoparticles-derived chemically ‘reactive’ coating on a fibrous substrate following the Michael addition reaction between the amine residues of BSA and an acrylate cross-linker.[31,32] Further, the post-chemical modification of the BSA-derived chemically ‘reactive’ coating with a hydrophobic alkylamine through Michael addition reaction resulted in superhydrophobicity. Moreover, the presence of residual reactivity allowed to tailor the water wettability and thus, control the release of bioactive small molecule.[32] Interestingly, naturally existing fish-scales and shark-skin that are made up of proteins display robust underwater superoleophobicity,[3] however, utilization of protein for the synthesis of a highly durable and artificial underwater superoleophobic coating has rarely been reported. Hence, the aim in this chapter was to obtain a bio-mimicked durable underwater superoleophobic coating from protein following the facile and scalable Schiff base reaction between amine and aldehyde.

In the past, the dynamic and covalent imine bond widely recognized as Schiff's base, has been synthesized through the condensation reaction between amine and aldehyde.[37-41] This facile chemical approach is the basis for synthesizing various functional and prospective materials, including covalent organic frameworks, organic cages, capsules, responsive coatings, biosensors, molecular motors and other functional polymeric materials.[40-42] Further, a simple reductive amination can convert the dynamic imine to a stable secondary amine.[43] In this chapter, this simple and scalable Schiff base chemistry was rationally integrated with BSA to achieve dynamically cross-linked, fluorescent, underwater superoleophobicity on a fibrous substrate. However, as expected, the protein-derived underwater superoleophobic interface consisting of the dynamic, covalently bonded imine failed to sustain aqueous acidic exposure and thus, the wettability transformed from underwater superoleophobicity to oleophobicity. However, the simple reduction of imine aids in restricting the dynamic nature of the imine bond and results in stably cross-linked BSA derived underwater superoleophobicity. After reduction, the resultant BSA derived underwater superoleophobic coating sustained prolonged (30 days) and continuous exposure to highly acidic (pH 1) aqueous phases. Moreover, the synthesized interface that was subjected to various, severe physical abrasions and other chemically complex aqueous conditions continued to display uninterrupted underwater superoleophobicity.

## 5.2. Experimental Section:

**5.2.1. Materials:** Bovine Serum Albumin (MW ~ 66.5 kDa, Faction V), sodium dodecyl sulfate (SDS), dodecyl trimethyl ammonium chloride (DTAB) and sodium borohydride were purchased from Sigma-Aldrich. Nile Red (CAS No. 7385-67-3) was purchased from Tokyo Chemical Industry. Absolute ethyl alcohol (CAS No. 64-17-5) was purchased from TEDIA Company (United States of America). Glutaraldehyde (25% aqueous solution), sodium chloride, magnesium chloride, calcium chloride, magnesium sulphate, sodium hydroxide was purchased from Merck Specialties Private Limited. Hydrochloric acid was purchased from Fischer Scientific (Hyderabad, India). Polyurethane fabric and calibration weights were procured from Amazon, India. Sand paper and adhesive tape was procured from a local stationary shop. Sand was collected from a local construction site in IIT Guwahati and rinsed with water, dried before use. River water was collected from Brahmaputra river, Guwahati, Assam.

**5.2.2 General Consideration:** The glass wares were washed with water and acetone thoroughly prior to use. Kruss Drop Shape Analyzer-DSA25 instrument with automatic liquid dispenser was used for contact angle measurements. The contact angles were measured using a droplet (5μL) of a model oil phase i.e. dichloromethane at four different locations of each sample. Field Emission Scanning Electron Microscope (FESEM) images were obtained using a Carl Zeiss Field Emission Scanning Electron Microscope. The samples were sputtered with gold coating prior to analysis. UV spectra was obtained using the Perkin-Elmer Lambda 750 (UV/Vis/NIR Spectrometer). Digital images were captured using a Canon Powershot SX420 IS digital camera. Phase contrast and fluorescence microscopic images were obtained using a ZEISS Axio Vert.A1 inverted microscope. Milli-Q grade water was used for all experiments.

### 5.2.3. Synthesis of Durable Underwater Protein Derived Superoleophobicity:

Briefly, 1 mL aqueous solution of 40 mg/mL bovine serum albumin (pH adjusted to 8.0 with 0.1 N NaOH) was taken in a beaker. To this solution of BSA, 7 ml of ethanol was added at a rate of 1 mL/min under continuous stirring at room temperature till faint turbidity was observed. Thereafter, a commercially available polyurethane based fibrous substrate (3 cm x 3 cm) was placed in the beaker to ensure the deposition of BSA followed by *in-situ* addition of 200 µl of 8% aqueous solution of glutaraldehyde (GA) to induce imine-based cross-linking in the freshly deposited BSA protein. The reaction was kept undisturbed for 12 hours under constant stirring. Subsequently, the imine derived cross-linked BSA coating (turbid brown solution) was subjected to reduction by addition of 25 mL sodium borohydride aqueous solution (70 mg/mL) and kept unperturbed for 6 hours. During this reduction process, the turbid brown solution became colourless. Thereafter, the fabric was taken out and washed thoroughly with water and the embedded underwater superoleophobic property was examined through contact angle measurements and digital images. To verify the process of cross-linking and reduction, the as obtained de-solvated BSA, GA-crosslinked BSA and the reduced GA-cross-linked BSA were subjected to centrifugation at 12000 rpm for 15 mins to collect the sediments, which were further washed thoroughly thrice with water before recording the UV spectrum.

**5.2.4. Physical and Chemical Durability Tests:** To examine the robustness of the embedded oil repellent property, various practically relevant and harsh physical and chemical durability tests were imposed on the protein derived underwater oil repellent fibrous substrate.

**5.2.4.1. Sand Paper Abrasion:** In sand paper abrasion, an abrasive sand paper was manually rubbed across the reduced-BSA coated fibrous substrate (4 cm x 2 cm) for ~50 cycles with 700 g load on top at a sliding speed of 4 cm/sec. Thereafter, the durability of the embedded oil repellent property was examined via contact angle measurements and digital images.

**5.2.4.2. Adhesive Tape Test:** The reduced-BSA coated substrate (4 cm x 2 cm) was placed under an adhesive tape with 700 g load on top to ensure uniform contact between the substrate and adhesive tape. Subsequently, the adhesive tape was peeled off from the surface of the fibrous substrate and the same process was repeated for 25 cycles, Thereafter, the freshly exposed interface was examined for its oil repellence property via contact angle measurements and digital images.

**5.2.4.3. Sand Drop Test:** In this particular test, 150 g of sand was poured from a height of 25 cm on the reduced-BSA coated fibrous substrate (4 cm x 2 cm) which was pre-tilted at an angle of 45°. After performing sand drop test, the underwater oil repellence was examined by measuring the underwater oil contact angles and the digital images.

**5.2.4.4. Knife Scratch Test:** Random scratches were made on the reduced-BSA coated fibrous substrate (4 cm x 2 cm) in all possible directions using a sharp-edged knife for multiple times (~30) and thereafter, the oil repellence was examined via contact angle measurements and digital images.

**5.2.5. Physical Manipulations:** The reduced-BSA coated fibrous substrate (5 cm x 2 cm) was manually bended, creased, twisted and winded for 25 times arbitrarily. Thereafter, the digital images were acquired, and the underwater oil contact angles were measured to examine the impact of these physical manipulations on the embedded underwater superoleophobicity. The protein-based fibrous substrate was also subjected to 150% tensile strain for 1000 cycles and subsequently, the digital images and oil contact angles were measured at regular intervals.

**5.2.6. UV irradiation:** The reduced-BSA coated fibrous substrate was exposed to both short (254 nm) and long (365 nm) wavelength UV irradiation for 30 days. The embedded oil repellence was examined at regular intervals by measuring the oil contact angles and acquiring digital images.

**5.2.7. Chemical Durability:** The underwater extreme oil repellence on the reduced-BSA coated fibrous substrate was examined at regular intervals after exposure to different chemically harsh aqueous conditions i.e. acidic water (pH 1), basic water (pH 12), surfactant contaminated water (SDS, 1 mM and DTAB, 1 mM), river water (Brahmaputra river, Assam, India) and seawater for 30 days. Artificial seawater was prepared by mixing $MgCl_2$ (0.226 g), $MgSO_4$ (0.325 g), NaCl (2.673 g) and $CaCl_2$ (0.112 g) in 100 mL of de-ionized water in a volumetric flask. All the interfaces were washed with DI water prior to examination of the oil-wettability.

## 5.3. Results and Discussions:

### 5.3.1. BSA Derived Dynamically Cross-linked Coating:

Glutaraldehyde (GA), a bifunctional cross-linker, is well-known to form imine-based linkages through the Schiff base reaction with amine-containing polymers, proteins, DNA, enzymes, antigens, antibodies, etc.[44-54] This simple chemical approach has been widely used to develop various bio-interfaces, functional nanotubes, microcapsules, etc.[55-63] for biosensing, gene therapy and inhibition of enzyme degradation. [44-63] Specifically, various proteins were rationally associated with glutaraldehyde to develop cell arrays, nanolithography of proteins, drug delivery vehicles, immuno-sensors, etc.[55-63] Recently, a biocompatible and biodegradable auto-fluorescent protein hydrogel was

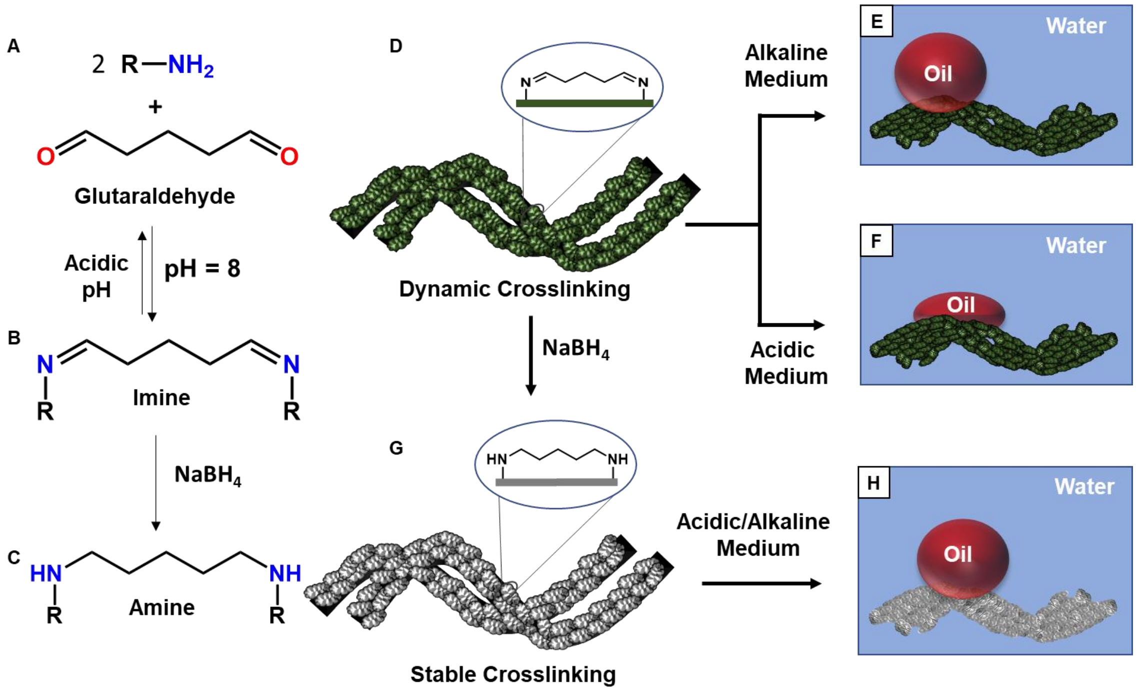

**Figure 5.1.** A-B) Depiction of the Schiff base reaction between amine and glutaraldehyde. The dynamic imine bond can revert in the presence of acidic media. This reversibility can be restricted via conversion of the imine bond to a secondary amine using sodium borohydride (C). D-F) The facile Schiff base assisted dynamic cross-linking process between the amine residues of bovine serum albumin protein and glutaraldehyde is expected to generate a fluorescent coating on a fibrous substrate displaying underwater superoleophobicity in alkaline media (E). However, the oil wettability would be compromised in acidic media owing to the hydrolysis of the imine bonds (F). Thus, the reduction of the imine bonds would result in a stable cross-linked BSA coating (G) capable of displaying unperturbed underwater superoleophobicity even in acidic media (H).

developed, where BSA protein was covalently cross-linked with GA through the Schiff base reaction.[64] Inspired by these earlier reports, the Schiff base reaction between BSA protein and GA (Figure 5.1A-B) was extended in this chapter to achieve fish scale-inspired underwater superoleophobic coating, that is covalently cross-linked on a selected fibrous substrate (Figure 5.1E). The deposited BSA was hypothesized to provide the a) essential topography to entrap the infiltrated aqueous phase and b) the hydrophilic moieties of BSA would stabilize the entrapped aqueous phase that is responsible for conferring extreme oil repellence under water. However, this dynamic, imine linkage in the fluorescent BSA derived coating would compromise the embedded oil repellence owing to the acidic hydrolysis of its imine bond, as shown in Figure 5.1A-B,F. To prevent the loss of super-oil wettability under acidic conditions, the facile reduction of imine (Figure 5.1D-G) was introduced to generate a BSA derived stably cross-linked coating (reduced imine) exhibiting durable underwater superoleophobicity (Figure 5.1H).

The widely used de-solvation technique was adopted here to achieve a BSA protein derived luminescent coating on a selected fibrous substrate. Prior to the study on BSA derived coating, the

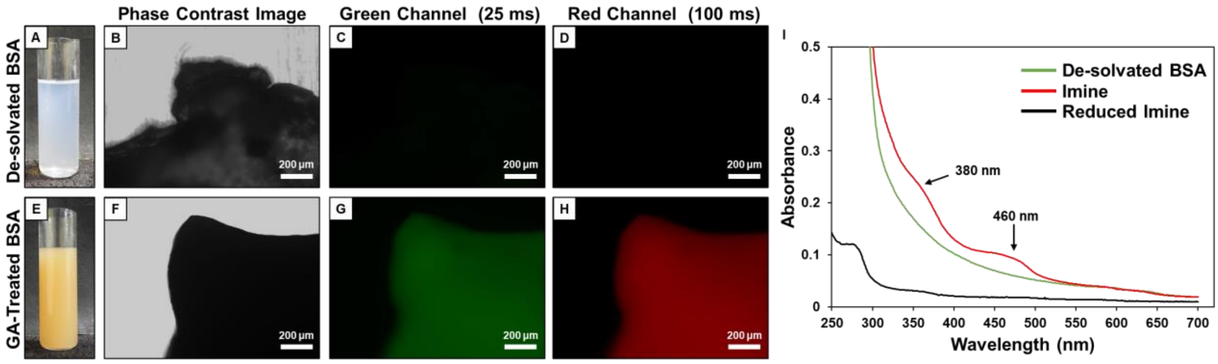

**Figure 5.2.** A) Digital image of the faintly turbid solution of BSA protein after de-solvating with ethanol. B-D) Phase contrast image (B) and fluorescence microscope images (C-D) of de-solvated BSA protein residues. E) Digital image of the brown solution of BSA protein after *in-situ* addition of glutaraldehyde to form imine. F-H) Phase contrast image (F) and fluorescence microscope images (G-H) of GA-crosslinked BSA protein. I) UV spectra of de-solvated BSA before (green), after (red) treatment with glutaraldehyde and after reduction of the imine bonds (black).

luminescence of the phase-separated BSA residue (indicated by faint turbidity, Figure 5.2A) was investigated under a fluorescence microscope before and after the GA-based cross-linking (brown solution indicates imine formation, Figure 5.2E). As expected, without GA treatment, no fluorescence signal was observed for the phase-separated BSA (Figure 5.2C-D). However, similar to the fluorescence activity of the earlier reported BSA-GA cross-linked hydrogel, the phase separated BSA that was cross-linked with GA displayed both green and red fluorescence under the optical microscope, as shown in Figure 5.2G-H. The n-π* transition in the imine bond[65,66] imparts fluorescence to the GA-crosslinked BSA residue. Further, the imine-based cross-linking between BSA protein and GA through the Schiff base reaction was investigated through UV-Vis spectral analysis. The milky white turbid solution of phase-separated BSA that turned into a brown coloured solution after the GA treatment (Figure 5.2A,E) was accompanied by the appearance of two characteristic UV-Vis peaks at 380 nm and 460 nm suggesting the Schiff base formation between the amines of BSA and aldehyde of GA, as shown in Figure 5.2I.

Thus, the same de-solvation of BSA followed by *in situ* treatment with GA was performed in the presence of a fibrous substrate. As expected, after GA-treatment, the BSA-derived coating displayed a uniform green and red fluorescence on the fibrous substrate, as shown in Figure 5.3E-F, which unambiguously revealed the deposition of the GA-treated BSA on the selected fibrous substrate. No fluorescence signals were observed in the native fibrous substrate (Figure 5.3B). Next, the underwater oil wettability was investigated on the fibrous substrate, before and after deposition of the GA-crosslinked BSA-coating. The uncoated fibrous substrate, a polyurethane fabric immediately soaked the beaded oil droplet underwater with oil contact angle (OCA) ~0°, as shown in Figure 5.3C-D. Interestingly, as hypothesized (Figure 5.1E), the GA-cross-linked BSA coating strongly repelled the

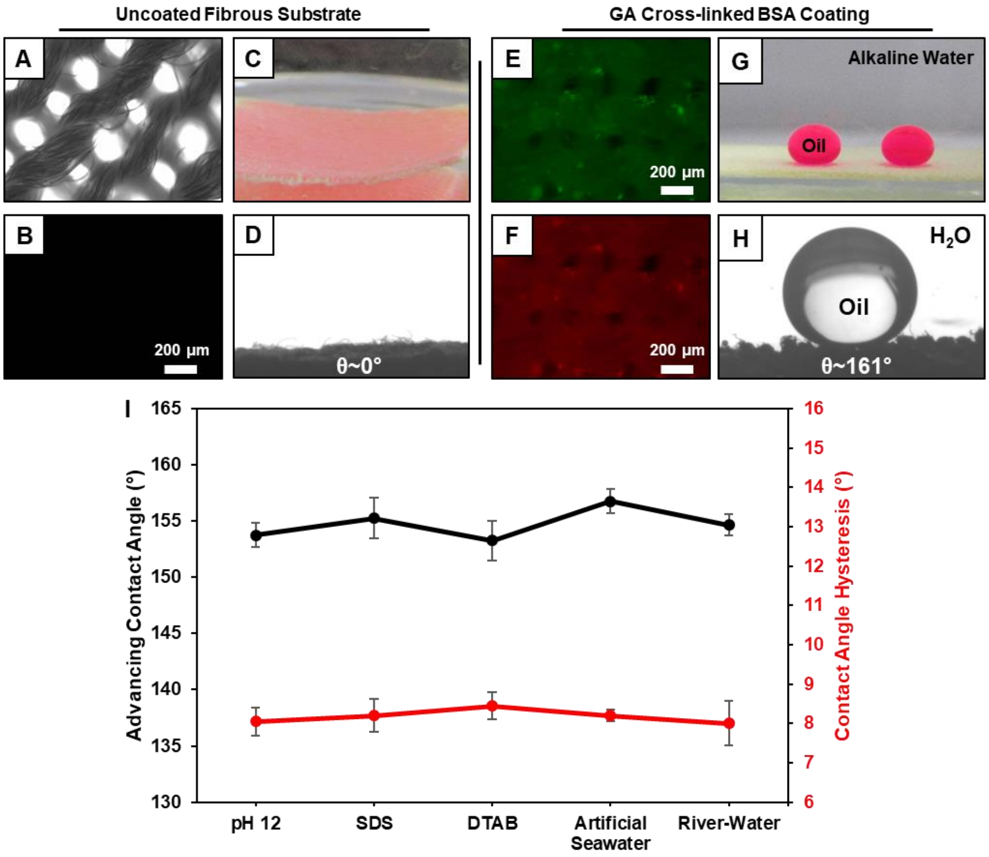

**Figure 5.3.** A-B) Phase contrast image (A) and fluorescence microscope images (B) of the commercially available, uncoated fibrous substrate. C-D) Digital image (C) and static OCA image (D) of the beaded model oil (dichloroethane, DCE) droplet underwater on the uncoated fibrous substrate. E-F) Fluorescence microscope images of the GA-crosslinked BSA deposited fibrous substrate. G-H) Digital image (G) and static OCA (H) of the beaded oil droplet on the GA-crosslinked BSA coated fibrous substrate after exposure to alkaline water for 12 h. I) Plot showing the change in advancing OCA and contact angle hysteresis, after exposing the GA-crosslinked BSA coated fibrous substrate to various chemically harsh aqueous media including basic water (pH 12), surfactant contaminated water (SDS, DTAB), river water and seawater for 30 days.

beaded oil droplet even after exposure to alkaline water for 12 h with OCA~161° as shown in Figure 5.3G-H. The GA-crosslinked BSA coating continued to display extreme oil repellence with advancing oil contact angles above 150° and contact angle hysteresis below 10°, even after 30 days exposure to chemically contaminated aqueous phases including alkaline water, surfactant contaminated water etc, as shown in Figure 5.3I.

However, the embedded extreme oil repellence was gradually compromised on exposure of the same coating to an acidic aqueous phase as shown in Figure 5.4. The exposure of the GA-crosslinked BSA coating to pH 1 for a short duration (4 h) led to a significant change in the static OCA of the beaded oil droplet from ~155° to ~128° (Figure 5.4A-D). Upon increasing the duration (12 h) of acidic exposure, the same interface became underwater oleophobic with static OCA~108° as shown in Figure 5.4E-F. Further, the fluorescence signal of the GA-crosslinked coating on the fibrous substrate

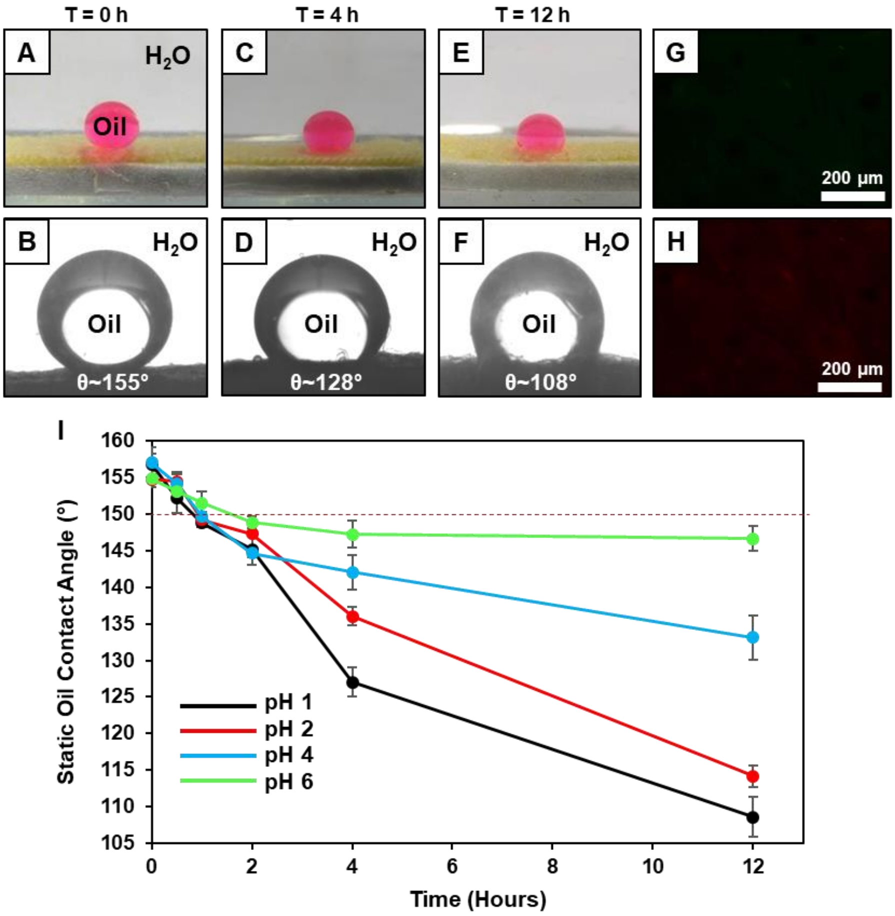

**Figure 5.4.** A-F) Digital images (A,C,E) and OCA images (B,D,F) of the beaded oil droplet (underwater) on the fibrous substrate coated with GA-crosslinked BSA—after exposure to acidic water (pH 1) at t= 0 h (A-B), t= 4 h (C-D) and t= 12 h (E-F). G-H) Fluorescence microscope images of the fibrous substrate coated with GA-crosslinked BSA after exposure to acidic media (pH 1) for 12 h. G) Plot accounting for the change in underwater OCA with time on the GA-crosslinked BSA coating after exposure to different acidic media i.e. pH 1 (black), pH 2 (red), pH 4 (blue) and pH 6 (green).

significantly diminished after exposure to the acidic aqueous phase for 12 h, as shown in Figure 5.4G-H. The compromise of underwater superoleophobicity was also observed on varying the acidic pH of the aqueous media with respect to time as shown in Figure 5.4I. The acidic hydrolysis of the dynamic covalent bond imine in the GA-based cross-linkage is responsible for the loss of bio-inspired underwater superoleophobicity during acidic aqueous exposure.[67]

### 5.3.2. Reduction of Dynamically Cross-linked BSA to Achieve Stably Cross-Linked Coating:

To prevent the acidic hydrolysis, the GA-crosslinked BSA coating was treated with sodium borohydride to reduce the imine bond into a stable secondary amine bond, as shown in Figure 5.1B-D,G-H to achieve highly tolerant underwater superoleophobicity. Even after exposure to highly acidic (pH 1) aqueous phase for 12 h, the same BSA-derived coating after reduction, remained extremely oil repellent with static OCA~162°, as shown in Figure 5.5A-B. The fluorescence signals of the BSA-

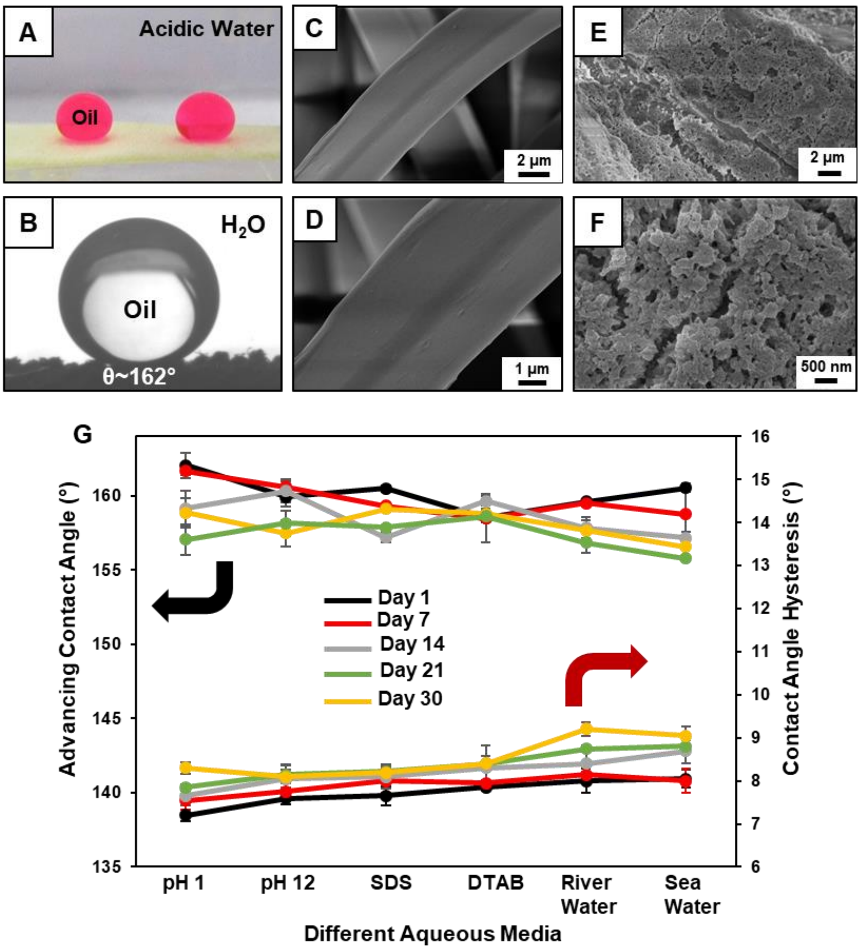

**Figure 5.5.** A-B) Digital image (A) and static OCA image (B) of the beaded oil droplet underwater on the BSA-coated fibrous substrate after reduction of imine followed by exposure to acidic water for 12 h. C-F) FESEM images of the uncoated fibrous substrate (C-D) and the BSA-derived coating on the fibrous substrate (E-F). G) Plot showing the changes in advancing OCA and contact angle hysteresis, after exposing the stable cross-linked (treated with sodium borohydride) BSA-coated fibrous substrate to various chemically harsh aqueous media including acidic water (pH 1), basic water (pH 12), surfactant contaminated water (SDS, DTAB), river water and seawater for 30 days.

derived coating were completely quenched following the reduction process. The durability of the underwater superoleophobicity after extended (12 h) exposure to a highly acidic phase re-validated the successful reduction of imine bonds in the BSA derived bio-inspired coating. Further, FESEM images of the BSA-derived underwater superoleophobic coating revealed the existence of granular aggregates (Figure 5.5E-F) on the otherwise featureless fibrous substrate (Figure. 5.5C-D). This topography likely plays an important role in achieving the heterogeneous oil wettability under water.

Further, the BSA-derived coating with secondary amine-based cross-linkages was exposed to various complex aqueous phases, including extremes pH values, sea water, river water and surfactant-contaminated aqueous phases upto 30 days with regular monitoring of the underwater oil wettability. As expected, the BSA-derived underwater superoleophobic coating withstood the prolonged and severe aqueous environments, wherein the embedded underwater superoleophobicity remained intact with advancing OCA above ~155° and contact angle hysteresis below 10°, as shown in Figure 5.5G.

### 5.3.3. Investigating the Durability of the BSA-Derived and Reduced Imine Coating

The BSA-derived and reduced imine linkage-based coating with embedded underwater superoleophobicity was exposed to various challenging physical abrasions to examine the durability of the coating and sustenance of the oil wettability for prospective practical applications. The reduced imine coating on the fabric was exposed to various relevant physical manipulations, including bending, twisting, and winding as shown in Figure 5.6A,D,G,J. However, the embedded underwater oil wettability remained unchanged even after performing these physical manipulation tests, where the oil droplet beaded with static OCA above 150° and contact angle hysteresis below 10° as shown in Fig. 5.6B-C,E-F,H-I,K-L and Table 5.1. Both the static OCA (Figure 5.6C,F,I,L) and dynamic oil contact angles (Table 5.1) were measured to reflect the non-adhesive underwater oil wettability. Thereafter, some standard and harsh physical abrasions were inflicted on the synthesized underwater superoleophobic coating. An abrasive sand paper with a 700 g load on top was rubbed on the reduced imine coated fabric in a back-and-forth motion multiple times (abrasion distance ~ 400 cm) during which the top portion of the synthesized interface was physically abraded (Figure 5.7A). However, the physically damaged interface continued to display underwater extreme oil repellence with static OCA~157° and contact angle hysteresis ~8°as shown in Figure 5.7B-C and Table 5.1. The abrasion tolerance of the synthesized interface was likely due to the uniform deposition of the BSA-derived coating on each individual fibre of the selected substrate. Further, an adhesive tape was repetitively

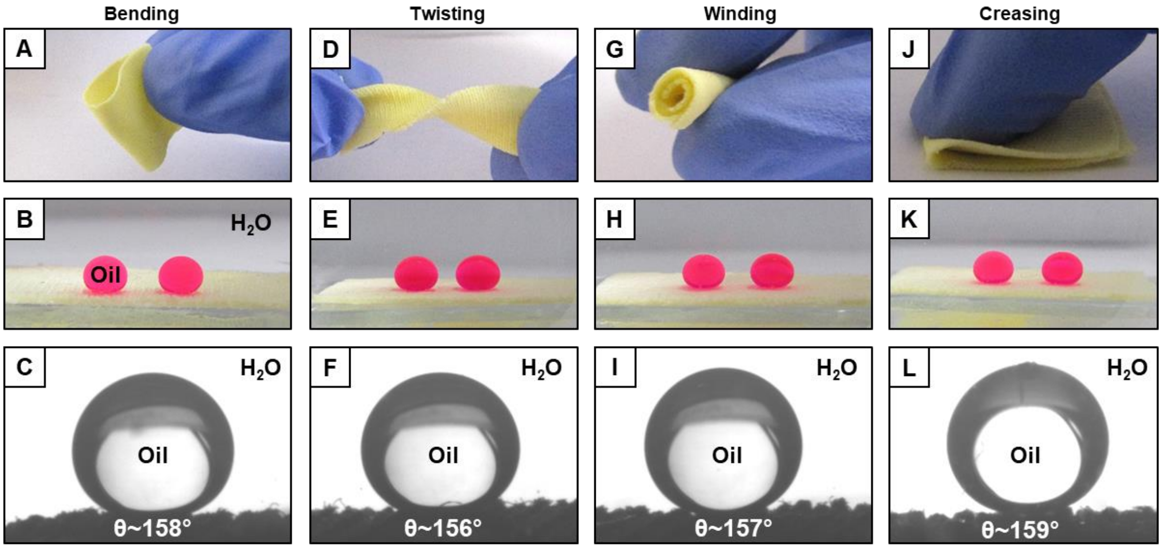

**Figure 5.6.** A-L) Digital images (A-B,D-E,G-H,J-K) and OCA images (C,F,I,L) of the beaded oil droplet underwater on the BSA-derived and reduced imine linkage-based fibrous coating after performing various physical manipulations including bending (A-C), twisting (D-F), winding (G-I) and creasing (J-L).

**Table 5.1.** Accounts for the change in advancing OCA and contact angle hysteresis after exposing the BSA-derived and reduced imine linkage-based fibrous coating to various physical manipulations and abrasions.

| Durability Test | Advancing Contact Angle (°) | Contact Angle Hysteresis (°) |
|---|---|---|
| **Bending** | 161.5 ± 0.3 | 7.3 ± 0.8 |
| **Creasing** | 162.7 ± 0.7 | 7.8 ± 1.0 |
| **Twisting** | 160.1 ± 1.1 | 7.1 ± 0.4 |
| **Winding** | 163.3 ± 0.3 | 6.9 ± 0.8 |
| **Adhesive Tape Test** | 158.8 ± 0.6 | 8.0 ± 1.3 |
| **Sand Paper Abrasion** | 157.3 ± 1.3 | 8.5 ± 0.7 |
| **Sand Drop Test** | 159.3 ± 0.4 | 8.1 ± 0.6 |
| **Knife Scratch Test** | 157.6 ± 1.1 | 7.7 ± 0.3 |

(25 times) peeled off from the coated substrate to disrupt the BSA reduced imine coating, as shown in Figure 5.7D, however, the embedded bio-inspired underwater superoleophobicity remained unperturbed as shown in Figure 5.7E-F and Table 5.1. Thereafter, standard sand drop test (Figure 5.7G) and knife scratch test (Figure 5.7J) were performed on the BSA derived and reduced imine based underwater superoleophobic interface. The investigation of oil wettability confirmed the existence of uninterrupted underwater oil repellence, as shown in Fig. 5.7H-I,K-L and Table 5.1. Thus, the superior durability of extreme oil repellence under water, even after performing these widely accepted physical abrasion tests on the synthesized bio-inspired interface revealed its potential applications at diverse and challenging practical settings.

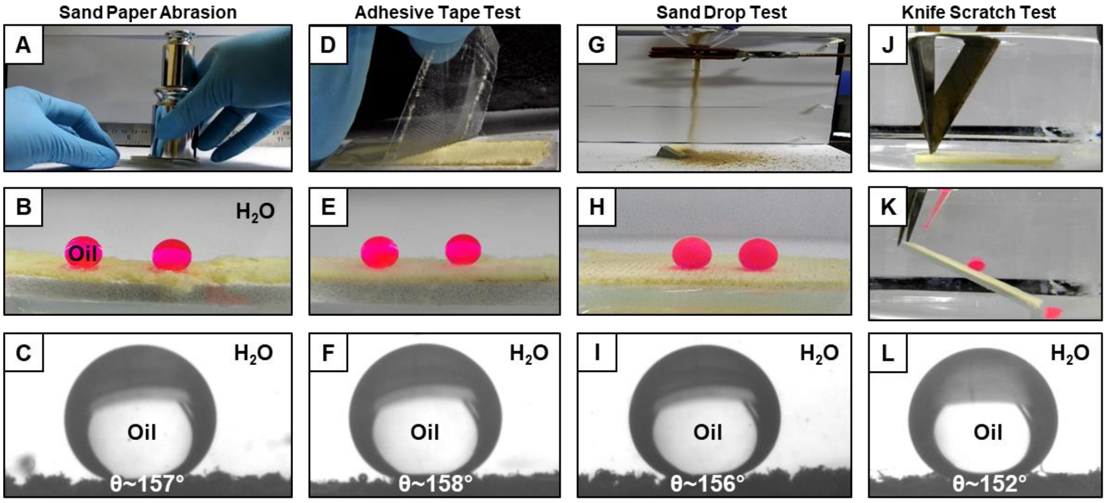

**Figure 5.7.** A-L) Digital images (A,B,D,E,G,H,J,K) and OCA images (C,F,I,L) images of the beaded oil droplet (underwater) on the reduced imine-based BSA-coated fibrous substrate after subjecting to various physically harsh abrasive tests including sand paper abrasion (A-C), adhesive tape test (D-F), sand drop test (G-I) and knife scratch test (J-L).

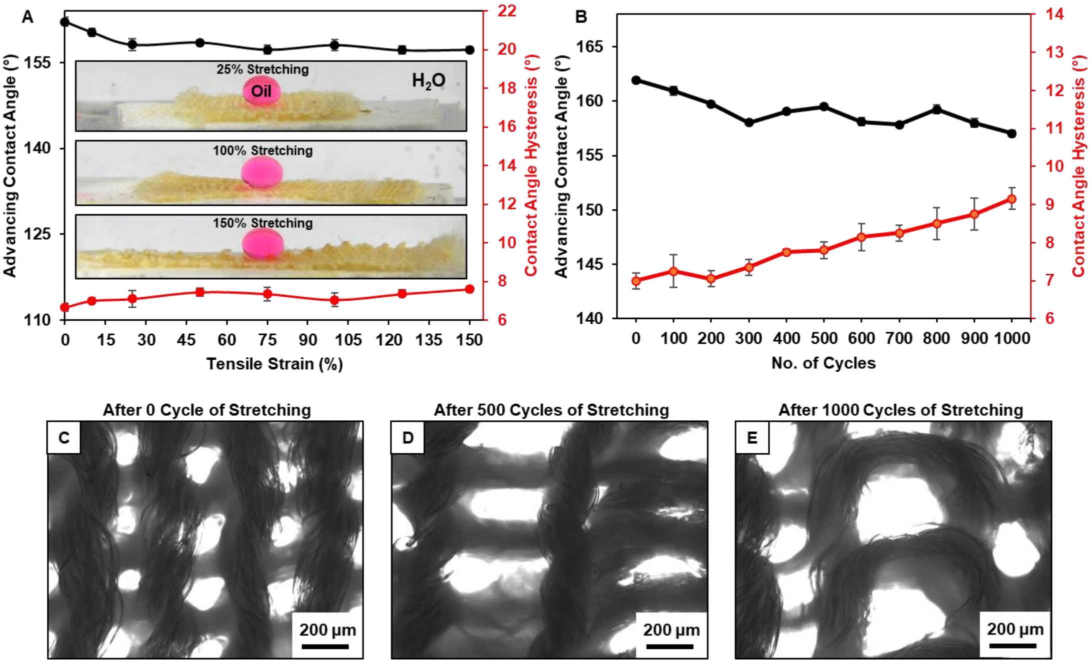

**Figure 5.8.** A) Plot accounting for the change in oil wettability on the reduced imine-based BSA-coated fibrous substrate after subjecting to different percentage of tensile strain ranging from 0% to 150%. B) Plot showing the advancing oil contact angle and contact angle hysteresis after subjecting the same fibrous substrate to 150% tensile deformation for 1000 cycles. C-E) Microscopic bright field images illustrating the change in the fibrous network of the used substrate after subjecting to repetitive 150% tensile deformation for 1000 cycles.

Furthermore, tensile strain was applied to the BSA derived reduced imine coated superoleophobic interface to investigate its ability to endure such practically relevant physical deformation. The tensile strain was gradually increased from 0 to 150% but the physically deformed interface continued to display underwater superoleophobicity with advancing OCA above 155° and contact angle hysteresis below 10°, as shown in Figure 5.8A. Further, such large (150%) physical deformation was repetitively imposed for 1000 times, but the underwater oil wettability remained intact with advancing oil contact

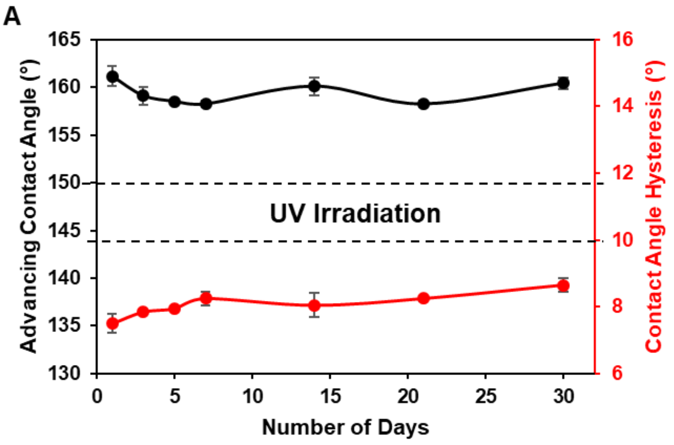

**Figure 5.9.** Plot showing the change in advancing oil contact angle and contact angle hysteresis after exposing the reduced imine-based BSA-coated fibrous substrate to UV radiation (254 nm and 365 nm) for 30 days.

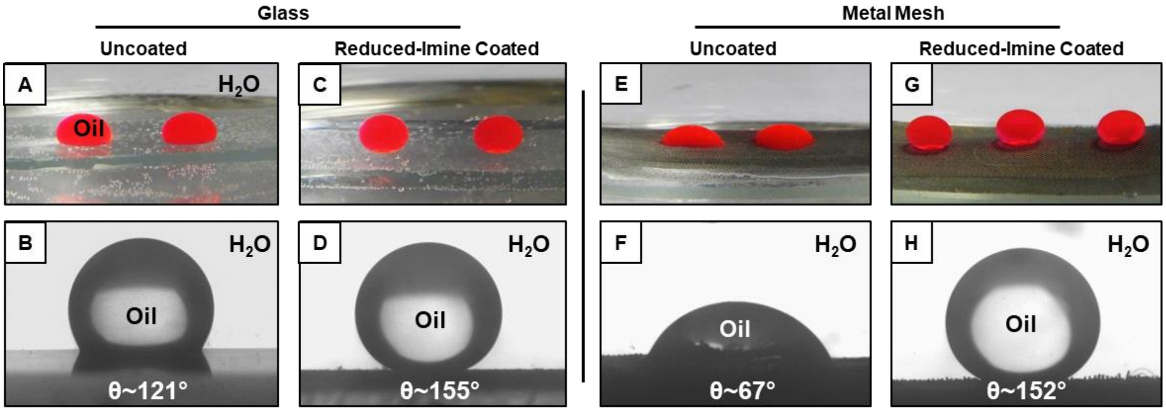

**Figure 5.10.** A-H) Digital images (A,C,E,G) and contact angle images (B,D,F,H) of the beaded oil droplet underwater on the uncoated (A-B, E-F) and reduced-imine based BSA-coated (C-D, G-H) glass slide (A-D) and metal mesh (E-H).

angles above 155° and contact angle hysteresis below 10° as shown in Figure 5.8B. Microscopic images further revealed the physical deformation of the fibres of the fabric after repetitive tensile stretching (Figure 5.8C-E) however, the underwater oil repellence behaviour remained unperturbed. Moreover, the same artificial underwater superoleophobic interface was subjected to prolonged UV irradiation (254 nm and 365 nm) for 30 days, however, the embedded oil repellence remained unperturbed with advancing OCA above 150° and contact angle hysteresis below 10°, as shown in Figure 5.9A.

Further, the BSA-derived reduced imine coating was successfully extended on planar (microscopic glass slide) and non-fibrous (metal mesh) substrates, where the uncoated glass slide is inherently oleophobic (OCA~121°) and the metal mesh is oleophilic (OCA~67°) underwater as shown in Figure 5.10A-B,E-F. However, the BSA-derived reduced imine coating rendered both the substrates underwater superoleophobic with static OCA above 150°, as shown in Figure 5.10C-D,G-H. Thus, this protein derived coating can be used to endow various substrates with underwater superoleophobicity.

## 5.4. Conclusion

Thus, in this chapter, the facile and reversible Schiff base reaction between amines and aldehydes was followed to generate underwater superoleophobicity. The mutual reaction between glutaraldehyde and bovine serum albumin (BSA) was adopted to develop a fluorescent coating on a fibrous substrate that displayed fish scale-inspired extreme oil repellence underwater. However, the synthesized underwater superoleophobicity failed to sustain under acidic aqueous exposure due to the predicted acidic hydrolysis of the imine bond, thus, transforming the wettability from superoleophobicity (OCA~155°) to oleophobicity (OCA~108°). Thus, a simple reduction of the dynamic imine cross-linkages was adopted to obtain a stable cross-linkages based underwater superoleophobic coating. The prepared coating sustained various physical abrasions, repetitive (1000 times) tensile strain (150%), prolonged exposure (30 days) to chemically complex aqueous phases, including extremes pH values (1 and 12), artificial sea water, river water and surfactant-contaminated (SDS, DTAB; 1 mM) aqueous phases and UV radiation (30 days). Thus, a facile chemical approach proved to be an efficient way to achieve sustainable underwater superoleophobicity that can perform under practically relevant and diverse conditions.

## 5.5. References

1. X. M. Li, D. Reinhoudt and M. Crego-Calama, *Chem. Soc. Rev.*, 2007, **36**, 1350-1368.
2. M. Liu, S. Wang, Z. Wei, Y. Song and L. Jiang, *Adv. Mater.*, 2009, **21**, 665-669.
3. B. Su, Y. Tian and L. Jiang, J. Am. Chem. Soc., 2016, 138, 1727. 4 X. Liu, J. Gao, Z. Xue, L. Chen, L. Lin, L. Jiang and S. Wang, *ACS Nano*, 2012, **6**, 5614-5620.
5. M. Tao, L. Xue, F. Liu and L. Jiang, *Adv. Mater.*, 2014, **26**, 2943-2948.
6. K. Chen, S. Zhou and L. Wu, *ACS Nano*, 2016, **10**, 1386-1394.
7. J. Li, D. Li, Y. Yang, J. Li, F. Zha and Z. Lei, *Green Chem.*, 2016, **18**, 541-549.
8. J. Yong, F. Chen, Q. Yang, J. Huo and X. Hou, *Chem. Soc. Rev.*, 2017, **46**, 4168-4217.
9. Z. Lian, J. Xu, Z. Yu, P. Yu, W. Ren, Z. Wang and H. Yu, *ACS Appl. Mater. Interfaces*, 2020, **12**, 6573-6580.
10. W. Chen, P. Zhang, R. Zang, J. Fan, S. Wang, B. Wang and J. Meng, *Adv. Mater.*, 2020, **32**, 1907413-1907420.
11. L. Lin, M. J. Liu, L. Chen, P. P. Chen, J. Ma, D. Han and L. Jiang, *Adv. Mater.*, 2010, **22**, 4826-4830.
12. X. Liu, J. Zhou, Z. Xue, J. Gao, J. Meng, S. Wang and L. Jiang, *Adv. Mater.*, 2012, **24**, 3401-3405.
13. L.-P. Xu, J. Peng, Y. Liu, Y. Wen, X. Zhang, L. Jiang and S. Wang, *ACS Nano*, 2013, **7**, 5077-5083.
14. L. P. Xu, J. Zhao, B. Su, X. L. Liu, J. T. Peng, Y. B. Liu, H. L. Liu, G. Yang, L. Jiang, Y. Q. Wen, X. J. Zhang and S. T. Wang, *Adv. Mater.*, 2013, **25**, 606-611.
15. Z. Cheng, H. Lai, Y. Du, K. Fu, R. Hou, C. Li, N. Zhang and K. Sun, *ACS Appl. Mater. Interfaces*, 2014, **6**, 636-641.
16. J. Yong, F. Chen, Q. Yang, U. Farooq and X. Hou, *J. Mater. Chem. A*, 2015, **3**, 10703-10709.
17. P. S. Brown and B. Bhushan, *Sci. Rep.*, 2015, **5**, 14030-14046.
18. Y. Cai, Q. Lu, X. Guo, S. Wang, J. Qiao and L. Jiang, *Adv. Mater.*, 2015, **27**, 4162-4168.
19. X. Meng and D. Deng, *J. Mater. Chem. A*, 2016, **4**, 6919-6925.

20. K. Han, L. Heng and L. Jiang, ACS Nano, 2016, 10, 11087. 21 S. Gao, J. Sun, P. Liu, F. Zhang, W. Zhang, S. Yuan, J. Li and J. Jin, *Adv. Mater.*, 2016, **28**, 5307-5314.

22. D. Zang, H. Yi, Z. Gu, L. Chen, D. Han, X. Guo, S. Wang, M. Liu and L. Jiang, *Adv. Mater.*, 2017, **29**, 1602869- 1602875.

23. S. Zhang, G. Jiang, S. Gao, H. Jin, Y. Zhu, F. Zhang and J. Jin, *ACS Nano*, 2018, **12**, 795-803.

24. X. Yuan, W.-C. Nie, C. Xu, X.-H. Wang, Q. Xiao, F. Song, X.-L. Wang and Y.-Z. Wang, *Adv. Funct. Mater.*, 2018, **28**, 1704956-1704963.

25. C.-L. Xu and Y.-Z. Wang, *J. Mater. Chem. A*, 2018, **6**, 2935-2941.

26. K. Chen, S. Zhou and L. Wu, *ACS Nano*, 2016, **10**, 1386-1394.

27. X. Meng, M. Wang, L. Heng and L. Jiang, *Adv. Mater.*, 2018, **30**, 1706634-1706642.

28. D. Wang, H. Liu, J. Yang and S. Zhou, *ACS Appl. Mater. Interfaces*, 2019, **11**, 1353-1366.

29. U. Manna and D. M. Lynn, *Adv. Funct. Mater.*, 2015, **25**, 1672-1681.

30. D. Parbat and U. Manna, *J. Mater. Chem. A*, 2018, **6**, 22027-22036.

31. A. Shome, A. M. Rather and U. Manna, *Nanoscale Adv.*, 2019, **1**, 1746-1753.

32. A. Shome, A. M. Rather, A. Ghosal, B. K. Bhunia, B. B. Mandal and U. Manna, *ACS Sustainable Chem. Eng.*, 2019, **7**, 7502-7509.

33. J. Lahann, *Nat. Nanotechnol.*, 2008, **3**, 320-321.

34. C. P. D. Brussaard, L. Peperzak, S. Beggah, L. Y. Wick, B. Wuerz, J. Weber, J. S. Arey, B. van der Burg, A. Jonas, J. Huisman and J. R. van der Meer, *Nat. Commun.*, 2016, **7**, 11206-11217.

35. Z. Xue, Y. Cao, N. Liu, L. Feng and L. Jiang, *J. Mater. Chem. A*, 2014, **2**, 2445-2460.

36. Z. Chu, Y. Feng and S. Seege, *Angew. Chem., Int. Ed.*, 2015, **54**, 2328-2338.

37. J.-M. Lehn and A. V. Eliseev, *Science*, 2001, **291**, 2331-2332.

38. S. J. Rowan, S. J. Cantrill, G. R. L. Cousins, J. K. M. Sanders and J. F. Stoddart, *Angew. Chem. Int. Ed.*, 2002, **41**, 898-952.

39. M. E. Belowich and J. F. Stoddart, *Chem. Soc. Rev.*, 2012, **41**, 2003-2024.

40. Y. Jia and J. Li, *Chem. Rev.*, 2015, **115**, 1597-1621.

41. J. L. Segura, M. J. Manchenoa and F. Zamora, *Chem. Soc. Rev.*, 2016, **45**, 5635-5671.

42. Y. Liu, Z. Tang, J. Chen, J. Xiong, D. Wang, S. Wang, S. Wu and B. Guo, *Polym. Chem.*, 2020, **11**, 1348-1355.

43. J. H. Billman and A. C. Diesing, *J. Org. Chem.*, 1957, **22**, 1068-1070.

44. Y. Sun, F. Yan, W. Yang and C. Sun, *Biomaterials*, 2006, **27**, 4042-4049.

45. S. Gan, P. Yang and W. Yang, *Biomacromolecules*, 2009, **10**, 1238-1243.

46. N. I. Bojorge-Ramirez, A. M. Salgado and B. Valdman, *Assay Drug Dev. Technol.*, 2007, **5**, 673-682.

47. S. V. Pavlukhina, J. B. Kaplan, L. Xu, W. Chang, X. Yu, S. Madhyastha, N. Yakandawala, A. Mentbayeva, B. Khan and S. A. Sukhishvili, *ACS Appl. Mater. Interfaces*, 2012, **4**, 4708-4716.

48. Y. Tian, Q. He, Y. Cui and J. B. Li, *Biomacromolecules*, 2006, **7**, 2539-2542.

49. L. Duan, W. Qi, X. H. Yan, Q. He, Y. Cui, K. W. Wang, D. X. Li and J. B. Li, *J. Phys. Chem. B*, 2009, **113**, 395-399.

50. L. Duan, X. H. Yan, A. H. Wang, Y. Jia and J. B. Li, *ACS Nano*, 2012, **6**, 6897-6904.

51. L. Ge, J. Yan, X. Song, M. Yan, S. Ge and J. Yu, *Biomaterials*, 2012, **33**, 1024-1031.

52. O. S. Kwon, S. J. Park, J.-Y. Hong, A. R. Han, J. S. Lee, J. S. Lee, J. H. Oh and J. Jang, *ACS Nano*, 2012, **6**, 1486-1493.

53. W. Zhao, H. Zhang, Q. He, Y. Li, J. Gu, L. Li, H. Li and J. Shi, *Chem. Commun.*, 2011, **47**, 9459-9461.

54. K. F. Ren, J. Ji and J. C. Shen, *Bioconjugate Chem.*, 2006, **17**, 77-83.

55. J.-H. Lim, D. S. Ginger, K.-B. Lee, J. Heo, J.-M. Nam and C. A. Mirkin, *Angew. Chem. Int. Ed.*, 2003, **42**, 2309-2312.

56. S. Hou, J. Wang and C. R. Martin, *Nano Lett.*, 2005, **5**, 231-234.

57. M. T. Zin, H.-L. Yip, N.-Y. Wong, H. Ma and A. K. Y. Jen, *Langmuir*, 2006, **22**, 6346-6351.

58. D. I. Rozkiewicz, Y. Kraan, M. W. T. Werten, F. A. Wolf, V. Subramaniam, B. J. Ravoo and D. N. Reinhoudt, *Chem. Eur. J.*, 2006, **12**, 6290-6297.

59. Y. Jia, Y. Cui, J. B. Fei, M. C. Du, L. R. Dai, J. B. Li and Y. Yang, *Adv. Funct. Mater.*, 2012, **22**, 1446-1453.

60. L. Gao, J. B. Fei, J. Zhao, W. Cui, Y. Cui and J. B. Li, *Chem. Eur. J.*, 2012, **18**, 3185-3192.

61. A.-M. Caminade and J.-P. Majoral, *Acc. Chem. Res.*, 2004, **37**, 341-347.

62. J. Zhao, J. Fei, L. Gao, W. Cui, Y. Yang, A. Wang and J. Li, *Chem. Eur. J.*, 2013, **19**, 4548-4555.

63. J. Yang and C. Gao, *Macromol. Rapid Commun.*, 2010, **31**, 1065-1070.

64. X. Ma, X. Sun, D. Hargrove, J. Chen, D. Song, Q. Dong, X. Lu, T.-H. Fan, Y. Fu and Y. Lei, *Sci. Rep.*, 2016, **6**, 19370-19382.

65. W. Wei, L. Yuan, G. Hu, L.-Y. Wang, H. Wu, X. Hu, Z. G. Su and G.-H. Ma, *Adv. Mater.*, 2008, **20**, 2292-2296.

66. Y. Jia, J. Fei, Y. Cui, Y. Yang, L. Gao and J. Li, *Chem. Commun.*, 2011, **47**, 1175-1177.

67. L. Tauk, A. P. Schr¨oder, G. Decher and N. Giuseppone, *Nat. Chem.*, 2009, **1**, 649-656.

# Chapter 6: Aloe Vera Mucilage Derived Abrasion-Tolerant Underwater Superoleophobicity*

In this chapter, the inherent underwater superoleophobicity of Aloe Vera Mucilage (AVM), a naturally existing hydrogel was discovered and strategically exploited for achieving a durable and highly stretchable underwater oil repellent coating on a fibrous substrate. The high content of aqueous phase (~99 wt%) entrapped within the mucilage imparted extreme oil repellent characteristics to the mucilage. Direct utilization of this mucilage to coat on a fibrous substrate led to the compromise of the embedded oil repellence behaviour on subjection to harsh physical abrasions and chemically contaminated aqueous settings. Therefore, the catalyst-free Michael addition reaction was strategically exploited to covalently cross-link the deposited mucilage and obtain a robust AVM coating on the fibrous substrate. Moreover, the presence of residual acrylate reactivity on this covalently deposited AVM aided in recovering the non-adhesive underwater superoleophobicity following the Michael addition assisted post covalent modification. The post covalently modified AVM coating was capable of sustaining various challenging chemical (pH 1, pH 12, surfactant water, sea water, and river water) settings upto 30 days and physical (150% tensile deformation, scratching and other abrasions) exposures without compromising the embedded underwater superoleophobicity. Further, the post-covalently modified, highly durable AVM coating on the fibrous substrate was extended for the gravity-driven, selective and repetitive (25 cycles) separation of the water phase from various oil/water mixtures with water separation efficiency above 97%, even under various severe practically relevant physically harsh settings and chemically harsh aqueous media.

---

*A. Shome *et al.*, *J. Mater. Chem. A*, 2018, **6**, 22465-22471.

## 6.1. Introduction

Nature-inspired anti-fouling interfaces have been artificially synthesized by strategic confinement of a third external phase between the solid interface and the beaded droplets of the probe liquid, and this immobilized third phase eventually provides the essential heterogeneous wettability.[1-11] In this context, the underwater superoleophobic property exhibited by 'fish-scales',[3] was mimicked through fabricating highly water compatible hierarchical interfaces, where the trapped aqueous layer contributed to the heterogeneous super oil wettability. Such bio-inspired underwater superoleophobic interfaces have emerged as an important avenue for developing smart materials for various practically relevant applications—including eco-friendly remediation of oil spillages, anti-biofouling coating, anti-platelet adhesion, smart robotics under water, etc.[12-18] Over the years, synthetic hydrogels, polyelectrolytic multilayers and metal oxides[3,17-27] were extensively used for developing underwater oil-repellent interfaces, however, these reported approaches have (a) poor durability[28-29] and (b) involve complex/tedious fabrication processes.[3,17-27] Recently, there were a few reports on mechanically durable underwater superoleophobic interfaces—where tensile moduli of the bio-mimicked artificial coatings are very high and physical deformation of the interfaces is highly restricted.[28-29] However, such designs are mostly inappropriate for developing durable and stretchable underwater superoleophobic membranes. Furthermore, utilization of naturally derived components over the synthetic counterparts would provide an economic and eco-friendly alternative for practical utility. Over the years, naturally derived chitosan,[30] nano-clay,[31] cellulose components[32] have been utilized to develop eco-friendly alternatives for developing materials for practical applications, but the prolonged durability concerns persist.[33-34] Thus, in this chapter we derived both the inspiration and ingredients from nature to develop durable and stretchable underwater superoleophobicity.

In the previous chapter, abundant proteins and waste papers were utilized to develop underwater superoleophobicity.[35] However, in this chapter, we have discovered the inherent underwater superoleophobicity of Aloe Vera mucilage and directly exploited it for developing sustainable underwater oil repellent interfaces. The naturally stored mucilage within the Aloe Vera leaf comprises of ~99 wt% water,[36] which imparted non-adhesive underwater superoleophobicity that remained intact even after exposure to extremes of temperature and chemically contaminated aqueous phases. Thus, this naturally abundant hydrogel was covalently cross-linked and embedded on a fibrous substrate following the Michael addition reaction at ambient conditions. The resultant, chemically modified hydrogel derived oil repellent interface could endure various severe physical abrasions, 150% tensile stretching and chemically contaminated aqueous phases for a prolonged duration (30 days), without compromising the embedded underwater oil repellence property. Thus, this highly durable, underwater oil-repellent interface was extended for the gravity-driven filtration based selective and repetitive (25 times) separation of both light and heavy oil/water mixtures wherein, selectively the water phase permeated through the oil-repellent interface with water separation efficiency above 97% even under extremes of physically and chemically challenging settings.

## 6.2. Experimental Section:

**6.2.1. Materials:** Di-pentaerythritol penta-acrylate (5Acl, MW = 524.51 g/mol), silicone oil (CAS No. 63148-58-3), rhodamine-6G (CAS No. 989-38-8), methylene blue (CAS No. 122965-43-9) and sodium dodecyl sulfate were obtained from Sigma Aldrich, (Bangalore, India). Dimethyl sulfoxide (DMSO) and hydrochloric acid were obtained from Fischer Scientific (Mumbai) India. Chloroform and tetrahydrofuran (THF) were obtained from FINAR. Sodium chloride, magnesium chloride, calcium chloride, magnesium sulphate, and sodium hydroxide were purchased from Merck Specialties Private Limited. Ethyl Alcohol (CAS No. 64-17-5, Lot No. 17030799) was purchased from TEDIA, United States of America. Adhesive Tape was obtained from Jonson tape Ltd Pvt., New Delhi, India. Nile Red (CAS No. 7385-67-3) and D-Glucamine (>95%) were purchased from Tokyo Chemical industry. Dichloroethane (CAS No. 107-06-2ADR) was purchased from Lobo Chemie Pvt. Ltd., Mumbai, India. Fibrous polyurethane (PU) fabric, vegetable oil and kerosene oil were purchased from a local shop in Guwahati City, Assam, India. Motor oil (Castrol Active 20W-40) was purchased from Castrol India Ltd. Sand was collected from a construction site at IIT, Guwahati and rinsed with water, dried prior to use. River water was collected from Brahmaputra river, Guwahati, Assam. Aloe Vera was generously obtained from the balcony garden of Mrs. Tumpa Manna Jana.

**6.2.2 General Consideration:** The glass wares were washed thoroughly with ethyl alcohol and acetone prior to preparing the desired solutions. Kruss Drop Shape Analyzer-DSA25 instrument with mechanical liquid dispenser was used for contact angle measurements at ambient temperature. The contact angles were measured using 5 μl model oil droplet (dichloroethane) at three different locations for each sample. Field Emission Scanning Electron Microscope (FESEM) images were obtained using a Carl Zeiss Field Emission Scanning Electron Microscope. FTIR spectra were recorded using a Perkin Elmer Instrument at ambient temperature by preparing KBr pellet with the sample. The digital photographs were captured by Cannon Powershot SX420 IS digital camera for all experimental demonstrations. Both the exterior green peel of the Aloe Vera leaf and the stored mucilage (hydrogel) within the leaf was lyophilized (Analytical Chemistry, 1973 45, 1296) using Labconco FreeZone Freeze Dryer instrument. The mucilage is exposed to liquid nitrogen for freezing the immobilized water, and then under the automated applied vacuum (0.310 mbar), the frozen aqueous phase sublimates. This approach is highly adopted in drying materials without destroying its structure.

### 6.2.3. Aloe Vera Mucilage Coating on a Stretchable, Fibrous Substrate:

In order to coat the stretchable polyurethane fabric (14 cm x 14 cm) with Aloe Vera Mucilage, the mucilage was collected by peeling off the rind (green portion that acts as a protective layer) and discarding the aloin (yellowish portion). Subsequently, Aloe Vera Mucilage weighing 8.5 g was squashed manually and coated over an area of 196 $cm^2$ using a paint brush in to-fro motion to ensure a uniform coating on the fabric. The fabric was allowed to air dry overnight and thereafter, the underwater oil wettability was examined using contact angle measurements and digital images.

### 6.2.4. Chemically 'Reactive' Aloe Vera Mucilage Coating and its Post Modification:

The Aloe Vera Mucilage coated fibrous substrate was thereafter treated in a solution of 5Acl (1.325 g in 10 mL of ethanol) for 2 h, this interface was denoted as the chemically 'reactive' AVM coating. Afterwards, it was washed thoroughly in ethanol to remove the excess 5Acl. Thereafter, the 5Acl modified AVM coated substrate was dipped in a solution of glucamine (5 mg/ml in DMSO) and kept overnight. Next, the glucamine post modified AVM substrate (denoted as Glu-AVM) was washed using DMSO and THF. Finally, the Glu-AVM was pre-wetted with water, and the oil wettability was examined through contact angle measurements and digital images.

### 6.2.5. Physical and Chemical Durability Tests:

Various practically relevant challenging physical and chemical settings were performed to examine the durability of the AVM derived underwater superoleophobicity on the fibrous substrate. The details of the durability tests have been outlined in the following sections.

**6.2.5.1. Sand Drop Test:** 100 g of sand was poured from a height of 25 cm onto both the AVM and Glu-AVM coated fibrous substrates (2 cm x 2 cm), titled at an angle of 45°. The underwater oil wettability after the sand drop test was investigated by measuring the oil contact angles and visual inspections.

**6.2.5.2. Sand Paper Abrasion Test:** Sand paper abrasion test was performed by fixing the respective AVM coated fibrous substrates (2 cm x 2 cm) onto a glass slide and subsequently rubbed with a sand paper in back and forth motion with a 500 g load on top for 50 cycles. Thereafter, the oil wettability was examined with contact angle measurements and digital images.

**6.2.5.3. Adhesive Tape Test:** The AVM coated fibrous substrates (2 cm x 2 cm) were horizontally exposed to an adhesive surface with an external load of 500 g on top and this set-up was kept undisturbed for 10 minutes to ensure uniform contact between the respective substrate and the adhesive interface. Thereafter, the fabric was peeled off form the adhesive tape manually and the underwater oil wettability was re-examined by following standard characterization processes. This process of exposing with the adhesive tape and subsequent peeling of the coating was repeated for 25 cycles.

**6.2.5.4. Knife Scratch Test:** Random scratches were made on the AVM coated fibrous substrate (2 cm x 2 cm) in all possible directions using a sharp-edged knife for multiple times (~30) and thereafter, the oil repellence was examined via contact angle measurements and digital images.

**6.2.5.4. Physical Manipulations:** Both the AVM and Glu-AVM coated substrates (5 cm x 5 cm) were manually bended, creased, twisted and winded arbitrarily for 25 times. Subsequently, the digital images were acquired, and oil contact angles were measured underwater to examine the impact of these physical manipulations on the embedded underwater superoleophobic property. Tensile strain was gradually applied on both the AVM and Glu-AVM coated substrates through manual stretching upto 150% and subsequently, the oil wettability under water was examined after regular intervals.

**6.2.5.5. Chemical Durability Tests:** The underwater oil wettability on the freshly exposed Aloe Vera Mucilage and its coating on the fibrous substrates were examined separately after exposing them to various chemically harsh aqueous phases i.e. artificial sea water, river water, extremes of pH (1 and 12), surfactant contaminated water (SDS, 1 mM) for 30 days. The artificial sea water was prepared by mixing $MgCl_2$ (0.226 g), $MgSO_4$ (0.325 g), NaCl (2.673 g) and $CaCl_2$ (0.112 g) in 100 mL of de-ionized water in a volumetric flask.

### 6.2.5.6. Examining the Impact of Heating on the Oil Wettability of Aloe Vera Mucilage:

The Aloe Vera mucilage was cut into a small piece (2 cm x 1.5 cm x 0.8 cm) and carefully fixed onto a glass slide with the rind acting as the base on the glass slide. The mucilage was subsequently submerged in de-ionized water (40 mL) in a glass beaker. This beaker was placed on a hot plate, and a mercury thermometer was used for continuously monitoring the temperature of the system. Nile red dyed dichloroethane droplet of size (15 µl) was placed on the mucilage exposed to water and the temperature of the system was gradually increased up to 100°C using a hot plate. The effect of this gradual heating of the aqueous phase on the oil wettability of the mucilage was examined through contact angle measurements and digital images.

### 6.2.6. Gravity-driven Oil/Water Separation:

The post covalently modified AVM derived durable underwater oil repellent fibrous substrate was used as a membrane for the separation of various oil/water mixtures. A lab made prototype was developed using a 50 mL falcon tube wherein the Glu-AVM derived stretchable underwater superoleophobic membrane (pre-wetted with water) was tied to the opening of the falcon tube and another hole was made near the closed end of the tube in order to pour the oil/water mixtures using a funnel. The aqueous phase was dyed with rhodamine-6G and methylene blue as required, and the oil was dyed with Nile Red for visual inspection. The water phase selectively impregnated through the underwater oil-repellent membrane and was subsequently collected in a beaker. The selective oil/water separation was performed even for chemically harsh aqueous phases, wherein the aqueous phase was contaminated with acid, base, surfactant, salt and river water. The selective water separation efficiency was calculated using the following formula,

$$\eta = \frac{V_f}{V_i} x\ 100$$

where, $V_i$ is the initial volume of water poured and $V_f$ is the final volume of water collected.

## 6.3. Results and Discussions:

### 6.3.1. Discovering the Underwater Superoleophobicity of Aloe Vera Mucilage

Aloe Vera Mucilage (AVM), a naturally existing hydrogel comprising of various bioactive agents including anthraquinones, carbohydrates, enzymes, amino acids, vitamins, etc was exploited over the years for wound healing, tissue engineering, drug delivery and edible coatings for food preservation.[36-38] In this chapter, the mucilage comprising of a large quantity of an immobilized aqueous phase (~99 wt%) was discovered to be inherently embedded with underwater superoleophobicity. The large content of the immobilized aqueous phase in AVM was hypothesized to contribute to the heterogeneous oil wettability (Cassie–Baxter state) underwater (Figure 6.1A).[3] The underwater oil wettability was examined in detail on an Aloe Vera leaf, where both the outer green exterior of the leaf and the mucilage were exposed to a 40 µL dichloroethane droplet (DCE; model heavy oil coloured red for visual inspection) under water as shown in Figure 6.1B. The outermost green skin of the Aloe Vera leaf was noticed to be oleophilic under water with oil contact angle (OCA) ~67° (Figure 6.1C), but interestingly, the encapsulated AVM repelled the beaded oil droplet extremely under water with static OCA~163° and contact angle hysteresis ~5° as shown in Figure 6.1D. The total immobilized water content in the exterior green peel of the Aloe Vera leaf was estimated to be ~7%, which is significantly lower than the amount (~99 wt%)[36] of aqueous phase immobilized within the AVM. Thus, the distinct difference in the underwater oil wettability in the exterior and interior of the leaf was attributed to the varying quantity of the immobilized aqueous phase. The trapped aqueous phase within the mucilage was concluded to be the key factor in controlling the super-oil repellence under water. The topography of the thick mucilage and the exterior of the leaf was characterized under field emission scanning electron microscope (FESEM) as shown in Figure 6.1E-F. Primarily, AVM was lyophilized for complete removal of the embedded water phase prior to imaging. The removal of a large amount of embedded water led to a folded morphology (Figure 6.1F) as observed under the FESEM, whereas the topography of the exterior of the leaf exhibited completely distinct and compact features as shown in Figure 6.1E. Further, an experiment was designed to examine the non-adhesive oil wettability on the interface of AVM, wherein a beaded oil droplet was moved from left to right as shown in Figure 6.1G-J. Interestingly, the beaded oil droplet completely receded from the interface of AVM without leaving behind any trace of the oil phase as shown in Figure 6.1J. Furthermore, the durability of the inherently embedded oil wettability in the AVM was investigated by subjecting it to practically relevant and challenging scenarios. The AVM was kept in boiling (100°C) water for 1 h and it was noted that the colour of the exterior green peel changed to yellow; however, both the physical integrity of the AVM and the embedded underwater oil wettability remained unaffected. The beaded oil droplet was repelled extremely with static OCA~160° and contact angle hysteresis ~6° as shown in Figure 6.1K-L. Another extreme condition was imposed on the AVM, where the interior of the AV leaf was exposed to liquid

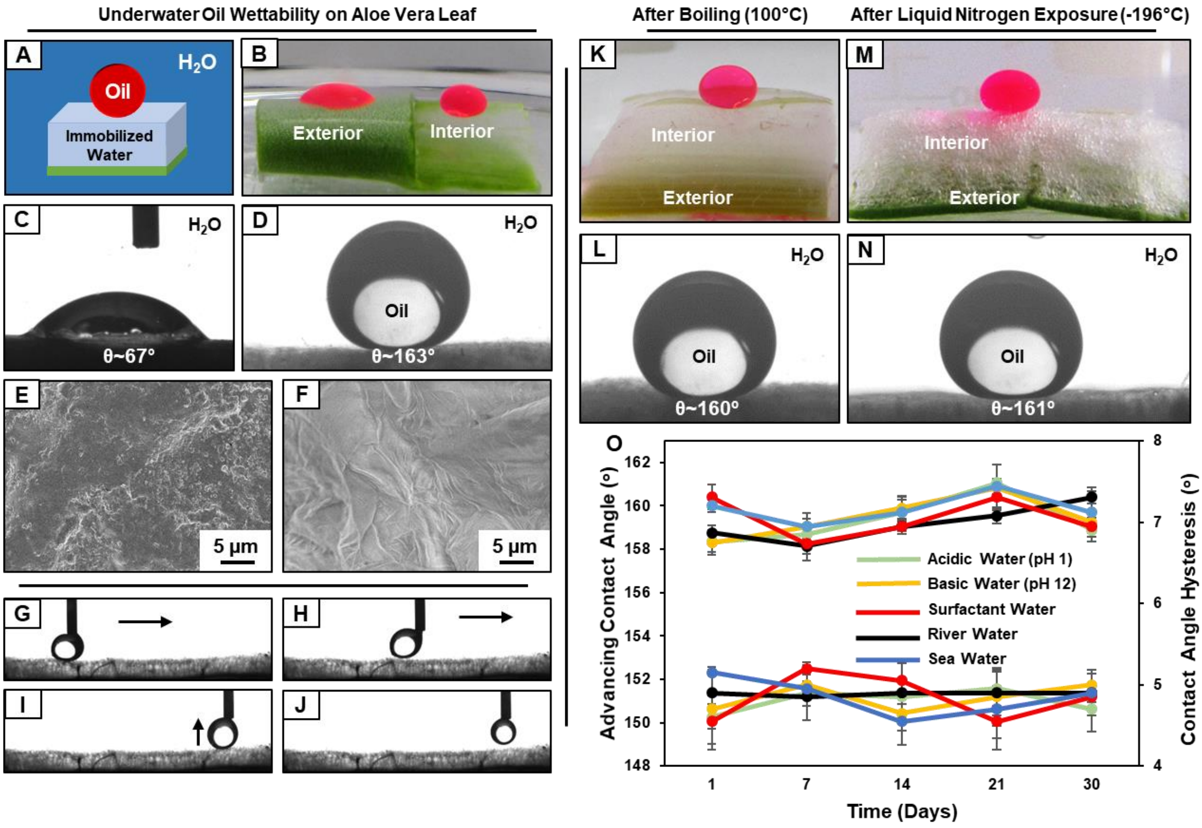

**Figure 6.1.** A) Schematic representation of oil wettability on the immobilized-aqueous phase under water. B-D) Digital image (B) and static OCA images (C-D) of the beaded oil droplets on the exterior (C) and interior (D) of the Aloe Vera leaf under water. E-F) FESEM images of the exterior (E) and interior (F) of the Aloe Vera leaf. G-J) Digital images displaying the translation of oil droplet on the top surface of AVM under water (G-I) and receding (J) of the beaded oil droplet from the AVM surface. K-N) Digital images (K,M) and OCA images (L,N) of the beaded oil droplet on the AVM under water after exposure to boiling water (K-L) and liquid nitrogen (M-N). O) Plot accounting for the advancing OCA and contact angle hysteresis of the beaded oil droplet on the AVM after exposing it to various harsh aqueous chemical conditions for 30 days.

nitrogen (-196°C) for 24 h and thereafter, the material was lyophilized. However, the lyophilized AVM remained efficient in displaying superoleophobicity with OCA~161° and contact angle hysteresis ~7°, after submerging in an aqueous phase (Figure 6.1M-N), where the external aqueous phase rapidly infiltrated the matrix and the immobilized water layer contributed to the extreme oil repellence. Furthermore, this AVM was exposed to various chemically severe conditions—including extremes of pH (1 and 12), surfactant (SDS; 1 mM) contaminated aqueous phase, artificial sea water and river water for 30 days. However, the embedded extreme oil repellence of AVM remained unperturbed with advancing OCA above 150° and contact angle hysteresis below 10° as shown in Figure 6.1O. Thus, the embedded oil wettability in the AVM was found to be extremely durable and capable of preserving its naturally embedded super-oil wettability even under highly drastic physical and chemical conditions, which provided a unique avenue to directly exploit the AVM for developing stretchable and durable underwater superoleophobic membranes for gravity-driven filtration-based oil/water separation.

### 6.3.2. Chemically Modulated Aloe Vera Mucilage derived Underwater Superoleophobic Coating

A commercially available fibrous and stretchable substrate, which is inherently oleophilic under water, was selected for coating with this naturally packaged underwater superoleophobic AVM. Fresh AVM (8.5 g) was uniformly deposited on the selected fibrous substrate (14 cm x 14 cm). The underwater oleophilic fibrous substrate (Figure 6.2A-B) transformed into an extremely oil repellent interface under water as measured through the static and dynamic oil contact angles where, the oil droplet beaded with static OCA~157° and contact angle hysteresis ~7° as shown in Figure 6.2C-D. Next, the durability of the embedded oil wettability on the AVM deposited fibrous substrate was examined adopting standard processes. Different physical manipulations including bending, twisting, creasing and winding were imposed on the AVM coated fibrous substrate for multiple times (25 times). However, the AVM coated

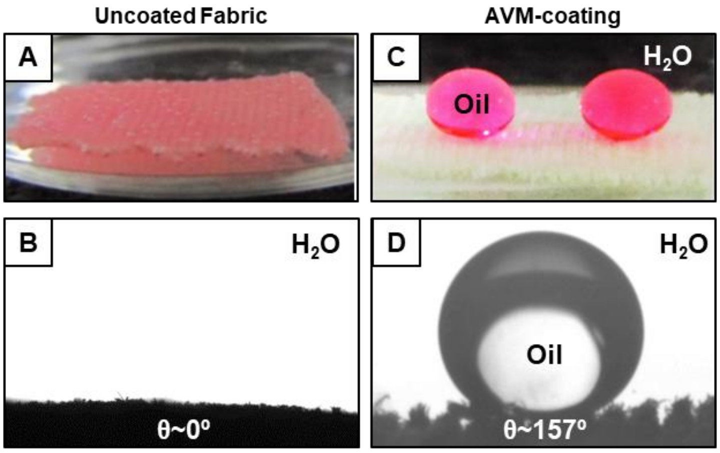

**Figure 6.2.** A-D) Digital images and static OCA images of the beaded oil droplet on the commercial, uncoated polyurethane fabric (A-B) and after coating the same fabric with Aloe Vera mucilage (C-D).

**Table 6.1** Illustrating the change in the advancing OCA and contact angle hysteresis of the beaded oil droplet under water on the AVM coated fibrous substrates after incurring various physical and chemical exposures.

| **Physical and Chemical Exposures** | **Aloe Vera Mucilage Coated Fabric** | |
|---|---|---|
| | **Advancing Contact Angle (°)** | **Contact Angle Hysteresis (°)** |
| **Bending** | 156.2 ± 1.5 | 7.5 ± 0.3 |
| **Creasing** | 155.6 ± 2.1 | 7.9 ± 0.6 |
| **Twisting** | 156.4 ± 1.8 | 8.1 ± 0.8 |
| **Winding** | 157.3 ± 2.3 | 7.8 ± 0.7 |
| **Acidic water (pH 1)** | 0 | - |
| **Alkaline water (pH 12)** | 158.0 ± 2.3 | 8.1 ± 0.5 |
| **Surfactant water (SDS)** | 159.2 ± 1.4 | 8.8 ± 0.8 |
| **Artificial sea-water** | 158.2 ± 1.7 | 8.3 ± 1.1 |
| **River water** | 157.8 ± 0.9 | 7.9 ± 1.3 |

substrate remained efficient in displaying non-adhesive superoleophobicity under water as shown in Table 6.1. Thereafter, severe physical abrasions, including adhesive tape peeling (Figure 6.3A), sand paper abrasion (Figure 6.3D) and sand drop test (Figure 6.3G), knife scratch test were performed on the AVM coated fibrous substrate, but it completely failed to survive under such challenging physical abrasions. The AVM coated fibrous substrate compromised the embedded nature-inspired underwater superoleophobicity with oil contact angles decreasing below ~105° as show in Figure 6.3B-C,E-F,H-I. The underwater superoleophobic coating survived exposure to various complex aqueous phases—including highly acidic water, alkaline water, artificial sea water, river water and surfactant

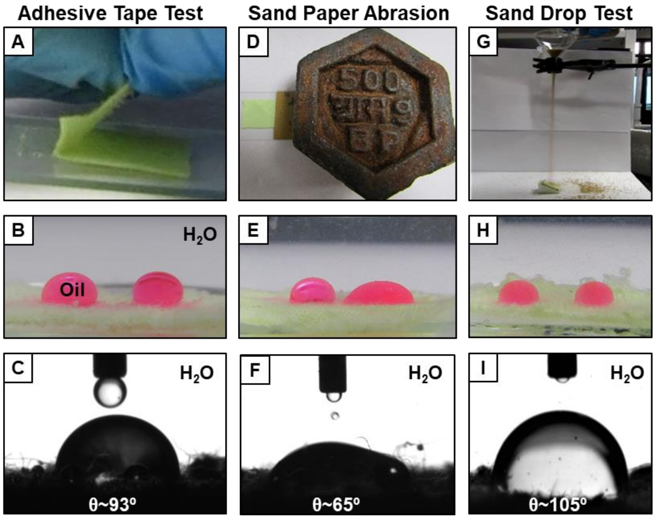

**Figure 6.3.** A, D, G) Digital images illustrating the set-up for different physical abrasions—including adhesive tape test (A), sand paper test (D) and sand drop test (G). Digital images and static OCA images of the beaded oil droplets under water on the AVM coated fibrous substrate after performing various physical abrasions, including adhesive tape test (A-C), sand paper abrasion (D-F), and sand drop test (G-I).

contaminated (SDS) water only upto 72 h as shown in Table 6.1. Thus, the AVM derived underwater superoleophobic coating on the fibrous substrate is capable of withstanding various physical manipulations, but at the same time, it is incapable of surviving severe physical abrasions (i.e., adhesive tape peeling test, sand paper test sand drop test and knife scratch test). To combat this challenge, a chemically 'reactive' and covalently cross-linked approach was rationally exploited for improving these noted physical durability issues, which are highly relevant for practical utility of the material. The inherently underwater superoleophobic AVM comprises of various amino acids and enzymes with amine functionalities[36] which provides a facile avenue for the further covalent chemical modifications.

In the current design, a multifunctional cross-linker (5Acl) was rationally associated with AVM following the catalyst-free Michael addition reaction between amines of AVM and the acrylate cross-linker as shown in Figure 6.4A-B. This simple chemical post modification (a) allowed the covalent cross-linking of the entire deposited AVM, and (b) the residual acrylate groups in the deposited AVM provided a facile basis to modulate the desired chemistry through the essential post-covalent modification process to achieve non-adhesive underwater superoleophobicity as shown in Figure 6.4C. For the proof-of-concept demonstration, AVM was treated with 5Acl in ethanol for 2 h. After this covalent cross-linking process, the oil wettability underwater transformed to adhesive superoleophobicity with static OCA~151° and contact angle hysteresis ~14° as shown in Figure 6.4D-E and Table 6.2. Further, the 5Acl treated AVM (denoted as AVM-5Acl) was characterized through FTIR analysis, where the appearance of the characteristic IR signature at 1735 $cm^{-1}$ corresponding to the carbonyl stretching frequency and 1410 $cm^{-1}$ for the symmetric deformation of the C–H bond for the β-carbon of vinyl groups revealed the existence of residual acrylate functional groups in the modified AVM as shown in Figure 6.4J (black). Such acrylate signatures are absent in the native AVM (Figure 6.4J; blue). The residual acrylate moieties rendered this AVM chemically 'reactive' and allowed the further induction of chemical functionality in AVM to modulate the oil wettability. The chemically 'reactive' AVM coated fibrous substrate was strategically modified with a hydrophilic small molecule—i.e. glucamine, which is well recognized for its inherent anti-biofouling property.[39] After the post covalent modification, the adhesive underwater superoleophobicity after 5Acl treatment (Figure 6.4D-E) transformed to non-adhesive underwater superoleophobicity with static OCA~162° and contact angle hysteresis ~6° (denoted as Glu-AVM) as shown in Figure 6.4F-G and Table 6.2. Both dynamic and static contact angles were measured to examine the non-adhesive underwater superoleophobicity. The successful post chemical modification of the chemically 'reactive' AVM with glucamine molecules was confirmed through standard FTIR analysis. During the Michael addition

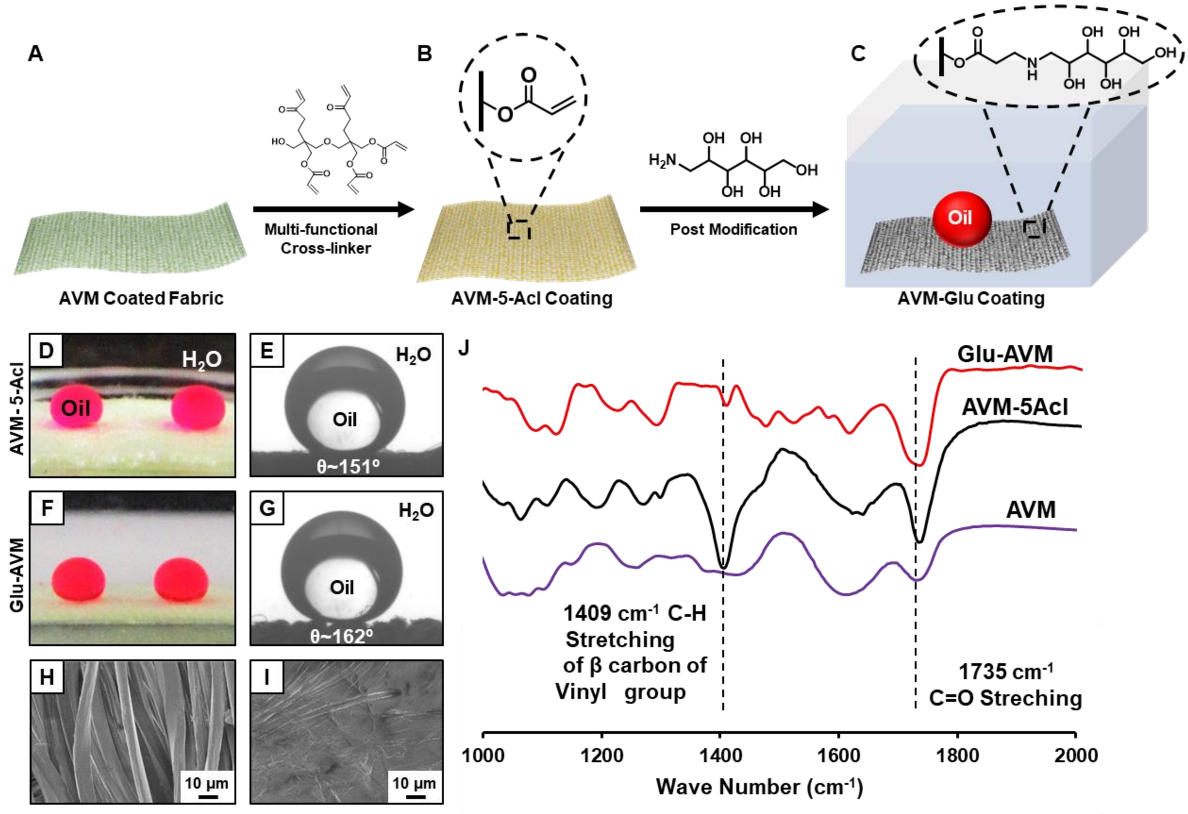

**Figure 6.4.** A-C) Schematic representing the covalent cross-linking of the deposited AVM on a fibrous substrate (A) with a multi-functional cross-linker following the Michael addition reaction between the amine groups of AVM and the acrylate cross-linker. The AVM-5Acl coating (B) comprises of residual acrylates that allows the post functionalization with a high surface energy molecule i.e. glucamine to obtain non-adhesive underwater superoleophobicity (C). D-G) Digital images and static OCA after treatment of the AVM coating with 5Acl (AVM-5Acl; D-E) and after glucamine treatment (Glu-AVM; F-G). H-I) FESEM images illustrating the morphological changes in the fibrous substrate before (H) and after (I) AVM coating. J) FTIR spectra of AVM (purple), AVM-5Acl coating (black) and after Michael addition reaction with glucamine, Glu-AVM (red).

reaction, the vinyl groups were consumed, while the carbonyl peak remained unaffected and provided an internal reference to monitor the progress of the reaction. The significant depletion of the IR peak intensity at 1410 cm$^{-1}$ with respect to 1710 cm$^{-1}$ strongly revealed the successful chemical modification as shown in Figure 6.4J (red). Further, the chemically modulated AVM coating on the fibrous substrate was characterized through FESEM, where the collapsed and folded layers on the otherwise smooth and featureless selected fibrous substrate (Figure 6.4H) confirmed the successful deposition of AVM as shown in Figure 6.4I.

**Table 6.2** Illustrating the change in the advancing OCA and contact angle hysteresis of the beaded oil droplet under water on the AVM coated fibrous substrates and after the chemical modification.

| Coating on Fibrous Substrate | Advancing Contact Angle (°) | Contact Angle Hysteresis (°) |
|---|---|---|
| **AVM** | 159.6 ± 1.3 | 7.1 ± 0.8 |
| **AVM-5Acl** | 153.4 ± 0.6 | 14.4 ± 1.2 |
| **Glu-AVM** | 161.8 ± 0.8 | 6.3 ± 0.5 |

### 6.3.3. Examining the Durability of the Chemically Modified, Underwater Oil-Repellent Aloe Vera Coating

The durability of the covalently cross-linked and post modified AVM coated substrate was examined in detail, where various physical manipulations—including bending, creasing, winding and twisting were repetitively imposed (25 times), however, the Glu-AVM coated substrate continued to display non-adhesive underwater superoleophobicity as shown in Table 6.3. Thereafter, harsh physical abrasions were imposed on the Glu-AVM substrates to examine the durability of the embedded oil repellence. A freshly exposed adhesive tape was brought in contact with the Glu-AVM coated fibrous substrate with an applied pressure of 12.25 kPa. After peeling off the adhesive tape, the oil wettability on the Glu-AVM coating was examined. Unlike the untreated AVM coated fibrous substrate, this glucamine modified AVM was capable of sustaining this severe physical exposure with static OCA~159° and contact angle hysteresis ~8° as shown in Figure 6.5A-B and Table 6.3. Next, 100 g of sand was dropped on the Glu-AVM coated fibrous substrate from a height of 25 cm, but the coated interface remained extremely oil repellent under water with static OCA~160° and contact angle hysteresis ~8° as shown in Figure 6.5C-D and Table 6.3. Other severe physical abrasions—including sand paper abrasion and knife scratching were also performed on this Glu-AVM coated fibrous substrate but the nature-inspired and nature-derived wettability remained intact with advancing OCA above 150° and contact angle hysteresis below 10° as shown in Table 6.3. Further, the Glu-AVM fibrous coating was exposed to various harsh chemically complex aqueous phases for 30 days including acidic, alkaline, surfactant-contaminated water, artificial sea water and river water, however, the Glu-AVM coated fabric continued to display uninterrupted underwater superoleophobicity as depicted in shown in Table 6.3 through the dynamic contact angles measured after 30 days.

**Table 6.3** Illustrating the change in the advancing OCA and contact angle hysteresis of the beaded oil droplet under water on the Glu-AVM coated substrates after incurring various physical and chemical exposures.

| Physical and Chemical Exposures | Glu-AVM Coated Fabric | |
|---|---|---|
| | Advancing Contact Angle (°) | Contact Angle Hysteresis (°) |
| **Bending** | 158.6 ± 1.3 | 6.5 ± 0.6 |
| **Creasing** | 157.4 ± 2.1 | 7.2 ± 1.3 |
| **Twisting** | 158.3 ± 1.6 | 7.1 ± 0.4 |
| **Winding** | 159.8 ± 1.9 | 6.9 ± 0.9 |
| **Adhesive Tape Test** | 159.2 ± 1.3 | 7.9 ± 0.7 |
| **Sand Paper Abrasion** | 158.7 ± 1.6 | 8.4 ± 1.1 |
| **Sand Drop Test** | 160.4 ± 1.3 | 7.6 ± 0.9 |
| **Knife Scratch Test** | 157.8 ± 1.9 | 8.5 ± 0.8 |

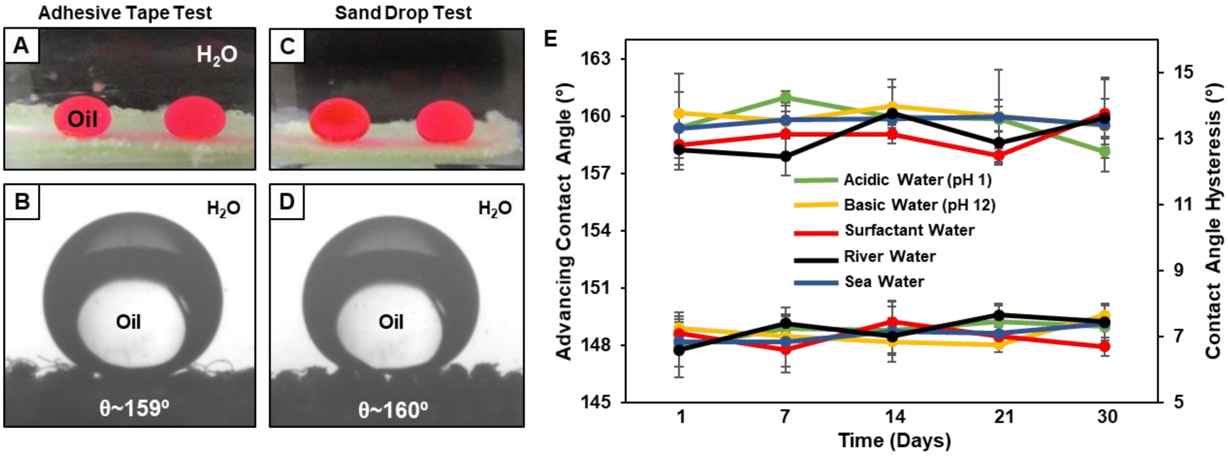

**Figure 6.5.** A-D) Digital images and OCA images of the beaded oil droplets on the Glu-AVM coated substrate under water after performing adhesive tape test (A-B) and sand drop test (C-D). E) Plot accounting for the advancing OCA and contact angle hysteresis of the beaded oil droplet on the Glu-AVM coated fibrous substrate after exposing it to various harsh aqueous chemical conditions for 30 days.

Furthermore, this Glu-AVM coated fibrous substrate was found to be extremely tolerant towards repetitive tensile deformations (150%) for 1000 cycles without affecting the embedded underwater superoleophobicity with advancing OCA above 150° and contact angle hysteresis below 10° as shown in Figure 6.6A-C.

Thus, the tremendous improvement of physical and chemical durability was unambiguously attributed to the strategic chemical modulation of the AVM coating and this development certainly allowed the

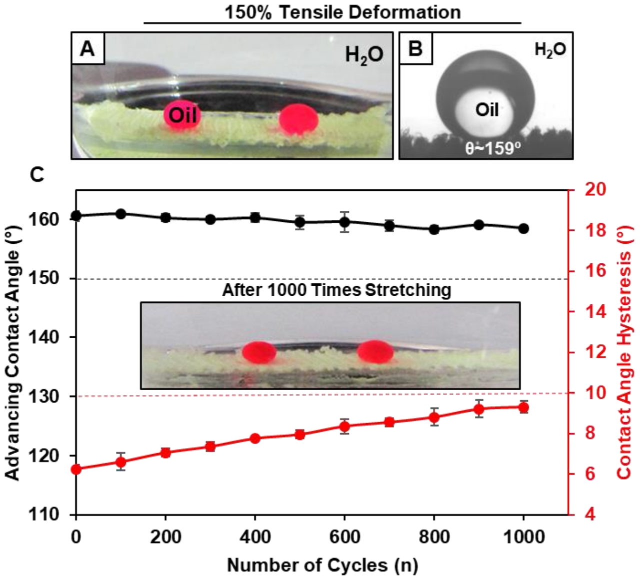

**Figure 6.6.** A-B) Digital image and OCA image of the Glu-AVM coated membrane before tensile deformation. C) Plot illustrating the changes in the advancing OCA (black) and contact angle hysteresis of the beaded oil droplets on the Glu-AVM coated fibrous substrate that was subjected to 150% tensile deformation repetitively for 1000 times. Inset image of the membrane after 150% stretching.

utilization of this naturally derived material for gravity-driven filtration-based separation even under practically relevant and extremely severe settings. The design of such naturally derived, stretchable and durable underwater superoleophobic coatings is rare in the literature.

### 6.3.4. Gravity-driven Oil/Water Separation at Challenging Settings

The covalently cross-linked and post modified, robust underwater oil-repellent interface derived directly from AVM, was further exploited for gravity-driven oil/water separation. The Glu-AVM coated fibrous substrate was used as a membrane and tied onto the open end of a lab-made prototype and mixtures of light (kerosene oil) and heavy (dichloroethane, DCE, model oil) oils were separated through selective filtration process. On pouring the light oil (Figure 6.7A-B) and heavy oil (Figure 6.7D-E) water mixtures, selectively only the aqueous phase was allowed to permeate through the Glu-AVM membrane as shown in Figure 6.7C,F while the oil phase remained restricted by the membrane. The Glu-AVM coated membrane was repetitively used for the separation of both light and heavy oils for a minimum of 25 times, and the water separation efficiency remained above 97% as shown in Figure 6.7G. Moreover, the Glu-AVM membrane was capable of successfully separating various oil/water mixtures, where oils of varying viscosities were taken, and water separation efficiency remained above 95% as shown in Figure 6.7H. Further, even viscous oil/water mixtures such as

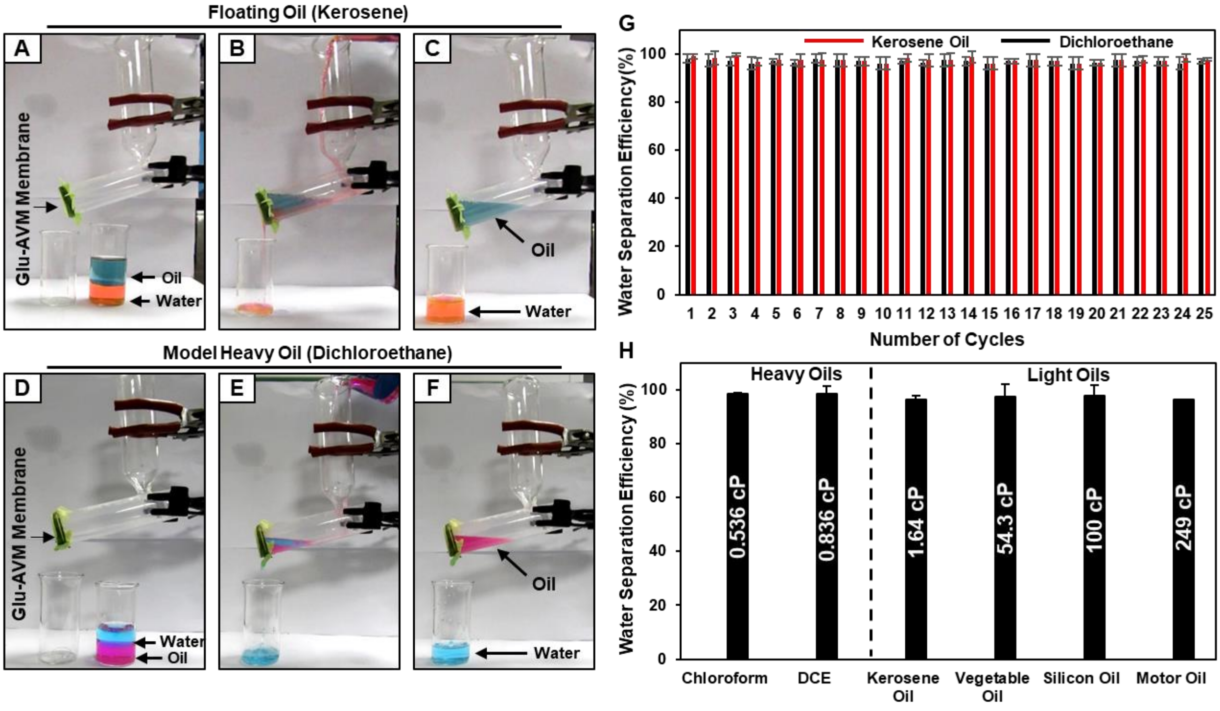

**Figure 6.7.** A-F) Digital images showing the gravity-driven separation of both light (kerosene oil; (A-C)) and heavy oils (dichloroethane, DCE; (D-F)) following the selective filtration of the aqueous phase through the Glu-AVM coated stretchable bio-mimicked membrane. G) Plot illustrating the water separation efficiency after repetitive use of the Glu-AVM coated membrane for both kerosene (red) and dichloroethane/water mixture (black). H) Plot displaying the water separation efficiency of various oil/water mixtures where oils with a wide range of densities and viscosities were used.

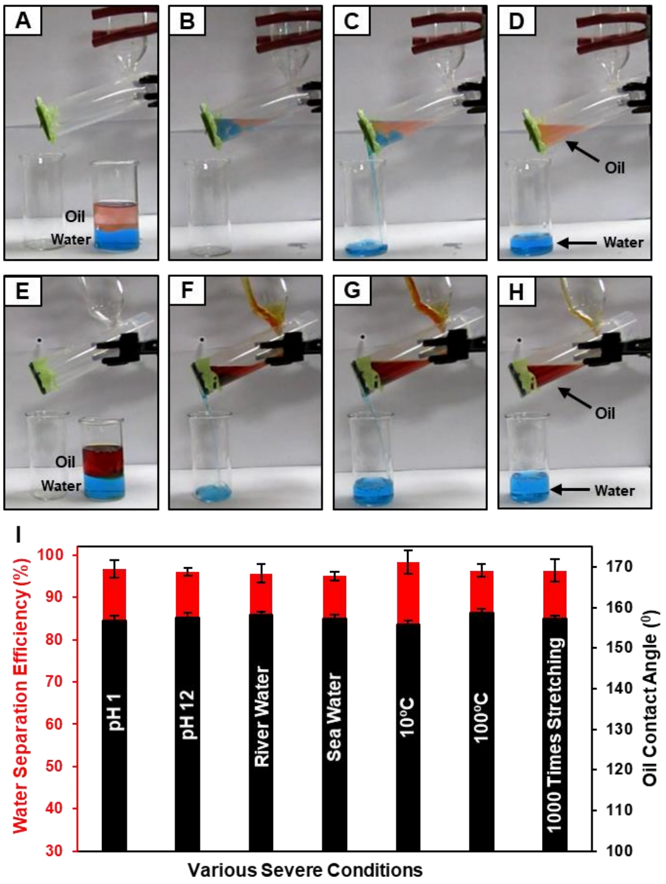

**Figure 6.8.** A-H) Digital images showing the separation of viscous oil/water mixtures i.e. silicon oil (A-D) and motor oil (E-H) through the Glu-AVM coated membrane. I) Plot depicting the water separation efficiency (red) through the Glu-AVM coated membrane for motor oil/water mixtures under various harsh aqueous chemical conditions, extremes of temperatures (10°C and 100°C) and after 1000 times stretching the membrane. The black bars represent the change in the oil contact angle on the Glu-AVM coated membrane after performing the oil/water separations at the respective severe settings.

silicone oil (Figure 6.8A-D) and motor oil (Figure 6.8E-H) could also be successfully separated using this robust underwater oil-repellent membrane. Furthermore, this bio-mimicked interface was exploited for oil/water separation under harsh aqueous conditions i.e. extremes of pH, artificial sea water, extremes of temperatures (10°C and 100°C) and even after physical deformation of the membrane for 1000 times, however, the water separation efficiency remained unperturbed (Figure 6.8I, red bar). Moreover, even after selective filtration of the aqueous phases under challenging conditions, the Glu-AVM coated interfaces continued to display underwater superoleophobicity with oil contact angles above 150° as shown in Figure 6.8I (black bar).

## 6.4. Conclusion

In this chapter, we introduced a simple environment-friendly approach for the strategic and direct use of the naturally preserved hydrogel from Aloe Vera leaf for developing robust underwater superoleophobicity. The Aloe Vera mucilage that mainly consists of an immobilized aqueous phase

(~99 wt%) was discovered to display highly tolerant underwater superoleophobicity and the embedded super-oil repellence remained intact even after subjection to severe challenging settings including extremes of temperatures (100°C and -196°C), extremes of pH (1 and 12), sea water, and surfactant contaminated water for 30 days. Further, this naturally derived hydrogel was directly applied on a selected (oleophilic) fibrous substrate to develop highly durable and stretchable super-oil-repellent membranes adopting the covalent modification of AVM following the catalyst-free Michael addition reaction between the amino acid residues of the mucilage and an acrylate cross-linker. The covalently modified AVM was subjected to post modification with a high surface energy molecules to impart non-adhesive underwater superoleophobicity that was found to be chemically and physically durable and thus, such a robust interface was extended for gravity-driven filtration-based oil/water separation of both light and heavy oils wherein selective passage of only the aqueous phase was allowed. This selective oil/water separation was performed repetitively (25 times) and even under practically relevant challenging aqueous settings circumstances with water separation efficiency above 97% for all cases. Such naturally derived, and extremely durable materials have immense potential for ‘real world’ prospective applications.

## 6.5. References

1. L. Feng, S. H. Li, Y. S. Li, H. J. Li, L. J. Zhang, J. Zhai, Y. L. Song, B. Q. Liu, L. Jiang and D. B. Zhu, *Adv. Mater.*, 2002, **14**, 1857-1860.
2. X. M. Li, D. Reinhoudt and M. Crego-Calama, *Chem. Soc. Rev.*, 2007, **36**, 1350-1368.
3. M. J. Liu, S. T. Wang, Z. X. Wei, Y. L. Song and L. Jiang, *Adv. Mater.*, 2009, **21**, 665-669.
4. Y. Y. Yan, N. Gao and W. Barthlott, *Adv. Colloid Interface Sci.*, 2011, **169**, 80-105.
5. T.-S. Wong, S. H. Kang, S. K. Y. Tang, E. J. Smythe, B. D. Hatton, A. Grinthal and J. Aizenberg, *Nature*, 2011, **477**, 443-447.
6. J. C. Bird, R. Dhiman, H. M. Kwon and K. K. Varanasi, *Nature*, 2013, **503**, 385-388.
7. L. Wen, Y. Tian and L. Jiang, *Angew. Chem., Int. Ed.*, 2015, **54**, 3387-3399.
8. B. Su, Y. Tian and L. Jiang, *J. Am. Chem. Soc.*, 2016, **138**, 1727-1748.
9. S. Amini, S. Kolle, L. Petrone, O. Ahanotu, S. Sunny, C. N. Sutanto, S. Hoon, L. Cohen, J. C. Weaver, J. Aizenberg, N. Vogel and A. Miserez, *Science*, 2017, **357**, 668-673.
10. Q. Cheng, M. Li, Y. Zheng, B. Su, S. Wang and L. Jiang, *Soft Matter*, 2011, **7**, 5948-5951.
11. Q. Cheng, M. Li, F. Yang, M. Liu, L. Li, S. Wang and L. Jiang, *Soft Matter*, 2012, **8**, 6740-6743.
12. L. Chen, M. Liu, H. Bai, P. Chen, F. Xia, D. Han and L. Jiang, *J. Am. Chem. Soc.*, 2009, **13**, 10467-10472.
13. X. Liu, J. Gao, Z. Xue, L. Chen, L. Lin, L. Jiang and S. Wang, *ACS Nano*, 2012, **6**, 5614-5620.

14. Z. Shi, W. Zhang, F. Zhang, X. Liu, D. Wang, J. Jin and L. Jiang, *Adv. Mater.*, 2013, **25**, 2422-2427.

15. Y. Wu, B. Su, L. Jiang and A. J. Heeger, *Adv. Mater.*, 2013, **25**, 6526-6533.

16. M. Tao, L. Xue, F. Liu and L. Jiang, *Adv. Mater.*, 2014, **26**, 2943-2948.

17. Y. Cai, Q. Lu, X. Guo, S. Wang, J. Qiao and L. Jiang, *Adv. Mater.*, 2015, **27**, 4162-4168.

18. K. Chen, S. Zhou and L. Wu, *ACS Nano*, 2016, **10**, 1386-1394.

19. L. Lin, M. J. Liu, L. Chen, P. P. Chen, J. Ma, D. Han and L. Jiang, *Adv. Mater.*, 2010, **22**, 4826-4830.

20. Z. Xue, S. Wang, L. Lin, L. Chen, M. Liu, L. Feng and L. Jiang, *Adv. Mater.*, 2011, **23**, 4270-4273.

21. X. Liu, J. Zhou, Z. Xue, J. Gao, J. Meng, S. Wang and L. Jiang, *Adv. Mater.*, 2012, **24**, 3401-3405.

22. F. Zhang, W. B. Zhang, Z. Shi, D. Wang, J. Jin and L. Jiang, *Adv. Mater.*, 2013, **25**, 4192-4198.

23. Z. Cheng, H. Lai, Y. Du, K. Fu, R. Hou, C. Li, N. Zhang and K. Sun, *ACS Appl. Mater. Interfaces*, 2014, **6**, 636-641.

24. J. Yong, F. Chen, Q. Yang, U. Farooq and X. Hou, *J. Mater. Chem. A*, 2015, **3**, 10703-10709.

25. S. Gao, J. Sun, P. Liu, F. Zhang, W. Zhang, S. Yuan, J. Li and J. Jin, *Adv. Mater.*, 2016, **28**, 5307-5314.

26. U. Manna and D. M. Lynn, *Adv. Funct. Mater.*, 2015, **25**, 1672-1681.

27. D. Parbat and U. Manna, *Chem. Sci.*, 2017, **8**, 6092-6102.

28. T. Guo, L. Heng, M. Wang, J. Wang and L. Jiang, *Adv. Mater.*, 2016, **28**, 8505-8510.

29. X. Meng, M. Wang, L. Heng and L. Jiang, *Adv. Mater.*, 2018, **30**, 1706634-1706642.

30. M. Wang, M. Peng, J. Zhu, Y.-D. Li and J. -B. Zeng, *Carbohydr. Polym.*, 2020, **244**, 116449-116456.

31. A. Prasannan, J. Udomsin, H. -C. Tsai, C. -F. Wang and J. -Y. Lai, Chem. Eng. J., 2020, 391, 123585-123598.

32. S. K. Hong, S. Bae, H. Jeon, M. Kim, S. J. Cho and G. Lim, *Nanoscale*, 2018, **10**, 3037-3045.

33. A. Milionis, C. S. Sharma, R. Hopf, M. Uggowitzer, I. S. Bayer and D. Poulikakos, *Adv. Mater. Interfaces*, 2019, **6**, 1801202-1801212.

34. N. A. Ivanovaa and A. B. Philipchenko, *Appl. Surf. Sci.*, 2012, **263**, 783-787.

35. A. Shome, A. Das, N. Rawat, A. M. Rather and U. Manna, *J. Mater. Chem. A*, 2020, **8**, 15148-15156.

36. A. Balaji, M. V. Vellayappan, A. A. John, A. P. Subramanian, S. K. Jaganathan, M. SelvaKumar, A. A. B. M. Faudzi, E. Supriyantoa and M. Yusofa, *RSC Adv.*, 2015, **5**, 86199-86213.

37. S. D. McConaughy, S. E. Kirkland, N. J. Treat, P. A. Stroud and C. L. McCormick, *Biomacromolecules*, 2008, **9**, 3277-3293.

38. D. K. Kim, B. R. Sim and G. Khang, *ACS Appl. Mater. Interfaces*, 2016, **8**, 15160-15168.

33. S. L. Bechler and D. M. Lynn, *Biomacromolecules*, 2012, **13**, 1523-1532.

# Chapter 7: Conclusion and Future Directions

This chapter provides an overview of the various works discussed in the individual chapters. The thesis revolves around the strategic use of naturally abundant, low-cost materials including natural polymers, waste materials and natural hydrogel to develop three-dimensional sponges and coatings embedded with abrasion-tolerant bio-inspired liquid repellence for proof-of-concept drug release and oil/water remediation applications.[1-6] In Chapter 1, I have provided a brief overview on the discovery of the naturally existing species with characteristic liquid repellent properties and the introduction of the theoretical models of liquid wettability on a solid surface. Moreover, I have outlined the various prospective applications of bio-inspired liquid wettability and the different types of non-biodegradable, environmentally hazardous synthetic components explored over the years to fabricate bio-inspired anti-wetting materials. Further, I have discussed the different kinds of naturally abundant, eco-friendly and low-cost components that have been exploited to develop anti-wetting materials and the associated durability concerns that hinder their practical applicability. Thereafter, I have enlisted my motivation and objectives for designing the chapters in this thesis. In Chapter 2, I covalently intertwined the amine containing bovine serum albumin nanoparticles with a multifunctional acrylate cross-linker following the catalyst-free Michael addition reaction to develop chemically 'reactive' protein nanoparticles that provided the appropriate topography and residual 'reactive' chemistry for constructing a durable protein-based coating on a fibrous substrate. The presence of residual chemical functionalities allowed the post covalent modification with the desired small molecules to embed a wide range of water wettability including hydrophobicity, adhesive superhydrophobicity and non-adhesive superhydrophobicity. The tailorable water wettability aided in the controlled and sustained release of the drug molecules loaded onto the three-dimensional, superhydrophobic fibrous substrate.[2] Since the mechanical property of the fibrous superhydrophobic substrate in the previous chapter could not be tailored, thus, in Chapter 3, silk-cocoon derived silk microfibers and silk fibroin were strategically combined to develop silk sponges with both tailorable mechanical property and abrasion-tolerant water wettability. The ethanol assisted controlled induction of beta sheet in the silk fibroin network that was reinforced with silk microfibers, allowed to tailor the mechanical property of the sponges. Further, the facile Michael addition reaction between the amine residues of silk protein and an acrylate cross-linker imparted chemical reactivity to the sponges to modulate the water wettability. The controlled introduction of beta sheet content in the silk cocoon derived sponges is specific for tailoring the mechanical property of only protein derived materials, thus, I further explored a single chemical avenue that allowed to modulate both the mechanical property as well as the water wettability in waste paper derived functional materials in chapter 4. The covalent integration of a silane moiety with waste paper provided a facile avenue to tailor the porosity and compressive modulus of the sponges. The Michael addition assisted covalent cross-linking of the silanized waste paper sponges with a multi-functional acrylate cross-linker allowed to develop physically and chemically durable, highly compressible paper sponges were extended for the selective, repetitive absorption of the oil phase from various oil/water mixtures even under harsh aqueous settings. The analogous waste paper derived membranes were extended for gravity-driven filtration-based, selective and repetitive oil/water separation even under harsh aqueous settings. In Chapter 5, the Schiff base reaction was exploited to introduce another type of liquid wettability i.e. underwater superoleophobicity. I derived inspiration from the protein constituent of fish-scales that aided in exhibiting extreme oil repellence underwater. The association of the amine residues of BSA protein with an aldehydic cross-linker followed by reduction of the as obtained imine bond generated highly sustainable underwater superoleophobic coatings on the selected fibrous and planar substrates. Subsequently, I discovered the inherent underwater superoleophobicity of Aloe Vera mucilage which was directly exploited following the Michael addition pathway for developing stretchable and robust underwater superoleophobicity on a fibrous substrate for selective filtration of the water phase from various oil/water mixtures even under challenging aqueous settings and extremes of temperatures as presented in Chapter 6.

The research works described in this thesis possess potential for various bio-medical, environmental and electronics applications. The substitution of the existing synthetic ingredients derived functional materials with naturally existing, low-cost counterparts would eliminate the concerns related to environmental hazards. In that context, superhydrophobic, blood-repellent coatings with hierarchical topography have recently garnered limelight for minimizing blood loss, easier wound dressing removal and triggering faster clotting.[7-8] The hierarchal topography associated with the water repellent interfaces aid in minimizing the effective surface area available for platelet adhesion.[9] Moreover, the textured surfaces alter the conformation of the blood proteins and thus, minimize the blood adherence to the surface. Thus, the bovine serum albumin derived hierarchically featured, coating on fibrous substrates with tuneable water wettability that was demonstrated for proof-of-concept drug delivery in this thesis, holds potential for fabricating mechanically deformable, superhydrophobic, blood-repellent bandage materials for use as external wound healing patches. The tuneability of a wide range of water wettability in such bio-viable functional materials is a facile avenue to control the rate of release of the drugs loaded in the blood-repellent patches, thus, preventing excessive blood loss and enabling faster clotting, as desirable. In the past, the water wettability of a surface has been well established to regulate stem cell differentiation.[10-11] In that context, the silk-cocoon derived sponges with tailorable mechanical property and water wettability possess immense potential for tissue engineering applications. Therefore, the opportunity for simultaneous tailoring of the water wettability and mechanical property would provide a platform for developing bio-degradable implants initiating stem cell differentiation. Moreover, silk-cocoon derived, or the waste paper based mechanically deformable substrates embedded with superhydrophobicity can be integrated with conductive 2D-nanomaterials to develop bio-compatible, wearable electronics where embedment of water repellence would enhance the longevity of the devices. Recently, porous xerogels and aerogels have been exploited to develop thermally insulating sponges, but the prolonged physical and chemical durability was not investigated in detail which limits its practical applicability.[12-15] Thus, the porous, highly compressible, superhydrophobic waste paper derived sponges with prolonged physical and chemical durability can be successfully extended for developing thermal insulators for practical applications. On the other side, underwater superoleophobicity coatings have recently been explored to study the platelet adhesion in order to minimize thrombosis and in-stent restenosis.[16-17] However, the existing reports mostly exploit synthetic polymers for demonstrating anti-platelet adhesion behaviour which limits its practical medical applicability. Thus, the naturally derived, stretchable and extremely abrasion-tolerant underwater superoleophobic coatings can be extended for developing coatings on implantable medical devices with tuneable liquid wettability to modulate the platelet adhesion. Moreover, association of such low-cost, highly durable underwater oil-repellent coatings with marine vessels have potential for reducing biofouling and bio-adhesion[18], thus, increasing the longevity and efficiency of the vessels. Thus, naturally derived components integrated with a smart chemical approach possess potential for a various prospective practical applications.

## References:

1. A. Shome, A. M. Rather and U. Manna, *Nanoscale Adv.*, 2019, **1**, 1746-1753.
2. A. Shome, A. M. Rather, A. Ghosal, B. K. Bhunia, B. B. Mandal and U. Manna, *ACS Sustainable Chem. Eng.*, 2019, **7**, 7502-7509.
3. A. Shome, J. C. Moses, A. M. Rather, B. Mandal and U. Manna, *ACS Appl. Mater. Interfaces*, 2021, **13**, 24258-24271.
4. A. Shome, A. M. Rather, A. Borbora, P. Srikrishnarka, A. Baidya, T. Pradeep and U. Manna, *Chem Asian J.*, 2021, **16**, 1988-2001.
5. A. Shome, A. Das, N. Rawat, A. M. Rather and U. Manna, *J. Mater. Chem. A*, 2020, **8**, 15148-15156.
6. A. Shome, A. M. Rather and U. Manna, *J. Mater. Chem. A*, 2018, **6**, 22465-22471.
7. Z. Li, A. Milionis, Y. Zheng, M. Yee, L. Codispoti, F. Tan, D. Poulikakos and C. H. Yap, *Nat. Commun.*, 2019, **10**, 5562-5573.

8. T. Zhu, J. Wu, N. Zhao, C. Cai, Z. Qian, F. Si, H. Luo, J. Guo, X. Lai, L. Shao and J. Xu, *Adv. Healthcare Mater.*, 2018, **7**, 1701086-1701093.

9. V. Jokinen, E. Kankuri, S. Hoshian, S. Franssila and R. H. A. Ras, *Adv. Mater.*, 2018, **30**, 1705104-1705114.

10. 40. K. S. Brammer, C. Choi, C. J. Frandsen, S. Oh and S. Jin, *Acta Biomater.*, 2011, **7**, 683-690.

11. Q. Lu, X. Hua, X. Wang, J. A. Kluge, S. Lu, P. Cebe and D. L. Kaplan, *Acta Biomater.*, 2010, **6**, 1380-1387.

12. W. Sakuma, S. Yamasaki, S. Fujisawa, T. Kodama, J. Shiomi, K. Kanamori and T. Saito, *ACS Nano*, 2021, **15**, 1436-1444.

13. Y. Kobayashi, T. Saito and A. Isogai, *Angew. Chem. Int. Ed.*, 2014, **53**, 10394-10397;

14. Y. Kobayashi, T. Saito and A. Isogai, *Angew. Chem.*, 2014, **126**, 10562-10565.

15. C. Jia, L. Li, Y. Liu, B. Fang, H. Ding, J. Song, Y. Liu, K. Xiang, S. Lin, Z. Li, W. Si, B. Li, X. Sheng, D. Wang, X. Wei and H. Wu, *Nat. Commun.* 2020, **11**, 3732-3745.

16. L. Chen, M. Liu, H. Bai, P. Chen, F. Xia, D. Han and L. Jiang, *J. Am. Chem. Soc.*, 2009, **131**, 10467-10472.

17. D. Parbat, B. K. Bhunia, B. B. Mandal and U. Manna, *Chem Asian J.*, 2021, **16**, 1081-1085.

18. X. Chao, X. Xiang, K. Cao, G. Yi, C. Dan, J. Fei, Z. Ze and H. Dong, *Colloids Surf. A Physicochem. Eng.* , 2021, **628**, 127323-127327.

# Publications Related to Thesis Work

1. **A. Shome,** A. M. Rather, U. Manna. Aloe Vera Mucilage Derived Highly Tolerant Underwater Superoleophobic Coatings, *J. Mater. Chem. A*, 2018, **6**, 17019-17031.
2. **A. Shome,** A. M. Rather, U. Manna. Chemically Reactive Protein Nanoparticles for Synthesis of a Durable and Deformable Superhydrophobic Material, *Nanoscale Adv.*, 2019, **1**, 1746-1753.
3. **A. Shome,** A. M. Rather, A. Ghosal, B. K. Bhunia, B. B. Mandal, U. Manna. Rational Chemical Engineering in Natural Protein Derived Functional Interface, *ACS Sustainable Chem. Eng.*, 2019, **7**, 7502-7509.
4. **A. Shome,** A. Das, N. Rawat, A. M. Rather, U. Manna. Reduction of Imine-based Cross-Linkages to Achieve Sustainable Underwater Superoleophobicity that Performs Under Challenging Conditions, *J. Mater. Chem. A*, 2020, **8**, 15148-15156.
5. **A. Shome**, J. C. Moses, A. M. Rather, B. Mandal and U. Manna. Unconventional and Facile Fabrication of Chemical Reactive Silk- Fibroin Sponges for Environmental Remediation, *ACS Appl. Mater. Interfaces*, 2021, **13**, 24258-24271.
6. **A. Shome**, A. M. Rather, A. Borbora, P. Srikrishnarka, A. Baidya, T. Pradeep and U. Manna. Design of a Waste Paper-Derived Chemically 'Reactive' and Durable Functional Material with Tailorable Mechanical Property Following an Ambient and Sustainable Chemical Approach, *Chem Asian J.*, 2021, **16**, 1988-2001.

# Other Publications

7. A. M. Rather, **A. Shome,** S. Kumar, B. K. Bhunia, B. B. Mandal, H. K. Srivastava, U. Manna. Alkali Metal-ion Assisted Michael Addition Reaction in Controlled Tailoring of Topography in a Superhydrophobic Polymeric Monolith, *J. Mater. Chem. A*, 2018, 6, 17019-17031.
8. A. M. Rather, **A. Shome**, B. K. Bhunia, B. B. Mandal, U. Manna. Simultaneous and Controlled Release of Two Different Bioactive Small Molecules from Nature Inspired Single Material, *J. Mater. Chem. B*, 2018, 6, 7692-7702.
9. **A. Shome,** K. Maji, A. M. Rather, A. Yashwanth, D. K. Patel, U. Manna. A Scalable Chemical Approach for the Synthesis of a Highly Tolerant and Efficient Oil Absorbent, *Chem. Asian J.*, 2019, 14, 4732-4740.
10. A. Das, D. Parbat, **A. Shome**, U. Manna. Sustainable Bio-mimicked Oil/Water Wettability that Perform Under Severe Challenges, *ACS Sustainable Chem. Eng.*, 2019, **7**, 11350-11359.

11. A. M. Rather, P. Srikrishnarka, A. Baidya, **A. Shome**, T. Pradeep and U. Manna, Evaluating the Impact of Tailored Water Wettability on Performance of $CO_2$ Capture, *ACS Appl. Energy Mater.*, 2020, **3**, 10541-10549.

12. **A. Shome,** † A. Das, † and U. Manna, Porous and Reactive Polymeric Interfaces: An Emerging Avenue for Achieving Durable and Functional Bio-Inspired Wettability, *J. Mater. Chem. A*, 2021, **9**, 824-856. († Equal Authors)

13. R. Dalapati, S. Nandi, C. Gogoi, **A. Shome** and S. Biswas**,** Metal–Organic Framework (MOF) Derived Recyclable, Superhydrophobic Composite of Cotton Fabrics for the Facile Removal of Oil Spills. *ACS Appl. Mater. Interfaces,* **2021**, *13*, 8563-8573.

14. **A. Shome,** † A. Das, † and U. Manna, Michael Addition Reaction Assisted Derivation of Functional and Durable Superhydrophobic Interfaces, *Chem. Mater.*, 2021, **33**, 23, 8941-8959. († Equal Authors)

15. M. Dhar, A. Das, **A. Shome**, A. Borbora and U. Manna, Design of 'Tolerant and Hard' Superhydrophobicity to Freeze Physical Deformation, *Mater. Horiz*., 2021, **8**, 2717-2725.

16. A. Shome, A. Das, A. Borbora, M. Dhar and U. Manna. Role of Chemistry on Bio-inspired Liquid Wettability *Chem. Soc. Rev.*, 2022, **51**, 5452-5497.

## Patents

1. U. Manna, V. Nandakumar, Karthick R, K. Maji, **A. Shome**, A. M. Rather, Selective and Super Oil Absorbent for Remediation of Oil Spills, Indian Patent: 201841029004, Filling Date: 01.08.2018.

2. U. Manna, V. P. Nandakumar, K. Ramalingam, M. Megur G. BHAT, P. K. Hegde, A. Das, **A. Shome**, M. Dhar, A Coating Composition and a Process of Preparation, Indian Patent: 202041020725, Filling Date: 16.05.2020.

3. U. Manna, V. Nandakumar, Karthick R, A. Das, K. Maji, **A. Shome**, A Process for Preparation of a Superhydrophobic Membrane, Indian Patent: 202041005525, Filling date : 07.02.2020.

## Conferences and Workshops Attended

1. Flash Talk at International Conference in Advanced Nanomaterials and Nanotechnology, **ICANN 2021** organized by Centre for Nanotechnology, IIT Guwahati.

2. Poster presentation at **National Science Day celebration, 2021** and National Seminar on Material Chemistry-Today and Tomorrow organised by Indian Chemical Society.

3. Oral presentation at the **57th Annual convention of chemists**, **2020**, **International Conference on Recent Trends in Chemical Sciences** organised by Indian Chemical Society.

4. Oral Presentation at National Conference on Issues and Challenges in Water Treatment and Allied Research for Sustainable Environment **(WATER 2020)** organized by Centre for Environment, IIT Guwahati.

5. Poster presentation at **Research Conclave 2019,** organized by Students Academic Board, IIT, Guwahati.

6. Oral Presentation at **Reflux 7.0, 2019** organized by Department of Chemical Engineering, IIT, Guwahati.

7. Oral Presentation at **National Conference in Green, Sustainable and Evolving Sciences, 2019** organized by Cotton University and Assam Science Society.

8. Poster Presentation at National Conference on Upstream Petroleum Engineering **(NCUPE), 2019** organized by Department of Chemical Engineering, IIT Guwahati.

9. Poster Presentation at **ICANN 2019** organized by Centre for Nanotechnology, IIT Guwahati.

10. Workshop on Thermal Analysis of Materials, 2019 organized by Department of Chemical Engineering, IIT, Guwahati and Guwahati Regional Centre Indian Institute of Chemical Engineers.

11. Poster presentation at **Frontiers in Chemical Sciences, 2018** organized by Department of Chemistry, IIT, Guwahati.

## Awards and Achievements

1. **AWSAR-DST 2019**, Popular Science Story Award for the article entitled ‘‘Cotton - The Trivialzed Treasure.’’

2. **Sir C V Raman Award of Excellence** for poster presentation at National Science Day celebration-2021 and National seminar on ’’Material Chemistry-Today and tomorrow’’ organised by Indian Chemical Society.

3. **Professor G. Gopalarao Centenary Young Scientist Award** for oral presentation at the 57th Annual convention of chemists, 2020, International conference on recent trends in chemical sciences organised by Indian Chemical Society.

4. **Best Oral Presentation** at National Conference on Issues and Challenges in Water Treatment and Allied Research for Sustainable Environment **(WATER 2020)** organized by Centre for Environment, IIT Guwahati.

5. **Best Oral Presentation** at Reflux 7.0, 2019 organized by Department of Chemical Engineering, IIT, Guwahati.

6. **Best Poster Presentation** at ICANN 2019 organized by Centre for Nanotechnology, IIT Guwahati.

7. **Best Poster Presentation** at National Conference on Upstream Petroleum Engineering **(NCUPE), 2019** organized by Department of Chemical Engineering, IIT Guwahati.

8. **Best Poster Presentation** at Frontiers in Chemical Sciences, 2018 organized by Department of Chemistry, IIT, Guwahati.